BRIGHTNESS TEMPERATURE CALIBRATION OF SAC-D/AQUARIUS MICROWAVE RADIOMETER (MWR)

by

SAYAK KRISHNA BISWAS
B.Tech. National Institute of Technology Calicut, 2005
M.S. University of Central Florida, 2009

A dissertation submitted in partial fulfillment of the requirements
for the degree of Doctor of Philosophy
in the Department of Electrical Engineering and Computer Science
in the College of Engineering and Computer Science
at the University of Central Florida
Orlando, Florida

Spring Term
2012

Major Professor: Linwood Jones

© 2012 Sayak Krishna Biswas

ABSTRACT

The Aquarius/SAC-D joint international science mission, between the National Aeronautics and Space Administration (NASA) of United States and the Argentine Space Agency (Comision Nacional de Actividades Espaciales, CONAE), was launched on a polar-orbiting satellite on June 10, 2011. This mission of discovery will provide measurements of the global sea surface salinity, which contributes to understanding climatic changes in the global water cycle and how these variations influence the general ocean circulation. The Microwave Radiometer (MWR), a three channel Dicke radiometer operating at 23.8 GHz H-Pol and 36.5 GHz V-& H-Pol provided by CONAE, will complement Aquarius (NASA's L-band radiometer/scatterometer) by providing simultaneous spatially collocated environmental measurements such as water vapor, cloud liquid water, surface wind speed, rain rate and sea ice concentration.

This dissertation focuses on the overall radiometric calibration of MWR instrument. Which means establishing a transfer function that relates the instrument output to the antenna brightness temperature (T_b). To achieve this goal, the dissertation describes a microwave radiative transfer model of the instrument and validates it using the laboratory and thermal-vacuum test data. This involves estimation of the losses and physical temperature profile in the path from the receiver to each antenna feed-horn for all the receivers. As the pre-launch laboratory tests can only provide a simulated environment which is very different from the operational environment in space, an on-orbit calibration of the instrument is very important. Inter-satellite radiometric cross-calibration of MWR using the Naval Research

Laboratory's multi-frequency polarimetric microwave radiometer, WindSat, on board the Coriolis satellite is also an important part of this dissertation. Cross-calibration between two different satellite instruments require normalization of T_b's to account for the frequency and incidence angle difference between the instruments. Also inter-satellite calibration helps to determine accurate antenna pattern correction coefficients and other small instrument biases.

Dedicated to the miracle of life, and to the beautiful planet where it happened for sure.

ACKNOWLEDGMENTS

This endeavor wouldn't have been successful without the help and support from many people. First of all I would like to express my sincere gratitude to my major advisor Dr. W. Linwood Jones. His dedication, sincerity and pursuit of excellence have been contagious. I will be forever indebted to him for his teaching and guidance. His unended support and trust in my research, boosted my self-confidence and helped me to overcome many challenges which I faced during this work. My deepest gratitude also due to the committee members: Dr. Thomas Wilheit, Dr.Michael Georgiopoulos and Dr. Parveen Wahid for their insightful comments and contribution to this work.

My sincere thanks go to CONAE for their financial support during my first visit to Argentina. I would specially thank Sandra Torrusio and Monica Rabolli for their unmatched hospitality and help during the annual trips to Argentina. I am indebted to Juan Cruz Gallo and Daniel Rocca for everything that I know about the MWR instrument. This work wouldn't have been possible if they hadn't taken time out of their busy schedule to answer my unnumerable questions. From time to time, they have translated useful information from their original Spanish documents to English for my comprehension. I want to share any credit that I deserve for this work, equally with them. Next, I would like to thank Sergio Masuelli of the MWR applications team for his hospitality and help during my six weeks at CONAE's Cordoba Space Center(CETT). My sincere thanks go to all the wonderful people whom I came across in CETT: March Jacob, Carolina Tauro, Carlos Moyano, Hector Raimondo, Nicolas Castro, Sebastian Heredia, Martin Labanda, Felipe Madero, Matas Marenchino and

others for their help, support, and friendship. I would like to make special mention of March Jacob and Marco Pantalone for their friendship and great hospitality.

My friends and colleagues at CFRSL has been an integral part of this journey. First, I would like to thank Kaushik Gopalan for his guidance and help during the initial days in the lab. My special appreciation goes to Spencer Farrar, Suleiman Alsweiss and Larry Schneider for all the insightful discussions that we had on different topics. I would like to acknowledge: Rafik Hanna, Pete Laupattarakasem, Salem El-Nimri and Ruba Amarin; interaction with them has always enriched me. I would like to make special mention of Yazan Hejazin who has helped me throughout this work. My sincere thanks go to Andrea-Santos Garcia and Shadi Aslebagh for helping me at the last days of this research. They have constantly supported me during the entire post-launch time period including the critical on orbit check-out phase of MWR. Finally, I want to acknowledge the help of Cathy May for assuming my responsibilities in another project so that I could concentrate on MWR calibration work.

I am indebted to my parents for inculcating in me the dedication and discipline to do whatever I undertake well. Despite their incomprehension about what I do, they have shown their unflagging belief that I must be saving the world. Thanks to my brothers for being the greatest friends a person could have during tumultuous times. I thank my wife for her love, understanding, patience and bringing joy to my life in so many different ways. This dissertation would not have been possible without her support and encouragements. My friends during graduate school, have always been great help to me. I have been fortunate to have many friends who cherish me despite my eccentricities. I would not name them here,

for I think they know who they are. Finally, I want to thank Dr. Tapanjyoti Banerjee, without whose help, the pursuit of my degree in United States would have been difficult.

I would like to acknowledge that the financial support to pursue my PhD program was sponsored by various NASA grants.

TABLE OF CONTENTS

LIST OF FIGURES . . . . . **xiv**

LIST OF TABLES . . . . . **xxiii**

CHAPTER 1 INTRODUCTION **1**

CHAPTER 2 AQUARIUS/SAC-D MISSSION AND SAC-D MWR **4**

2.1 Aquarius Mission **4**

2.2 MWR Sensor Geometry **6**

2.3 MWR Hardware **13**

CHAPTER 3 MWR CALIBRATION : PRE-LAUNCH **15**

3.1 Internal Calibration of MWR Receivers **16**

3.2 External Calibration of MWR Receivers **29**

3.3 Antenna Switch Matrix Calibration **39**

3.3.1 Front-End Hardware Radiative Transfer Model **42**

3.3.2 Thermal/Vacuum Antenna Temperature Cal/Val **50**

CHAPTER 4 MWR CALIBRATION : POST-LAUNCH 59

4.1 Inter-Satellite Calibration With WindSat 60

4.1.1 Choice of WindSat 60

4.1.2 Radiative Transfer Modelling 65

4.1.3 Datasets 71

4.1.4 Inter-Satellite Radiometric Calibration Method 75

4.2 Results 79

4.2.1 MWR Anomalies 93

CHAPTER 5 CONCLUSIONS 114

APPENDIX A MWR RF COMPONENT DATA-SHEETS 118

A.1 K Band Receiver 119

A.1.1 Circulator Switch 119

A.1.2 Isolator 120

A.1.3 Coupler 121

A.1.4 Filter 122

A.1.5 Low Noise Amplifier (LNA) 124

A.1.6 Noise Diode 126

A.1.7 Wave Guide Termination (Match Load) 127

A.2 Ka Band Receiver 128

A.2.1 Ortho-Mode Transducer (OMT) 128

A.2.2 Circulator Switch 129

A.2.3 Isolator 130

A.2.4 Coupler 131

A.2.5 Filter 133

A.2.6 Low Noise Amplifier (LNA) 135

A.2.7 Noise Diode 137

A.2.8 Wave Guide Termination (Match Load) 138

APPENDIX B MWR RECEIVER SCHEMATICS 139

B.1 K Band Receiver Schematics 140

B.2 Ka Band Receiver Schematics 141

APPENDIX C MWR WAVEGUIDE LENGTHS 142

C.1 Waveguide Length Computation Example 143

C.2 K Band Waveguide Lengths 144

C.3 Ka Band V-pol Waveguide Lengths 145

C.4 Ka Band H-pol Waveguide Lengths 146

APPENDIX D MWR SWITCH MATRICES 147

D.1 K Band Switch Matrix 148

D.2 Ka Band Switch Matrix (H-pol) 149

D.3 Ka Band Switch Matrix (V-pol) 150

APPENDIX E MWR THERMAL VACUUM TEST 151

E.1 K Band Absorber Temperature sensors 152

E.2 Ka Band Absorber Temperature sensors 153

E.3 Thermal Vacuum Test Data Readme 154

APPENDIX F MWR LEVEL 1 DATA PRODUCTS 160

F.1 CONAE L1A Data (HDF5) 161

F.2 CONAE L1B Data (HDF5) 198

F.3 CFRSL L1 Data (.mat) 223

LIST OF REFERENCES 226

LIST OF FIGURES

Figure 1.1 Historical SSS Measurements compared with Aquarius measurements. . . 2

Figure 2.1 Aquarius mission instruments on SAC-D spacecraft 5

Figure 2.2 MWR sensor geometry. 7

Figure 2.3 MWR instrument configuration. 10

Figure 2.4 Schematic of the Ka band radiometer in the MWR system [1]. 11

Figure 2.5 MWR Timing Diagram [1]. 12

Figure 3.1 Microwave radiometer 15

Figure 3.2 Block diagram of a total power radiometer. There are three major components: the band pass filter and amplifier amplifies the received radiation only over the desired bandwidth. The square law detector's output voltage is proportional to the power of the input signal. The final low pass filter acts as an integrator to reduce the noise in the power measurement. 17

Figure 3.3 MWR receiver block diagram with internal calibration technique. The guided radiation from the antenna is fed into the receiver through a directional coupler. When

turned on, the signal from the calibration noise diode is attenuated and coupled to the incoming antenna signal and provides a calibration reference. The Dicke switch constantly switches between the internal reference load (T_o) and the signal from the coupler output to provide another calibration point. 19

Figure 3.4 Simplified internal calibration model for MWR. The equivalent noise temperature (T_{REC}) of the receiver and calibration circuit is dumped at the coupler input. The transmission coefficient of the calibration circuit is assumed to be L (ratio).The equivalent increase in brightness at the radiometer input due to the calibration noise diode is assumed to be T_n K. 20

Figure 3.5 (a) Computer rendering of the Ka band MWR receiver and switch matrix are shown. The red line separates the two. (b) Schematic of the Ka band radiometer with red line separating the switch matrix from the receiver. (c) Simplified Cal-model applied to MWR receiver (Forward radiative transfer equations). 24

Figure 3.6 Calibration waveguide connected to a MWR receiver during external calibration test. The end of the 'blue' waveguide is terminated in a matched load. A platinum temperature sensor is attached to the termination. The matched termination is heated and cooled to simulate hot and cold calibration reference. 26

Figure 3.7 Radiative transfer through the calibration waveguide. The waveguide is divided into small sections. The radiative transfer equations are solved using assumed temperature variation along the length of the waveguide. 27

Figure 3.8 Assumed temperature distribution of the calibration waveguide.(a) Temperature distribution along the length of the waveguide is shown while the warm load was connected. Temperature exponentially decays from load end to the receiver end. (b) Temperature distribution when cold load is connected. Temperature exponentially rises from load end to the receiver end. 28

Figure 3.9 Least square linear regression through three calibration points, cold load (T_c), reference load (T_o) and the hot load (T_h). Slope of the line is radiometer gain (G). . 32

Figure 3.10 Temperature of the internal reference load during HOT and COLD load tests (Ka band H-pol Rx) 33

Figure 3.11 Counts for the internal reference during HOT and COLD load tests (Ka Band H-pol Rx) 34

Figure 3.12 Noise diode deflection counts for HOT and COLD load tests. (Ka Band H pol receiver). The deflection is higher for the cold input load compared to the hot input load case. 35

Figure 3.13 MWR K & Ka-band antenna feed-horn and switch-matrix assembly. The receiver and antenna reflectors are not shown here. Ka band system uses OMT to guide both V & H pol components of the incoming radiation to respective receivers. The K band only measures H-pol component through a circular to rectangular waveguide adapter connected to the horns. The feed horn numbers are shown; the even numbered horns are in the top plane and the odd numbered ones are in the bottom plane for each antenna system. 40

Figure 3.14 MWR antenna switch matrix radiative transfer model schematic. A necessary orientation of the circulator switches are shown, to guide radiation incident on horn i to the receiver. In the primary path, the radiation has to pass through four waveguide sections and three switches. 41

Figure 3.15 (a) Picture of the MWR instrument covered with thermal blanket, prepared for the T/V test. The flight reflectors are replaced by blackbody calibration targets. The whole instrument is put inside the coffin before taking inside the T/V chamber (Fig. (b)). (c) There are total five temperature sensors attached at the face of the blackbody absorber target to monitor its temperature. 51

Figure 3.16 (a) Computed Tin from the model using assumed losses and reflection coefficients for the entire duration of the T/V test. (b) Tin calculated from the radiometer counts during T/V test. 53

Figure 3.17 Computation of antenna temperature (T_{ap}) from radiometer counts based on the radiative transfer model inversion. The red line is the computed T_{ap}. The black line is the measured T_{ap}. The model does not follow the measured T_{ap} very well. 54

Figure 3.18 Antenna temperature (T_{ap}) computed based on regression based model (red). The blue line is the model based inversion algorithm which assumes losses and reflection coefficients to guess coefficients.The black line is the measured T_{ap} 55

Figure 4.1 STK Simulation of the (a) ascending and (b) descending collocations between MWR (green) and WindSat (magenta) swaths. The red colored points show corners of collocated 0.5^o resolution boxes.[2] 62

Figure 4.2 $0.5^o \times 0.5^o$ collocation boxes between MWR and WindSat in $\sim$ 45 hours as simulated in STK.[2] 63

Figure 4.3 Frequency spectrum of top-of-the-atmosphere brightness temperature (T_b) as seen by a downward looking radiometer at 53° incidence angle for three different columnar WV densities $\sim$ 6 mm (red), $\sim$ 20 mm (green) and $\sim$ 70 mm (blue) for a fixed ocean surface conditions: wind speed 5 m/s, Sea Surface Temperature 300 K and salinity 36 ppt. Even though atmospheric emissions are not polarized, greater dynamic range of T_b is observed at H pol (panel (b)) compared to V-pol (panel (a)) due to surface reflection modulation. The T_b's peak up at 22.2 GHz WV resonance line. 68

Figure 4.4 MWR and WindSat $1^o \times 1^o$ collocation boxes for first 65 MWR revs. . . 78

Figure 4.5 Comparison between MWR real observations (y-axis) and Simulated MWR based on WindSat (x-axis) observations for K band H-pol Horn#1, before (a) and after (b) slope offset correction. 81

Figure 4.6 Comparison between MWR real observations (y-axis) and Simulated MWR based on WindSat (x-axis) observations for Ka band H-pol Horn#1, before (a) and after (b) slope offset correction. 82

Figure 4.7 Comparison between MWR real observations (y-axis) and Simulated MWR based on WindSat (x-axis) observations for Ka band V-pol Horn#1, before (a) and after (b) slope offset correction. 83

Figure 4.8 Ka band (36.5 GHz) H-pol brightness temperature image for first five days (Aug 31st - Sept 4th, 2011) combining all ascending passes. The colorbar is in Kelvin. 86

Figure 4.9 Ka band (36.5 GHz) V-pol brightness temperature image for first five days (Aug 31st - Sept 4th, 2011) combining all ascending passes. The colorbar is in Kelvin. 87

Figure 4.10 K band (23.8 GHz) H-pol brightness temperature image for first five days (Aug 31st - Sept 4th, 2011) combining all ascending passes. The colorbar is in Kelvin. 88

Figure 4.11 MWR 23.8 GHz H-pol bias histograms for all horns before (v2.0) and after (v2.2) final slope/offset correction. 90

Figure 4.12 MWR 36.5 GHz H-pol bias histograms for all horns before (v2.0) and after (v2.2) final slope/offset correction. 91

Figure 4.13 MWR 36.5 GHz V-pol bias histograms for all horns before (v2.0) and after (v2.2) final slope/offset correction. 92

Figure 4.14 (a) Comparison between MWR real observations (y-axis) and Simulated MWR based on WindSat (x-axis) observations for K band H-pol Horn#1 using v2.1 algorithm. The colorbar represents positive bias in K. (b) The positive biases <16 K is plotted on global map. Most of these points are located near coast line and islands. . 94

Figure 4.15 36.5 GHz H-pol brightness temperature (T_b) measurements over Australia for consecutive ascending passes showing T_b anomalies over land and ocean. 95

Figure 4.16 Description of MWR data frame containing 240 ms of integrated measurement. 97

Figure 4.17 Image of noise diode deflection ($C_{a+n} - C_a$) counts for 36.5 GHz H-pol, gridded in $0.5^o \times 0.5^o$ boxes over the earth. The colorbar unit is radiometer counts. Due to the non-linearity of the receiver the deflection is lower over high T_b scenes like land, weather etc. 101

Figure 4.18 Image of noise diode deflection ($C_{a+n} - C_a$) counts after non-linearity correction for 36.5 GHz H-pol, gridded in $0.5^o \times 0.5^o$ boxes over the earth. The colorbar unit is radiometer counts. The deflection does not depend on the scene T_b anymore. . . . 102

Figure 4.19 Image of reference load temperature (T_o) for 36.5 GHz H-pol, gridded in $0.5^o \times 0.5^o$ boxes over the earth. The colorbar unit is in K. Due to the sun angle variation in orbit T_o is warmer in the northern hemisphere compared to southern hemisphere. The instrument gain is supposed to follow the reverse trend which is observed in the deflection of Fig. 4.18. 103

Figure 4.20 The difference image of Fig. 4.18 and Fig. 4.17 showing the degree of correction in terms of count to correct for non-linearity effect. The correction has a dynamic range of 40 counts which is equivalent to 2.44 K in terms of brightness temperature. 104

Figure 4.21 Variation of the physical temperature (in K) of the internal reference load for 23.8 GHz (K band) receiver during a one month period in February, 2012. The periodic drop in temperature approximately every 1.5 days is due to the resetting of MWR's thermal control caused by planned PAD reboot. The overall decreasing trend in the mean orbit temperature is due to the Sun-angle change in the given period. 110

Figure 4.22 Variation of the physical temperature (in K) of the internal reference load for 23.8 GHz (K band) receiver on Valentine's Day, 2012. The PAD was reset at $\sim$ 10

hrs GMT and it was back on $\sim$ 50 minutes after. It took approximately 7 hrs for the temperature transient to come back to the normal range. 111

LIST OF TABLES

Figure 3.1 Injected Noise Diode T_b values for MWR receivers 39

Figure 4.1 MWR and WindSat Similarities 61

Figure 4.2 K band (23.8 GHz) LSB identifier and corresponding feed horn # 98

Figure 4.3 Ka band (36.5 GHz) LSB identifier and corresponding feed horn # . . . 98

CHAPTER 1
INTRODUCTION

"The cycling of water and energy through the atmosphere and oceans is crucial to life on Earth. Yet the ties among the water cycle, ocean circulation, and climate are poorly understood. Interestingly, global measurement of Sea Surface Salinity (SSS) over time provides a clear way to resolve these relationships. By tracking SSS we can directly monitor variations in the water cycle: land runoff , sea ice freezing and melting, evaporation and precipitation over the oceans. Global SSS data will allow us to create unprecedented computer models that bridge ocean-atmosphere-land-ice systems, with the goal of predicting future climate conditions." [3]

Existing SSS data is much too sparse in space and time to study the climatic interaction between ocean and atmosphere. The current global knowledge of SSS from ships and buoys is shown in the left panel of Fig. 1.1 [4]. This data is acquired over 125 years and is limited mostly to summertime observations in shipping lanes. The Aquarius mission is designed to provide complete global observations of SSS once every 7 days from a satellite orbiting the earth 657 kilometers above the surface. It will deliver a monthly global map of SSS with 150 km spatial resolution and 0.2 (PSS-78, practical Salinity Scale 1978) accuracy [1]. Top right panel of Fig. 1.1 is a simulated example of Aquarius SSS data obtained over 7 days. The perspicuous advantage of the mission is evident in the lack of observations in existing historic SSS data shown in the bottom right panel.[5]

[1] Achieve SSS accuracy of 0.2 psu: this is about a "pinch" (i.e., 1/8th of a teaspoon) of salt in 1 gallon of water

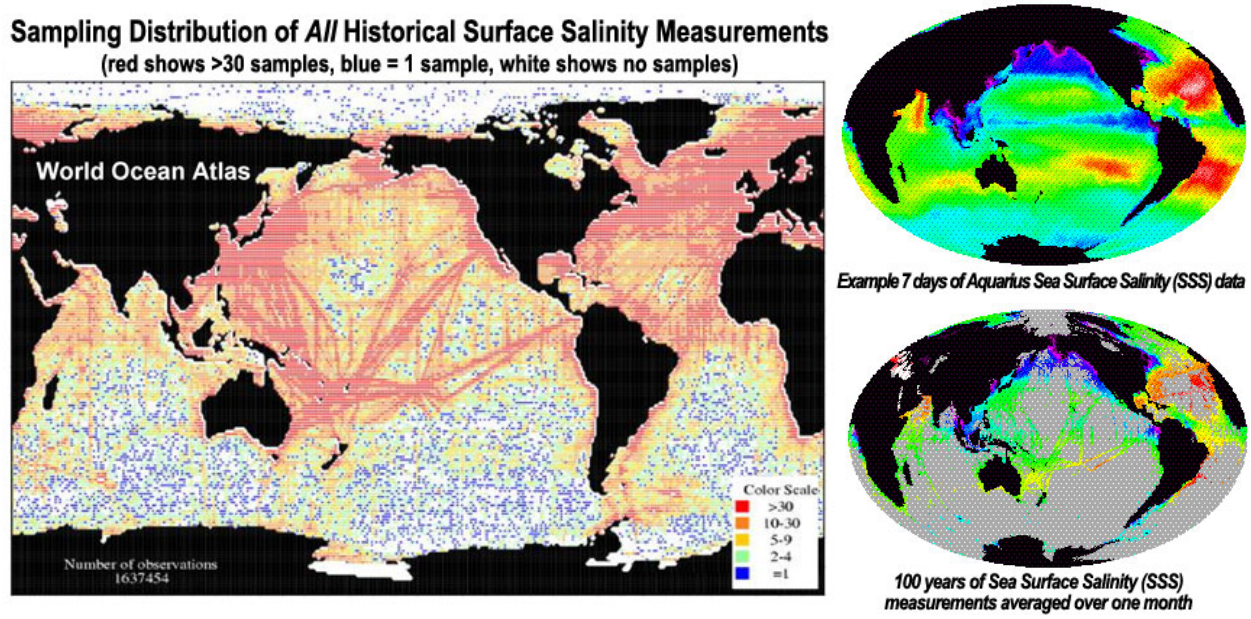

Figure 1.1: Historical SSS Measurements compared with Aquarius measurements.

The remote-sensing of SSS is achieved by measuring microwave radiation (in terms of brightness temperature, T_b) emitted by salty ocean. The variation of salinity, changes the dielectric properties of sea water which in turn modulates the low frequency (L-band) microwave emission from the ocean surface. The heart of the Aquarius instrument is a radiometer which measures L-band (1.413 GHz) T_b. There are several error sources which makes accurate SSS measurement very challenging from space. From the pre-launch error analysis using simulated data it is discovered that the largest single error source is roughness effects due to wind and waves [6]. Also the presence of rain and sea-ice contributes a significant amount of measurement uncertainty. The L-band frequency used by Aquarius radiometer is not suitable for measuring above mentioned geo-physical error sources. To this

end another payload of the SAC-D satellite, the Microwave Radiometer (MWR) developed by CONAE becomes invaluable. The MWR will make T_b measurements in K(23.8 GHz) and Ku(36.5 GHz) band frequencies in an overlapping swath pattern with Aquarius. From these measurements rain, wind and sea ice could be measured. The MWR data will be used by Aquarius data processor for flagging rain and sea ice, and also for a rain and wind-speed correction algorithm.

This dissertation discusses the process of converting raw instrument measurements (counts) to an antenna main-beam T_b measurement for the CONAE MWR. The overall radiometric calibration process spans over pre- and post-launch periods. The pre-launch radiometric calibration algorithm development involved analysis of data from instrument's calibration tests and thermal vacuum chamber (TVAC) test. During the post-launch commissioning phase of the instrument an antenna pattern correction algorithm is developed by comparing near simultaneous collocated T_b measurements by the WindSat radiometer onboard Coriolis satellite. It has been shown that the calibration algorithm is capable of eliminating instrument self-emission and the antenna pattern effects, and the measured T_b is able to produce preliminary geo-physical retrievals.

CHAPTER 2
AQUARIUS/SAC-D MISSSION AND SAC-D MWR

This chapter provides a brief overview of the Aquarius project and points out the implications of MWR. Keeping in mind that MWR is an auxiliary instrument for the Aquarius mission and recognizing that its design is greatly influenced by the Aquarius instrument, the measurement geometry for both the instruments are presented together. Finally the MWR hardware is described in brief along with some information on instrument's along and cross-track resolution.

2.1 Aquarius Mission

The Aquarius/SAC-D Mission (AQ) is a cooperative international scientific mission developed between the National Aeronautics and Space Administration (NASA) of United States of America (USA) and the Comision Nacional de Actividades Espaciales (CONAE) of Argentina, which includes instrument contributions from Italian Space Agency (Agenzia paziale Italiana, ASI), French Space Agency (Centre National d'Etudes Spatiales, CNES), and the Canadian Space Agency (CSA)[7]. The satellite bus (SAC-D service platform) was provided by CONAE and NASA provided the launch. SAC-D spacecraft was launched (using a Boeing Delta-II vehicle) on June 10th, 2011 from the Western Test Range (WTR) at Vandenberg Air Force Base (VAFB), California. The Aquarius Mission focuses on understanding the interactions between global water cycle, ocean circulation and climate through

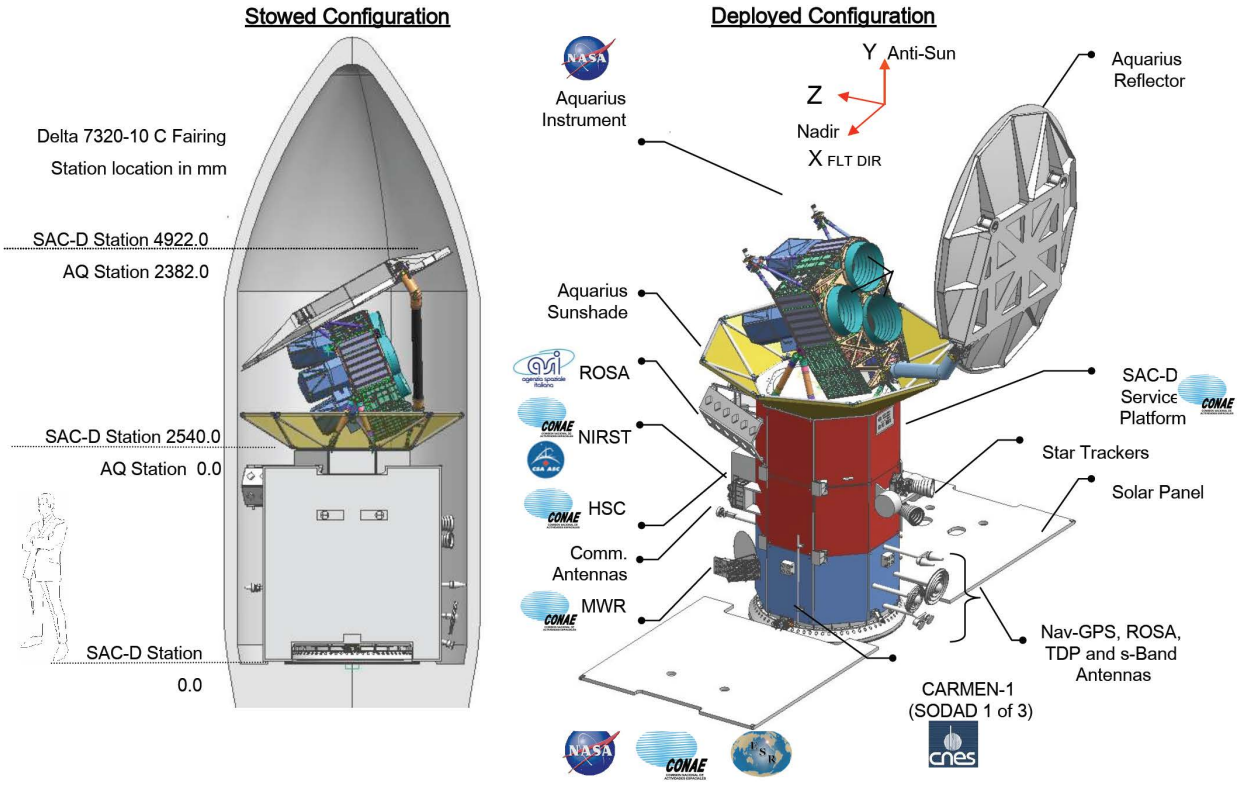

Figure 2.1: Aquarius mission instruments on SAC-D spacecraft

the measurement of Sea Surface Salinity (SSS). Fig. 2.1 shows the SAC-D space-craft in stowed and deployed configuration. The left hand side of the Fig. 2.1 is a cartoon depicting the stowed SAC-D in side Delta II rocket flaring at launch. Sketch of a human body is provided by the side to give an estimate of the size of the observatory. The right hand side of this figure is showing fully deployed Aquarius antenna reflector and SAC-D solar panels during mission mode. The X,Y,Z axes triads are pointing to the flight direction, anti-sun direction and the nadir direction respectively. All the science instruments are pointed out on the spacecraft along with their corresponding agency logos.

The prime instrument of the mission, a L-band radiometer/scatterometer known as Aquarius (built jointly by NASA's Goddard Space Flight Center and Jet Propulsion Laboratory), provides global measurements of salt concentration (salinity) at the ocean surface. The Aquarius instrument comprises a passive microwave radiometer operating in the protected "radio astronomy" frequency band at 1.413 GHz and an active scatterometer in the space-radar frequency band at 1.26 GHz [7]. The measurement of L-band T_b by the Aquarius radiometer is the primary means for remote sensing SSS, and the ocean backscatter measurements from the scatterometer provides a critical roughness correction for the passive SSS retrievals. In addition, the Microwave Radiometer (MWR, provided by CONAE), operating at K(23.8 GHz)/Ka(36.5 GHz) bands, measures the surface T_b in the frequency range sensitive to geophysical parameters over the ocean such as surface wind speed, rain rate, water vapor, cloud liquid water, and sea ice. These geophysical products are useful to the Aquarius microwave radiometer for key T_b corrections required to derive accurate sea surface salinity estimates.

2.2 MWR Sensor Geometry

The Aquarius instrument consists of three L-band horn antennas sharing a common parabolic reflector. The secondary (reflected) antenna pattern of these three horns produce three elliptical foot-prints (yellow) on the ground in a cross-track direction (away from the Sun) with respect to the flight direction as shown in the 3D cartoon in Fig. 2.2(a). With the

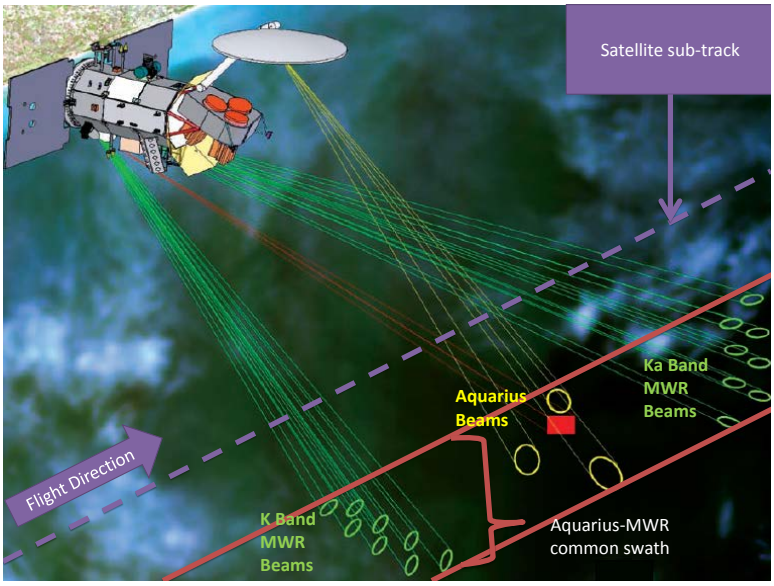

(a)

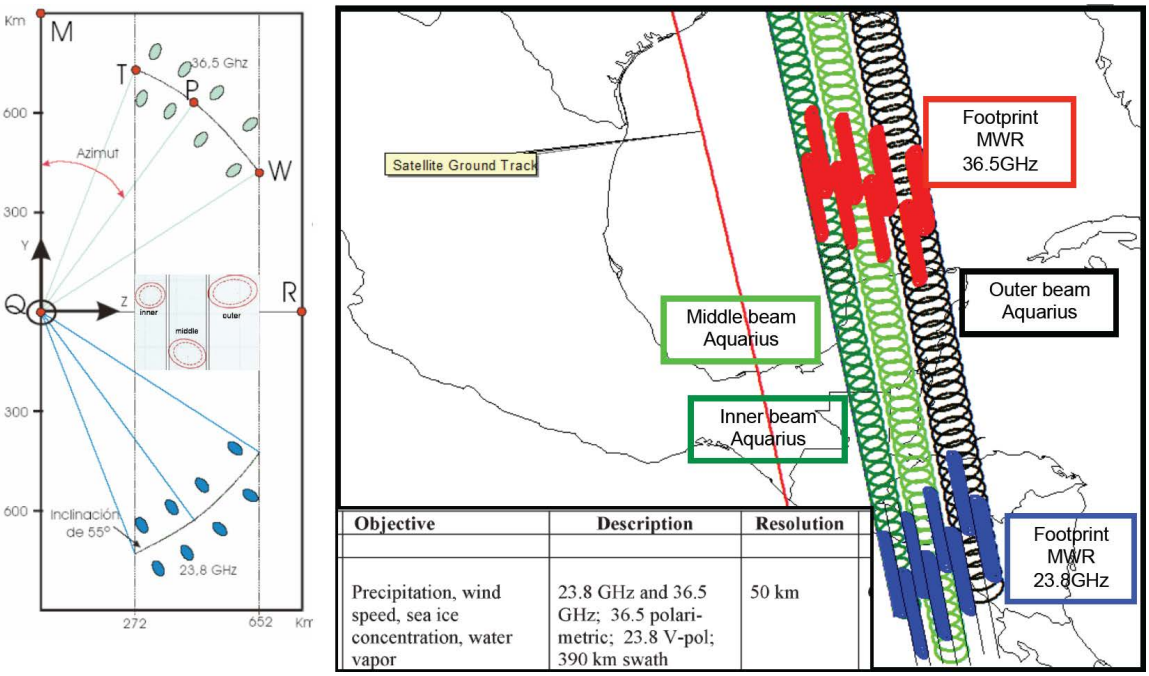

Objective	Description	Resolution
Precipitation, wind speed, sea ice concentration, water vapor	23.8 GHz and 36.5 GHz; 36.5 polarimetric; 23.8 V-pol; 390 km swath	50 km

(b)

Figure 2.2: MWR sensor geometry.

motion of the satellite these three beams produces a continuous swath along track on the anti-sun side of the orbit, which is shown in the right hand panel of Fig. 2.2(b). The two swath edges are marked by two red-lines in Fig. 2.2(a). The choice of one-sided (anti-sun side) swath is to avoid reflected solar intrusion off the ocean surface in the Aquarius main beams. Being in a sun-synchronous orbit the Sun never crosses the orbit plane thus Aquarius is always protected from main-beam solar intrusion with this particular swath geometry.

The CONAE MWR is designed to make measurements in Aquarius swath with a higher spatial resolution than Aquarius. Several trade-offs between meeting the science requirements and practical mission constraints produced the final design of the instrument. MWR consists of two radiometer instruments operating at K and Ka band looking aft and forward respectively with respect to the flight direction. Each radiometer is connected to a set of eight feed-horns arranged in two rows of four feeds which illuminate a parabolic torus reflector as shown in Fig. 2.3. The reflectors are scaled to match the 3dB beam width of the secondary antenna pattern at both the frequencies.The common 3db beam-width is 1.64°, which results in Instantaneous Field of View (IFOV) with resolution of 50 Km on ground. Each row of feed-horn produces IFOV's lying on a conical arc on the ground. The left-hand side panel of Fig. 2.2(b) depicts the conical geometry of MWR beams. The IFOV's within a conical arc, closer to the sub-satellite point along the radial direction, are at 52° incidence angle and those within the conical arc farther from the sub-satellite point are at 58° incidence angle. The right hand side panel of Fig. 2.2(b) shows the time progression of MWR IFOVs. The forward IFOVs at 36.5 GHz are marked in red and the aft IFOVs at

23.8 GHz are marked blue. It should be noted that there is a time lag between the forward and aft beams in sampling the same point on the Earth. This sensor geometry produces a swath width of 380 Km, displaced 272 Km across-track (towards the right), which exactly overlaps with the Aquarius instrument swath.

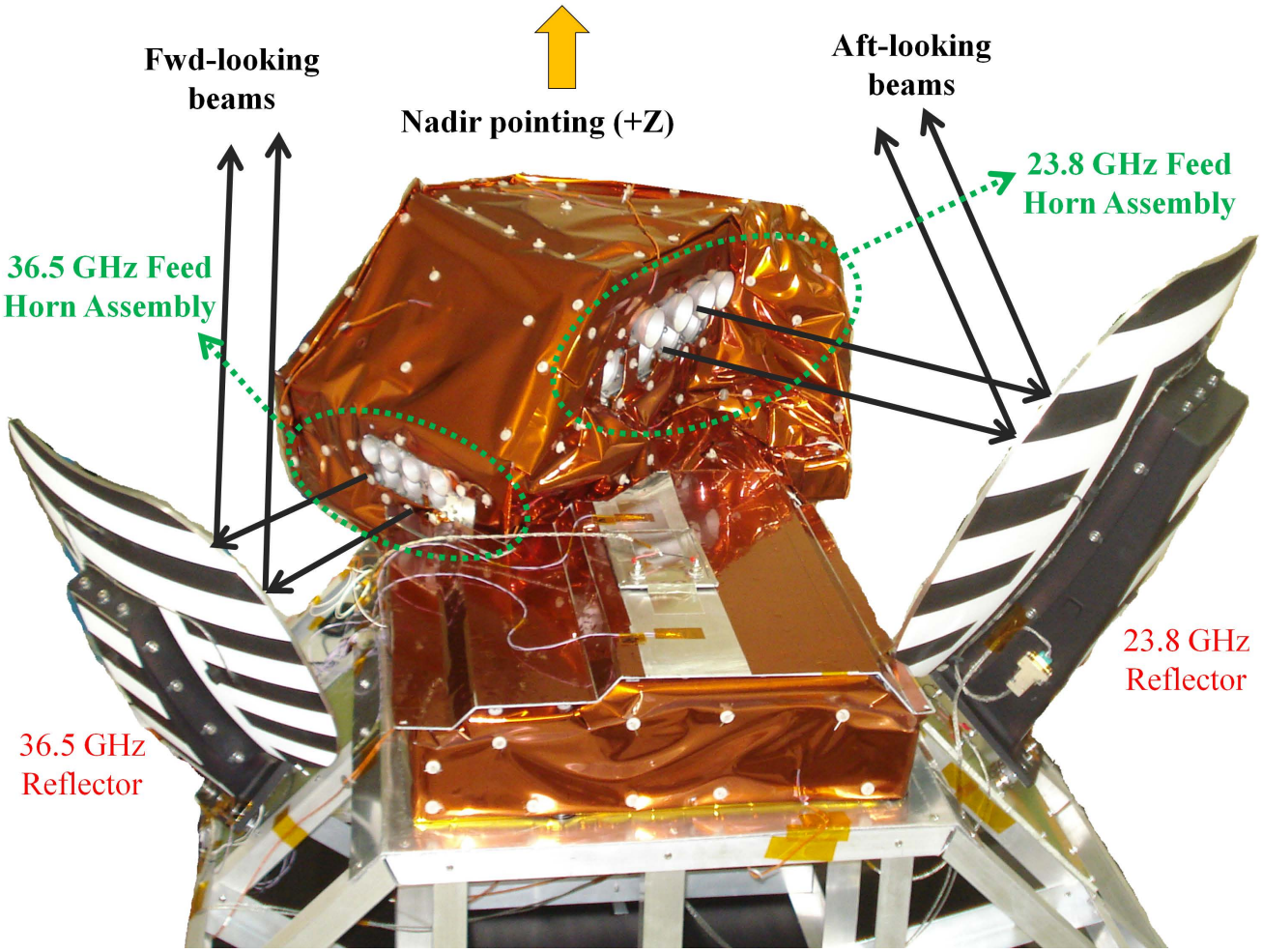

Figure 2.3: MWR instrument configuration.

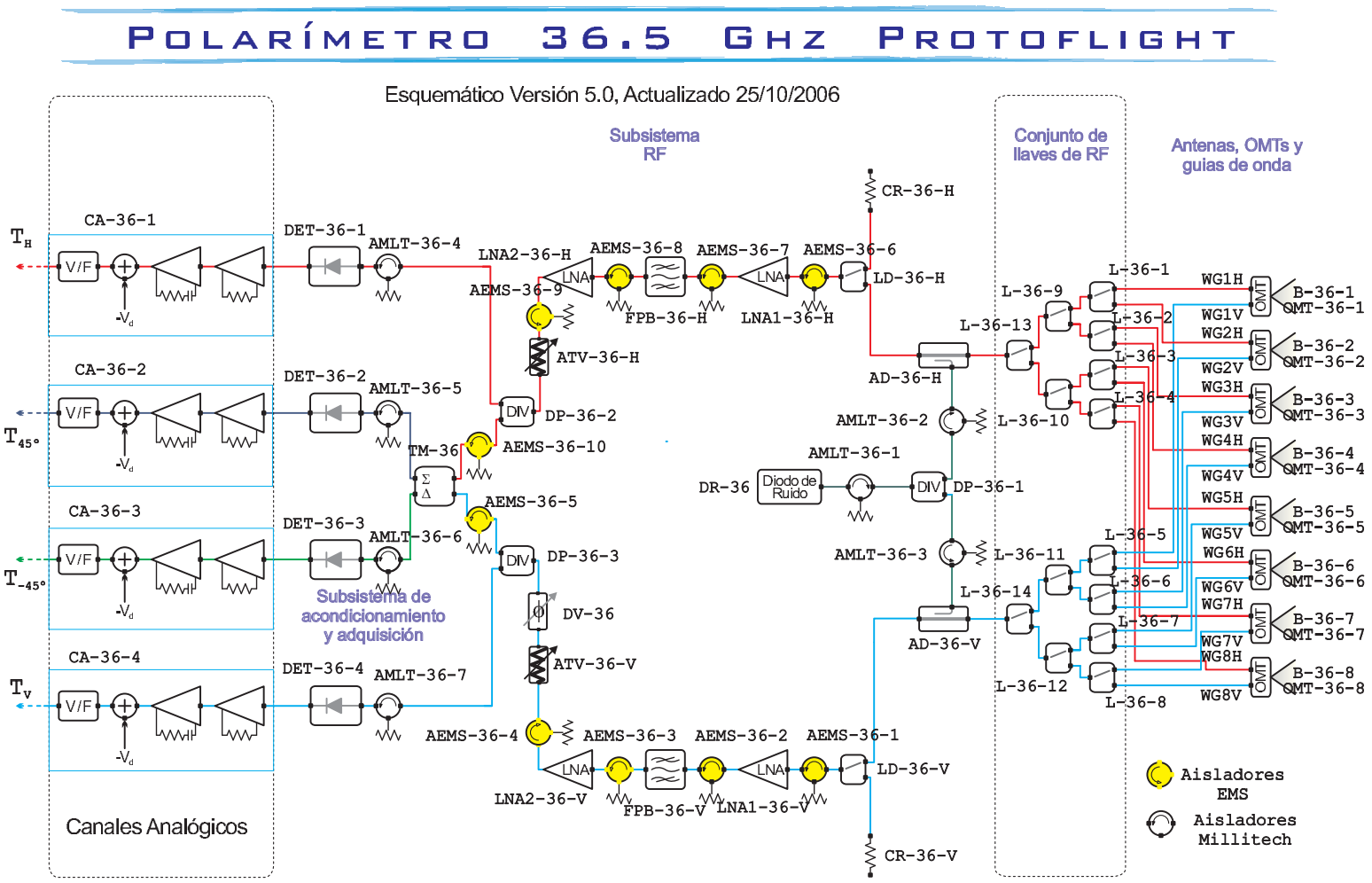

Figure 2.4: Schematic of the Ka band radiometer in the MWR system [1].

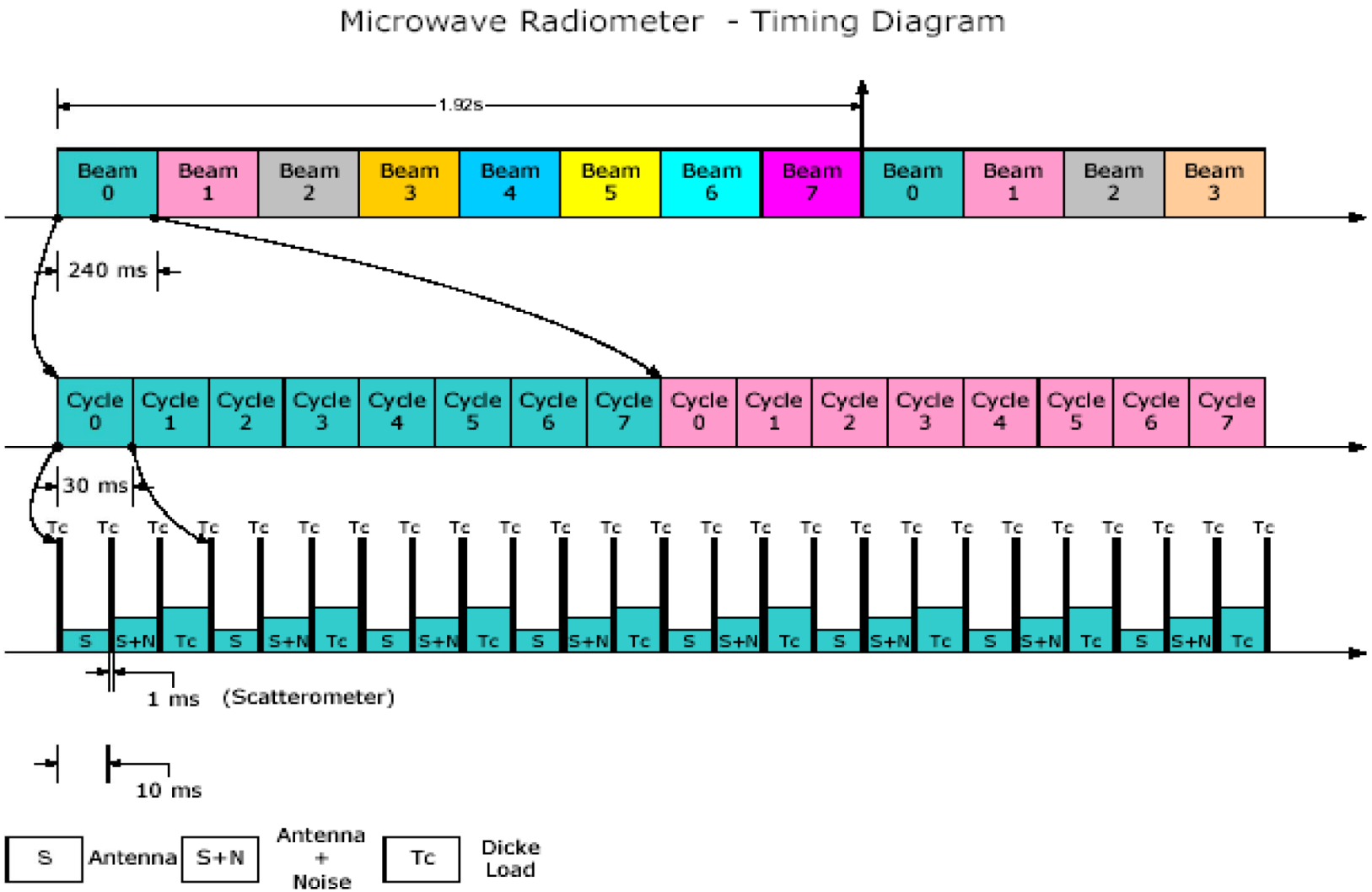

Figure 2.5: MWR Timing Diagram [1].

2.3 MWR Hardware

The MWR instrument measures four polarization states of the electromagnetic radiation at Ka band. The horizontal(H) and vertical(V) polarization component of the signal from a Ka band horn antenna is separated using an ortho-mode transducer (OMT). After the OMT these two signal components are guided through two separate wave-guide paths and received by two separate radiometer receivers. Fig. 2.4 shows the schematic of the Ka band receiver. The $+45°$ & $-45°$ polarized channels are synthesized by cross-correlating the V and H pol electric field signals using a hybrid coupler. Four separate detectors are used to detect all four polarimetric channels. These measurements enable MWR to produce first three of the Stoke's parameters at Ka band. Stoke's parameters are very useful in finding ocean surface wind direction and thus to correct for wind-direction induced wind-speed estimation error. For K band measurements there is only one radiometer receiver and one detector which only measure the H pol component of the antenna signal. The K band channel is mainly used to estimate the water vapor content of the atmosphere.

The whole MWR system consists of three Dicke type radiometers (one K- and two Ka-band channels), which calibrate themselves against gain fluctuations and thermal noise variations, by taking measurements of antenna temperature, noise (controlled) injected antenna temperature and a known reference temperature. For each of the radiometer three layers of switches are added at the front-end just after the OMTs to connect the eight feed horns on a time-shared basis. The eight MWR beams of a given polarization are input to a single radiometer receiver. These beams are sampled sequentially with an integration time

of 0.24 s as shown in Fig. 2.5. The beam number indicates the feed horn at any time. The 0.24s integration period is subdivided into eight subintervals of 30 ms duration and comprises an antenna measurement (S), an antenna plus noise measurement (S+N), and the reference load measurement (Tc). Thus 10 ms is allocated for taking each temperature measurement. During the last 1 ms of each of these 10 ms interval the Dicke switch connects the receiver to the reference load to protect MWR from potential Radio Frequency Interference (RFI) produced by the Aquarius scatterometer transmit pulses. The 0.24 s integration time of each beam results in a beam sampling time of 1.92 s (i.e., each beam is sampled once each 1.92 s). At an altitude of 657 Km, the SAC-D satellite travels with a velocity (Vs/c) of 7.53 Km/s, which corresponds to a ground velocity (Vg) of 6.82 Km/s. At this ground velocity, in 1.92 s beam sampling time, the beams travel an along-track distance of 13.1 Km [2]. Thus MWR footprints have 70% overlap in consecutive along-track sampling (considering a 50 km footprint size). However in the cross-track direction there is no overlap and the cross-track resolution is limited by the footprint size.

CHAPTER 3
MWR CALIBRATION : PRE-LAUNCH

A microwave radiometer is a very sensitive instrument used to measure the radiant power of blackbody electromagnetic radiation in terms of brightness temperatures (T_b), in the microwave region of the spectrum. In general, a microwave radiometer has two parts; an antenna and a receiver(as shown in Fig. 3.1). The antenna collects the energy radiated by the scene under observation and delivers it to the receiver. In modern radiometers the receiver output is typically a digital number, called "count", which is proportional to the received signal power. Thus the calibration goal for a microwave radiometer is to establish a relation between the instruments counts and the brightness temperature incident at the antenna aperture. For earth remote-sensing scenario, the received noise signal is very weak and typically below the noise floor of the receiver. This calls for high precision in the received power measurements. The total power at the output of the radiometer receiver is the sum of several sources. Some components are external in origin and others come from the radiometer itself. If the unwanted components are not properly accounted for, errors in T_b calibration result. Therefore, the characteristics of the radiometer must be well

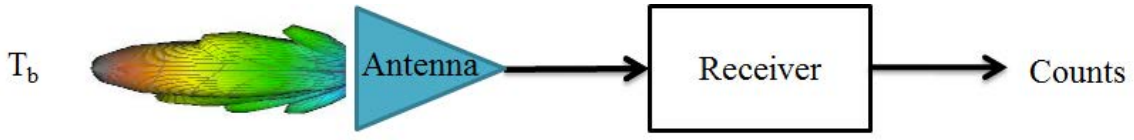

Figure 3.1: Microwave radiometer

understood. The antenna performance needs to be known; the receiver gain and equivalent noise temperature must be characterized, etc. All of these can be done by careful and complete radiometer calibration.

The complete end to end calibration of CONAE MWR can be temporally divided into pre- and post-launch time periods. In this chapter only the pre-launch calibration activities are discussed. The first section discusses the internal calibration of the MWR receivers and points out the need for an external calibration based on the laboratory test. Laboratory tests to calibrate MWR receiver using external hot and cold loads are discussed in the second section. The last section documents the details of MWR antenna switch matrix calibration.

3.1 Internal Calibration of MWR Receivers

A typical total power radiometer block diagram is shown in Fig. 3.2. Microwave radiation from the object under observation propagating in unbounded medium gets transformed into a guided electromagnetic wave in a transmission line by the antenna and sent to the receiver. A microwave radiometer antenna is typically a broad band structure and receives radiation from a wide frequency band. The signal strength at the receiver input is very weak and typically at or below the noise level of the receiver thermal noise. To make measurements of the signal strength in the desired frequency band, the first stage of the receiver consists of a low-noise amplifier that is followed by a bandpass high gain amplifier. Next, a square law detector is used to extract the power in the amplified signal followed by a low-pass filter

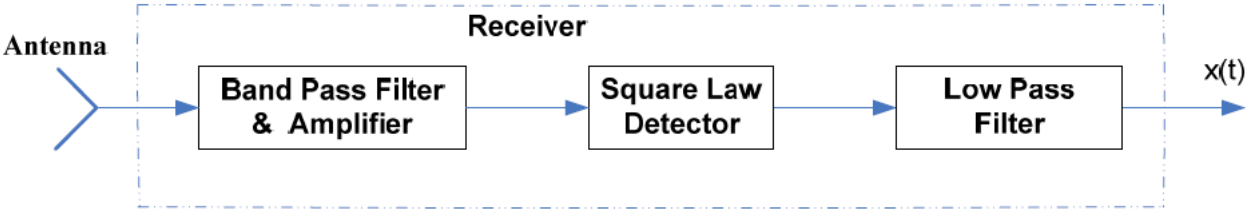

Figure 3.2: Block diagram of a total power radiometer. There are three major components: the band pass filter and amplifier amplifies the received radiation only over the desired bandwidth. The square law detector's output voltage is proportional to the power of the input signal. The final low pass filter acts as an integrator to reduce the noise in the power measurement.

to remove high-frequency fluctuations from the measured power. The DC component of the output from the low-pass filter is proportional to the brightness temperature at the receiver input for the desired microwave bandwidth. The bandwidth of the low-pass filter determines the integration time of the measurement.

There are two fundamental error sources present in a total power radiometer receiver.

1)Finite Integration Time and Bandwidth

A microwave radiometer measurement of brightness temperature (T_b) is an estimate of the variance of a random thermal emission signal derived from samples of the signal. Because the number of samples is always finite, the estimate is itself a random signal. The standard deviation of the estimate is given by the "radiometer uncertainty equation" $\Delta T = KT_{sys}/\sqrt{B\tau}$, where K is an instrument specific constant, T_{sys} is the system noise

temperature of the radiometer, B is its pre-detection bandwidth, and τ is the integration time of the measurement [8]. The "ΔT" of a radiometer measurement is of fundamental importance and often determines the precision with which geophysical parameters of interest can be estimated from measurements of T_b.

2)Receiver Gain Variation

The high gain amplifiers used in radiometer receivers have temperature sensitive components and their stability plays a critical role in a radiometer's performance. For a total power radiometer, the statistical uncertainty ΔT and the gain uncertainty ΔT_G can be considered to be uncorrelated because that they are caused by unrelated physical mechanisms. The total RMS uncertainty is given by [9]

$$\Delta T_{total} = \sqrt{(\Delta T)^2 + (\Delta T_G)^2} = T_{sys}\sqrt{\frac{1}{B\tau} + (\frac{\Delta G}{G})^2} \tag{3.1}$$

where,

G is system power gain & ΔG is the rms value of the receiver gain variation

B is the pre-detection bandwidth of the receiver

τ is the integration time

T_{sys} is the system noise temperature

Let us consider a radiometer with 20 MHz bandwidth (B) having an integration time τ = 0.1 s. If we consider a 1% gain uncertainty then for a receiver with system noise temperature of 370 K the contribution of noise uncertainty in the total RMS uncertainty is 0.26 K whereas the gain uncertainty contributes 3.70 K.

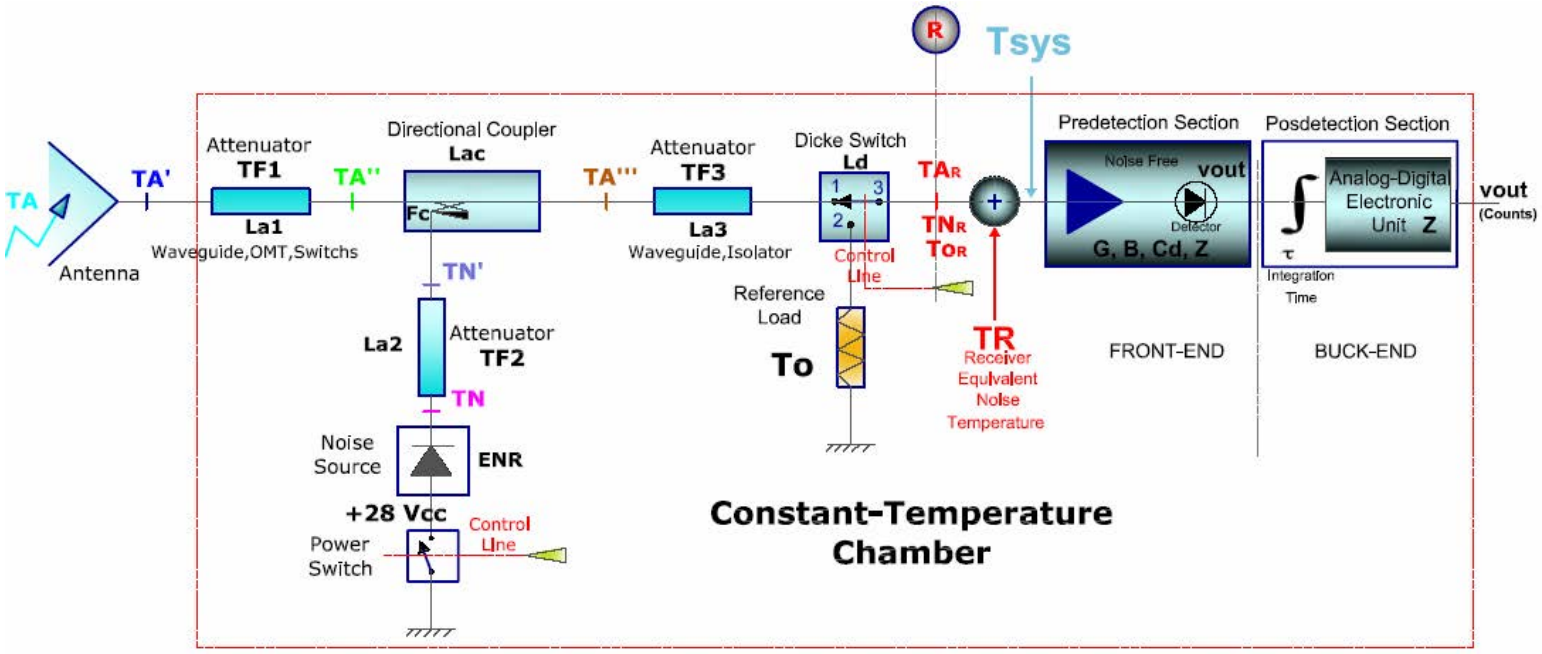

Figure 3.3: MWR receiver block diagram with internal calibration technique. The guided radiation from the antenna is fed into the receiver through a directional coupler. When turned on, the signal from the calibration noise diode is attenuated and coupled to the incoming antenna signal and provides a calibration reference. The Dicke switch constantly switches between the internal reference load (T_o) and the signal from the coupler output to provide another calibration point.

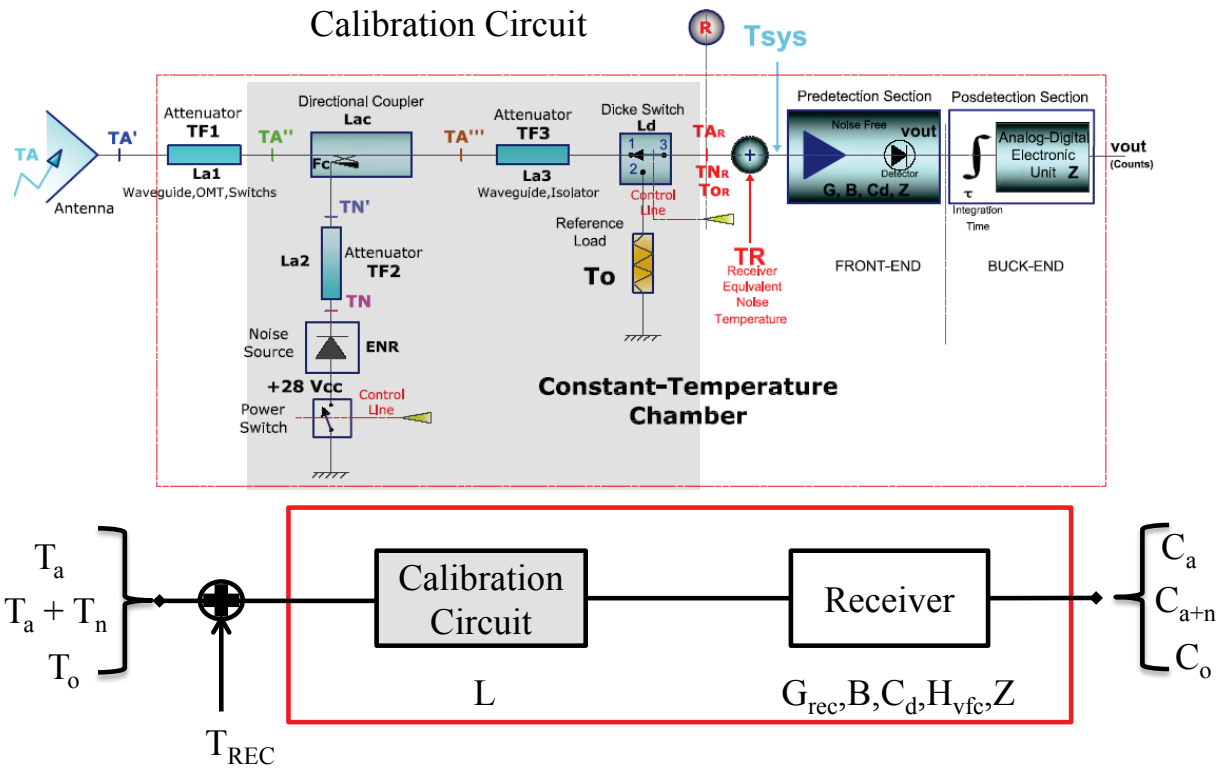

Figure 3.4: Simplified internal calibration model for MWR. The equivalent noise temperature (T_{REC}) of the receiver and calibration circuit is dumped at the coupler input. The transmission coefficient of the calibration circuit is assumed to be L (ratio).The equivalent increase in brightness at the radiometer input due to the calibration noise diode is assumed to be T_n K.

To reduce the effect of receiver gain variation, the receiver is usually housed in a temperature regulated chamber. Even though the gain variation is minimized by controlling the temperature, for accurate radiometric measurements receiver gain variation/drift has to be tracked from one integration period to the other. In MWR receivers this is achieved by using two internal noise sources with different noise levels. One is a matched load whose brightness temperature is its physical temperature, and the other is an active noise diode source of known T_b. A switch (Dicke switch, named after the inventor of this type of calibration scheme) connects the receiver sequentially between two calibration loads and antenna. Fig. 3.3 shows the implementation of this calibration technique in the MWR receiver. Signal from antenna enters the MWR receiver through a microwave directional coupler and arrives at the port 1 of the Dicke switch. A noise diode is turned on and off sequentially to inject a precise amount of brightness (TN') into the antenna brightness temperature through the directional coupler. This noise diode brightness serves as one calibration point. After taking measurements for antenna and antenna + injected noise, the Dickie switch connects the reference load (T_o) (at port 2) to the receiver (at port 3). The reference load is a matched wave-guide termination (no reflection, blackbody) whose physical temperature is the brightness temperature. As the receiver switches between 3 states (ant, ant+noise and reference load) sequentially, it is called a "three state Dicke radiometer".

Let the receiver's equivalent noise temperature be TR and i represents the switching state of the receiver. For example i could be equal to A(antenna look) or N(antenna+noise) or O (reference load). The total system noise temperature detected by the receiver for the

i-th state is given by $T^i_{sys} = (Ti_R + TR)$, where Ti_R is the brightness temperature for the i-th switching state entering the noise free receiver at the reference line R. Hence the total power entering the noise free receiver at the R-line is given by,

$$P_i = kT^i_{sys}B \tag{3.2}$$

where,

k is the Boltzman constant

B is the receiver bandwidth

T^i_{sys} is the system noise temperature for the i-th switching state

The circuit diagram in Fig. 3.3 could be simplified if we consider the equivalent block diagram shown in Fig. 3.4. We can model the MWR radiometer by inserting a calibration block with lumped loss (transmission coefficient L) between the antenna block and the receiver block. The shaded region of the circuit diagram in Fig. 3.4 shows the portion included in the calibration block. Using microwave theory we can represent all the noise generated by the calibration circuit and the receiver with a single noise temperature T_{REC} at the input of the calibration circuit i.e. the direction coupler's antenna input. Then the receiver and calibration circuit can be modeled as a series of noise free components with only transmission coefficients. Thus for an antenna temperature T_a at the coupler input if the radiometer count is C_a then we can write the following forward equation to relate C_a to T_a

$$C_a = k(T_a + T_{REC})BLG_{rec}C_dH_{vfc} + Z \tag{3.3}$$

where,

k is the Boltzman constant

T_{REC} is receiver noise temperature referenced to the coupler input B is the receiver bandwidth

L is the equivalent transmission coefficient of the calibration circuit

G_{rec} is the receiver amplifier gain

C_d is the diode detector constant

H_{vfc} is the transfer function of the voltage to frequency converter including the transfer function of the post detection analog gain stages

Z is the digital and analog offsets of the receiver

Equation 3.3 can be further simplified by,

$$C_a = gain \times T_a + offset \tag{3.4}$$

where, gain $= kBLG_{rec}C_dH_{vfc}$ and offset $= kT_{REC}BLG_{rec}C_dH_{vfc} + Z$

Thus to apply equation 3.4 in MWR we define a calibration reference plane for the receiver. The calibration reference plane separates the antenna and receiver and is defined at the input of the coupler as shown in Fig. 3.5. The top left hand side panel showing a CAD model of the MWR Ka band receiver. The top right panel shows the schematic of the same receiver. The bottom panel is a simplified radiometer block diagram where equation 3.4 is applied for three switching states of the radiometer. The calibration reference plane is marked by a red line in all the diagrams. In the radiometer block-diagram in Fig. 3.5, the antenna temperature T_{ap} after going through the antenna switch matrix becomes T_{in} at the calibration reference plane. With T_{in} being input to the receiver the equations for the three

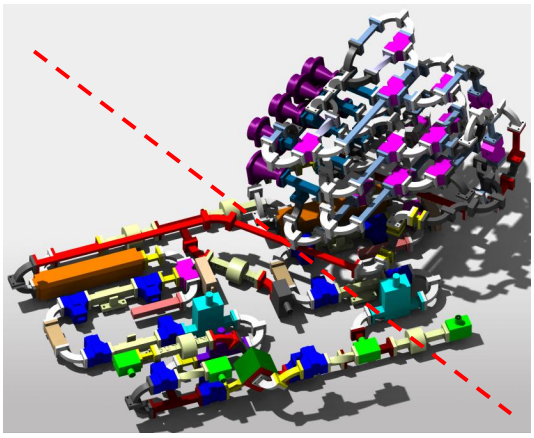

(a)

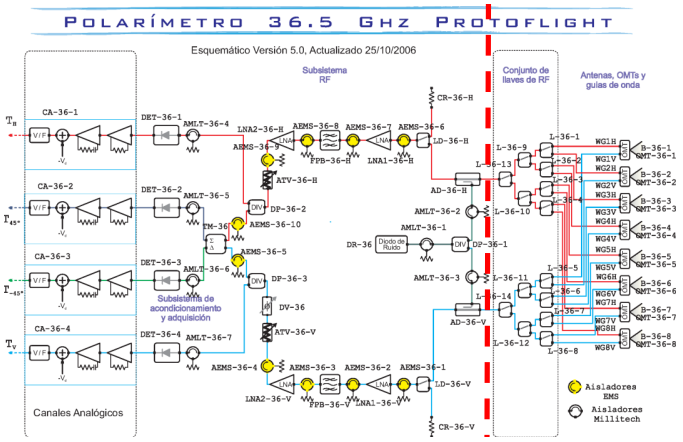

(b)

$C_{in} = GT_{in} + offset$

$C_{in+n} = G(T_{in} + T_n) + offset$

$C_o = GT_o + offset$

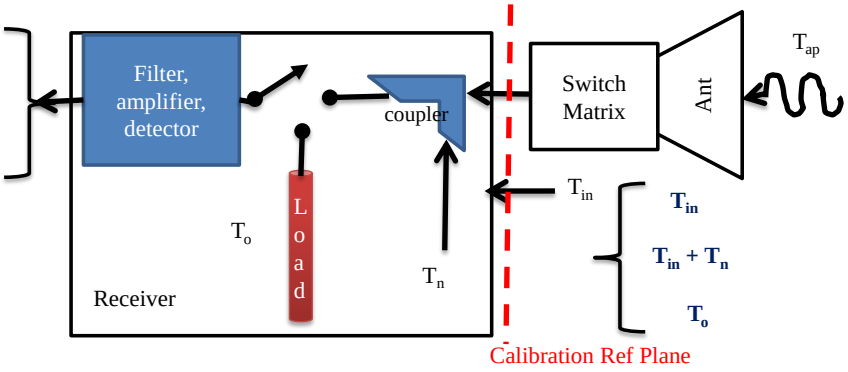

(c)

Figure 3.5: (a) Computer rendering of the Ka band MWR receiver and switch matrix are shown. The red line separates the two. (b) Schematic of the Ka band radiometer with red line separating the switch matrix from the receiver. (c) Simplified Cal-model applied to MWR receiver (Forward radiative transfer equations).

switching states are

$$C_{in} = GT_{in} + O \tag{3.5}$$

$$C_{in+n} = G(T_{in} + T_n) + O \tag{3.6}$$

$$C_o = GT_o + O \tag{3.7}$$

It should be noted here as represented by equation 3.6 that the effect of turning on the noise diode inside the receiver is represented by an addition of brightness level of T_n K at the input of the receiver. Using equation 3.5, 3.6 and 3.7 we can solve for T_{in},

$$T_{in} = \frac{(C_{in} - C_o)}{(C_{in+n} - C_{in})} \times T_n + T_o \tag{3.8}$$

Equation 3.8 enables us to determine T_{in} from the radiometer counts given T_o and T_n are known. T_o is obtained in real time from MWR's internal temperature sensors. T_n is measured in laboratory using external calibration loads before launch and the assumption is it does not during flight.

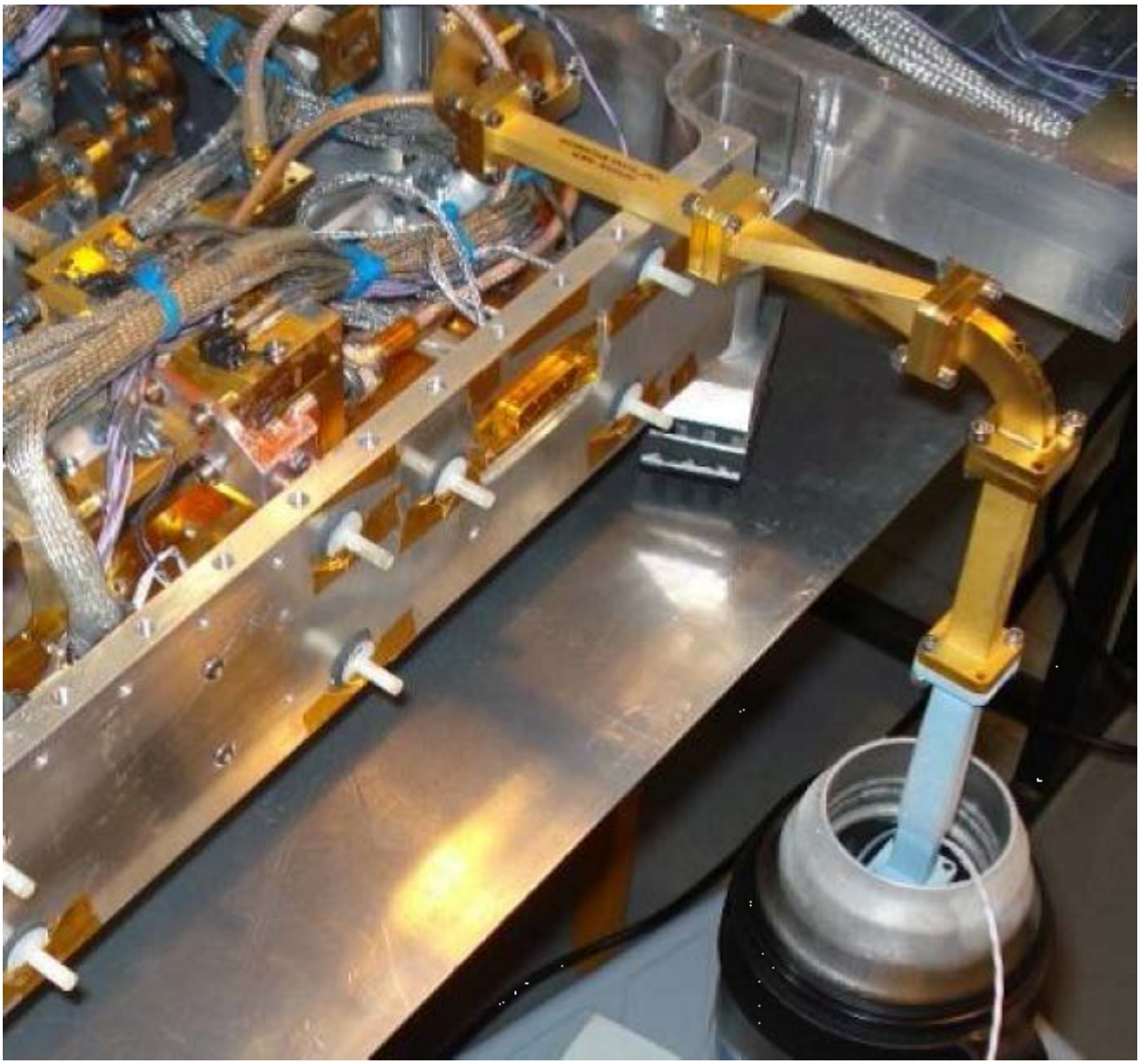

Figure 3.6: Calibration waveguide connected to a MWR receiver during external calibration test. The end of the 'blue' waveguide is terminated in a matched load. A platinum temperature sensor is attached to the termination. The matched termination is heated and cooled to simulate hot and cold calibration reference.

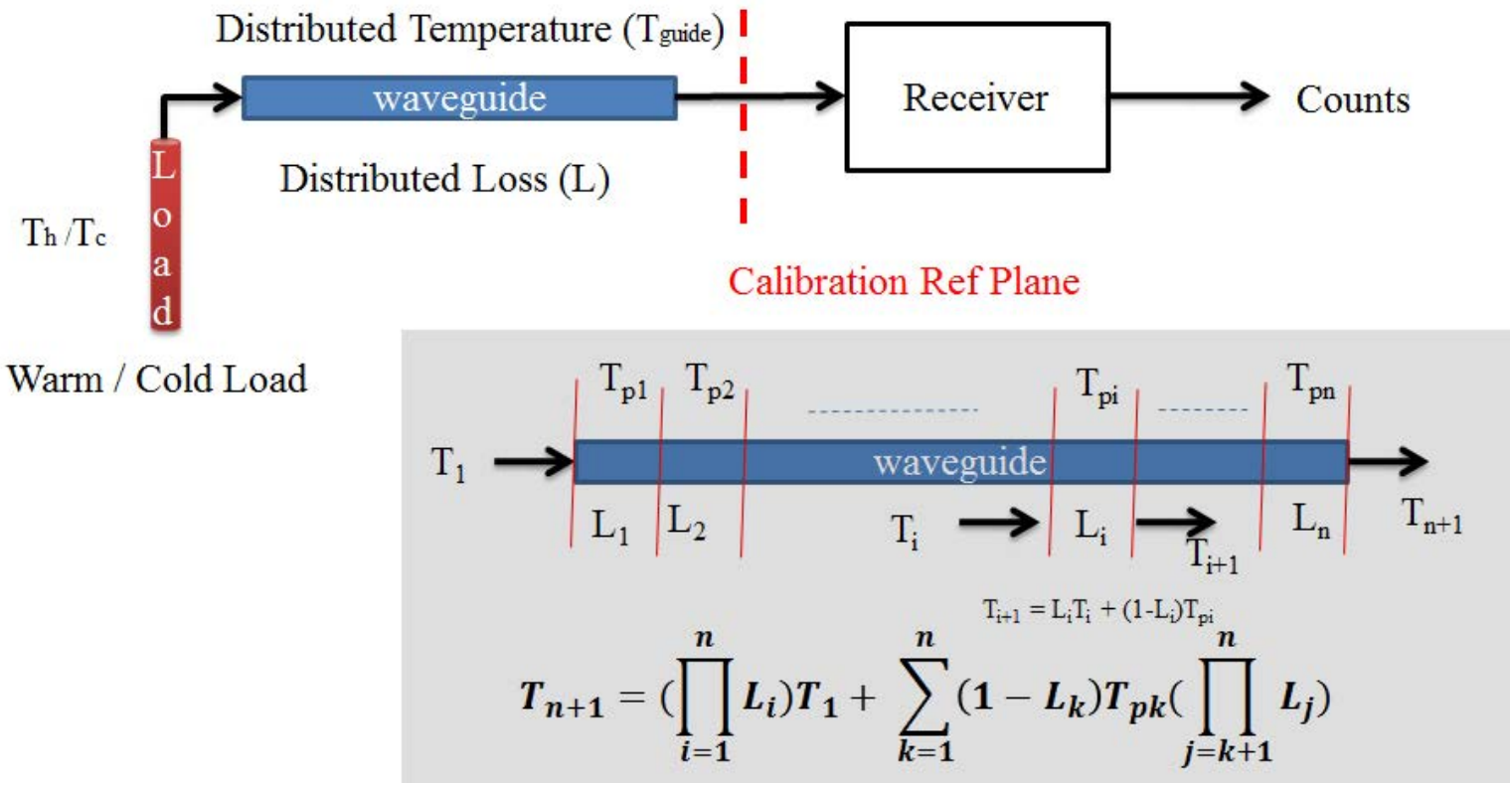

Figure 3.7: Radiative transfer through the calibration waveguide. The waveguide is divided into small sections. The radiative transfer equations are solved using assumed temperature variation along the length of the waveguide.

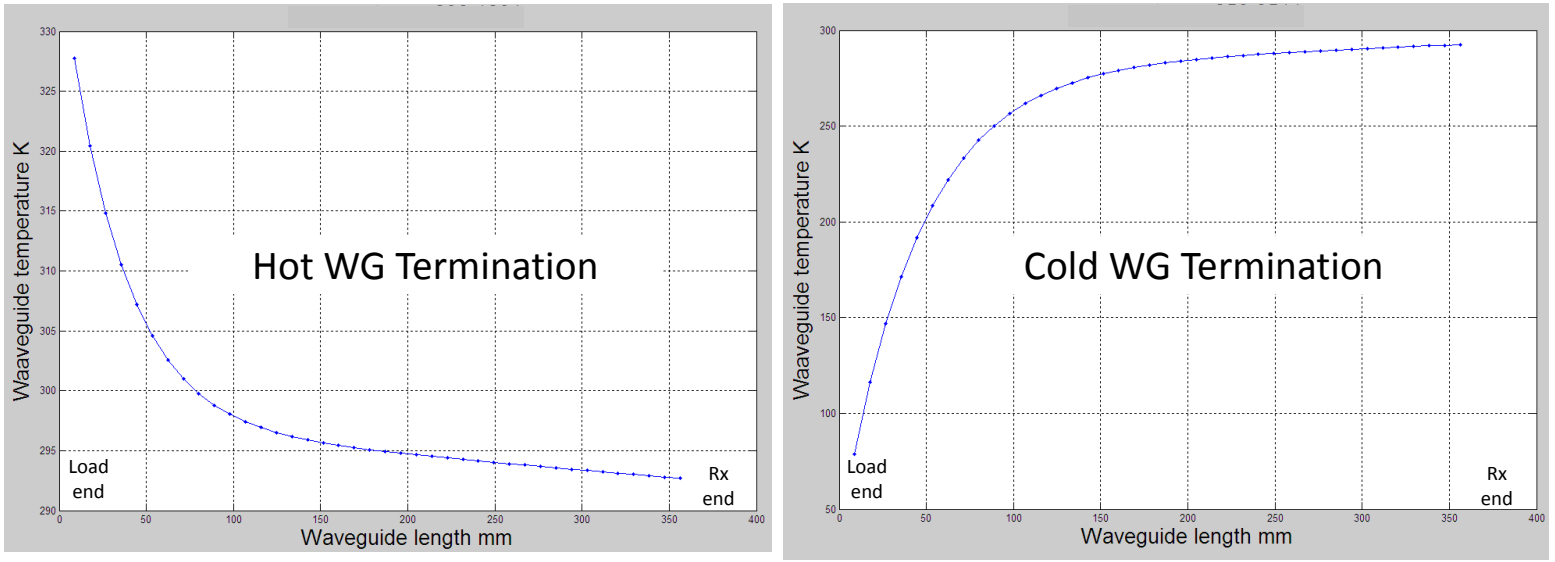

(a) (b)

Figure 3.8: Assumed temperature distribution of the calibration waveguide.(a) Temperature distribution along the length of the waveguide is shown while the warm load was connected. Temperature exponentially decays from load end to the receiver end. (b) Temperature distribution when cold load is connected. Temperature exponentially rises from load end to the receiver end.

3.2 External Calibration of MWR Receivers

The main goal for external calibration is to determine T_n required for the counts-to-T_{in} conversion. For this purpose the receiver and the antenna switch matrices were disconnected at the calibration reference plane. Receiver is then connected to a calibration waveguide terminated in a matched load. As there is no reflection from the matched load termination it acts as a blackbody with unit emissivity. Thus the physical temperature of the termination is equal to the brightness temperature emitted by termination towards the receiver. Thus by heating (warm water) and cooling (liquid nitrogen) the termination external T_b sources are created at two different noise levels. The 'hot' and 'cold' T_b sources cover a wide dynamic range of T_b [77K, 330K] including the range of possible T_b observations from space. The calibration waveguide connected to one of the MWR receiver is shown in Fig. 3.6. The long piece of waveguide has a loss of about -0.18dB and this should be taken into account while computing T_n. The radiometer equations 3.5-3.7 relates brightness temperatures at the calibration reference plane to the output counts. Due to the loss in the waveguide the T_b that arrives at the coupler input is different than the T_b generated by the matched load termination. To accurately determine the input to the radiometer we need to apply radiative transfer theory through the waveguide. Fig. 3.7 shows the block-diagram of the test setup where the receiver calibration reference plane is shown with the red line. The hot/cold load T_b's (T_h/T_c) after passing through the waveguide becomes T_h' and T_c' at the receiver input. Let us divide the length of the waveguide into n different sections with transmission coefficients represented by L_1 to L_n and physical temperatures represented by T_{p1} to T_{pn}

respectively. If the input to the waveguide is T_1 and the output from the nth section be T_{n+1} then it can be derived that,

$$T_{n+1} = (\prod_{i=1}^{n} L_i)T_1 + \sum_{k=1}^{n}(1 - L_k)T_{pk}(\prod_{j=k+1}^{n} L_j) \tag{3.9}$$

During the calibration test only the temperature of the termination was measured. So the waveguide loss and temperature distribution both are unknown. However from the measured length of the waveguide we estimated the loss by assuming standard loss/unit length for silver waveguide (MWR's waveguides are silver coated from inside). Even though the temperature distribution of the waveguide was not measured the temperature at both the ends were known. Matched load termination end was measured by precision temperature sensor and the receiver end was at the receiver internal temperature (which was controlled). Using these two boundary conditions we assumed a 'realistic' exponential temperature distribution along the length of the waveguide as shown in Fig. 3.8. The left and right hand panel of the figure are showing hot and cold waveguide terminations respectively. As you can see for the 'hot' case the temperature at the load/termination end is higher than the receiver internal temperature, so the temperature distribution is exponentially decaying from load end to the receiver end. In the 'cold' case the trend is opposite; the temperature rises exponentially from the cold termination end to the receiver temperature on the other side. For the Ka band H pol receiver the measured temperature of the hot termination was 330.86 K and it was 77.4 K when cooled using liquid nitrogen. Using these two T_b's as input (T_1) to our waveguide radiative transfer equation 3.9 we compute the waveguide output T_b to be 329.5 K and 84.8 K respectively. It should be noted that the loss affects the brightness of cold end

more than the hot end. This is because the average physical temperature of the waveguide loss is closer to the 'hot' T_b. In a microwave network, if the physical temperature of a loss is equal to the input T_b then the loss doesn't affect the output of the network i.e. the loss becomes transparent and the network can be assumed to be lossless with unity transmission coefficient.

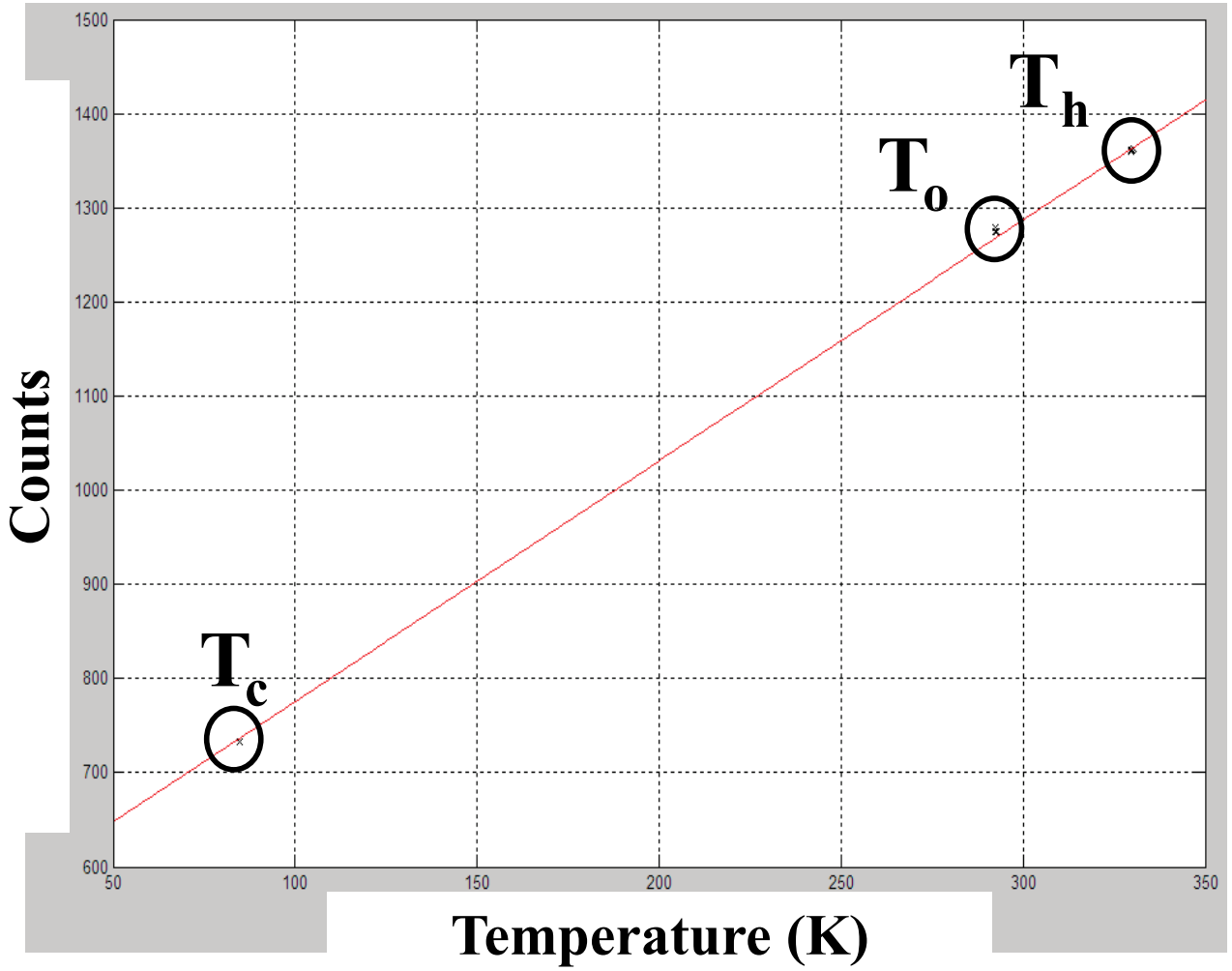

Figure 3.9: Least square linear regression through three calibration points, cold load (T_c), reference load (T_o) and the hot load (T_h). Slope of the line is radiometer gain (G).

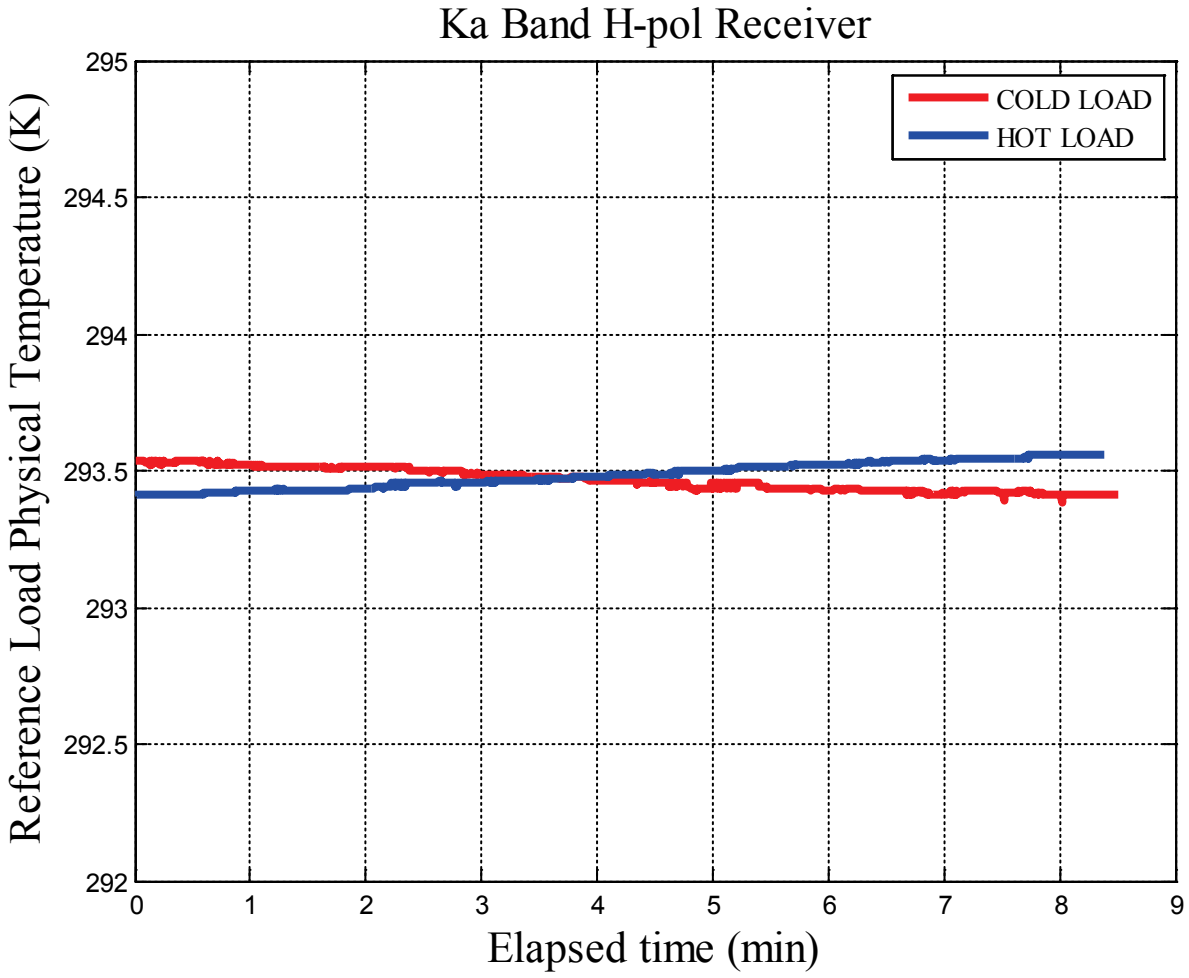

Figure 3.10: Temperature of the internal reference load during HOT and COLD load tests (Ka band H-pol Rx)

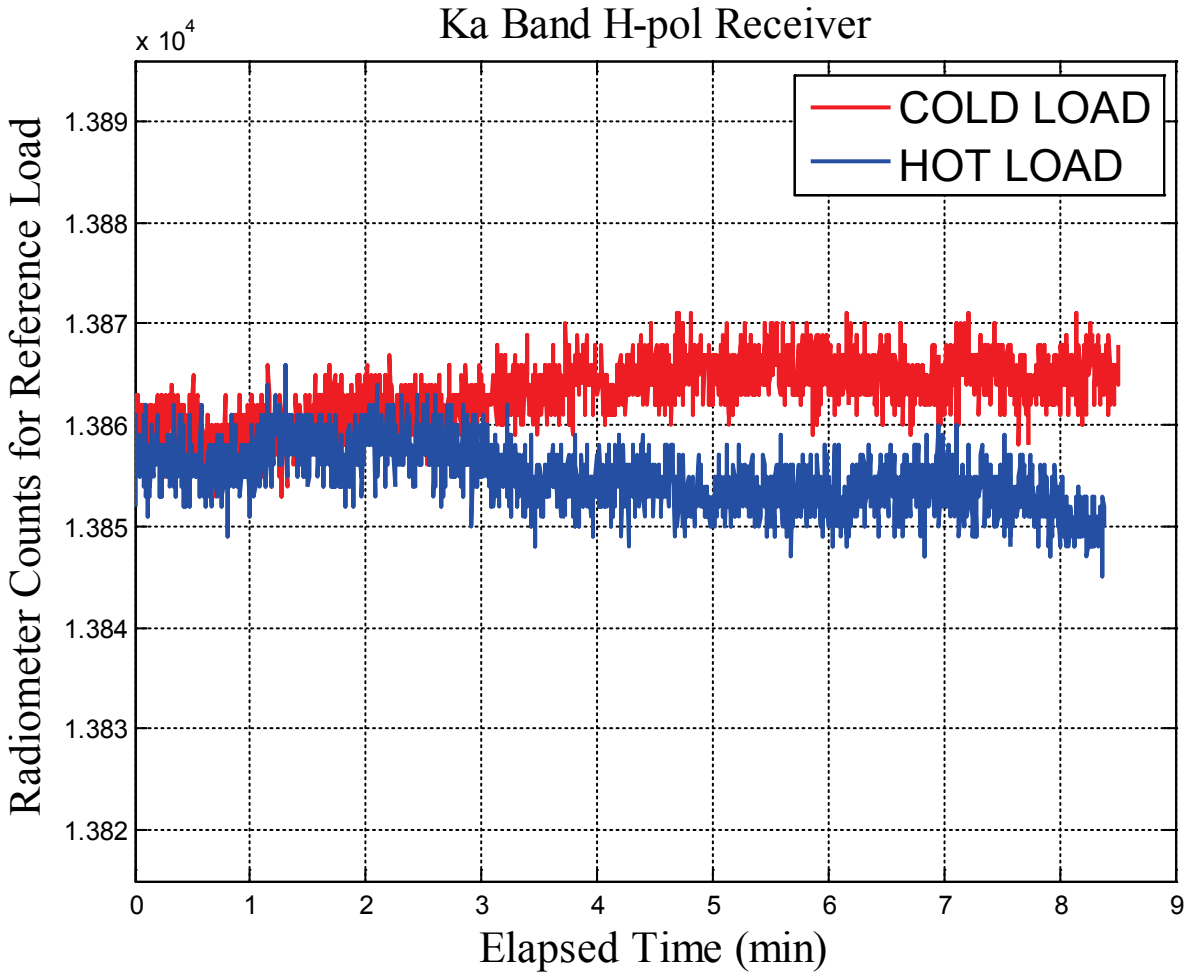

Figure 3.11: Counts for the internal reference during HOT and COLD load tests (Ka Band H-pol Rx)

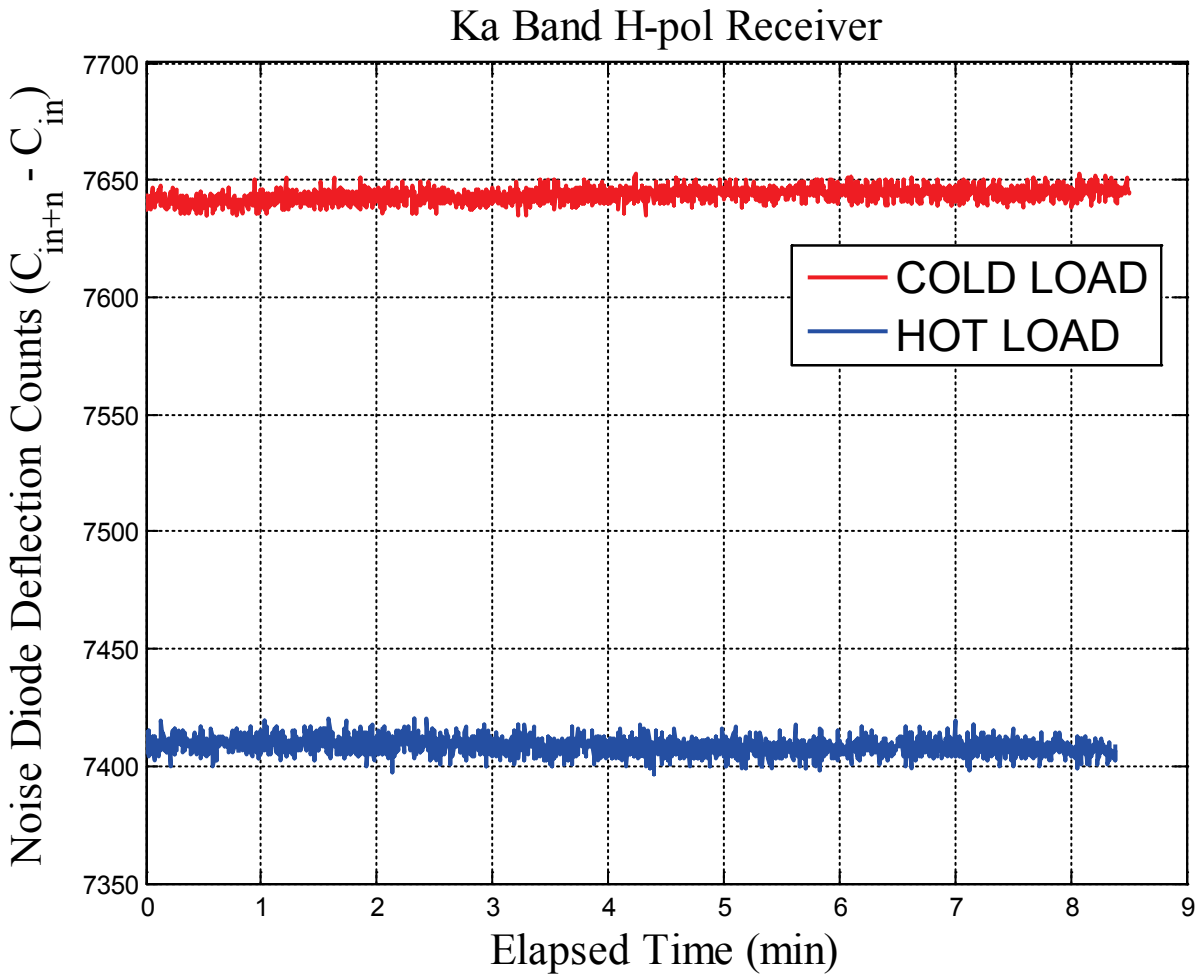

Figure 3.12: Noise diode deflection counts for HOT and COLD load tests. (Ka Band H pol receiver). The deflection is higher for the cold input load compared to the hot input load case.

With T_b values on the x-axis and corresponding measured counts on the y-axis a least-square regression line is fitted using three points for each receiver. The x values corresponding to the points are : 1) computed T_b values for the 'hot' case, 2) computed T_b values for the 'cold' case and 3) measured value of the average T_o. The gain of each receiver is readily obtained by computing the slope of the regression line (Δy/Δx). An example is shown in Fig. 3.9.The assumption in the above calibration procedure is that the receiver gain does not change during the cold and hot measurements. This was achieved by maintaining the radiometer internal temperature at a controlled level. Figure 3.10 shows that the temperature of the internal reference load varied less than 0.2 K (radiometer sensitivity is $\sim$ 0.5 K) during the two tests. Figure 3.11 shows the radiometer output due to the input temperatures of Fig. 3.10. The relationship between the count and input temperature for the receiver is defined by equation 3.4. It is noteworthy that the radiometer counts are decreasing for an increasing input temperature (blue) and vice versa (red). This is caused by the fact that radiometer gain is very sensitive to internal temperature variation and it decreases with increase in temperature and vice versa. It is clear from Fig. 3.11 that the radiometer gain is almost identical for the first 3 minutes of the calibration test data. Therefore, only the first 3 minutes of data is averaged for the calibration test so that we can safely assume that the gain of the radiometer did not change considerably between the hot and cold measurements. To solve for injected noise diode temperature (T_n) we need to subtract equation 3.5 from equation 3.6,

$$(C_{in+n} - C_{in}) = G(T_n) \tag{3.10}$$

Equation 3.10 is known as "noise diode deflection equation" in the radiometer terminology. Pertaining to the receiver calibration test C_in could be either counts due to hot load (C_h) or counts due to cold load (C_c) connected to the receiver input. Thus there are two independent solution of T_n possible given by,

$$(C_{c+n} - C_c) = G(T_n) \tag{3.11}$$

$$(C_{h+n} - C_h) = G(T_n) \tag{3.12}$$

Where, C_{c+n} and C_{h+n} are antenna counts while the internal noise diode was 'on' for cold load and hot load cases respectively. The injected noise diode temperature (T_n) does not depend on the external load T_b, and we already verified that the receiver gain (G) is essentially the same (except for a small drift) for both the calibration load cases. Therefore if we plot and compare left hand side of the equation 3.11 and 3.12 they will show exactly same number of counts, except a small drift similar to the drift in Fig. 3.11. However while plotted in Fig. 3.12 for Ka band H pol receiver, the noise diode counts are 250 counts lower in the HOT case compared to the COLD case. This is a non-ideal result. The small gain difference is not the cause as the gain drift pattern (of Fig. 3.11) is not visible in the Fig. 3.12. For the Ka band H-pol receiver, the antenna + noise count for COLD case is $\sim$ 15500 and for HOT case $\sim$ 22200. If the receiver has a very small non-linearity it will be dominant when the input is high. The nonlinearity may be expansive or compressive. What we are seeing here is (in Fig. 3.12) the deflection count due to noise injection is less in HOT case compared to COLD case. This suggests that the non-linearity is compressive.

In MWR the non-linearity is caused by the following components in the hardware: RF

Amplifiers, Diode detector, Video amplifiers and Voltage to Frequency Converter (VFC). The RF amplifiers are operated well below their 1 dB compression ratio and the video amplifiers being consist of low THD (Total Harmonic Distortion) op-amps the non-linearity contribution of these devices is negligible. The major sources of non-linearity are therefore the diode-detector and the VFC. The square law diode detectors generally contribute 'expansive' non-linearity while operated in the non - square-law region of the diode characteristic. On the other hand the VFC acts compressive. Therefore, Fig. 3.12 demonstrate the domination of VFC non-linearity over the detector non-linearity. The over-all effect is compressive. To correct for the non-linear behavior of the receiver we need to formulate a linearizing model function using receiver internal temperature and output counts (detected power). Unfortunately, no suitable test data are available at this time to characterize the non-linearity accurately. Because of this limitation, we have to assume that the receiver is linear over the dynamic range of ocean observation (100K - 300K). And it only becomes significantly non-linear when a noise diode Tb (> 270 K) is injected with an antenna temperature of $\sim$ 300K (hot load). This assumption could be backed by the fact that a linear least-square line is accurately fitted using the 3 points in Fig. 3.9 with minimum error. With this assumption we can use equation 3.11 to obtain T_n which will calibrate the MWR T_b's over ocean. If the non-linearity is not corrected in future, the MWR will not produce accurate T_b's over land (> 300K). Using cold load deflection the computed noise diode brightness are given in Table 3.1 for the three MWR receivers. The Tn values from Table 3.1 is used in equation 3.8 to determine the brightness temperature at the radiometer input (T_{in}) from the measured

Table 3.1: Injected Noise Diode T_b values for MWR receivers

T_n (K)		
K H-pol	Ka V-pol	Ka H-pol
390	274	270

counts. The only assumption here is the injected noise brightness is stable and does not change during flight.

3.3 Antenna Switch Matrix Calibration

As described in chapter 2, in MWR system a single receiver is time-shared between eight feed-horn antennas by means of a microwave waveguide 1x8 switching network. The total radiation brightness (T_{ap}) captured by any particular antenna feed horn under observation is guided to the receiver through this switching network. The feed-horn and all successive components in the path of the signal from antenna to the receiver have finite losses and corresponding self-emissions, which modifies T_{ap}. Also the reflections at the horn aperture and leakage through the switches modify the input/output relationship of the radiative transfer. Hence, a hardware radiative transfer model for the entire waveguide switch matrix path from antenna aperture to the receiver is discussed. The forward model is inverted to predict T_{ap} from measured brightness at the input of the radiometer receiver (T_{in}).

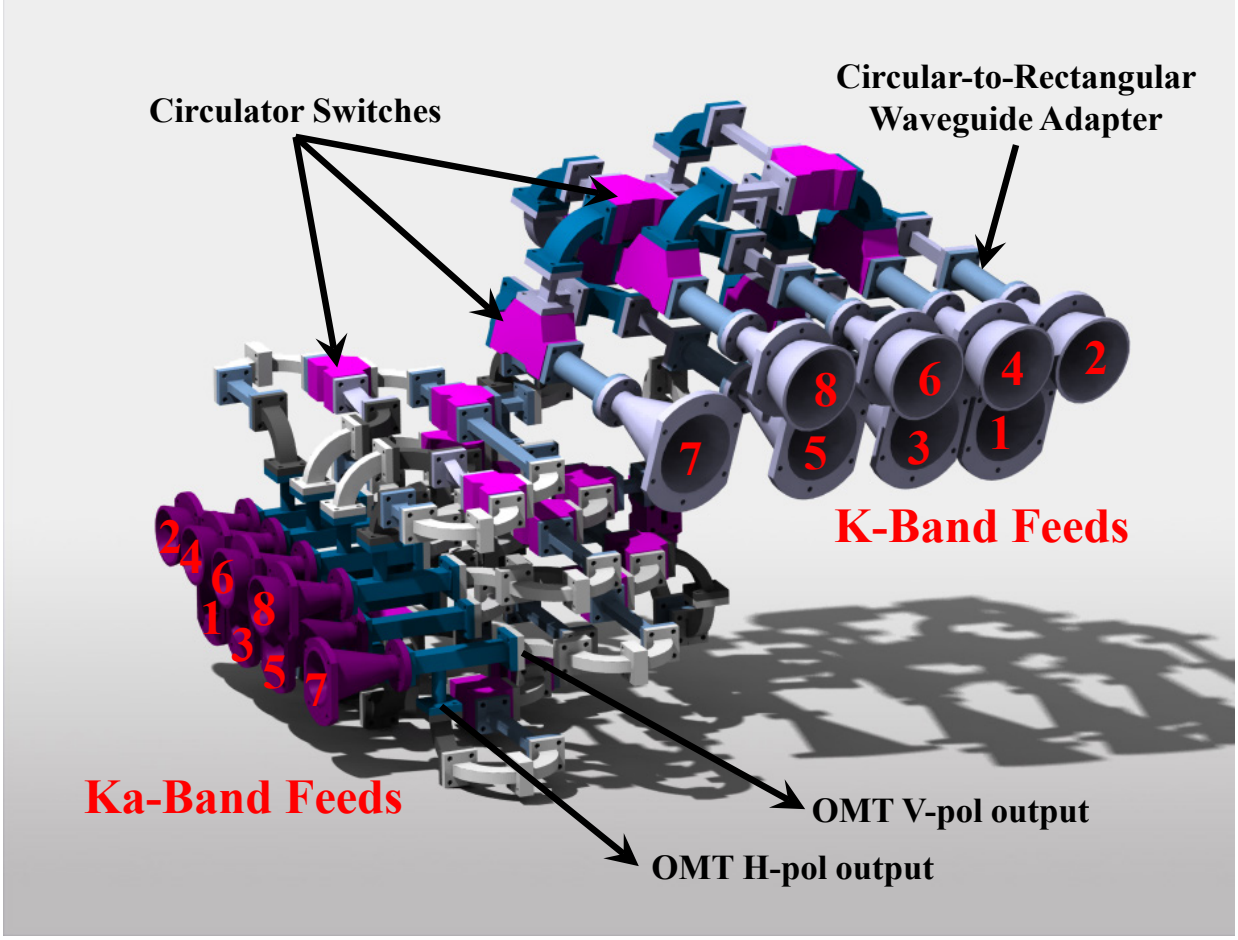

Figure 3.13: MWR K & Ka-band antenna feed-horn and switch-matrix assembly. The receiver and antenna reflectors are not shown here. Ka band system uses OMT to guide both V & H pol components of the incoming radiation to respective receivers. The K band only measures H-pol component through a circular to rectangular waveguide adapter connected to the horns. The feed horn numbers are shown; the even numbered horns are in the top plane and the odd numbered ones are in the bottom plane for each antenna system.

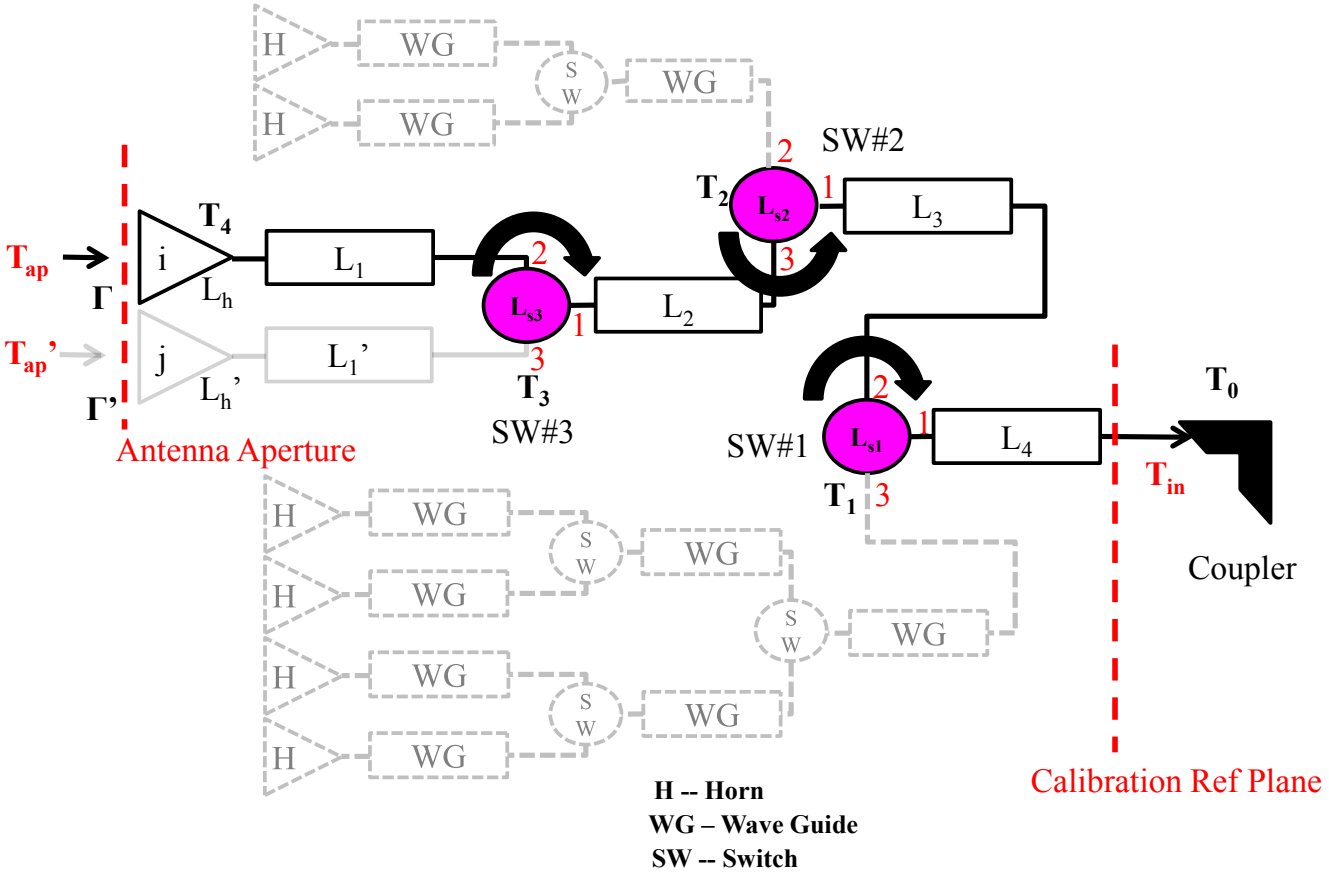

Figure 3.14: MWR antenna switch matrix radiative transfer model schematic. A necessary orientation of the circulator switches are shown, to guide radiation incident on horn i to the receiver. In the primary path, the radiation has to pass through four waveguide sections and three switches.

3.3.1 Front-End Hardware Radiative Transfer Model

A computer rendering of the MWR antenna system is shown in Fig. 3.13. It should be noted that only the feed horns and the switching networks are shown, the reflectors and receivers are not included in the figure. The Ka band antenna system uses an ortho-mode transducer (OMT) to guide Vertical and Horizontal polarization components of the feed-horn incident radiation through two separate waveguide paths. However for K band, a circular to rectangular wave-guide adaptor is used to guide only the H-pol component of the incident radiation to the receiver. After the OMT/Adaptor the guided radiation passes through three layers of ferrite circulator switches. The 'magenta' switches are shown in the 3D rendering of Fig. 3.13. The three layers of the switch matrix comprise (staring from feed-horn side) four switches, two switches and one switch respectively. Thus MWR antenna switching matrix has all together seven switches for each channel, totaling 21 switches for all three channels (K band H-pol, Ka band H & Ka Band V-pol). Figure 3.13 also shows the numbering scheme of the antenna feed-horns. It is based on the location of the antenna foot-prints on the ground with respect to the satellite sub-track e.g., horn 1 foot-prints are being closest and horn 8 are being furthest to the satellite sub-track. To compensate for the earth's diurnal rotation, SAC-D space-craft is yaw steered in a manner so that the K band horn n foot-prints exactly overlaps with Ka band horn n foot-prints for every horn number n (n = 1,2,...,8).

The antenna switch matrix for any particular channel (e.g. K-H or Ka-H or Ka-V) of MWR could be simplified by the schematic shown in Fig. 3.14. Let us consider that horn i is being sampled by the radiometer receiver. To guide the incident radiation T_{ap} (in K)

from the feed-horn to the input of the coupler (i.e. receiver input) all the ferrite circulator switches in the path are connected in a particular orientation by sending control signals to the individual switch drivers. The switches in horn i path are colored in 'magenta' and the ports are numbered in Fig. 3.14. In these three port circulator switches, switching between ports is achieved by sending a current by the driver circuit to change the polarity of a magnetic field sustained by a ferrite puck inside the switch. There is always a low-loss path between any two adjacent ports of the switch. However, the way the ports are connected (clockwise or counter-clockwise) is determined by the orientation of the magnetic field applied to the ferrite puck. For example in Fig. 3.14, SW#1 and SW#3 are given a clockwise polarity to establish a low loss path between port 2 to port 1 (also, port 1 to 3 and port 3 to 2 are connected). And SW#2 is given an anti-clockwise polarity to connect between port 3 to port 1 (also, port 1 to 2 and port 2 to 3 are connected).

An antenna acts as an impedance transformer between free-space propagating unbounded radiation and a guided wave inside microwave waveguide. In practice even in a well-designed antenna there is a small amount of reflection present due to imperfect impedance transformation at the antenna free-space boundary (i.e. at the antenna aperture). Let Γ (unit-less ratio) be the power reflection coefficient at the aperture of horn i. Thus the guided radiation $(1-\Gamma)T_{ap}$ passes through the feed horn and OMT (or, waveguide adapter for K band) loss L_1, SW#3 loss L_{s3}, waveguide loss L_2, SW#2 loss L_{s2}, waveguide loss L_3, SW#1 loss L_{s1} and waveguide loss L_4. Here L_h, L_1, L_{s3}, L_2, L_{s2}, L_3, L_{s1} and L_4 are power transmission coefficients (unit-less ratio) of the corresponding losses. The incoming radiation

power that reaches the receiver input is given by (unit in K),

$$(1-\Gamma)L_hL_1L_{s3}L_2L_{s2}L_3L_{s1}L_4T_{ap} \tag{3.13}$$

The switches SW#1, SW#2 and SW#3 are set to guide radiation entering horn i to the receiver and isolate any radiation that might try to enter the receiver through other feed-horns. It should be noted here that irrespective of the state of the other four switches in the switching matrix free-space radiation can always find a low loss path up to the port 3 of SW#3, port 2 of SW#2 and port 3 of SW#1. So the isolation of these switches is very important for proper functioning of the MWR antenna system. From the manufacturer data sheets in Appendix A.1.1 and A.2.2 it is evident that the average isolation over the bandwidth of the receiver varies between -30 dB to -35 dB, hence it is safe to assume that the contribution from switch leakages is negligible. Even though free-space radiation from other horns doesn't leak through the switches, incident brightness T'_{ap} from adjacent horn j finds a low-loss path through SW#3 to the aperture of the horn i. The reflection coefficient Γ at the horn i aperture is in the order of -17 dB. For a 200 K signal the reflection is close to 4 K, which cannot be ignored. In general, T_{ap} and T'_{ap} are not correlated signals. This is because the beam bore-sight of horn i and horn j look at scenes on earth separated approximately 100 km apart (footprints of any two adjacent horns which share a 3rd level switch e.g. SW#3, are separated by another horn footprint on ground i.e. $|i-j|$ is always 2; assuming $\sim$ 50 km footprint size the beam bore-sight separation is $\sim$ 100 km). Thus the power (in K) of the two uncorrelated signals could be added at the horn aperture as,

$$(1-\Gamma)T_{ap} + (1-\Gamma')L'_hL'_1L_{s3}L_1L_h\Gamma T'_{ap} \tag{3.14}$$

The assumption in equation 3.14 is that the transmission coefficient between port 3 and port 2 of SW#3 is same as that between port 2 and port 1 (L_{s3}). The total brightness that arrives at the port 2 of SW#2 finds a low loss path through port 3. This guided radiation flows through the low loss path between port 1 and port 3 of SW#3 and gets reflected at aperture of the horn j. This reflected signal travels further towards horn i in a way similar to T'_{ap} and suffers one more reflection at the antenna-free space boundary. The double reflection reduces the signal strength by $\sim$ -34 dB (-17 dB per reflection); thus, it is safely ignored in the forward radiative transfer model. Similarly, the brightness that enters port 3 of SW#1 is also ignored. From equation 3.13 and 3.14 , the total free-space brightness that arrives at the receiver input is given by,

$$\{(1-\Gamma)T_{ap} + (1-\Gamma')L'_h L'_1 L_{s3} L_1 L_h \Gamma T'_{ap}\} L_h L_1 L_{s3} L_2 L_{s2} L_3 L_{s1} L_4 \tag{3.15}$$

Next, thermal self-emission of all the components in the signal path needs to be considered in the radiative transfer modeling. In MWR the entire antenna switch matrix is housed inside a temperature controlled environment. High precision platinum resistor temperature sensors (PRT) are put on each of the front-end switches. All the feed-horns are mounted on an aluminum plate with negligible temperature gradient ensuring all the horns (for a particular antenna system, K or Ka band) are maintained at the same temperature. There is only one temperature sensor on the aluminum plate which represents the physical temperature of all the eight horns for any particular antenna (K or Ka band). On orbit, The feed-horns are exposed to cold space of temperature 2.73 K , hence they acts as thermal radiators. The receiver is heated by active heaters attached under an aluminum plate on which all the

microwave components are mounted. Thus there is a natural heat flow from receiver end to the feed-horns via the waveguides and switches of the switching matrix which has no active thermal control. To achieve the requirement of $\pm 1^o$ C temperature stability on orbit, this heat-flow needs to be controlled. For this reason, a heater is put on the horn plate. Thus a uniform temperature gradient could be established across the switching network by controlling the temperatures at both ends. The temperature sensor data is obtained as a part of MWR's telemetry data packet and each sensor is sampled once in every 0.24 s (same as MWR's integration time). Let us assume that the physical temperatures of SW#1, SW#2, SW#3 and Feed horns in Fig. 3.14 are T_1,T_2,T_3 and T_4 respectively. In MWR there are no PRT sensors attached to the waveguides. Therefore for the radiative transfer modeling, we will assume that the physical temperature of any waveguide in the switching matrix is the average of the physical temperatures of the components at its both ends. For example, in Fig. 3.14, physical temperature of L_1 is $0.5(T_4 + T_3)$ K and physical temperature of L_4 is $0.5(T_1 + T_o)$ K etc. Here, T_o represents the physical temperature of the coupler at the input of the receiver. It should be noted that in MWR there is no temperature sensor on the coupler. Thus, T_o, the temperature of the internal reference load, which is measured by a PRT sensor, is used. As all the receiver components are in close-proximity and are mounted on aluminum plate with negligible temperature gradient, this is a very safe assumption.

The thermal self-emission from horn i has a direct and reflected (at the antenna aperture) path to the receiver. If the relative electrical phase length between these two paths are

denoted by Φ, then the contribution to the output by the feed horn i is,

$$(1 - L_h)T_4L_1L_{s3}L_2L_{s2}L_3L_{s1}L_4|1 + \sqrt{(\Gamma L_h)}e^{j\Phi}|^2 \tag{3.16}$$

Note, however, that the feed losses are distributed over the length of the component, not lumped at a single point. Each differential part of the loss will have its own relative phase length associated with it. If the component is an appreciable number of half-wavelengths long, then these phase lengths will tend to average out. There will be no net constructive or destructive interference between the direct and the reflected emission from the feed to the receiver input. In this case, the power in the two contributions can be added directly. The contribution to the output by the feed is, then

$$(1 - L_h)T_4L_1L_{s3}L_2L_{s2}L_3L_{s1}L_4(1 + \Gamma L_h) \tag{3.17}$$

Similarly, the self-emission from the waveguide loss L_1 will add in power from the direct and reflected paths. This contribution to the output is,

$$(1 - L_1)0.5(T_4 + T_3)L_{s3}L_2L_{s2}L_3L_{s1}L_4(1 + \Gamma L_hL_1) \tag{3.18}$$

Finally, self-emission contribution of SW#3 due to direct and reflected path is,

$$(1 - L_{s3})T_3L_2L_{s2}L_3L_{s1}L_4(1 + \Gamma L_1^2L_h^2L_{s3}) \tag{3.19}$$

The thermal self-emission of feed-horn j and the wave-guide loss L_1' both has a direct and reflected (at the horn j aperture) path. After passing through SW#3 they both reflect at the horn i aperture. Ignoring double reflection path, the horn j contribution to the output is,

$$(1 - L_h')T_4L_1'\Gamma L_h^2L_1^2L_{s3}^2L_2L_{s2}L_3L_{s1}L_4 \tag{3.20}$$

Similarly, output contribution of waveguide L_1' is,

$$(1 - L_1')0.5(T_4 + T_3)\Gamma L_h^2 L_1^2 L_{s3}^2 L_2 L_{s2} L_3 L_{s1} L_4 \tag{3.21}$$

The self-emissions of all the components after SW#3, e.g. waveguides L_2, L_3, L_4 and switches SW#2, SW#1 find no single reflection path to the switch matrix output, hence the multiple reflected paths are ignored. The direct self-emission contribution of all these components are given by,

$$\begin{aligned}
&(1 - L_2)0.5(T_3 + T_2)L_{s2} L_3 L_{s1} L_4 \\
&+(1 - L_{s2})T_2 L_3 L_{s1} L_4 \\
&+(1 - L_3)0.5(T_2 + T_1)L_{s1} L_4 \\
&+(1 - L_{s1})T_1 L_4 \\
&+(1 - L_4)0.5(T_1 + T_o)
\end{aligned} \tag{3.22}$$

The total brightness that appears at the input to the receiver (T_{in}) is obtained by combining equations 3.15 and 3.17 through 3.22. It is given by,

$$\begin{aligned}
T_{in} &= \{(1-\Gamma)T_{ap} + (1-\Gamma')L'_h L'_1 L_{s3} L_1 L_h \Gamma T'_{ap}\} L_h L_1 L_{s3} L_2 L_{s2} L_3 L_{s1} L_4 \\
&+(1-L_h)T_4 L_1 L_{s3} L_2 L_{s2} L_3 L_{s1} L_4 (1+\Gamma L_h) \\
&+(1-L_1)0.5(T_4+T_3) L_{s3} L_2 L_{s2} L_3 L_{s1} L_4 (1+\Gamma L_h L_1) \\
&+(1-L_{s3})T_3 L_2 L_{s2} L_3 L_{s1} L_4 (1+\Gamma L_1^2 L_h^2 L_{s3}) + (1-L'_h)T_4 L'_1 \Gamma L_h^2 L_1^2 L_{s3}^2 L_2 L_{s2} L_3 L_{s1} L_4 \\
&+(1-L'_1)0.5(T_4+T_3)\Gamma L_h^2 L_1^2 L_{s3}^2 L_2 L_{s2} L_3 L_{s1} L_4 + (1-L_2)0.5(T_3+T_2) L_{s2} L_3 L_{s1} L_4 \\
&+(1-L_{s2})T_2 L_3 L_{s1} L_4 + (1-L_3)0.5(T_2+T_1) L_{s1} L_4 \\
&+(1-L_{s1})T_1 L_4 + (1-L_4)0.5(T_1+T_o) \qquad (3.23)
\end{aligned}$$

Acknowledging the fact that all the transmission and reflection coefficients are going to be constant and not expected to change during MWR's mission life time, the expression for T_{in} can be simplified as,

$$T_{in} = gT_{ap} + g'T'_{ap} + a_o T_o + a_1 T_1 + a_2 T_2 + a_3 T_3 + a_4 T_4 \qquad (3.24)$$

where,

$g = (1-\Gamma)L_h L_1 L_{s3} L_2 L_{s2} L_3 L_{s1} L_4$,

$g' = (1-\Gamma')\Gamma L'_h L'_1 L_h^2 L_1^2 L_{s3}^2 L_2 L_{s2} L_3 L_{s1} L_4$,

$a_o = 0.5(1-L_4)$, $a_1 = 0.5(1-L_4) + (1-L_{s1})L_4 + 0.5(1-L_3)L_{s1}L_4$,

$a_2 = 0.5(1-L_3)L_{s1}L_4 + (1-L_{s2})L_3 L_{s1} L_4 + 0.5(1-L_2)L_{s2}L_3 L_{s1} L_4$,

$a_3 = 0.5(1-L_2)L_{s2}L_3 L_{s1} L_4 + 0.5(1-L'_1)\Gamma L_h^2 L_1^2 L_{s3}^2 L_2 L_{s2} L_3 L_{s1} L_4$

$+(1-L_{s3})L_2 L_{s2} L_3 L_{s1} L_4 (1+\Gamma L_1^2 L_h^2 L_{s3}) + 0.5(1-L_1)L_{s3} L_2 L_{s2} L_3 L_{s1} L_4 (1+\Gamma L_h L_1)$,

and

$$a_4 = 0.5(1 - L_1')\Gamma L_h^2 L_1^2 L_{s3}^2 L_2 L_{s2} L_3 L_{s1} L_4 + (1 - L_h')\Gamma L_1' L_h^2 L_1^2 L_{s3}^2 L_2 L_{s2} L_3 L_{s1} L_4$$

$$+0.5(1 - L_1) L_{s3} L_2 L_{s2} L_3 L_{s1} L_4 (1 + \Gamma L_h L_1) + (1 - L_h) L_1 L_{s3} L_2 L_{s2} L_3 L_{s1} L_4 (1 + \Gamma L_h).$$

3.3.2 Thermal/Vacuum Antenna Temperature Cal/Val

The thermal vacuum (T/V) test for MWR was performed during a four day time-period in the month of September, 2009 in CONAE's Teofilo Tabanera Space Center or CETT (Centro Espacial Teofilo Tabanera), Cordoba, Argentina. There were several goals of this test namely: to measure the performance of the instrument's thermal control over a wide range of temperature variation, to check the accuracy of the thermal model of the instrument (which is used to predict the temperature of various parts of the instrument on orbit) and finally to perform the radiometric calibration of the MWR instrument. The radiometric calibration test requires a 'known' target temperature to be seen by the feed horns. For this reason, MWR's flight reflectors were replaced by broadband foam absorbers (Fig. 3.15(a) & 3.15(c)). These absorbers' pyramidal geometry simulates a continuous change in dielectric constant for incident microwave radiation and thereby absorbs it based on the principle of tapered impedance. By steadily increasing the impedance from that of "free space" at the incident surface of the absorber to a high impedance, lossy material at the rear surface, energy is progressively absorbed and attenuated through ohmic loss as it propagates through the absorber. Hence these absorbers act as blackbody targets at microwave frequencies,

(a)

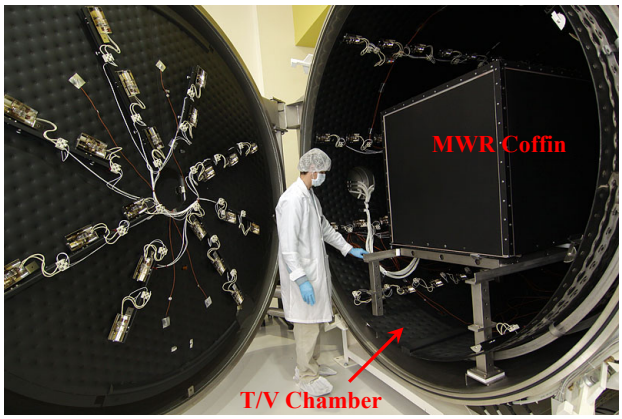

(b)

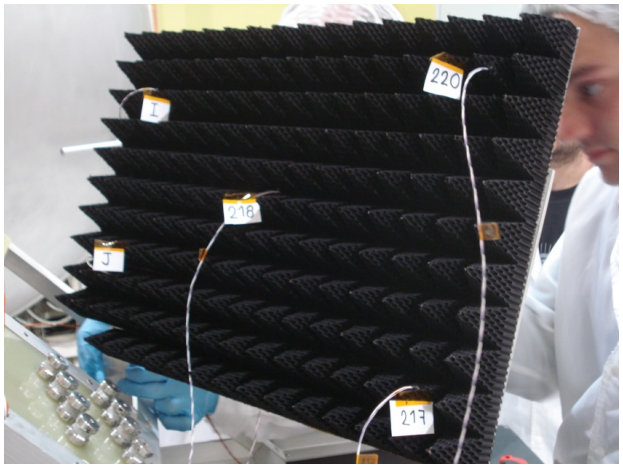

(c)

Figure 3.15: (a) Picture of the MWR instrument covered with thermal blanket, prepared for the T/V test. The flight reflectors are replaced by blackbody calibration targets. The whole instrument is put inside the coffin before taking inside the T/V chamber (Fig. (b)). (c) There are total five temperature sensors attached at the face of the blackbody absorber target to monitor its temperature.

producing brightness equal to their respective physical temperatures. To have a uniform brightness temperature over the entire target cross section the absorber was mounted on aluminum plate with high thermal conductivity. Platinum temperature sensors were put at four corners and at the center of the calibration target, inside the foam material near the base of the pyramid (Fig. 3.15(c)) to measure the physical temperature. Assuming a blackbody target with unity emissivity, the temperature measured by these sensors were used as the brightness seen by the feed horns. There were several other temperature sensors at the back of the absorber, on the aluminum plate, to monitor any possible thermal gradient that might exist during the test. The MWR instrument was covered with thermal blanket as it would be in the flight configuration. The instrument and the calibration targets were put inside an aluminum box (MWR coffin), coated with infrared (IR) absorbing paint (Aeroglaze Z306, Absorptive Polyurethane) in both inside and outside. This box was then placed inside the T/V chamber as shown in Fig. 3.15(b). In the T/V chamber air was evacuated to create a vacuum, simulating space like environment. The MWR coffin was insulated from the chamber so that negligible conductive heat transfer was possible. Radiative heating was performed by IR heaters inside the chamber, and the chamber was cooled by liquid nitrogen. During the four day period of the test the minimum temperature attained by the calibration target was 180 K. The T/V test data provides us with various combination of temperatures at different parts of the antenna switch matrix and MWR receivers while the feed-horn were looking at 'known' calibration targets. This is very useful to estimate the coefficients of equation 3.24 for each feed-horn for all receivers.

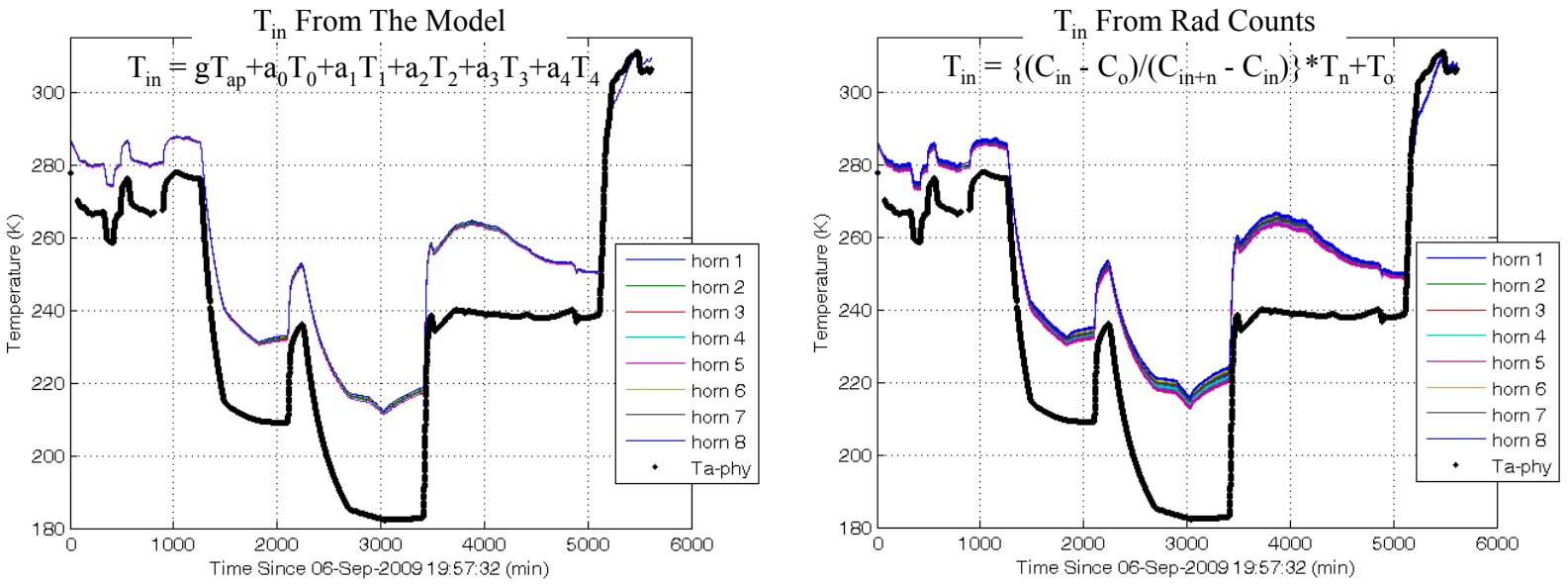

(a) (b)

Figure 3.16: (a) Computed Tin from the model using assumed losses and reflection coefficients for the entire duration of the T/V test. (b) Tin calculated from the radiometer counts during T/V test.

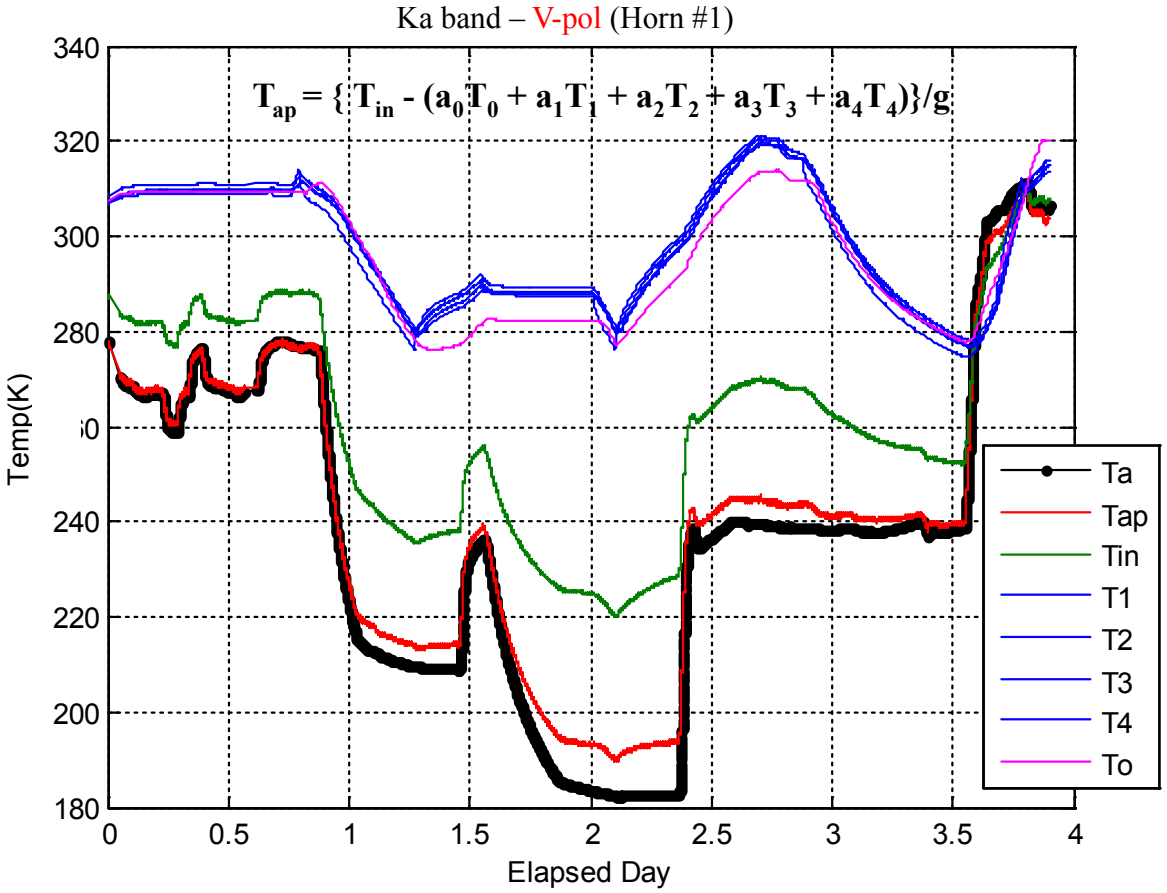

Figure 3.17: Computation of antenna temperature (T_{ap}) from radiometer counts based on the radiative transfer model inversion. The red line is the computed T_{ap}. The black line is the measured T_{ap}. The model does not follow the measured T_{ap} very well.

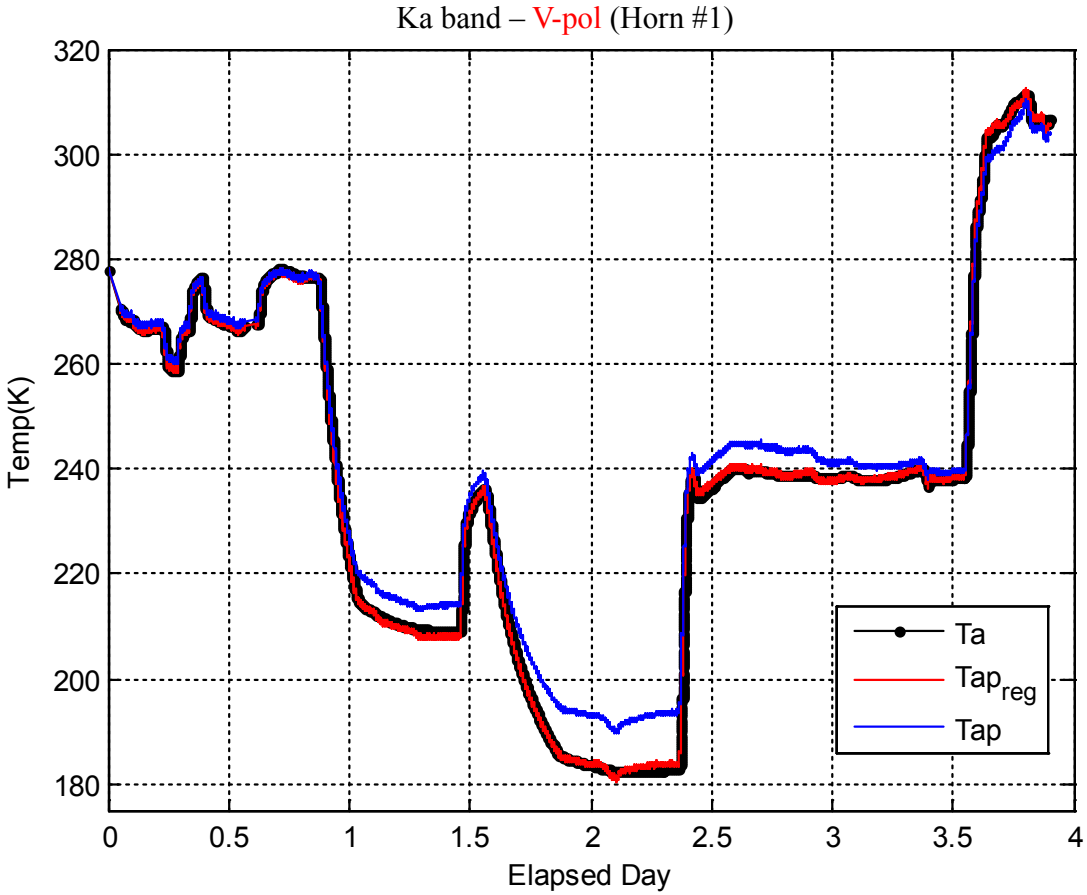

Figure 3.18: Antenna temperature (T_{ap}) computed based on regression based model (red). The blue line is the model based inversion algorithm which assumes losses and reflection coefficients to guess coefficients.The black line is the measured T_{ap}

Before empirically estimating the coefficients, a functional verification of the hardware radiative transfer model was done using the radiometer's T/V data. To calculate the forward model coefficients in equation 3.24 various assumptions about losses and reflections were made. For example, standard loss value for silver waveguide -0.5117 dB/m was used as the MWR waveguides are silver coated from inside. To get the total loss for each waveguide section, their lengths were measured from the CAD model. The lengths of each waveguide section for the all three channels are given in Appendix C. All the switches were assumed to have the same insertion loss of -0.2 dB (the datasheets in Appendix A suggests that it is smaller in practice). The reflection coefficients at the horn aperture was computed using the VSWR (Voltage Standing Wave Ratio) values from the OMT data sheets. In the T/V test since all the horns are looking at the same calibration target T_{ap} and T'_{ap} in equation 3.24 are the same. The T_{ap} input to the RTM was obtained by averaging all the five sensor temperatures from the face of the calibration target. The coefficients g and g' were represented by only one coefficient g. All other temperatures T_o, T_1, T_2, T_3 and T_4 were obtained from MWR's internal telemetry data packets. Thus using equation 3.24 T_{in} is computed for the entire T/V test duration. This is shown in the Fig. 3.16(a), where, the black line represents the temperature of the calibration target (T_{ap}) and different colored plots are T_{in} computed for various feed horn paths using the RTM for Ka Band H-pol channel. T_{in} measured by the radiometer (calculated using equation 3.8) is plotted in the Fig. 3.16(b). The similarity of Fig. 3.16(a) and 3.16(b) verifies the fact that our model is able to predict the receiver input signal with considerable accuracy. There is a larger variation among the T_{in} values measured

by the radiometer compared to those obtained from the model. This is because the model did not have accurate estimate of the different switch losses and reflection coefficients for different paths and also the waveguide losses were assumed to be "standard". The imperfection of the model assumption is demonstrated in Fig. 3.17. Here, similar to Fig. 3.16 the target temperature T_{ap} is plotted using the black line. The green line represents the T_{in} computed from the radiometer counts for the Ka band V pol receiver, Horn# 1. Using this value of T_{in} and inverting equation 3.24, T_{ap} is solved and plotted in Fig. 3.17 using the red line. As we can see the red plot does not exactly follow the black plot. Thus a better estimate of the forward model coefficients are required. In Fig. 3.17 the switch matrix temperatures are plotted using blue lines and the receiver internal temperature is represented by a magenta line. As we can see, because of the active thermal control of the MWR instrument there is a very high correlation among the switches and horn plate temperatures. Therefore for a regression based algorithm these temperatures fails to become an independent estimator of T_{ap} . The following form of the regression model is assumed,

$$T_{ap} = b_1 + b_2 T_{in} + b_3 T_{in}^2 + b_4 T_o + b_5 T_{av} \tag{3.25}$$

Where, $T_{av} = (T_1 + T_2 + T_3 + T_4)/4$

The motivation behind the quadratic term is to correct for the small non-linearity of the receiver observed during the receiver external calibration tests. The coefficients b_1 to b_5 were estimated for each feed-horn path and for all receivers. Selected regions of the T/V data were chosen for the regression so that the coefficients do not get biased by the temperature plateaus in the data. The temperature of the black-body target was used as T_{ap} to train

the model. T_{in} was computed using counts and all other temperatures were obtained from MWR's internal telemetry. The T_{ap} computed from the regression based algorithm (red line) is plotted in Fig. 3.18. The blue line in the same plot is the forward model inversion based algorithm (v1.0) which assumed nominal values of losses and reflections. From Fig. 3.18 it is clear that the regression algorithm matches the measured antenna temperature (black line) much better than the previous algorithm.This version of the calibration algorithm is v2.0

There are several limitations of this regression based Pre-Launch algorithm (v2.0). The assumption of the antenna temperature (T_{ap}) equal to the physical temperature of the absorber is only valid if the emissivity of the absorber target is unity. This assumption was never verified by any laboratory test. It was also assumed that the feed-horn only capturing radiation from the target absorber, the effect of feed-horn spill-over in the T/V chamber was not considered. Finally, it was assumed that the brightness of the noise diode was constant and equal to the laboratory measurement. Because the physical temperature of the noise diode varied during the T/V test, this may have caused a small change in the diode T_n, which was not considered. Unfortunately, the stability of the noise diode was not measured over temperature.

CHAPTER 4
MWR CALIBRATION : POST-LAUNCH

As mentioned in the chapter 3, there are several limitations of the "Pre-Launch Algorithm". The assumption of the antenna temperature (T_{ap}) equal to the physical temperature of the absorber is only valid if the emissivity of the absorber target is unity. This assumption was never verified by any laboratory test. It was also assumed that the feed-horn only capturing radiation from the target absorber, the effect of feed-horn spill-over in the T/V chamber was not considered. Furthermore, no end to end T_b calibration was done in the laboratory using the flight reflectors. MWR's reflectors are made of pure metallic aluminum. This eliminates the problem of them being emissive [10, 11].Therefore no separate laboratory test was done to characterize reflector emissivity. The pre-launch anechoic chamber tests to determine MWR's antenna patterns were done only over a restricted range of $\pm 40^o$ azimuth and $\pm 30^o$ elevation angles. This is not sufficient to formulate an accurate antenna pattern correction algorithm. Also, irrespective of the knowledge of the entire 4π steredian antenna pattern, it is almost impossible to simulate the space environment in laboratory to estimate the contributions of far side lobes and spill overs in the measured antenna temperatures. Finally, it was assumed that the brightness of the noise diode was constant and equal to the laboratory measurement. Because the physical temperature of the noise diode varied during the T/V test, this may have caused a small change in the injected T_n, which was not considered. Unfortunately, the stability of the noise diode was not measured over temperature.

In this chapter, post-launch calibration of MWR is discussed. On-orbit calibration

is necessary to estimate accurate antenna pattern correction (APC) coefficients and other residual instrument biases. The first section describes the inter-satellite calibration using the polarimetric radiometer WindSat, on board Naval Research Laboratory's Coriolis satellite. WindSat and MWR shares similarities in orbit ground track and radiometric frequencies, enabling the possibility of obtaining a large number of collocated radiometric measurements which could be easily compared. Also, WindSat mission, to investigate the use of microwave radiometers to measure both wind speed and direction over the ocean, is extremely demanding on the quality of the calibration and the sensor had commensurate care applied to its calibration.

4.1 Inter-Satellite Calibration With WindSat

4.1.1 Choice of WindSat

WindSat is a polarimetric microwave radiometer developed by the Naval Research Laboratory Remote Sensing Division and the Naval Center for Space Technology (NCST) for the U.S. Navy and the National Polar-orbiting Operational Environmental Satellite System (NPOESS) Integrated Program Office (IPO) as a risk reduction mission for NPOESS [12]. It was launched on January 6, 2003 on board the United States Air Force (USAF) Coriolis satellite in an 840 km near circular sun-synchronous polar orbit. WindSat comprises 22 channels operating at 5 frequencies: 6.8, 10.7, 18.7, 23.8, 37.0 GHz, of which the 10.7-, 18.7-,

Table 4.1: MWR and WindSat Similarities

Parameter	**WindSat**	**MWR**
Altitude	840 Km	657 Km
Eccentricity	0.00134	0.00120
Orbit Inclination	98.7°	98.01°
Ascending Node	6 p.m.	6 p.m.
Channels	6.5, 10.7, 18.7, 23.8 & 37 GHz (V,H)	23.8 GHz (H) & 36.5 GHz (V,H)
Swath Width	$\sim$ 950 Km	$\sim$ 380 Km
Earth Incidence Angle	53°	52° & 58°

and 37.0-GHz channels are fully polarimetric (V/H, $\pm 45^o$, and left- & right-hand circular polarized) with incidence angles ranging from 50° to 55°. This conically scanning instrument has a forward-looking swath of approximately 950 km and an aft-looking swath of about 350 km. WindSat shares similarities with MWR in satellite groundtrack and radiometric frequencies. Both the sensors fly in sun-synchronous orbit with similar inclination angles and eccentricities. They also share the same local equatorial crossing times for ascending (6 p.m.) and descending (6 a.m.) nodes. Although the viewing angles are different, the 3 channels of MWR are a subset of the WindSat channels. Moreover, the WindSat swath is much wider (950 Km) than the MWR swath (380 Km), which allows considerable radiometric collocations between the two sensors. Table 4.1 lists the similarities between MWR and WindSat [2].

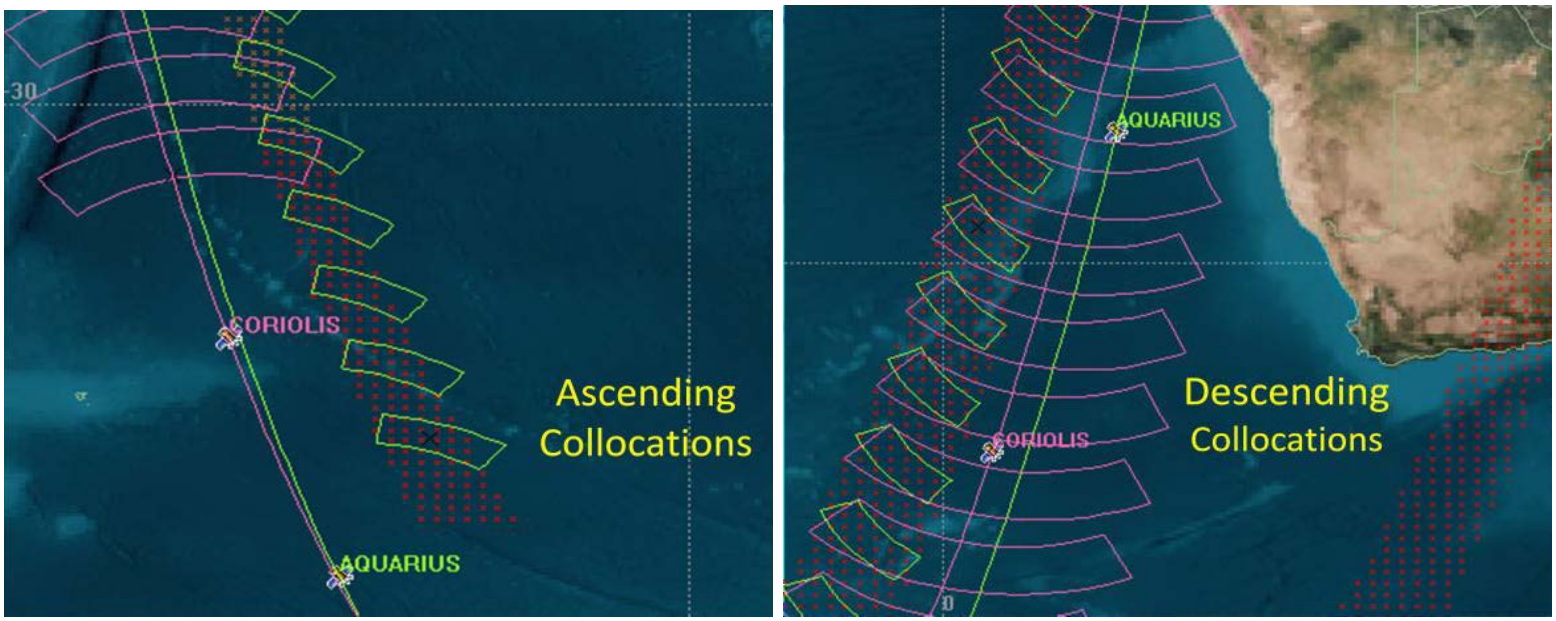

(a) (b)

Figure 4.1: STK Simulation of the (a) ascending and (b) descending collocations between MWR (green) and WindSat (magenta) swaths. The red colored points show corners of collocated 0.5^o resolution boxes.[2]

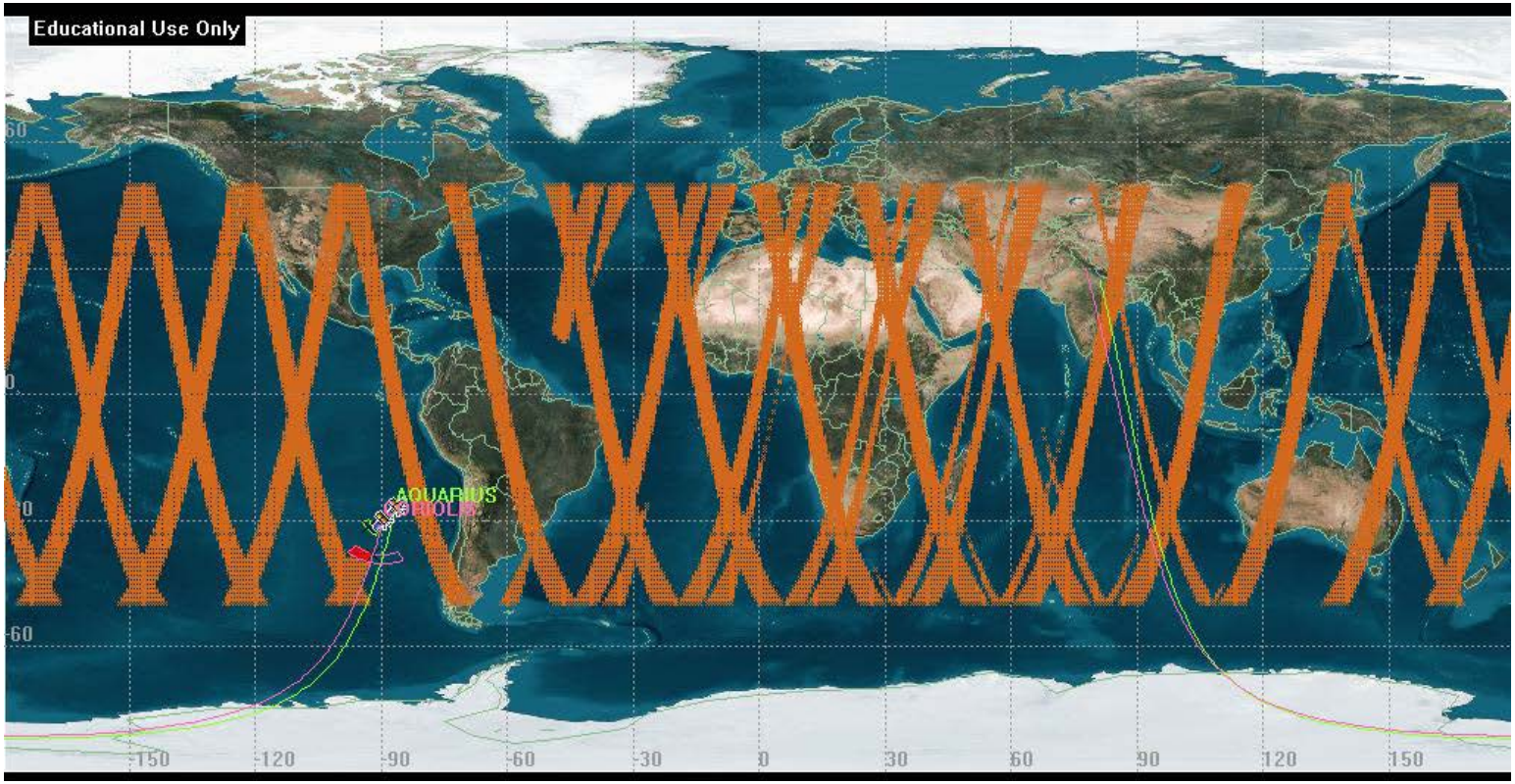

Figure 4.2: $0.5^o \times 0.5^o$ collocation boxes between MWR and WindSat in $\sim$ 45 hours as simulated in STK.[2]

In the pre-launch time period the orbits of the two satellites were simulated in Satellite Toolkit (STK) software [13]. SAC-D, orbiting at a lower altitude than Coriolis, has a higher velocity and therefore, laps the Coriolis satellite in approximately 45 hours and 36 mins (lap time) [2]. For the simulation if we start with zero orbital phase between the two satellites, as SAC-D begins to lead Coriolis, the ground-tracks gradually phase out to a maximum value and then again phase in. When the temporal spacing between the two satellites is exactly half of an orbit period ($\sim$ 45 min), the ground-tracks are maximally out of phase. It was also observed that it takes about 57 days for the satellites to become collocated at approximately the same point on the surface of the earth. This orbit repeat period consists of $\sim$ 30 lap times i.e., after SAC-D laps Coriolis 30 times in approximately 57 days, the ground tracks will repeat [2].

The STK simulations also suggested that MWR has a significant swath overlap with WindSat. This will provide many spatial/temporal collocations, required for the post-launch radiometric calibration of MWR using WindSat as a reference. The inter-satellite spatial/temporal radiometric collocations were evaluated by simulations using Satellite Toolkit (STK) software. The collocations were observed in a 0.5^o resolution earth grid, restricted between $\pm 50^o$ latitudes, with a $\pm$45 min separation window. Fig. 4.1 shows the ascending and descending collocations between MWR (green) and WindSat (magenta) swaths. The red colored points show corners of collocated 0.5^o resolution boxes. Fig. 4.2 shows the collocation swath coverage in $\sim$ 45 hours. There are about 19,000 (0.5^o lat/lng boxes within $\pm 50^o$ lat., $\pm$45 min window) collocations in a 45 hour period. The swaths have maximum

collocation when the ground-tracks of the two satellites are in-phase and they have minimum collocation when the ground-tracks are out of phase [14].

4.1.2 Radiative Transfer Modelling

Inter-satellite calibration utilizes satellite observations that are collocated spatially & temporally. In the simplest sense, if two radiometers of identical design made an observation over the earth at the exact time and space, difference in T_b should reflect the radiometric calibration bias between the satellites. Unfortunately, for radiometers of different design the situation is more complicated because the scene brightness varies with the observing frequency and viewing geometry (primarily earth incidence angle or EIA); therefore, normalization between the sensors is required, before estimating the radiometric bias between the satellites. In the context of MWR and WindSat, since MWR channels are a subset of WindSat channels, there is no need for T_b normalization due to observation frequency difference. However, due to the EIA difference between MWR beams and WindSat normalization of T_b is required before comparison.

The method used here for this normalization utilizes microwave radiative transfer theory to translate the measurement of WindSat to MWR's viewing parameters. This technique uses the double-difference of theoretical Tb difference minus the observed Tb difference bwtween the two instruments, which minimizes the impact of the Radiative Transfer Model (RTM) used. The need for a well predicted theoretical T_b adds constraints to the nature

of the observed scene where this comparison could be done. Global Ocean is chosen for its homogeneous nature and the availability of accurate ocean surface emissivity models. Also the experiment is done for "clear sky" conditions where there is negligible atmospheric contribution to the observed T_b. The RTM used here is NASA's Precipitation Measurement Mission (PMM) Science Team's Inter-Calibration Working Group's (A.K.A. XCAL) RTM that uses a combination of surface models developed by Meissner and Wentz [15], Elsaesser [16], Wilheit [17], Hollinger [18], and Stogryn [19] for ocean isotropic emissivity (ignoring small wind direction effects) to account for frequency and incidence angle. An in-depth discussion of radiative transfer theory can be found in Ulaby, Moore and Fung [9] and Elachi [20].

For "clear-sky" ocean scenes used in our calibration, the brightness temperature is dominated by the surface emission. The XCAL emissivity (ϵ) model requires sea surface temperature (SST), wind speed (WS), salinity, frequency and incidence angle as inputs. It calculates the isotropic ocean surface emissivity and ignores small wind direction effects, which were investigated and found to average to zero globally and have negligible effect on the relative biases. In the frequency range of our interest 22-37 GHz (for this intercomparison) and for EIA between 52° to 58°, the sensitivity of surface emission to WS is almost an order in magnitude greater for H-pol compared to V-pol. There is high confidence in these RTM calculations over wind speed based upon excellent wind speed retrievals compared to ocean buoys reported by Wentz [21]. The strongest variation in the ocean radiance

with environmental parameters is associated with SST. In EIA range of interest the V-pol exhibits higher sensitivity to SST compared to H-pol.

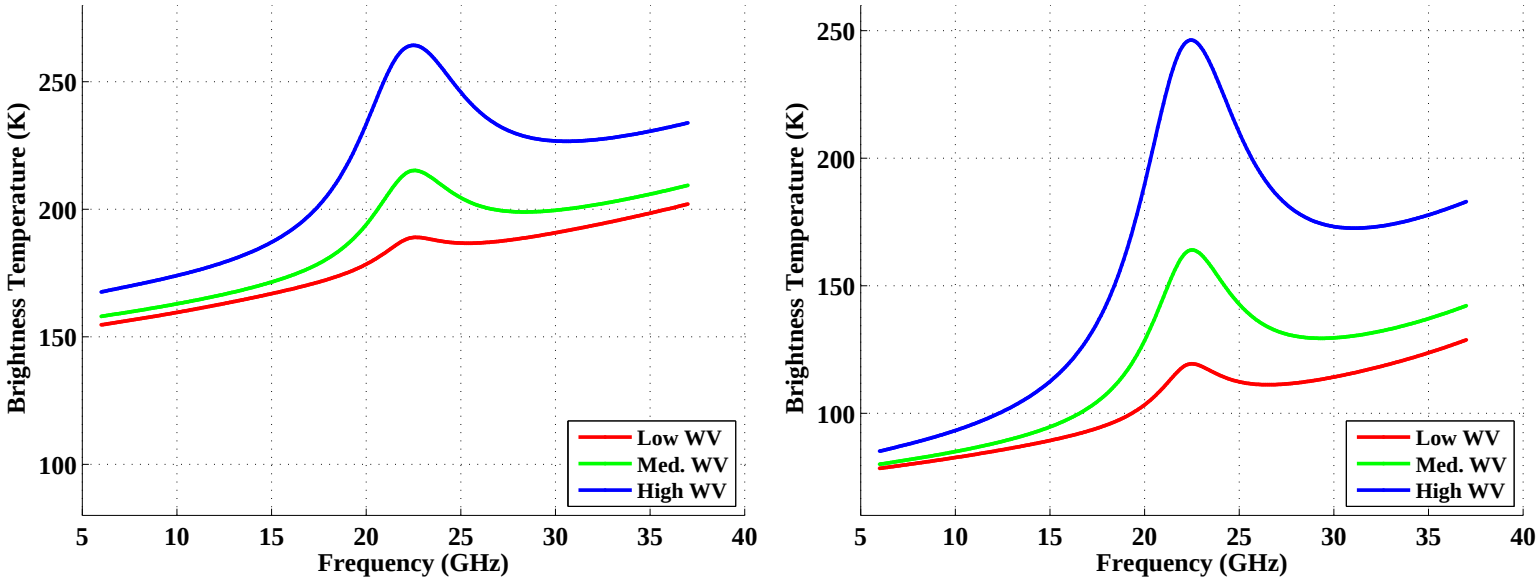

(a) (b)

Figure 4.3: Frequency spectrum of top-of-the-atmosphere brightness temperature (T_b) as seen by a downward looking radiometer at 53° incidence angle for three different columnar WV densities $\sim$ 6 mm (red), $\sim$ 20 mm (green) and $\sim$ 70 mm (blue) for a fixed ocean surface conditions: wind speed 5 m/s, Sea Surface Temperature 300 K and salinity 36 ppt. Even though atmospheric emissions are not polarized, greater dynamic range of T_b is observed at H pol (panel (b)) compared to V-pol (panel (a)) due to surface reflection modulation. The T_b's peak up at 22.2 GHz WV resonance line.

Rosenkranz models for water vapor (WV) [22], cloud liquid water (CLW) [23], oxygen (O_2) [24] and nitrogen (N_2) [25] absorption in the atmosphere are used to calculate the atmospheric absorption coefficients. The largest contribution to the atmospheric absorption in the 18 GHz - 37 GHz frequency range comes from water vapor. For a set of oceanic surface parameters, WS = 5 m/s, SST = 300 K, EIA = 53°, and salinity = 36 ppt, Fig. 4.3(a) & 4.3(b) illustrates the top of the atmosphere apparent T_b spectrum (6 to 37 GHz) for 3 categories of columnar WV low ($\sim$ 6 mm), medium ($\sim$ 20 mm), and high ($\sim$ 70 mm) for V- & H-Pol, respectively. Our model captures the WV absorption for V & H-Pol, with H-Pol having the expected larger dynamic range than V-Pol, reflecting larger T_b differentials between the three WV categories. The absorption coefficient is low for the low frequencies, peaks at 22.2 GHz and drops again before rising monotonically for frequencies higher than 33 GHz. For the simulation in Fig. 4.3, CLW is assumed to be zero mm. Even though CLW has a significant effect on the T_b simulation, for calibration purposes, we usually look at "clear sky" scenes with very low CLW (CLW $<$ 0.1 mm) to avoid uncertainties in simulated T_b's. There is extremely strong O_2 absorption signal near 60 GHz, which does not affect the inter-calibration analysis, as our radiometer channels are far removed from that frequency. Thus, WV and CLW are the two atmospheric parameters that significantly affect 10.7 to 37 GHz frequency emissions. Hence, over the range of frequencies of interest, these two parameters, along with SST and wind speed are the four geophysical parameters that significantly impact the RTM modeled T_b.

The environmental inputs to the RTM are obtained from the ancillary data (GDAS),

which provides model outputs at 0000, 0600, 1200 and 1800 GMT and on a 100 km ($1^o \times 1^o$) grid. These data include the atmospheric profiles of various parameters at different pressure levels as well as columnar cloud liquid water, sea surface temperature, and ocean wind speed at 10 m height. The atmosphere is divided into 100 layers of 200 m thickness each; therefore, the atmosphere is modeled up to a height of 20 km, which extends beyond the height of the tropopause [26]. Furthermore, the air in the atmosphere above the tropopause is extremely rarified and does not significantly affect the apparent T_b. Thus, the RTM adequately models the entire extent of the atmospheric contribution to the radiometer T_b. The atmospheric profiles from the ancillary data are interpolated to the heights of the 100 layers in the RTM, using a piece-wise linear distribution for temperature and piece-wise exponential distributions for pressure and water vapor. The lapse rates of the temperature, pressure and water vapor have significant differences between the upper and lower layers for some cases. Thus, generating a single fit for the entire vertical profile would have resulted in large re-sampling errors for these cases. Therefore, piecewise interpolations were used to adequately represent the non-uniform variation of environmental parameters in the different layers. A uniform distribution is used for cloud liquid water, and the heights of the cloud top and bottom are obtained from ocean climatology based on the ENVIMOD model developed by Wisler and Hollinger [27]. These environmental parameters are matched-up with the mean T_b observations for each 1° lat-lon box and are used to calculate the predicted T_b for that box.

4.1.3 Datasets

The available T_b data and the ancillary (GDAS) datasets are all in different formats and varying temporal and spatial resolution.To enable inter-comparison between WindSat and MWR their respective datasets are mapped into a common Latitude/Longitude grid on earth. The ancillary data (GDAS) required as input to the RTM is also mapped to the same grid points.

4.1.3.1 WindSat Data

The WindSat data product used for the on-orbit calibration of MWR is the WindSat Sensor Data Record (SDR). The SDR file contains calibrated, collocated, averaged brightness temperatures for all WindSat channels. The file is composed of data records spaced in time for every fourth 37 GHz V/H measurement along scan and every scan along track. This results in approximately a 12.5×12.5 km grid locally. This T_b product includes antenna pattern correction, (including spillover) and corrections for polarization rotation angle (PRA) variations, which change the polarization basis of the antenna. The data from each frequency band are then resampled to the 37 V/H locations. The data are then averaged to a common spatial resolution. The swath of the SDR data is defined as the common swath of all channels at 10.7, 18.7, 23.8 and 37.0 GHz.[28]

For our analysis we only use data from 23.8 GHz H-pol and 37.0 GHz V/H-pol channels.

The raw sensor T_b's are averaged spatially into 1° boxes, which typically have 50-100 samples. For quality control purposes, these boxes are then filtered to remove outliers using the standard deviation of these T_b measurements. Since high standard deviations are indicative of nonhomogeneous environmental conditions, including weather fronts with rain and small island contamination, these boxes are removed when standard deviations exceed 2 and 3 K for vertical and horizontal polarizations, respectively. For ocean observations, further editing is applied at all frequencies based on the upper limits of brightness temperatures expected from rain-free ocean, and a conservative land mask is also applied to filter out nearby land pixels. Apart from these filters, we also filter ocean data based on SDR "Surface_type" flag.

4.1.3.2 MWR Data

MWR's binary data packets are multiplexed with other three instrument data streams, viz. DCS (Data Collection System), NIRST (New InfraRed Sensor Technology) and ROSA (Radio Occultation Sounder for Atmosphere) on SAC-D space-craft by the PAD (Data Acquisition and Processing Subsystem) and transmitted down to the ground station. After a successful downlink PAD packets are checked for CRC error by the ground processing systems and dumped into a storage server following proper timestamp and naming conventions. From this binary data dump MWR frames are parsed to produce raw MWR serial data stream. This data does not contain any geolocation information, hence it is not suitable for inter-satellite calibration. CONAE's ground processing system merges SAC-D naviga-

tion data (satellite ephemeris) with the raw MWR instrument serial data stream to produce MWR Level 1A data (Appendix F.1). This L1A data reports radiometer samples (counts) for every 240 ms, where all the feed-horn measurements are time multiplexed (Fig. 2.5). This dataset does not contain calibrated T_b measurements and location of antenna foot-prints on ground for each feed-horn. The calibrated T_b measurements along with individual foot-print locations for feed-horns are provided in the MWR Level 1B (Appendix F.2) dataset. The form of this data is suitable for inter-satellite calibration and comparison. However, during the early phase of mission and especially in the pre-launch period, the algorithm for producing calibrated T_b was not finalized. Therefore CFRSL has produced an experimental dataset in MATLAB binary (.mat) format for internal cal/val purposes and for the purpose of defining the final counts to T_b algorithm coefficients. This CFRSL L1 dataset (Appendix F.3) is produced by gathering the MWR serial data from CONAE L1A files, then applying the CFRSL calibration algorithm to converts counts to T_b and finally attaching the geolocation information read from the CONAE L1B files. The data is grouped separately for three receivers and for individual feed horn. A detail description of this dataset is given in Appendix F.3. This data is used for the on-orbit calibration of MWR discussed in this dissertation. It should be noted that CONAE L1B is the official MWR brightness temperature data product which is currently implementing the CFRSL T_b calibration algorithm.

The raw sensor T_b's are gridded into 1° boxes by treating each feed horn for each receiver separately. This results in 8 feeds $\times$ 3 receivers or 24 separate radiometer channels

being individually collocated with WindSat 1° boxes. The RTM is run separately for each of this 24 radiometer channels.

4.1.3.3 GDAS Data

The ancilliary dataset used here is the NCEP (National Centers for Environmental Prediction) FNL (Final) Operational Global Analysis. This product is from the Global Data Assimilation System (GDAS) that continuously collects observational data from the Global Telecommunications System (GTS), and other sources, for many analyses. The FNLs are made using the same model that NCEP uses to create Global Forecast System (GFS). From this point forward these data will be addressed as GDAS. GDAS is prepared operationally every six hours on a $1^o \times 1^o$ lat/lon grid. The grid points are centered at integer values of lat/lon points, including latitude grids at 90^oS, 0° and 90^oN, resulting in 181 x 360 grid boxes. The atmospheric profile data are provided in 26 pressure levels from 1000 mb to 10 mb; but for input to our RTM, we only use the first 21 levels between pressures of 1000 mb and 100 mb. Out of a plethora of GDAS environmental parameters we use the following: height, temperature and relative humidity profiles, sea surface temperature, columnar cloud liquid water and the u- and v-components of 10 meter wind speed.

4.1.4 Inter-Satellite Radiometric Calibration Method

The inter-satellite radiometric calibration method involves collocating 1° brightness temperature grids with ancillary data. The $1^o \times 1^o$ T_b grids over ocean are generated per orbit basis for each sensor (MWR & WindSat), for each radiometer channel. The average time of all the observations falling in an one-degree box is assigned as the observation time of that box. There are four environmental parameter file per day, generated at 00, 06, 12 and 18 hours Greenwich Mean Time (GMT). A file with time within ± 3 hours of the box observation time is chosen for collocation. Let us consider that the average T_b for a particular channel, observed by a sensor in a 1° box, is T_b^{obs}. The RTM is run using the collocated environmental parameters and given sensor parameters (frequency, incidence angle and polarization). If the RTM output T_b is represented by T_b^{rtm}, then the single difference bias (B_{SD}) is computed as,

$$B_{SD} = T_b^{obs} - T_b^{rtm} \tag{4.1}$$

Ideally, for all the radiometer sensors, we expect B_{SD} statistic to be normally distributed with zero mean. Since the RTM input parameters are only an estimation of the true geophysical scene under observation and the RTM (physics and absorption coefficients) is not a perfect simulator, absolute biases may be present in the simulated brightness temperatures. Therefore, a nonzero mean of B_{SD} in equation 4.1 doesn't necessarily points to an absolute calibration error. Even though magnitude of B_{SD} does not help us estimating absolute calibration errors, B_{SD} can be further analyzed to determine if the sensor is consistent with itself. For example, B_{SD} is checked for possible correlation with several instrument

and flight parameters: scan position, solar heating (Sun beta angle), orbit phase, distance from landmass, ascending/descending node time (for sunsynchronous satellites) etc. If a significant correlation is found, a correction is introduced before considering the instrument for inter-calibration. This technique has been successfully demonstrated for TMI solar bias correction in [11] and [29].

The limitations of RTM are greatly overcome by the pairwise comparison of B_{SD}'s from two different satellite sensors. This technique is called "Inter-Satellite Calibration". In this method, the bias for an arbitrary sensor A with respect to another sensor B is given by the double difference of individual B_{SD}'s,

$$\begin{aligned} B_{DD}(AB) &= B_{SD}(A) - B_{SD}(B) \\ &= (T_b^{obs} - T_b^{rtm})_A - (T_b^{obs} - T_b^{rtm})_B \end{aligned} \tag{4.2}$$

The terms in equation 4.2 can be rearranged to represent the bias of sensor A with respect to sensor B as a single difference term,

$$B_{DD}(AB) = (T_b^{obs})_A - (T_b^{pred})_{AB} \tag{4.3}$$

Where, $(T_b^{pred})_{AB}$ is the predicted T_b of sensor A based on the observation made by sensor B, and is given by,

$$(T_b^{pred})_{AB} = (T_b^{obs})_B + \{(T_b^{rtm})_A - (T_b^{rtm})_B\} \tag{4.4}$$

The second term in the right hand side of equation 4.4 is a difference in the RTM T_b's of sensor A and B. This difference essentially cancels out any absolute bias that may exist in the RTM and provides us with an estimate of the theoretical difference between the observed

T_b's due to difference in sensor parameters (e.g. frequency, incidence angle) only. Thus, adding this theoretical difference to the sensor B observed brightness temperature $(T_b^{obs})_B$, produces a theoretical prediction of sensor A T_b. If sensor B is known to be well-calibrated and tested to be self-consistent, then using $B_{DD}(AB)$ instead of $B_{SD}(A)$ for checking sensor A self-consistency, is a much more robust method.

In the scenario of MWR and WindSat, we want to check the calibration of MWR (sensor A) against WindSat (sensor B). Due to the nature of the WindSat mission the calibration requirements and design of the instrument is far superior compared to MWR and most of the other existing space-borne radiometers. From equation 4.3 The double difference bias of MWR with respect WindSat is given by,

$$MWRBias = (T_b^{obs})_{MWR} - (T_b^{pred})_{MWR-WindSat} \tag{4.5}$$

Where, $(T_b^{pred})_{MWR-WindSat}$ is the predicted T_b of MWR based on the observation made by WindSat, and is given by,

$$(T_b^{pred})_{MWR-WindSat} = (T_b^{obs})_{WindSat} + \{(T_b^{rtm})_{MWR} - (T_b^{rtm})_{WindSat}\} \tag{4.6}$$

From now onwards, "MWR Bias" given by equation 4.5 will be referred as simply "bias" unless otherwise mentioned.

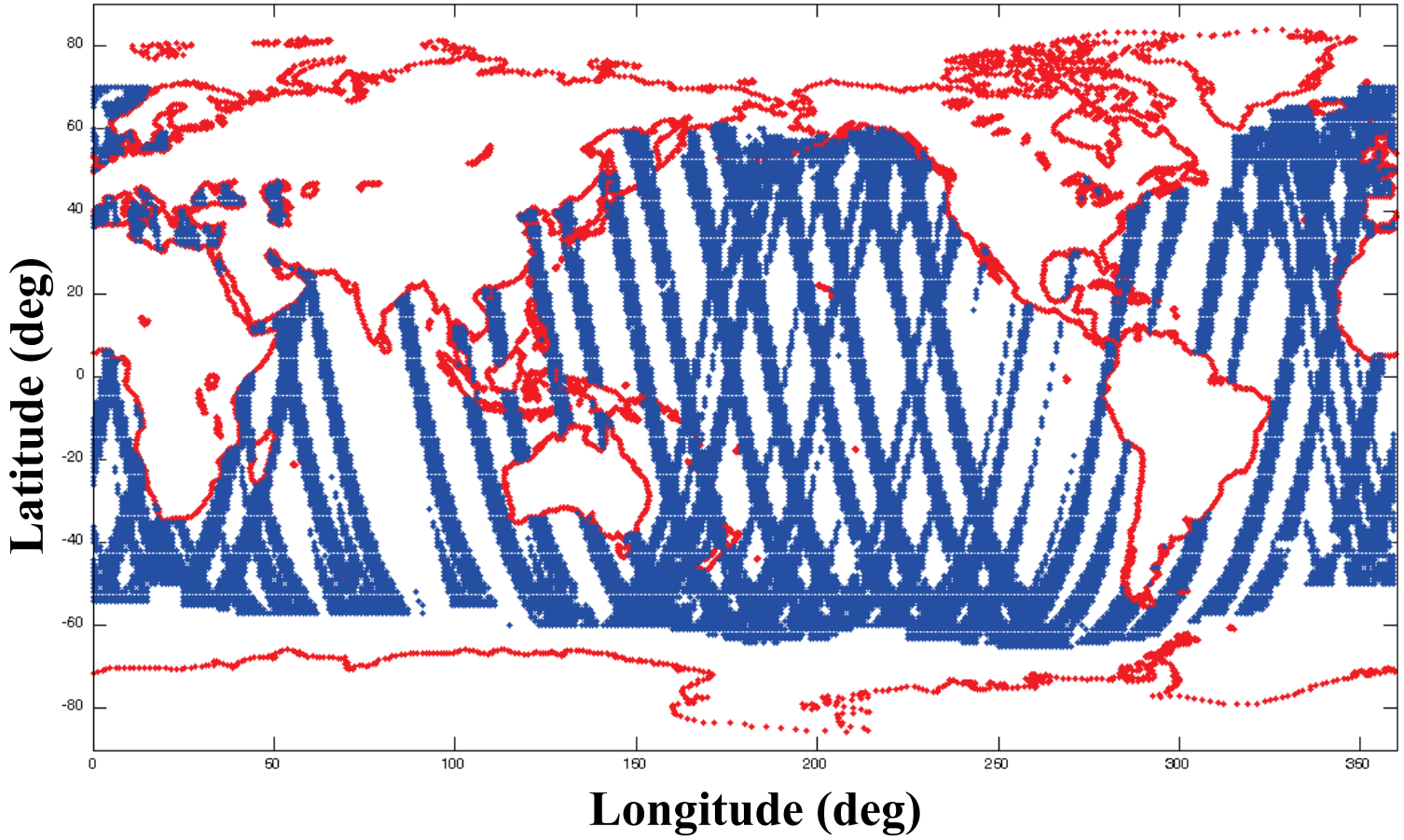

Figure 4.4: MWR and WindSat $1^o \times 1^o$ collocation boxes for first 65 MWR revs.

4.2 Results

The MWR instrument was powered on after 81 days from SAC-D launch on August 30th, 2011. The first T_b images were produced using the pre-launch algorithm (v2.0) $\sim$ 6 hours after the data reception on Wednesday, August 31st, 2011. The v2.0 algorithm is based on the analysis of the T/V data and as mentioned earlier, it gives an estimate of the antenna temperature (T_a) but not the actual main beam brightness temperature (T_b). Thus a comparison of the MWR T_a with WindSat T_b is performed after gathering 65 MWR orbits. Figure 4.4 shows the location of $1^o \times 1^o$ collocation boxes over earth using these 65 MWR revs. The MWR bias computed from this dataset is a bias between MWR T_a and the true scene T_b. Thus the bias equation in equation 4.5 can be re-written as,

$$MWRBias = (T_a^{obs})_{MWR} - (T_b^{pred})_{MWR-WindSat} \tag{4.7}$$

Where, $(T_a^{obs})_M WR$ is the MWR observed T_a computed using v2.0 of the calibration algorithm. Now, if we model this bias as a linear function of $(T_a^{obs})MWR$,

$$MWRBias = slope \times (T_a^{obs})_{MWR} + offset \tag{4.8}$$

then the MWR observed T_b can be calculated as,

$$(T_b^{obs})_{MWR} = (T_a^{obs})_{MWR} - (slope \times (T_a^{obs})_{MWR} + offset) \tag{4.9}$$

The form of equation 4.9 is an effective antenna pattern correction (APC) [9]. Figure 4.5(a) shows the comparison between $(T_a^{obs})_{MWR}$ and $(T_b^{pred})_{MWR-WindSat}$ in equation 4.7 for K band Horn#1. The purple line passing through the origin is of unity slope. If the v2.0

algorithm output were 'true' MWR T_b (at least with respect to WindSat) then the scatter diagram would have lined up along the purple line. Instead, we can see a slope and offset error which needs to be corrected using equation 4.9. Figure 4.5(b) shows how the comparison looks like after correction. Note that the estimation of slope and offset is done for each beam separately and for each receiver. The 'strange' outliers, visible above the purple line away from the dense region, are not considered while estimating correction coefficients. These outliers will be discussed later in the "MWR Anomalies" sub-section.Figure 4.6 and 4.7 shows the same comparison for Ka band H- and V-pol repectively. Note that, there is smaller slope error compared to K band channel. The offset for Ka band V-pol seems to be larger than all other channels. All the comparisons shown here are for Horn#1 of each antenna system. This correction is implemented in the v2.1 of the calibration algorithm.

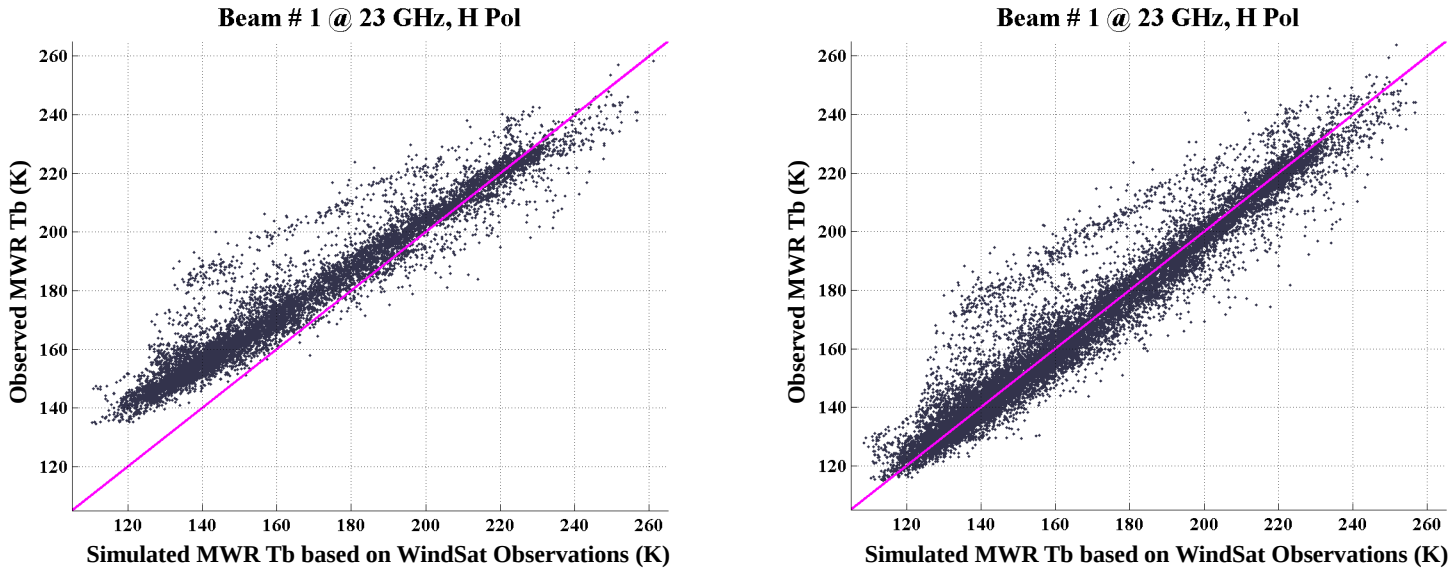

(a) (b)

Figure 4.5: Comparison between MWR real observations (y-axis) and Simulated MWR based on WindSat (x-axis) observations for K band H-pol Horn#1, before (a) and after (b) slope offset correction.

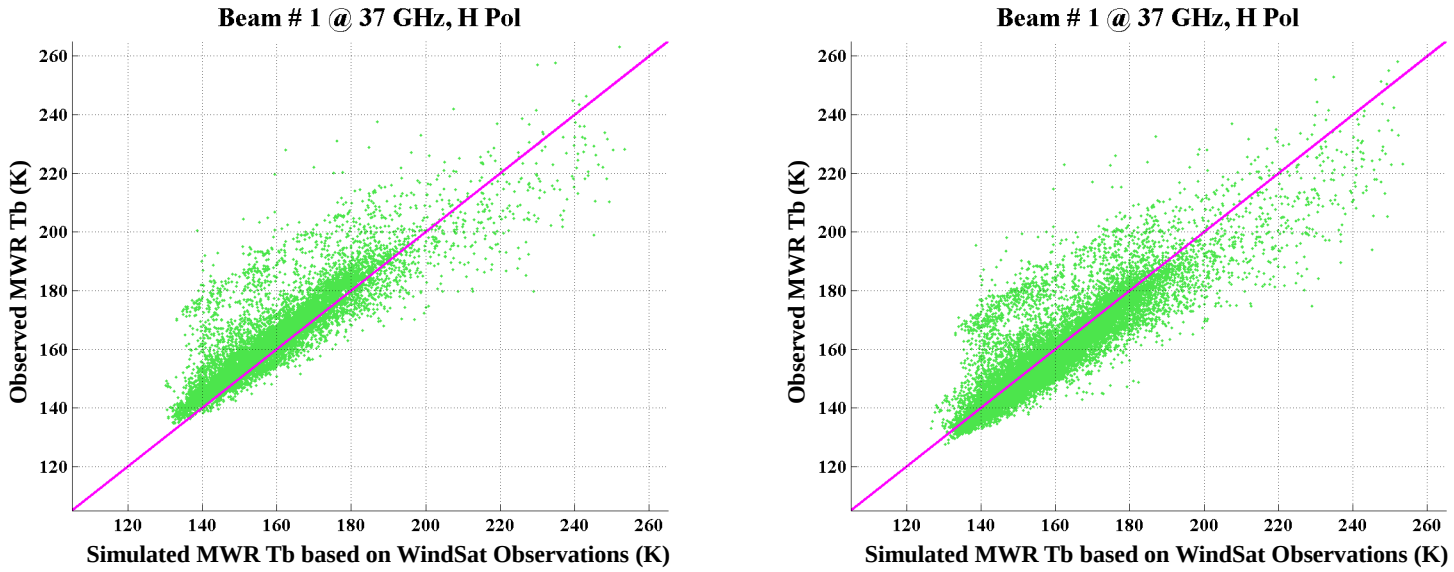

(a) (b)

Figure 4.6: Comparison between MWR real observations (y-axis) and Simulated MWR based on WindSat (x-axis) observations for Ka band H-pol Horn#1, before (a) and after (b) slope offset correction.

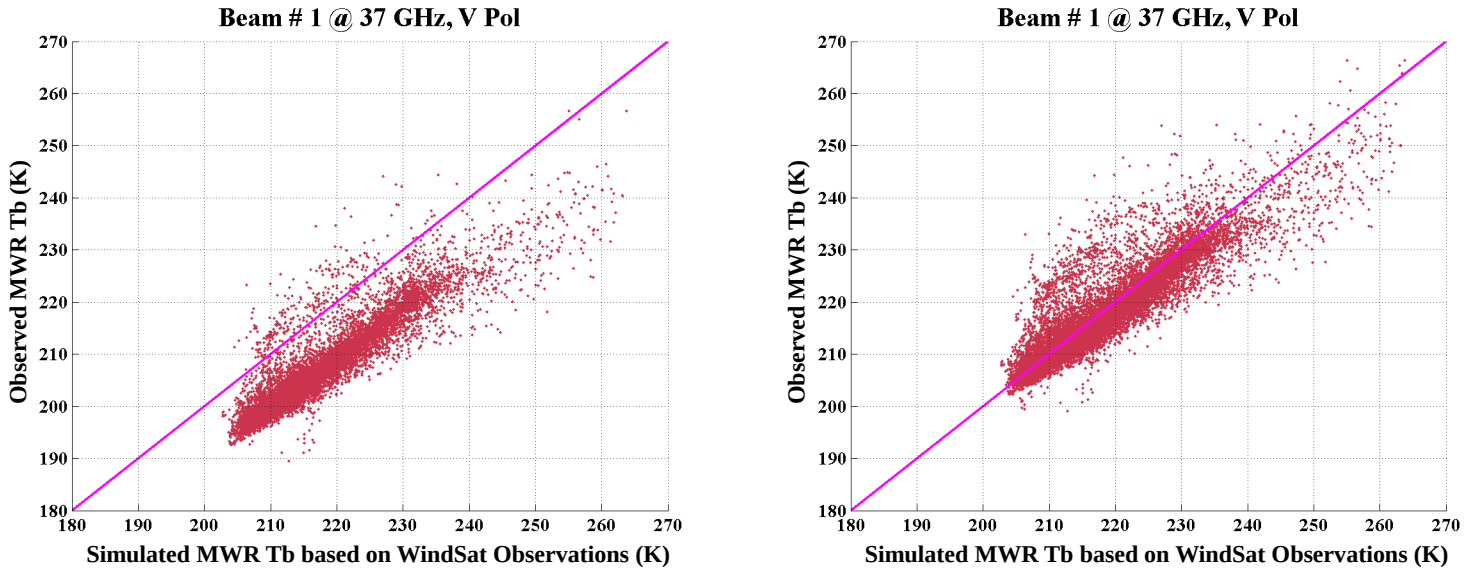

(a) (b)

Figure 4.7: Comparison between MWR real observations (y-axis) and Simulated MWR based on WindSat (x-axis) observations for Ka band V-pol Horn#1, before (a) and after (b) slope offset correction.

The earth-located brightness temperature images using v2.1 of MWR calibration algorithm are shown in Figs. 4.8 to 4.10 for Ka band H-pol, Ka band V-pol and K band H-pol respectively. These were the first global images from MWR instrument including only ascending portions of all orbits from Aug 31st through Sept 4th, 2011. The along-track visible gaps in the T_b images suggests that the one sided narrow swath of ascending MWR is unable to completely cover the entire earth in five consecutive days. There is no spatial averaging or gridding done to generate these images. The bore-sight location of the T_b's are plotted here, appending ascending portions of the consecutive orbits. The idea was to make a 7 day global coverage map, similar to what is produced by the Aquarius instrument but due to technical problem with PAD memory MWR data was lost starting Sept 5th, 2011. The PAD was reset and data capturing again started after 9 days on Sept 14th. Therefore, being the first of their kind, Figs. 4.8 to 4.10 has historical significance in MWR mission, even though they fail to cover the entire earth. The figures are physically meaningful and they prove proper functioning of the instrument hardware. For example, at Ka band, in the range of MWR incidence angles (52° and 58°) the vertical polarized component of the ocean emission is much stronger compared to the horizontal polarized component. This phenomenon is captured in Figs. 4.8 and 4.9 where for Ka band H-pol (Fig. 4.8) the average ocean T_b is close to 140 K and for the V-pol (Fig. 4.9) it is above 200 K. Another interesting feature in the Fig. 4.9 is the visible stripes caused by the measured T_b difference between MWR even and odd numbered beams which are at two different incidence angles (52° and 58°). The sensitivity of ocean emission to the incidence angle variation is greater at V-pol compared to the H-pol.

Hence the stripes are only visible in Fig. 4.9 but not in Fig. 4.8. As demonstrated by the RTM simulations in Fig. 4.3 the T_b sensitivity to WV is higher for frequencies near 22 GHz water vapor line. Thus MWR's 23.8 GHz channel is expected to have strongest response to atmospheric WV. This is demonstrated in Fig. ch4fig9; a much warmer T_b is observed near ITCZ (Inter-Tropical Convergence Zone) and other precipitating regions where a higher WV density is expected. The Ka band (36.5 GHz) images also show these features but the contrast is much lower compared to K band (23.8 GHz). Also the presence of sea ice on the ocean surface warms up the T_b emission for all the MWR channels. The sea ice edges in the Antarctic region can be easily seen in the three images. The emissivity difference between land ice and sea ice is also demonstrated in the figure. For example, there is a distinct difference in color between the Greenland (land ice) and the ice sheet at the edge of Antarctica (sea ice). It is exciting to notice some of the severe weather features like a typhoon near Japan coast and a tropical storm in the Gulf of Mexico etc. The geolocation accuracy of these images were verified separately and found to be exceeding the mission requirements [30].

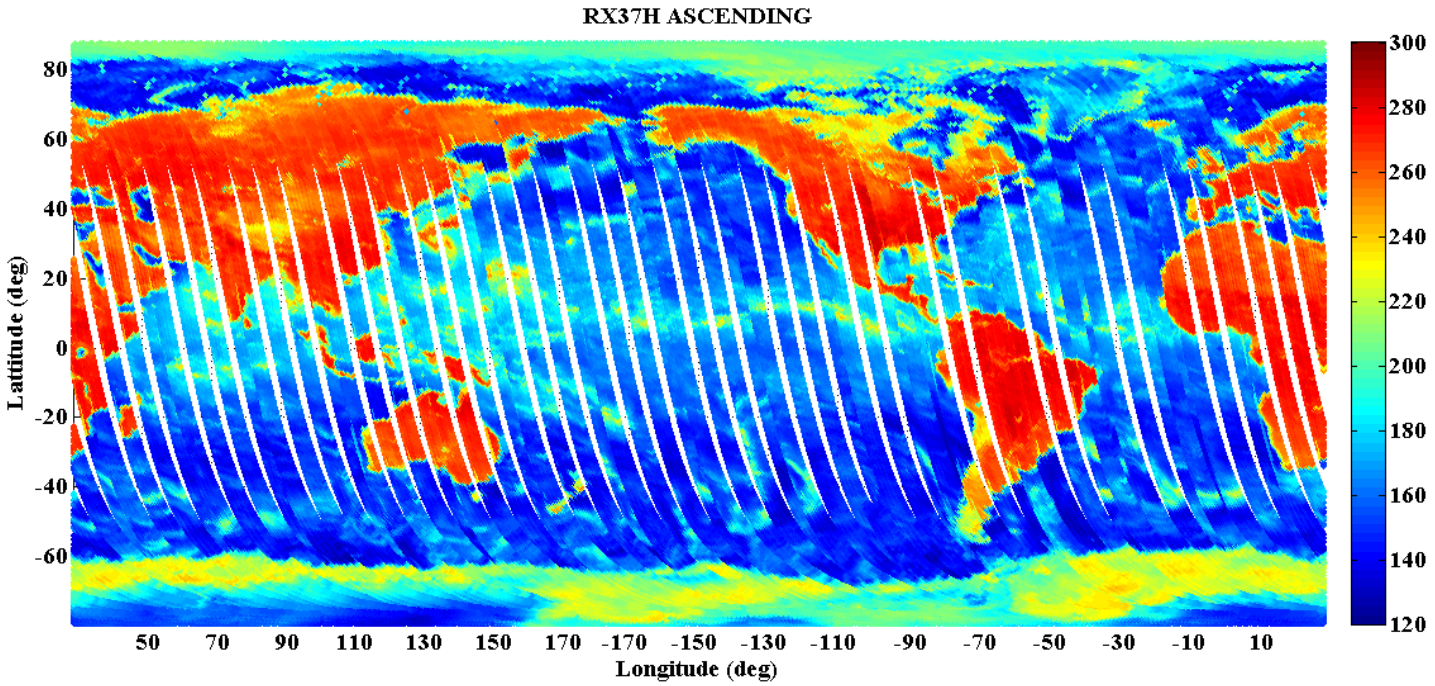

Figure 4.8: Ka band (36.5 GHz) H-pol brightness temperature image for first five days (Aug 31st - Sept 4th, 2011) combining all ascending passes. The colorbar is in Kelvin.

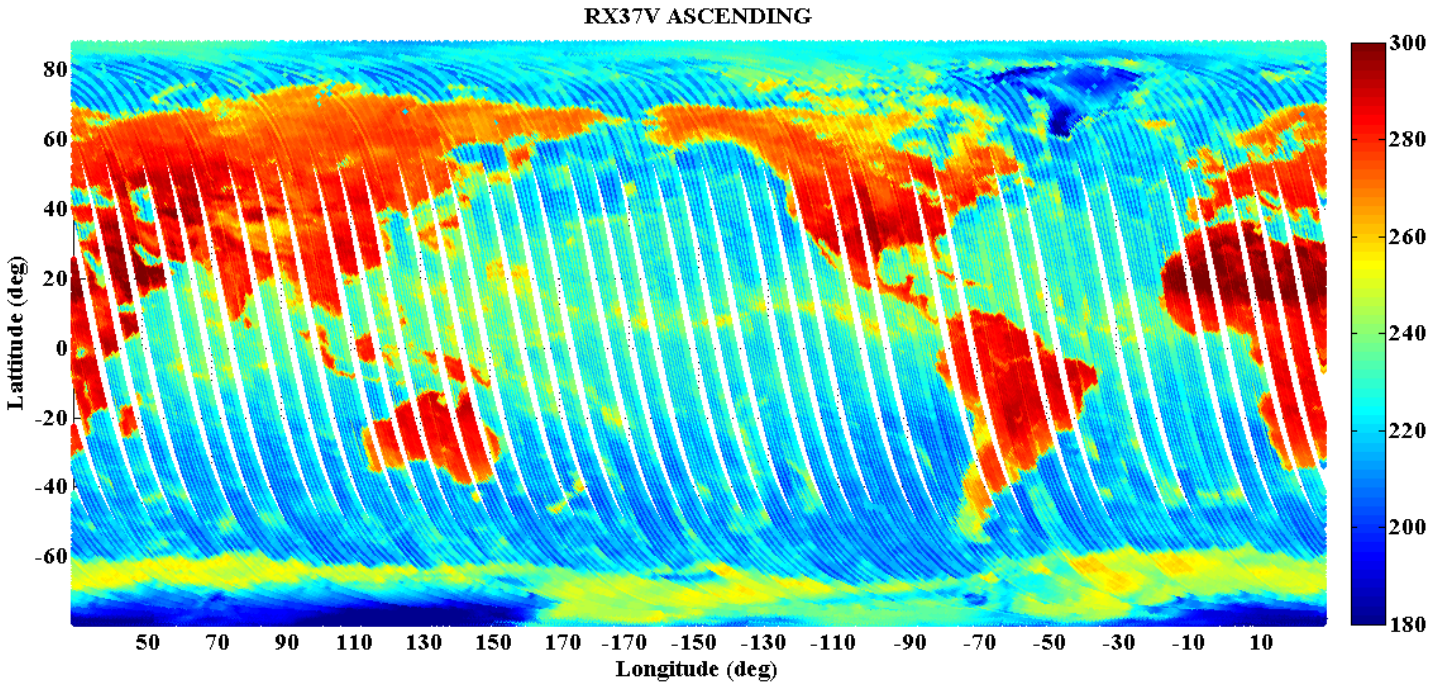

Figure 4.9: Ka band (36.5 GHz) V-pol brightness temperature image for first five days (Aug 31st - Sept 4th, 2011) combining all ascending passes. The colorbar is in Kelvin.

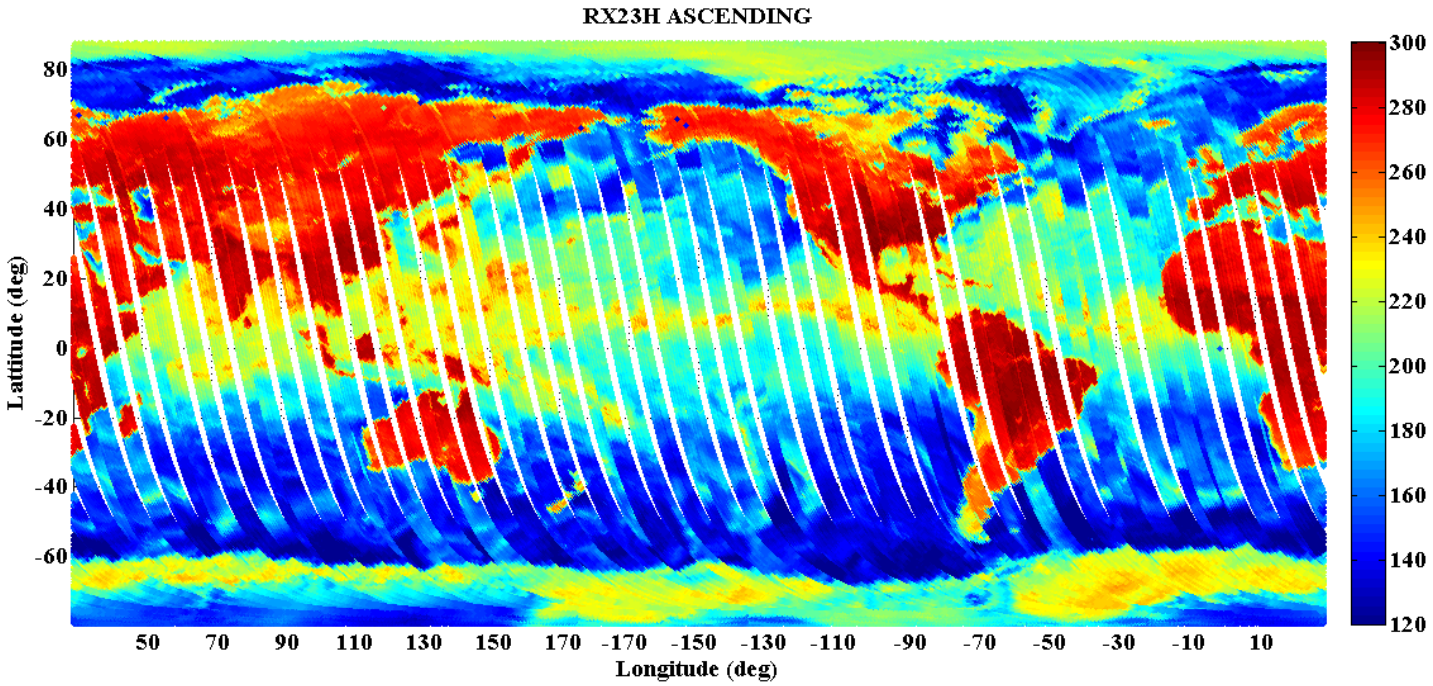

Figure 4.10: K band (23.8 GHz) H-pol brightness temperature image for first five days (Aug 31st - Sept 4th, 2011) combining all ascending passes. The colorbar is in Kelvin.

The PAD was rebooted on Sept 14th, 2011 and MWR data capturing was resumed. The slope/offset correction coefficients of v2.1 algorithm are further tuned after obtaining 127 revs of MWR data. The mean biases are observed to get shifted when the v2.1 algorithm is applied to the new data. These shifts are adjusted in v2.2 algorithm. A comparison between MWR bias histograms using pre-launch (v2.0) and the improved post-launch (v2.2) calibration algorithm is shown in Fig. 4.11, for the 23.8 GHz H-pol channel. It should be noted that the v2.0 bias histograms (marked with dashed lines) are severely distorted and not any close to the ideal Gaussian shape. Whereas, after the slope/offset correction, the v2.2 bias histograms (solid line) are zero mean and of Gaussian shape. Also the biases for all the beams are balanced with respect to each other. Figure 4.12 and 4.13 show similar histogram plots for 36.5 GHz H- and V-pol respectively. At the time of writing this dissertation the v2.2 data is already distributed to the Aquarius cal/val science team for evaluation.

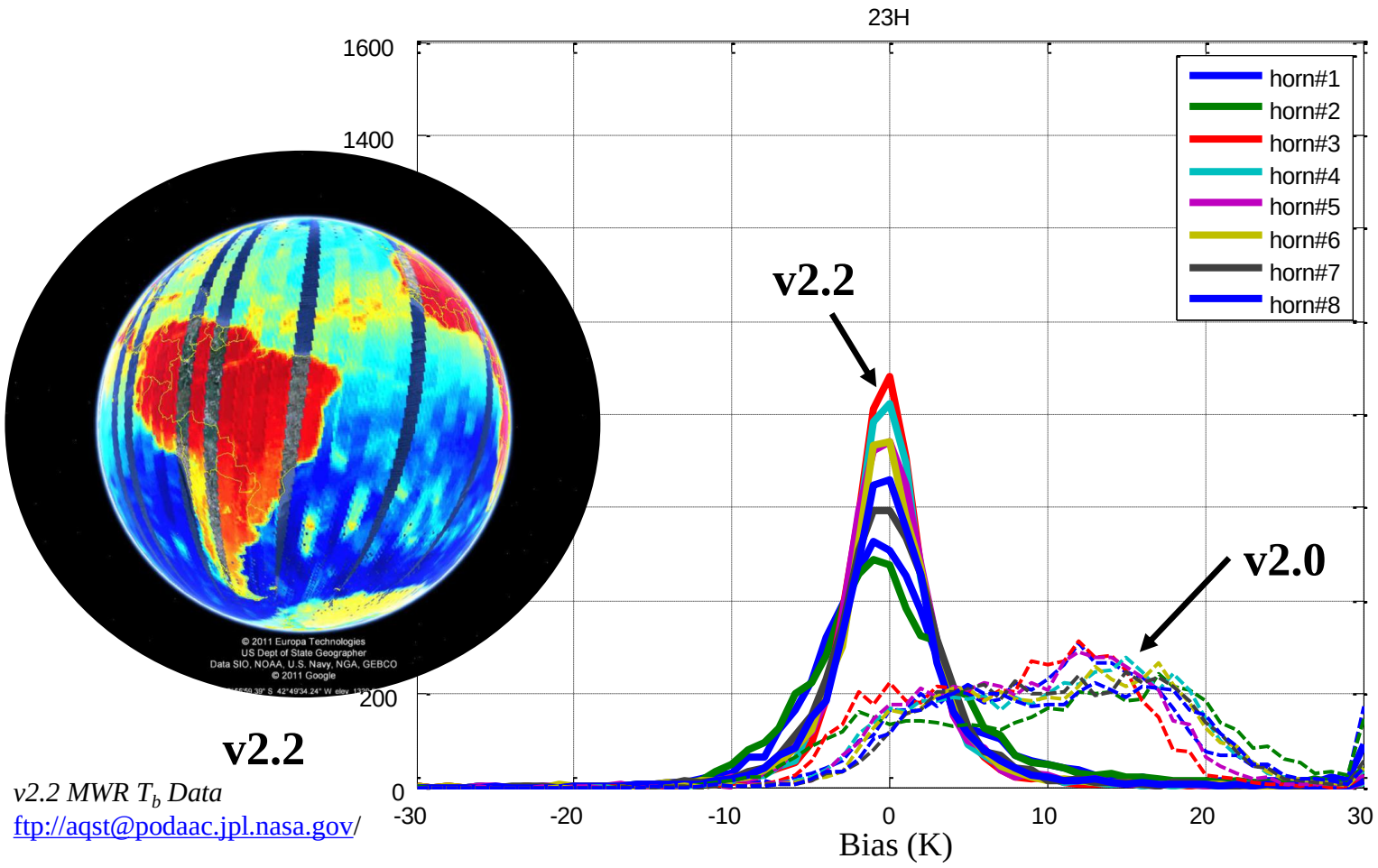

Figure 4.11: MWR 23.8 GHz H-pol bias histograms for all horns before (v2.0) and after (v2.2) final slope/offset correction.

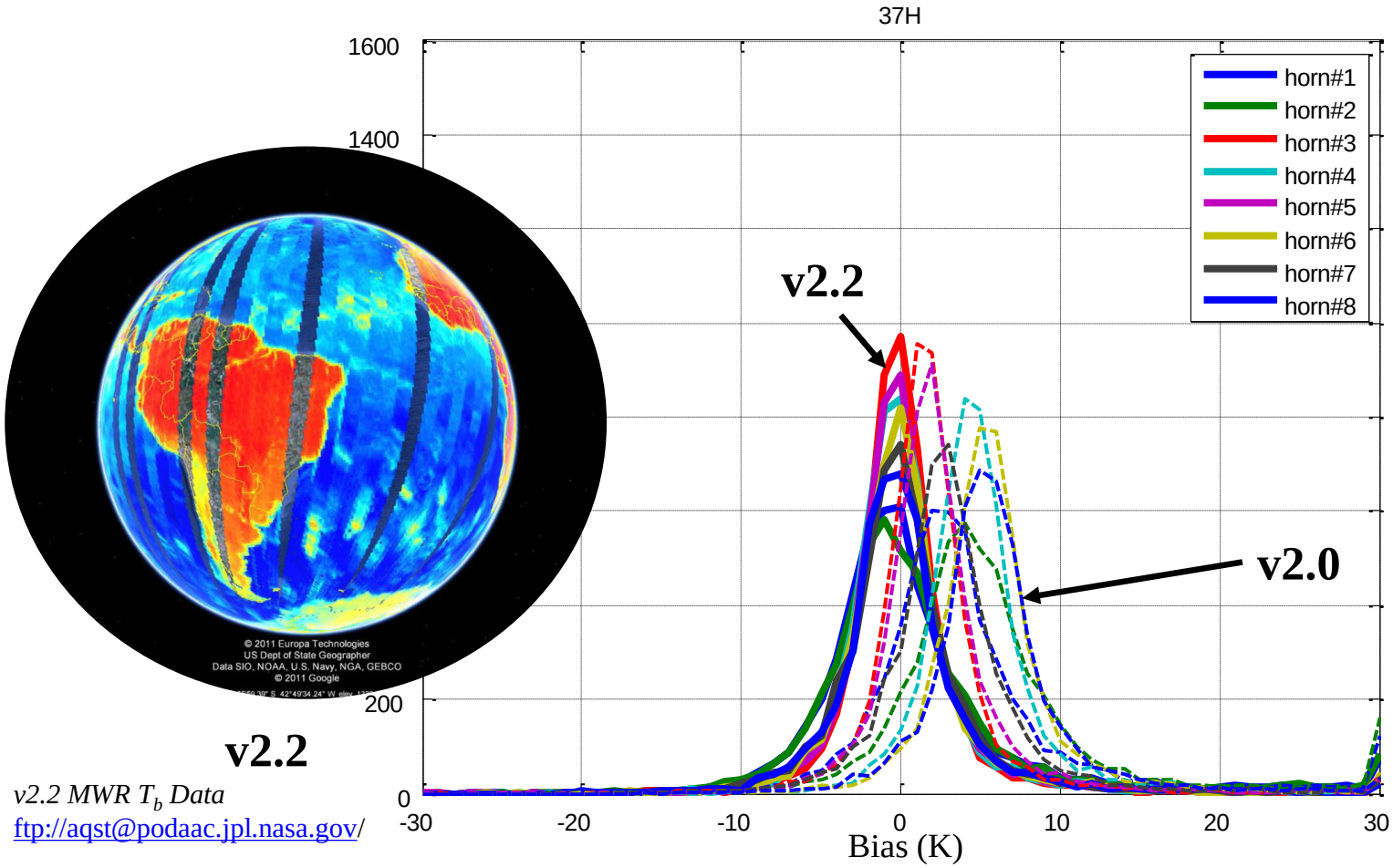

Figure 4.12: MWR 36.5 GHz H-pol bias histograms for all horns before (v2.0) and after (v2.2) final slope/offset correction.

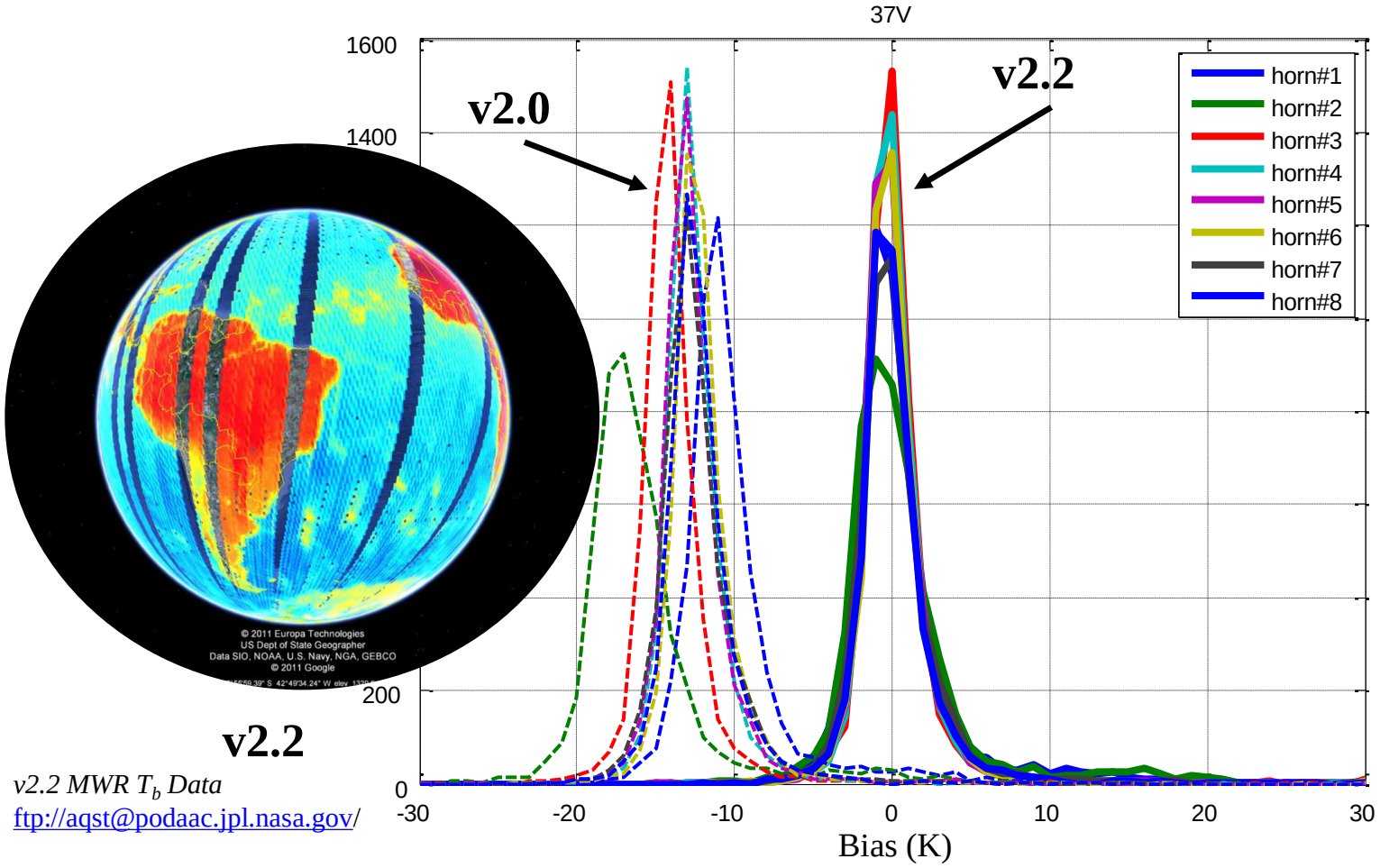

Figure 4.13: MWR 36.5 GHz V-pol bias histograms for all horns before (v2.0) and after (v2.2) final slope/offset correction.

4.2.1 MWR Anomalies

The MWR "On Orbit Check Out (OOCO)" period began just after the instrument turn on. In this period several issues with MWR T_b's were observed. The three major issues which affect MWR T_b calibration are discussed in this section.

4.2.1.1 Beam Smearing

To investigate the outliers in Fig. 4.5 to 4.7 the plot in Fig. 4.5(a) is reproduced in Fig. 4.14(a) with colorbar representing the positive bias magnitude in unit of Kelvin. The $1^o \times 1^o$ bias boxes with bias value <16 K are plotted on a global map in Fig. 4.14(b). Close inspection revealed that these boxes are near coastline and near small islands in the ocean. Also it can be seen that most of the times there are series of boxes aligned along the MWR flight track. To understand these anomalies further Australia coast is chosen. Figure 4.15 shows an image of MWR 36.5 GHz H-pol channel made by combining few consecutive ascending passes over Australia. The beam bore-sights are plotted with color indicating T_b values in K. It is found that the ocean measurements near land getting affected by land brightness. For example in region #1 & #2, in Fig. 4.15, non-physical warm T_b over ocean is seen along the flight track for some of the MWR beams. These are the cause of the large outliers in T_b biases as shown in Fig. 4.14.

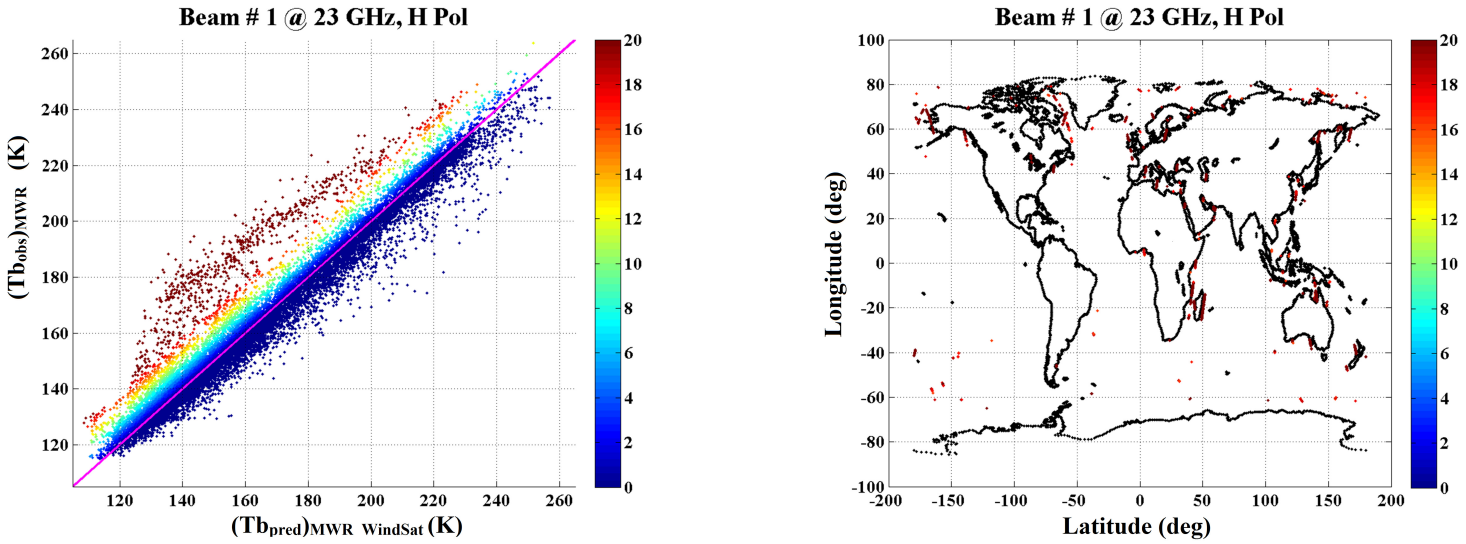

(a) (b)

Figure 4.14: (a) Comparison between MWR real observations (y-axis) and Simulated MWR based on WindSat (x-axis) observations for K band H-pol Horn#1 using v2.1 algorithm. The colorbar represents positive bias in K. (b) The positive biases <16 K is plotted on global map. Most of these points are located near coast line and islands.

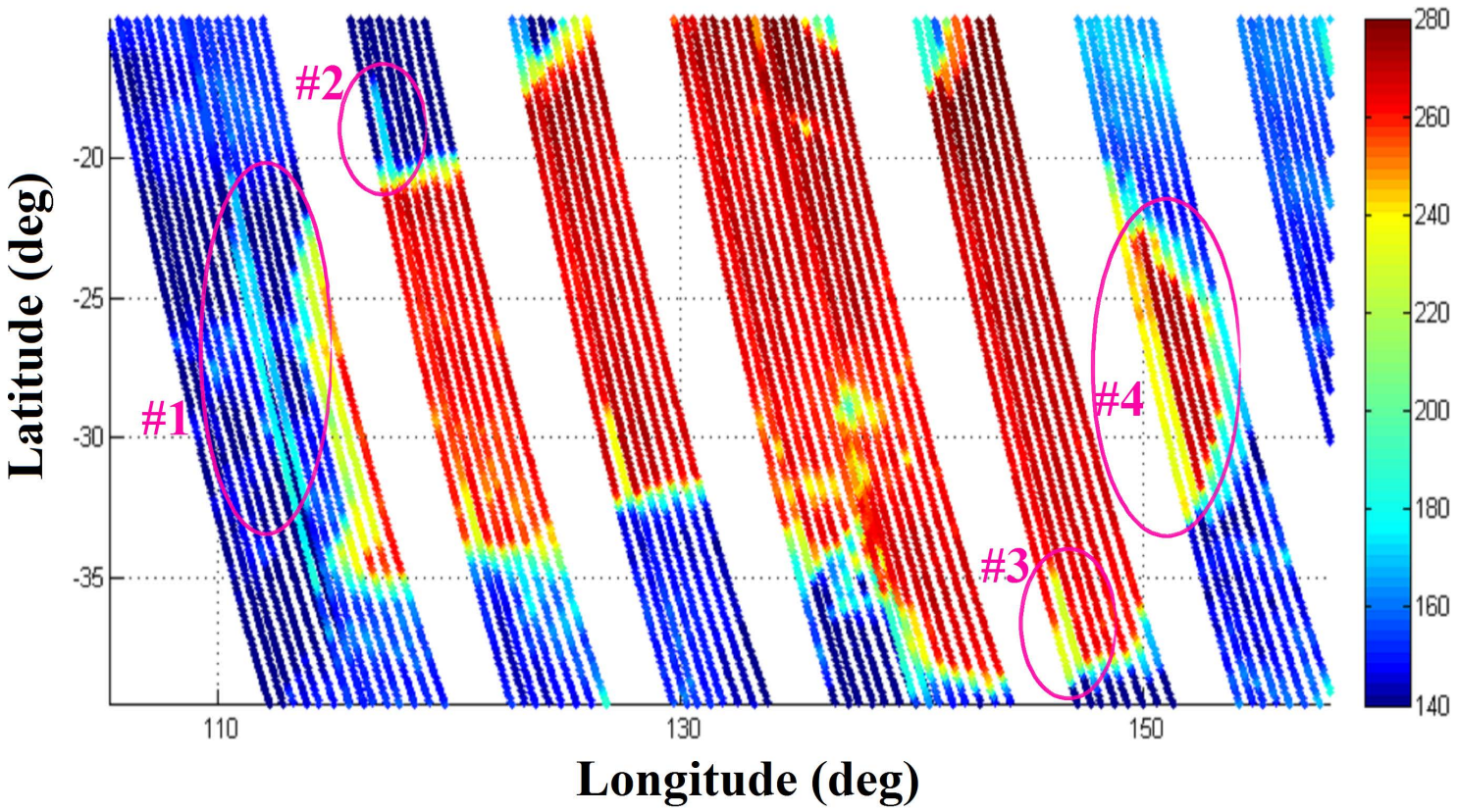

Figure 4.15: 36.5 GHz H-pol brightness temperature (T_b) measurements over Australia for consecutive ascending passes showing T_b anomalies over land and ocean.

From Fig. 4.15 another thing came into notice was that, it is not only ocean T_b's that are getting affected but the land T_b's also showing similar anomaly. For example, in region #3 and #4, non-physical colder T_b over land along the flight track for some of the MWR beams was observed. The cause for these T_b anomalies, visible near land-water crossings, is being analyzed at this moment.At the time of writing this dissertation CONAE has figured out an effective correction at the "count" level to tackle this problem.

MWR receivers are time-shared between different horns. The antenna-switching network ensures that only the incident T_b from the horn under observation enters the receiver during a complete observation period of 240 ms. This 240 ms is composed of 8 samples from each of the radiometer states - antenna, antenna + noise and reference load [Fig. 2.5]. MWR's digital back-end adds these 8 measurements for each state to produce a single science measurement for a particular horn, which is then stored as a single MWR data frame on-board PAD and transmitted later via downlink. All the receivers of MWR operate in parallel. For example in a given 240 ms interval each of the outputs K band H, Ka band V, H, +45 and -45 generate counts for three radiometer states - total 15 count values. All the data from an integration period (240 ms) is put in one MWR data frame. There is a pre-defined sequence in which MWR horns are being sampled by the receiver. This information is encoded in the least significant byte (LSB) of the two bytes long "MWR ID" field in each MWR frame (Fig. 4.16). The mapping of antenna horn # and LSB identifier value is different for 23.8 GHz and 36.5 GHz receiver.

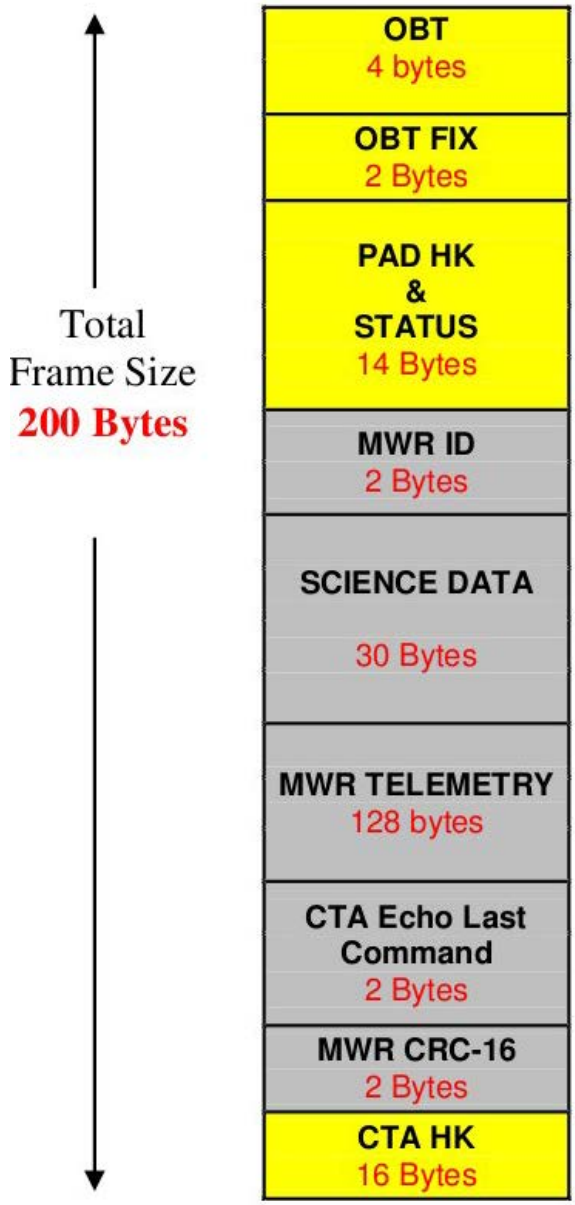

Figure 4.16: Description of MWR data frame containing 240 ms of integrated measurement.

Table 4.2: K band (23.8 GHz) LSB identifier and corresponding feed horn #

23.8 GHz Antenna	
Observed Horn	LSB Identifier
Horn #2	0x01
Horn #4	0x02
Horn #6	0x03
Horn #8	0x04
Horn #1	0x05
Horn #3	0x06
Horn #5	0x07
Horn #7	0x08

Table 4.3: Ka band (36.5 GHz) LSB identifier and corresponding feed horn #

36.5 GHz Antenna	
Observed Horn	LSB Identifier
Horn #1	0x01
Horn #3	0x02
Horn #5	0x03
Horn #7	0x04
Horn #2	0x05
Horn #4	0x06
Horn #6	0x07
Horn #8	0x08

Table 1 and 2 tabulates the relationship for 23.8 GHz and 36.5 GHz receivers respectively.

It should be noted that for K band the horn sampling sequence is 7, 2, 4, 6, 8, 1, 3, 5, 7, 2,

while the corresponding sequence for Ka band is 8, 1, 3, 5, 7, 2, 4, 6, 8, 1, . CONAE's initial investigation revealed that the "beam smearing" problem visible near land-water crossings, is due to mixing of T_b from the previously sampled horn in the current horn under observation. For example, in the K band receiver, horn# 2 T_b is contaminated by horn# 7 T_b and horn# 4 T_b is contaminated by horn# 2 T_b etc. The same is true for the Ka band system also where horn# 1 is affected by horn# 8 and all the successive measurements are affected by their previous measurements. Thus the T_b's are recursively coupled. This effect is the minimum when consecutive horns are looking at same range of brightness temperature. Thus over the Ocean in clear weather condition or over landmasses with not much T_b variation, this artifact in T_b image is not clearly visible. The effect is the maximum when the two consecutive horns are looking at Tb scenes with a very large difference, e.g. one foot-print is over land and other is over ocean. The maximum effect is observed in horn# 2 (contaminated by horn #7) because of the large spatial separation of the footprints of horn# 7 and horn# 2. Similar problem exists also in horn# 1 due to horn#8. The findings of CONAE team and the correction algorithm is reported in [31]. Even though a seemingly right correction is in place the reason for this anomaly is not yet fully justified. More analysis is in progress.

4.2.1.2 Receiver Non-Linearity

During the laboratory calibration test using external "hot" and "cold" T_b sources it was found the MWR receivers have a compressive non-linearity at higher input power level (see

section 3.2). Figure 3.12 demonstrates that the noise diode deflection is lower for high input power level (i.e. input $T_b \sim 300$K) because of the compression. It was also mentioned that, if the non-linearity is not corrected in future, the MWR will not produce accurate T_b's over Land (T_b¿300K). In equation 3.25 a quadratic term is introduced to take care of the non-linear behavior of the receiver, but since non-linearity is a function of physical temperature, a fixed coefficient for quadratic term may not work in practice. The presence of non-linearity in MWR counts is experimentally verified using on-orbit data. In Fig. 4.17 the noise diode deflection counts $(C_{a+n} - C_a)$ is gridded into $0.5^o \times 0.5^o$ boxes over earth with color showing average number of deflection counts in a box. In an ideal linear radiometer, the plotted quantity should be independent of antenna signal. The noise diode deflection $(C_{a+n} - C_a)$ is equal to the radiometer gain (G) times the injected noise diode temperature (T_n). Since T_n is assumed to be a stable reference, the deflection is a measurement of instrument gain G. In Fig. 4.17, however we can see the landmasses and some of the strong weather patterns over ocean. The noise diode deflection cannot be correlated with the geophysical scene under observation, thus the image is definitely not of pure instrument gain. It should be noted that the deflection is less in the regions where high value of scene T_b is expected; for example, over land and strong weather etc. Thus it could be concluded that the receiver is compressing high input power signal from land and weather causing systematic low deflection counts for those scenes.

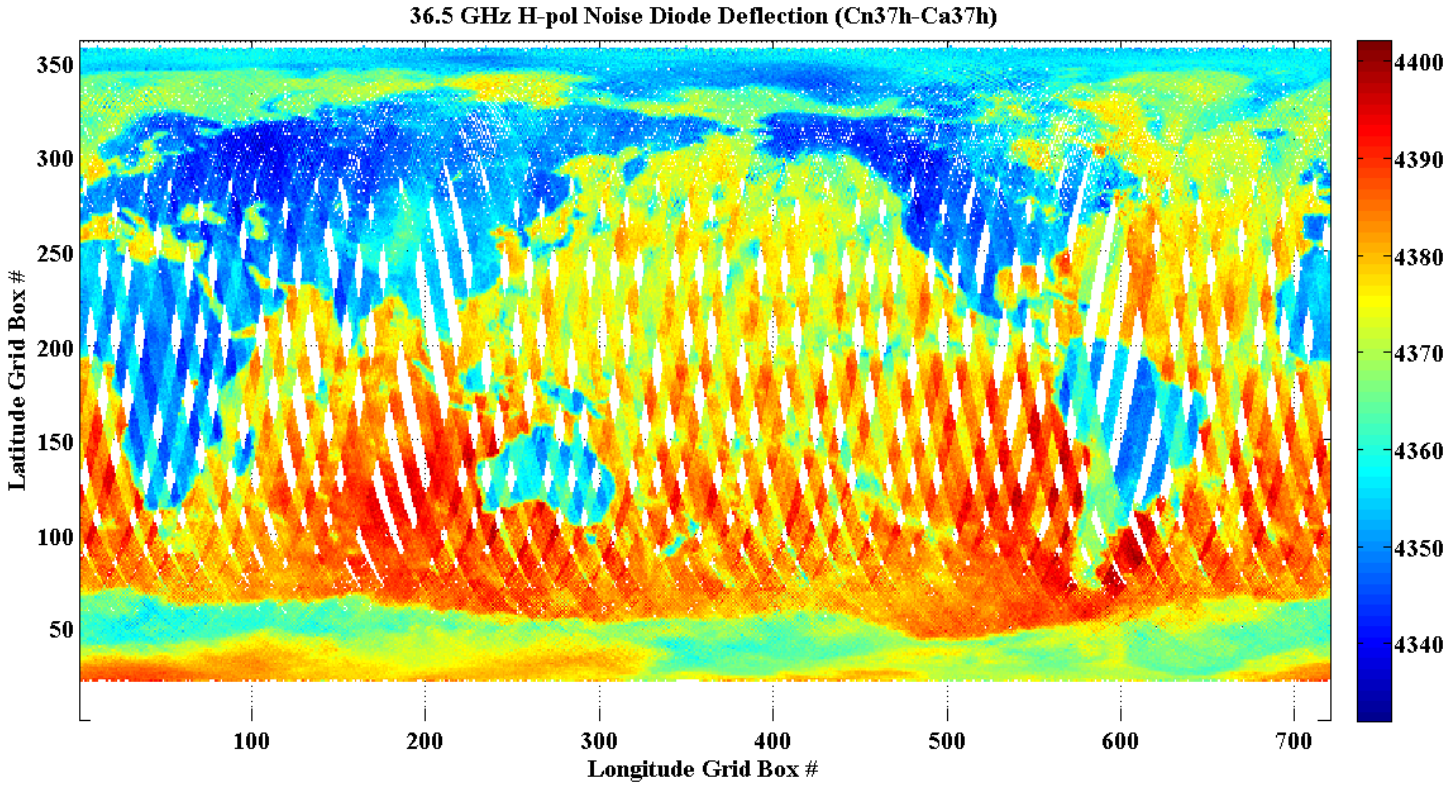

Figure 4.17: Image of noise diode deflection ($C_{a+n} - C_a$) counts for 36.5 GHz H-pol, gridded in $0.5^o \times 0.5^o$ boxes over the earth. The colorbar unit is radiometer counts. Due to the non-linearity of the receiver the deflection is lower over high T_b scenes like land, weather etc.

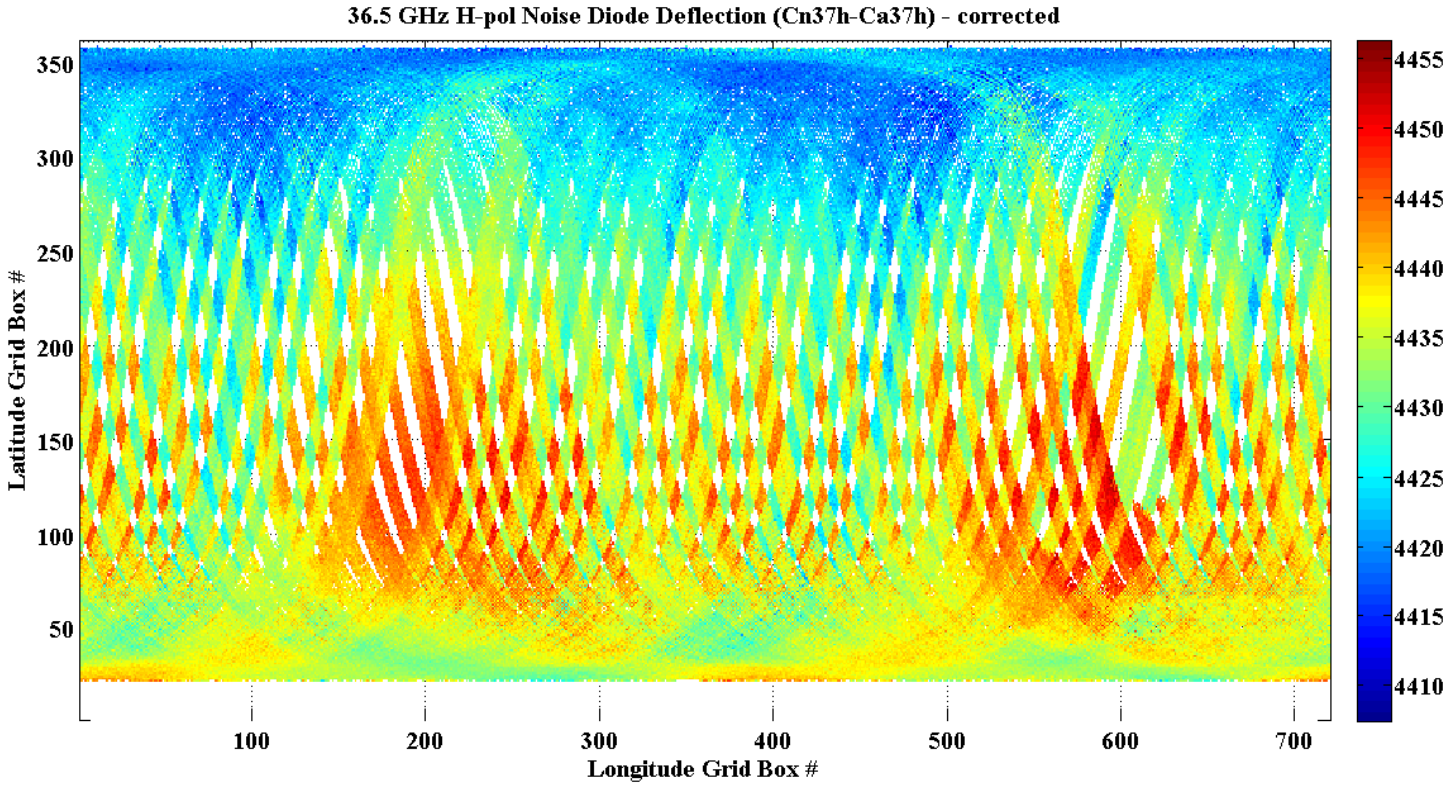

Figure 4.18: Image of noise diode deflection ($C_{a+n} - C_a$) counts after non-linearity correction for 36.5 GHz H-pol, gridded in $0.5^o \times 0.5^o$ boxes over the earth. The colorbar unit is radiometer counts. The deflection does not depend on the scene T_b anymore.

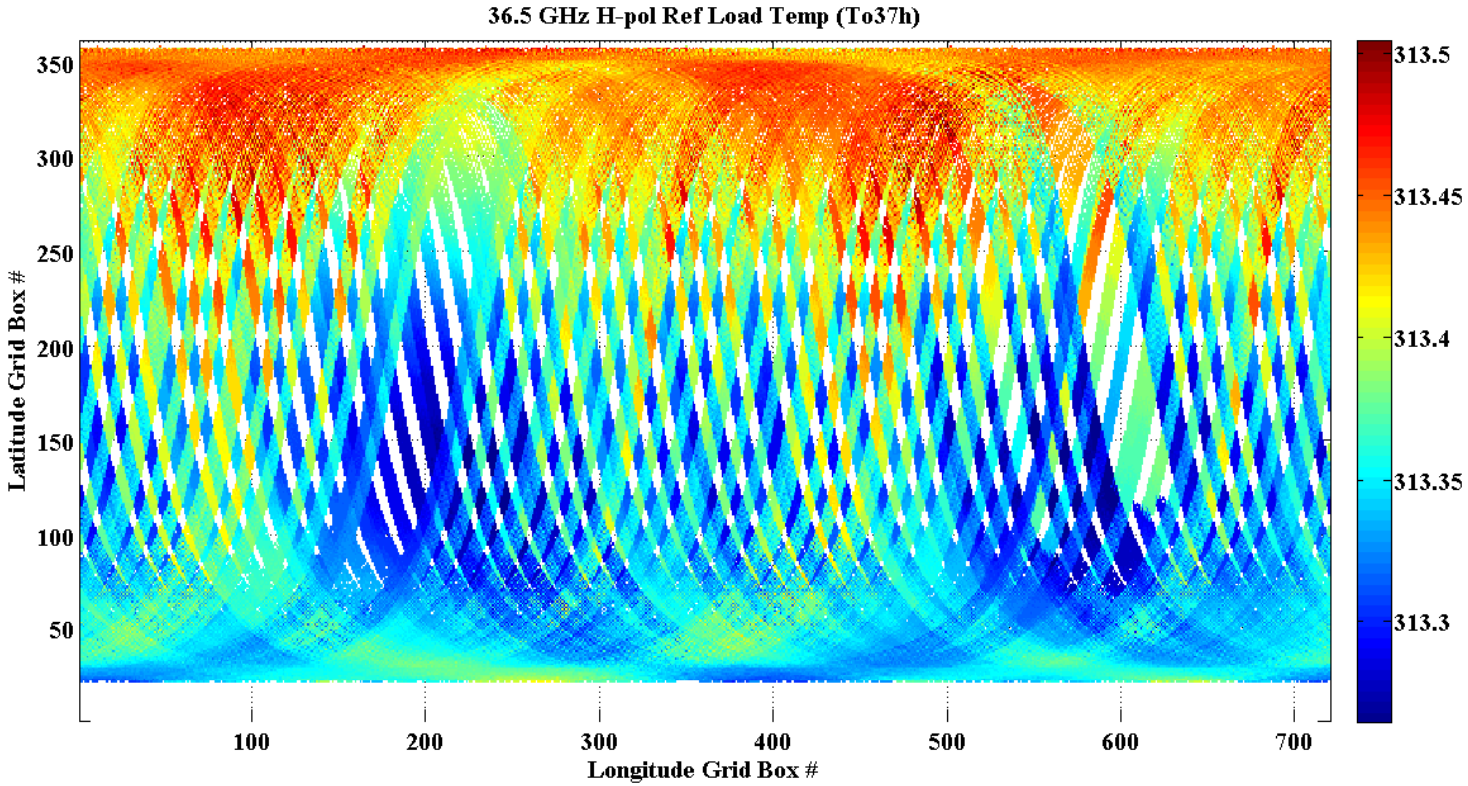

Figure 4.19: Image of reference load temperature (T_o) for 36.5 GHz H-pol, gridded in $0.5^o \times 0.5^o$ boxes over the earth. The colorbar unit is in K. Due to the sun angle variation in orbit T_o is warmer in the northern hemisphere compared to southern hemisphere. The instrument gain is supposed to follow the reverse trend which is observed in the deflection of Fig. 4.18.

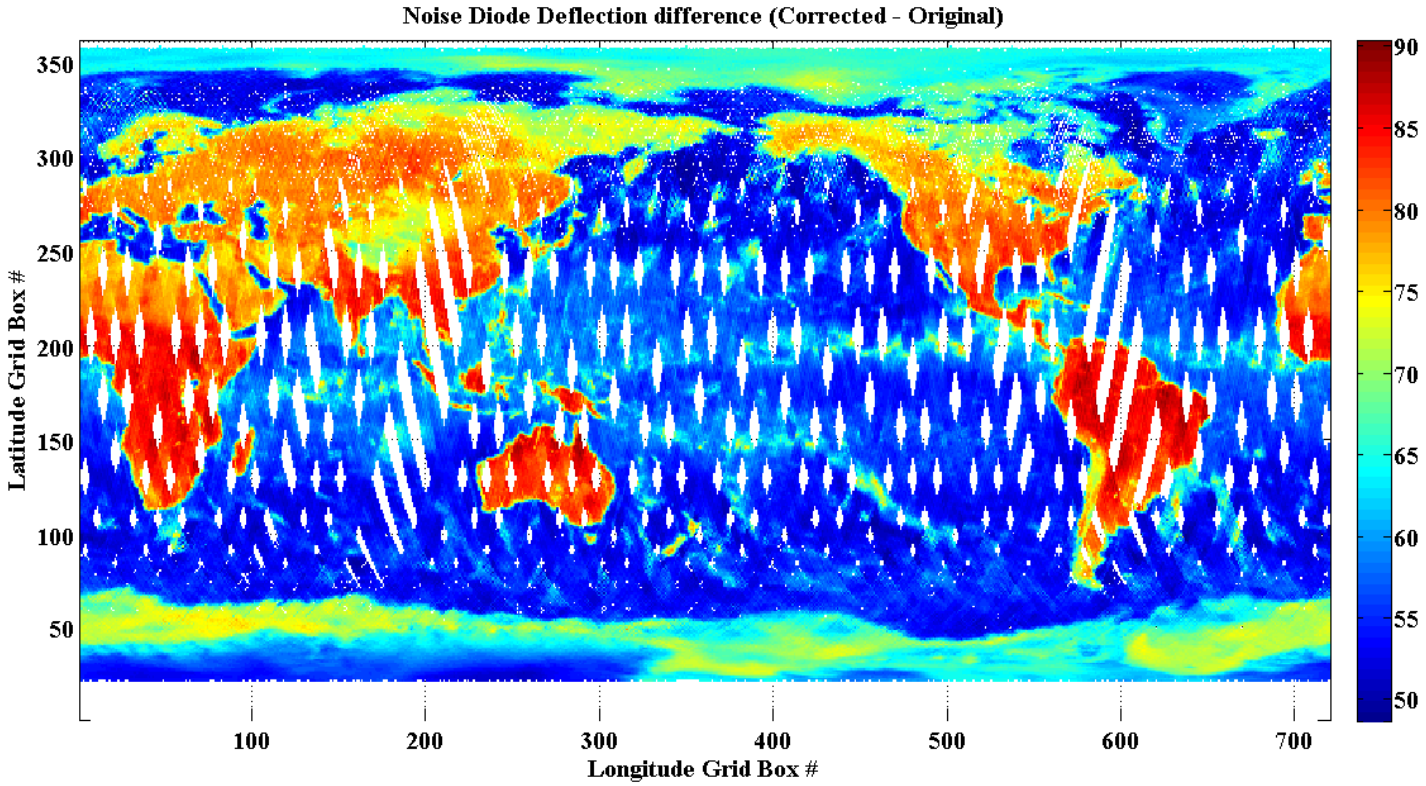

Figure 4.20: The difference image of Fig. 4.18 and Fig. 4.17 showing the degree of correction in terms of count to correct for non-linearity effect. The correction has a dynamic range of 40 counts which is equivalent to 2.44 K in terms of brightness temperature.

As mentioned earlier, non-linearity is a strong function of physical temperature of the receiver. The best possible correction method can be implemented on the raw MWR measurement counts if the non-linear transfer function of the receiver could be characterized over range of physical temperatures. For example, if the count from the non-linear receiver is C, then the linearized count C_{lin} could be modeled as,

$$C_{lin} = f(C, T_{phy}) \tag{4.10}$$

The function $f(C, T_{phy})$ is basically a polynomial function of counts where the coefficient of the polynomial are a function of physical temperature (T_{phy}) of the instrument. A generic form of this correction could be

$$f(C, T_{phy}) = a_0 + a_1 C + a_2 C^2 + \ + a_n C^n \tag{4.11}$$

where, the coefficients a_i's are function of T_{phy}. In simplest form they are linear functions of the form,

$$a_i = b_{0i} + b_{1i} T_{phy} \tag{4.12}$$

The polynomial expression in the equation 4.11 can be written in a compact form utilizing mathematical functions. For example, in the case of MWR we know that the observed nonlinear transfer function of the instrument is compressive. To correct for it we need an expansive transfer function. A function of the form

$$f(C, T_{phy}) = C(1 + (1/a)exp(C/a)) \tag{4.13}$$

is tested on the data used to create Fig. 4.17. Instead of n number of coefficient in equation 4.11 there is only one coefficient $'a'$ in equation 4.13 which is a function of T_{phy}. A single

coefficient is easier to manipulate and might be convenient while experimentally determining the best fit.

The image in the Fig. 4.17 is reproduced in Fig. 4.18 using linearized counts from equation 4.10 and 4.13 with a = 3500. Since the variation of T_o over the entire-period was less than 1 K (see Fig. 4.19), a fixed value of a = 3500 is used. The land and weather features in the deflection are not present in the corrected image of Fig. 4.18. Note that the decompression algorithm modifies the range of count values hence the colorbar is slightly adjusted so that the images could be compared appropriately. The difference between the corrected image (Fig. 4.18) and the original image (Fig. 4.17) is shown in Fig. 4.20. As the absolute values of the counts are increased by the expansive correction technique, the original image is subtracted from the corrected image to keep the difference positive. The dynamic range of this correction is 50 to 90 counts according to Fig. 4.20. Assuming the mean deflection (from Fig. 4.18) to be 4425 and T_n = 270 K the equivalent correction corresponding dynamic range of 40 counts is 2.44 K.

Unfortunately, there is no laboratory data available to characterize the non-linearity with various physical temperatures so the 'a' coefficient is determined based on several trials. This correction is not implemented in current MWR calibration algorithms. Any form of non-linearity correction affects the entire range of instrument counts including linear to non-linear regions. Therefore, care should be taken so that the linear regions of the receiver not get affected by the correction.

A vicarious way of correcting the effect of non-linearity is by introducing the quadratic

term in equation 3.25, as mentioned before. If T_{in} is the computed brightness temperature using the non-linear counts then the correct value of T_{in} can be obtained by [32],

$$(T_{in})_{corrected} = (T_{in} - a)^2 \tag{4.14}$$

This is equivalent to a 2nd order non-linear correction. The coefficient 'a' is a function of T_{phy} and can be approximated using a linear equation of the form in equation 4.12. Equation 4.14 is the motivation of introducing 2nd order term in equation 3.25.

In future we are hoping to characterize it properly after accumulating enough data statistics. If not corrected, the estimation of receiver gain using noise diode deflection in the calibration equations will be erroneous. Thus the calibrated T_b over land will always be lower than its true value. The effect of non-linearity is expected to be small over the normal range of ocean brightness. The inter-calibration of MWR Ocean T_b's with WindSat is also expected to correct for some of the non-linearity biases.

4.2.1.3 PAD Reset Transients

The Data Acquisition and Processing Subsystem (PAD) is the interface between the NIRST, MWR, DCS and ROSA instruments and the service platform (S/P). In particular, all these instruments do not have a direct interface with neither the S/P nor the downlink but via the PAD. The thermal control algorithm for all these instruments including MWR is implemented in the PAD computer. The memory storage requirement of these instruments is also satisfied by the PAD mass memory. PAD subsystem is cold redundant and composed

by two equivalent electronic boxes: PAD-A and PAD-B, each of them including the complete PAD functionality. Only one is powered by the RTU (Remote Terminal Unit) at any given time, being the selection made by Earth command. The stored information cannot be shared between units as they are never simultaneously operative.

MWR commanding and data handling (C & DH) is controlled by PAD, which receives all commands routed through the S/P C&DH. A total of 128 MB of the PAD mass memory is allocated for storing the MWR science packets, which include both Science data and the high rate HKT (House Keeping Temperature) data. This memory allocation permits two complete days of science and HK data storage without downloading, being flexible to a S/P problem. Six days after MWR turn-on, on 5th September, 2011 a problem with PAD memory was detected. This resulted in loss of MWR science and high rate HKT data. Initial investigations failed to determine the root-cause of the issue and a temporary fix was implemented by resetting the PAD computer on 14th September, 2011. The rebooting of PAD solved the problem for next few days and soon the problem re-surfaced. It should be noted that there are two identical PAD boxes, PAD-A and PAD-B. In the current stage of the mission PAD-A is only active. PAD-B is a complete back-up and will only be active if a hardware failure with PAD-A is determined. However, the memory problem of PAD-A seemed to be associated with the PAD software and most likely to repeat even after turning on the back-up PAD-B. Considering several situations it was determined by the SAC-D project team that unless the problem with PAD-A is fully understood the cold redundant PAD-B will not be turned on. Instead, the project team agreed on a periodic resetting of

the PAD computer approximately every 1.5 days. The rebooting of PAD is planned in a way that most of the time it should occur over land so that the loss of ocean data is minimized.

The periodic rebooting of PAD has a serious effect on the stability of the instrument. As mentioned earlier, MWR's thermal control is implemented in the PAD computer. Therefore, PAD computer reset causes a disruption of MWR's thermal control. This results in temperature transients inside the instrument, which lasts for several orbits.

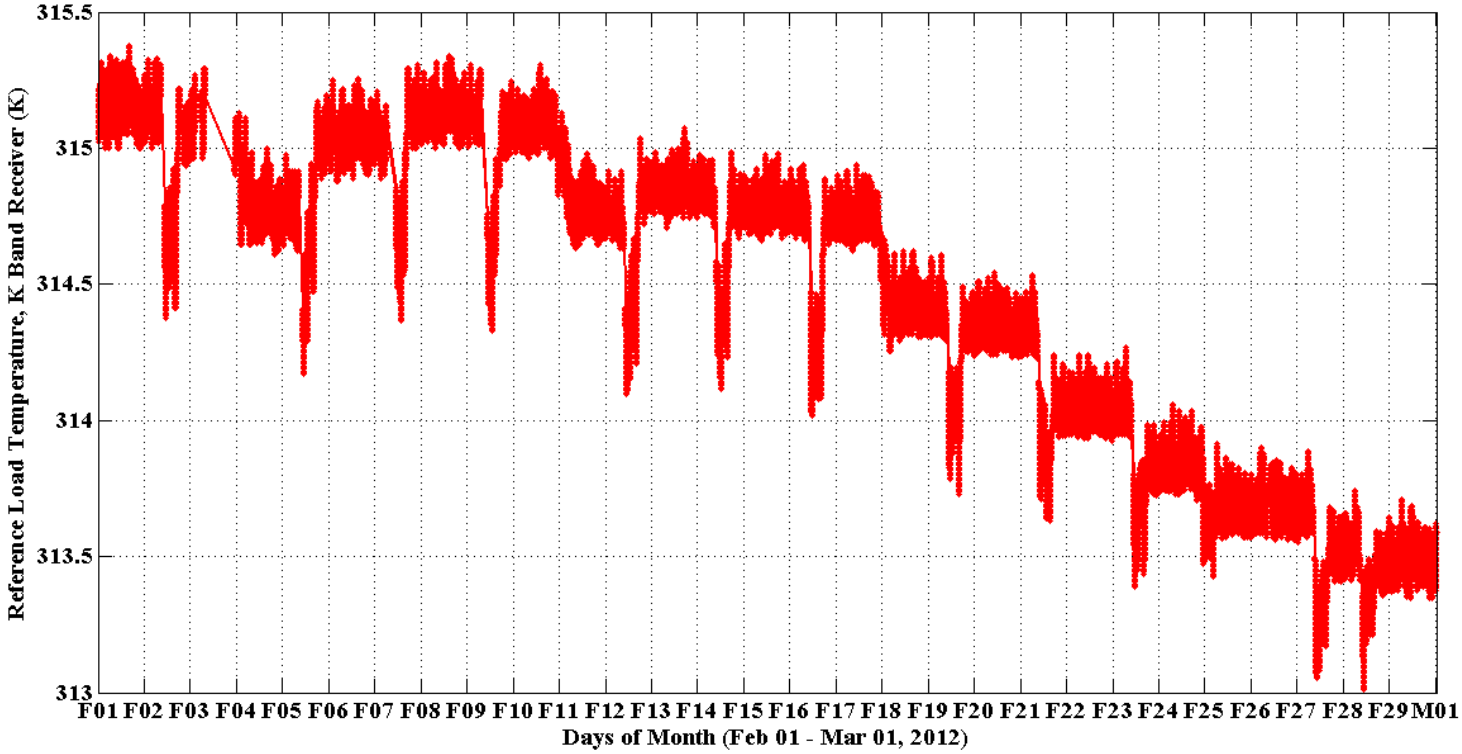

Figure 4.21: Variation of the physical temperature (in K) of the internal reference load for 23.8 GHz (K band) receiver during a one month period in February, 2012. The periodic drop in temperature approximately every 1.5 days is due to the resetting of MWR's thermal control caused by planned PAD reboot. The overall decreasing trend in the mean orbit temperature is due to the Sun-angle change in the given period.

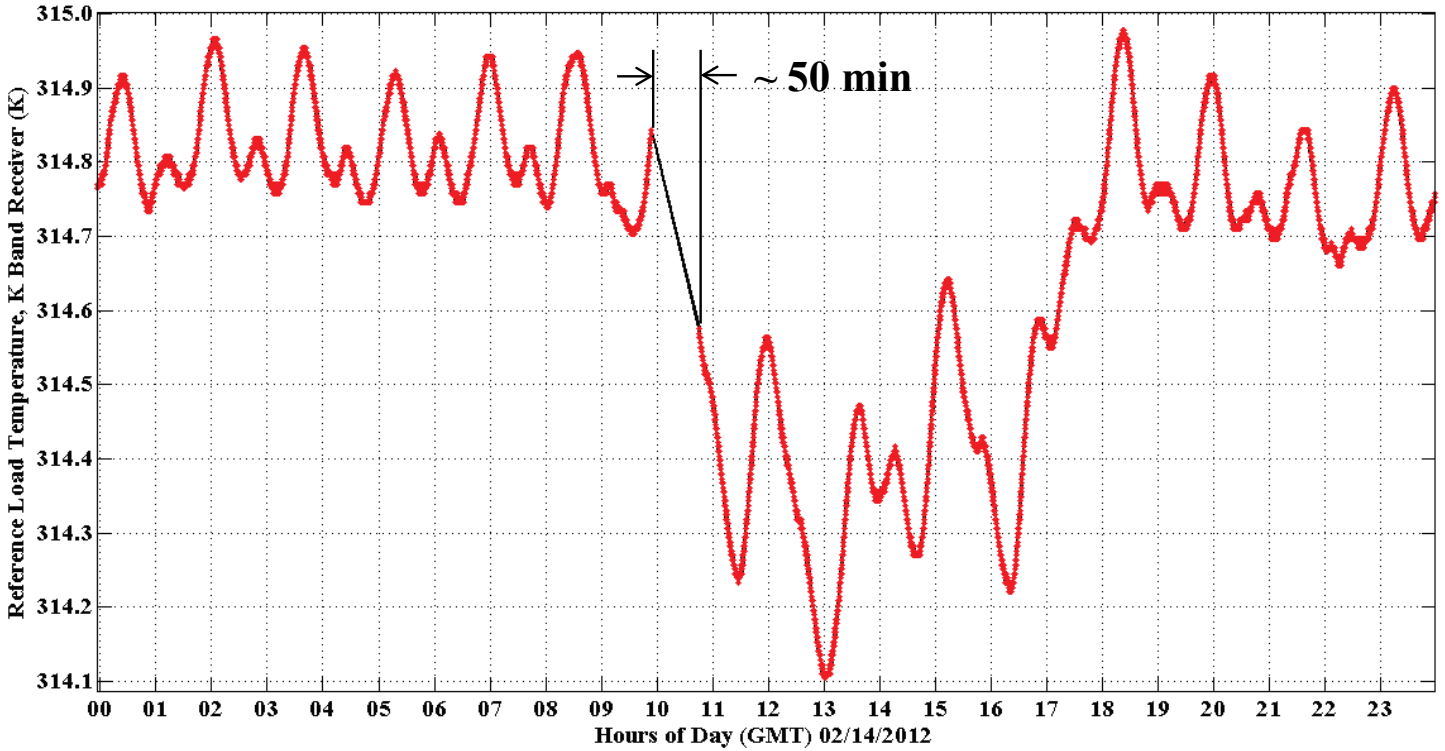

Figure 4.22: Variation of the physical temperature (in K) of the internal reference load for 23.8 GHz (K band) receiver on Valentine's Day, 2012. The PAD was reset at $\sim$ 10 hrs GMT and it was back on $\sim$ 50 minutes after. It took approximately 7 hrs for the temperature transient to come back to the normal range.

Figure 4.21 shows the Variation of the physical temperature (in K) of the internal reference load for 23.8 GHz (K band) receiver during a one month period in February, 2012. The periodic drop in temperature approximately every 1.5 days is due to the resetting of MWR's thermal control caused by planned PAD reboot. As mentioned in chapter 3, MWR's thermal control uses heaters to control temperature of the instrument. These heaters are driven by pulse width modulated current sources. The duty cycle of the driver current determine the total heat (power) output of the heater. During the time period of Fig. 4.21, MWR's thermal control was programmed such a way that always the heaters are driven with 10% duty cycle. So after every reset the thermal control returns to the same 10% duty cycle mode irrespective of the temperature of the instrument. The reason for such a setting was to track the mean orbit temperature variation over season due to Sun-angle variation and to find the maximum possible temperature on orbit. This information is very useful in deciding a proper thermal control approach. Therefore, in Fig. 4.21 we can see the overall decreasing trend in the mean orbit temperature due to the Sun-angle change in the given period. The same temperature variation for a PAD reset day in February, 2012 is plotted in Fig. 4.22. Note that the reset took place just before $\sim$ 10 hrs GMT and lasted for $\sim$ 50 minutes. During this time the value of mean T_o dropped by 0.4-0.5 K and it took approximately 7 hours for the heaters to stabilize the temperature again. There is a much larger peak to peak oscillation of T_o in the transient region and at the end of the large fluctuations the temperature steadily rises up to the normal level. However, due to the decreasing trend in the mean orbit temperature and fixed heat supply from the heaters, To doesn't recover fully

to the previous level after the PAD reset.

The effect of these transient on MWR calibration is being analyzed now. The analysis will be better when an active thermal control is in place i.e. the thermal control always bring back MWR to a fixed temperature set point instead of floating. In any case, resetting of thermal control will hurt the long term stability of the instrument. Hence, a solution to the PAD problem in near future is quite essential.

CHAPTER 5
CONCLUSIONS

Aquarius/SAC-D is the first NASA mission to measure global sea surface salinity from space. This unprecedented mission has several stringent requirements to be met for its data to be useful to the science community. One of the major sources of SSS error comes from the increase in Aquarius L-band T_b due to the presence of atmospheric liquid water (L) in the forms of rain and cloud. Here is an excerpt from a technical memo written by Frank J. Wentz on this topic:" *The overall error in salinity retrievals due to atmosphere liquid water is about 0.07 to 0.08 psu. Although this average global error is relatively small, its real impact is that it is spatially correlated with rain systems and can become quite large in areas of intense rain. About 11% of the Aquarius observations will have a salinity error greater than 0.1 psu if no flagging or correction procedure is implemented.*"[33]. Later in this memo the author proposes three options, the first and the best of which is:" *Aquarius will have a 23/37 GHz radiometer onboard that is collocated with the 1.4 GHz salinity observations. If this radiometer operates successfully, it will provide an ideal tool for flagging and correcting observations that are affected by large L values. For this application, the requirements on the 23/37 GHz radiometer calibration are not very stringent. The radiometer only needs to be stable over time scales of 10-minutes to measure the contrast between rain and no-rain scenes. Furthermore, this T_B contrast only needs to be measured to an accuracy of a few Kelvin. These requirements are well within the design goals of the 23/37 GHz radiometer.*" Apart from the flagging/correcting for rain contamination in Aquarius SSS retrievals, MWR

instrument is capable of producing geo-physical retrievals of its own e.g. atmospheric water vapor content, ocean surface wind vector, atmospheric liquid water (rain) and sea ice concentration. Being the first satellite microwave radiometer of CONAE, MWR's data will be used by a great number of scientists in Argentina for various applications over ocean, land and ice.

This dissertation presents a system level description of the SAC-D MWR instrument and its internal calibration scheme. It also addresses some of the requirements that had driven the design of this instrument. Just like any other microwave radiometer, calibration is an absolute necessity for MWR's data to be useful for scientific study. In the pre-launch period, MWR's receivers were calibrated in laboratory using external blackbody noise sources with brightness temperatures at both high and low ends of the earth viewing T_b dynamic range. A method to obtain the injected noise diode temperature from this test is described here. Using the internal reference load temperature and the injected noise diode brightness, the instrument's forward model equations are inverted to obtain the relationship between measured digital counts and the T_b at the receiver input. In MWR system, T_b's from multiple antenna feed horns are observed by a common receiver for a particular channel (frequency and polarization). This is implemented using a microwave waveguide switching network. The presence of a switching network with finite loss between the antenna and the receivers attenuates the T_a captured by the antenna. The self-emission of this loss adds an unwanted component to the antenna signal measured by the receiver. A radiative transfer model for the antenna switching network is presented here to quantify these effects and remove them

from the T_b measurements. The thermal vacuum (T/V) test data is used to calibrate this correction algorithm. Finally, in the post launch period MWR T_b's are compared against the T_b measurements from the WindSat instrument. The comparison is used to estimate an effective antenna pattern correction for MWR.

Initial On-orbit-checkout and T_b comparison with Windsat revealed several problems with the MWR data. The most prominent of these is the beam smearing problem described in Section 4.2.1.1. At the time of writing this dissertation there is an empirical correction that is being put by CONAE and the results are being analyzed. Like any other empirical correction, this is not going to eliminate the problem completely but hopefully the residual error will be reduced to an acceptable level. The second issue with the MWR T_b's come from the presence of receiver non-linearity which is not being accounted for in the calibration algorithm. This problem, if not corrected, will affect the T_b's over land, ice and heavy rain. Approximately a maximum of 2.5 K T_b error is estimated over land due to non-linearity effect. The third problem with MWR comes from the frequent resetting of the MWR's thermal control system due to an unresolved issue with the flight computer (PAD) memory. This compromises the thermal stability of the instrument causing drift in its calibration.

Irrespective of the current issues with the instrument, the calibration algorithm described here is able to produce MWR T_b's, which statistically match well with the collocated WindSat T_b observations. The preliminary geo-physical retrieval algorithms has already produced water vapor density, wind speed and sea ice concentration from the MWR T_b's with reasonable accuracy. The thermal instability issue with MWR is expected to be solved soon

resulting in a more stable T_b product. More data and analysis is needed to correct for the non-linearity and smearing problem accurately. The calibration of $\pm 45^o$ polarization channels of the Ka band system is not addressed in this dissertation. This is an important and required future effort. The proper calibration of these channels will enable MWR to detect ocean surface wind direction. The retrieval of wind vector (magnitude and direction) will improve other geophysical retrievals.

APPENDIX A
MWR RF COMPONENT DATA-SHEETS

A.1 K Band Receiver

A.1.1 Circulator Switch

EMS Technologies

Space & Technology/Atlanta
Ferrite Components Group

EMS S/N: 005
EMSr P/N: 142331AT23G8

Operator: 2783
Date: 6/5/2008

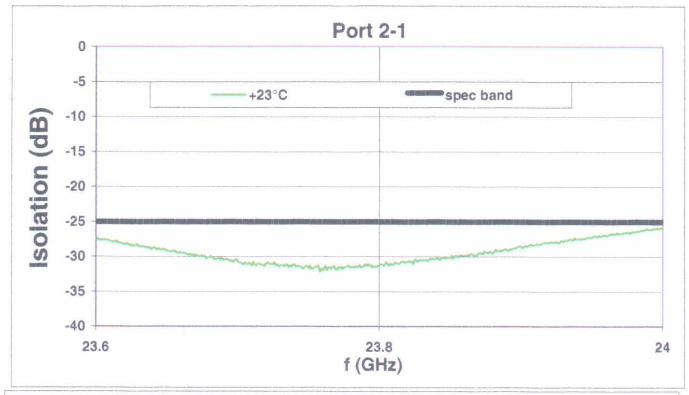

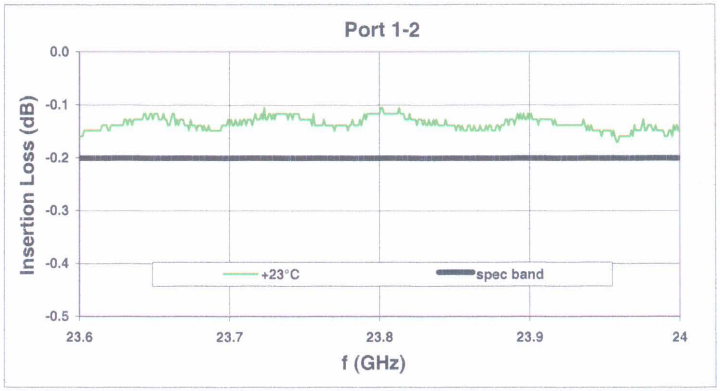

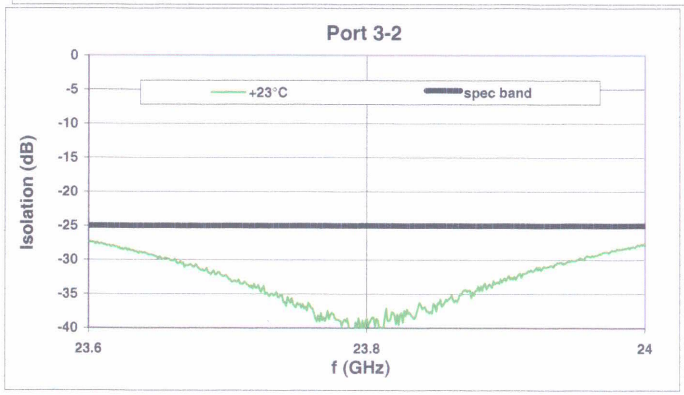

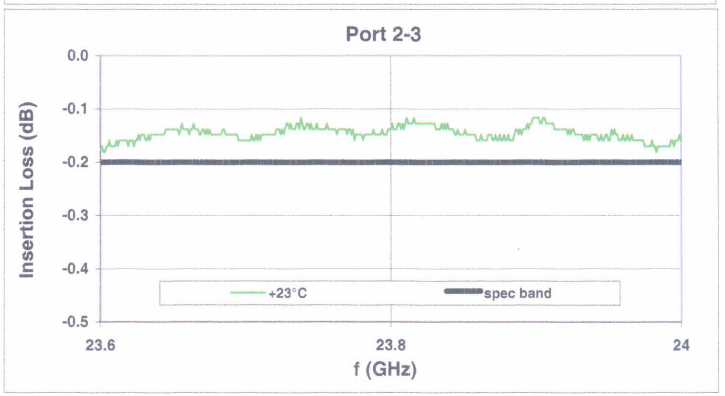

A.1.2 Isolator

EMS Technologies

Space & Technology/Atlanta
Ferrite Components Group

EMS S/N: 005
P/N: 142330AT23G8

Operator: 2783
Date: 5/19/2006

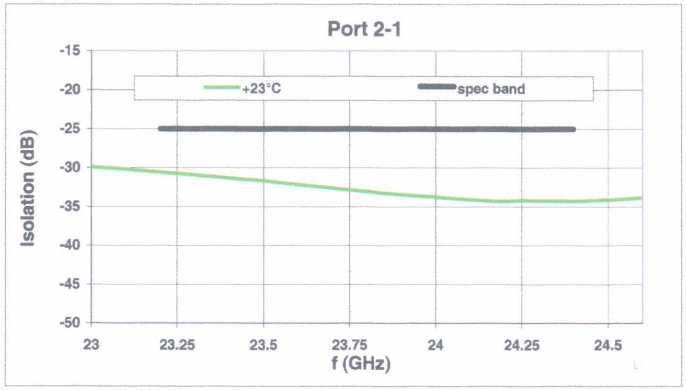

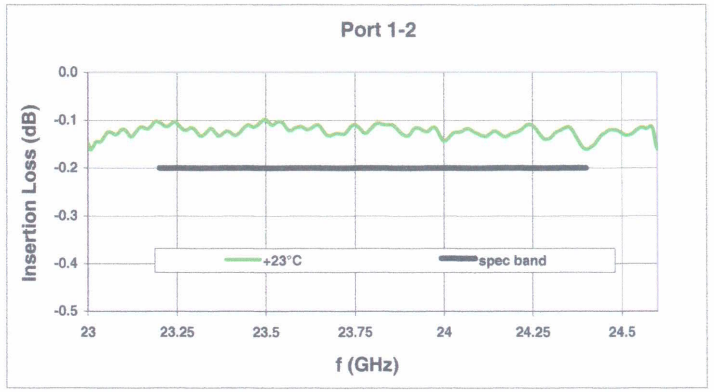

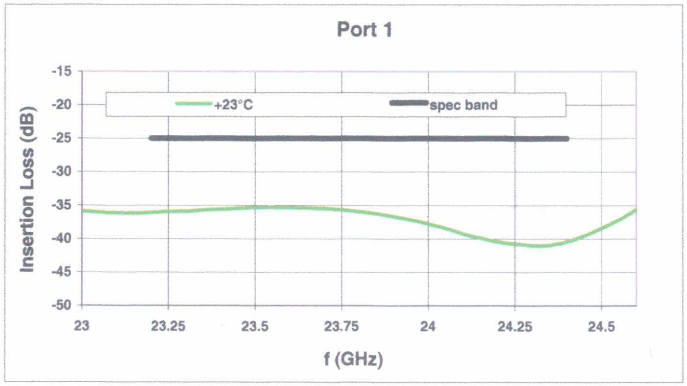

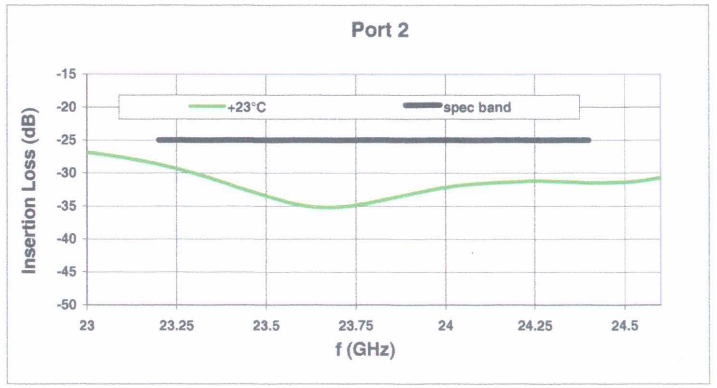

A.1.3 Coupler

millitech®

Coupler Test Data Sheet*

Customer:	Mollendo Equipment Co.,Inc.	**P.O. No:**	466/CON
Model No:	CL3-42-S2000	**Serial No:**	91
Description:	Coupler,3-Port High Directivity	**Date:**	05/04/05
Sales Order:	A12933.001	**Ref No:**	

Specifications and Requirements

Frequency:	18.0 – 26.5	GHz	**VSWR Main Port:**	1.05:1	
Insertion Loss:	0.8	dB (max)	**VSWR Secondary Port:**	1.10:1	
Coupling:	20.0	dB	**Directivity:**	32.00	dB (min)
Flatness:	+/-0.7	dB (max)			

Operating / Test Conditions

Test Frequency: 18.0-26.5 GHz

Test Data

Frequency (GHz)	Coupling (dB)	Insertion Loss (dB)	Flatness (dB)	Directivity (dB)	VSWR Main	VSWR Secondary
18.00	19.73	0.26	+/-0.48	32.95	1.05:1	1.07:1
22.25	20.60					
26.50	20.34					

*****CAUTIONS*****

****Waveguide flange #4-40 torque 5~6 in-lb****

Comments:

Signatures

Technician:	Helena Drowski	**Quality Assurance:**	
Print Name:	Helena Drowski	**Print Name:**	

*Covers Series CL3, CGC

Millitech, Inc. • 29 Industrial Dr. East • Northampton, MA 01060
Ph. (413) 582-9620 • Fax (413) 582-9622
Email: info@millitech.com • Web Site: www.millitech.com

A.1.4 Filter

millitech®

Filter Test Data Sheet*

Customer:	Mollendo Equipment Co., Inc.	**P.O. No:**	466/CON
Model No:	FNP-42-02000	**Serial No:**	13
Description:	Filter, Bandpass, Narrow	**Date:**	06/14/05
Sales Order:	A12933.007	**Ref No:**	

Operating / Test Conditions

Frequency Passband: 23.6 – 24.0 GHz **Center Frequency:** 23.8 GHz

Test Data

Test Parameter	Specification	Measurement
Insertion Loss (max):	1.60 dB	0.67 dB
VSWR (max):	1.50:1	1.24:1
Rejection Low:	40.0 dB (min) @ 23.1 GHz	40.63 dB (min) @ 23.1 GHz
Rejection High:	30.0 dB (min) @ 24.6 GHz	33.31 dB (min) @ 24.6 GHz

*****CAUTIONS*****

****Waveguide flange #4-40 torque 5~6 in-lb****

Comments:

Signatures

Technician: Bonnie Poku **Quality Assurance:**
Print Name: Bonnie Poku **Print Name:**

*Covers Series FHP, FLP, FNP

Millitech, Inc. • 29 Industrial Dr. East • Northampton, MA 01060
Ph. (413) 582-9620 • Fax (413) 582-9622
Email: info@millitech.com • Web Site: www.millitech.com

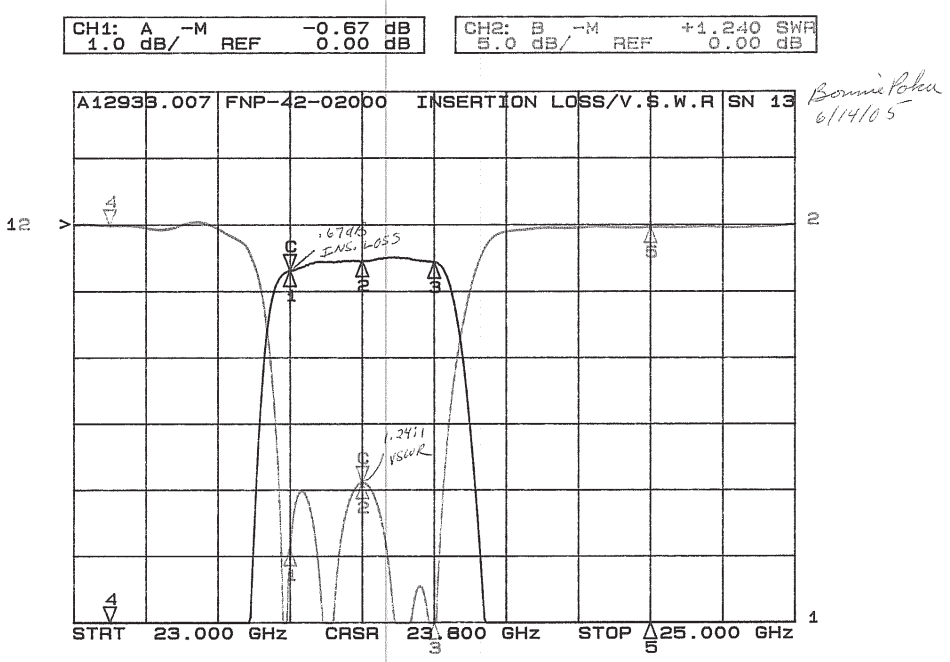
CH1: A -M -0.67 dB
1.0 dB/ REF 0.00 dB
CH2: B -M +1.240 SWR
5.0 dB/ REF 0.00 dB
A12933.007 FNP-42-02000 INSERTION LOSS/V.S.W.R SN 13
Bonnie Poku
6/14/05
.67dB
INS. LOSS
1.24:1
VSWR
STRT 23.000 GHz CRSR 23.800 GHz STOP 25.000 GHz

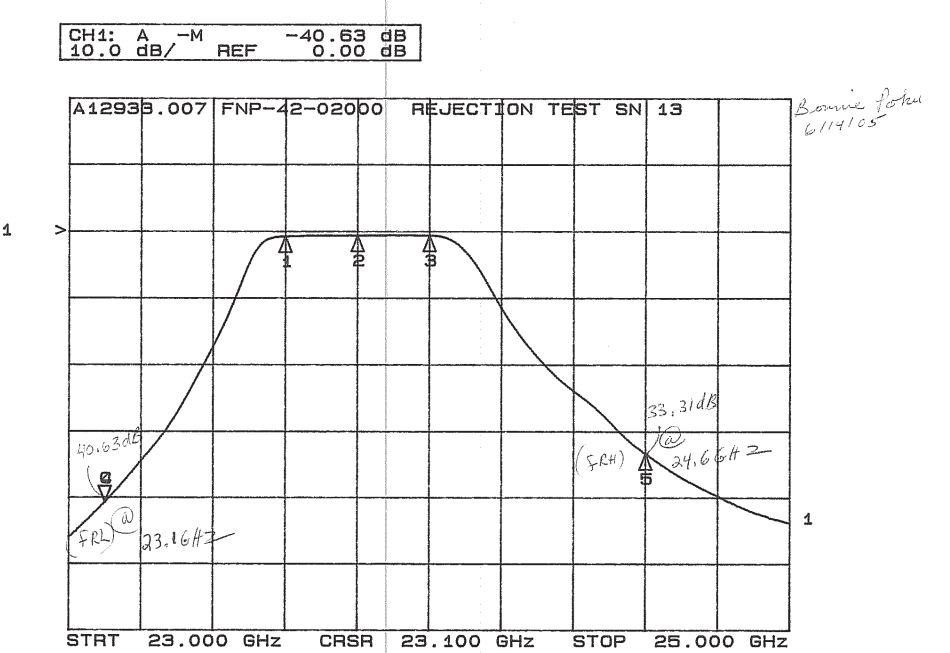
CH1: A -M -40.63 dB
10.0 dB/ REF 0.00 dB
A12933.007 FNP-42-02000 REJECTION TEST SN 13
Bonnie Poku
6/14/05
40.63dB
(FRL) @ 23.1GHz
33.31dB
(FRH) @ 24.6GHz
STRT 23.000 GHz CRSR 23.100 GHz STOP 25.000 GHz

A.1.5 Low Noise Amplifier (LNA)

MITEQ

100 Davids Drive

Hauppauge, NY 11788

Tel: (631) 436-7400

Serial #
1108762

Model #
JDM2-23002450-22-OPSH-FM

Project #
MQ0162287

Customer
CONAE / COMISION NACIONAL

Customer PO
1408

Stock #
1611

Voltage (V)
+12V

Current (mA)
158 Pass <= 200

Temp (°C)
23

Tested By
Richard Schwinn

Comments

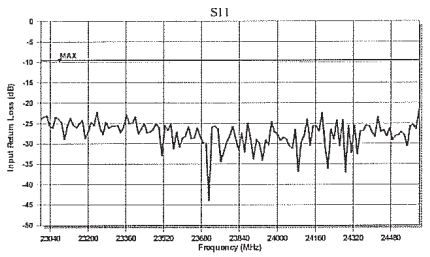

23000	-23.85
23200	-27.12
23400	-23.41
23600	-28.66
23800	-28.08
24000	-27.75
24200	-30.70
24400	-27.29
24600	-21.70
MAX	-21.70
SPEC:	-9.54
ID:6535	PASS

12/10/2008 3:06:47 PM ID:6535 V2.1.1672

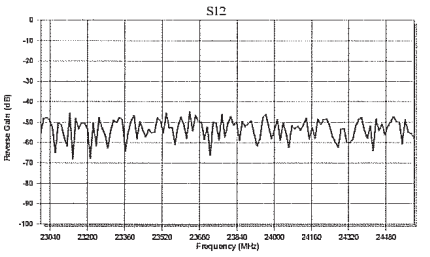

23000	-55.04
23200	-53.25
23400	-46.69
23600	-47.45
23800	-50.69
24000	-53.99
24200	-51.13
24400	-57.96
24600	-57.71
ID:6537	PASS

12/10/2008 3:07:00 PM ID:6537 V2.1.1672

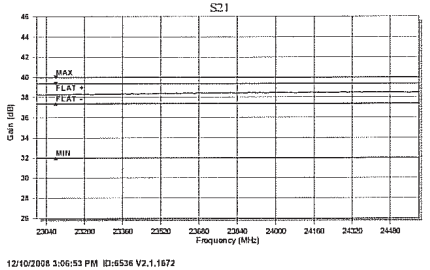

23000	38.25
23200	38.28
23400	38.35
23600	38.38
23800	38.42
24000	38.44
24200	38.46
24400	38.48
24600	38.50
MIN	38.21
SPEC:	32.00
MAX	38.53
SPEC:	40.00
FLAT+/-	0.16
SPEC+/-	1.00
ID:6536	PASS

12/10/2008 3:06:53 PM ID:6536 V2.1.1672

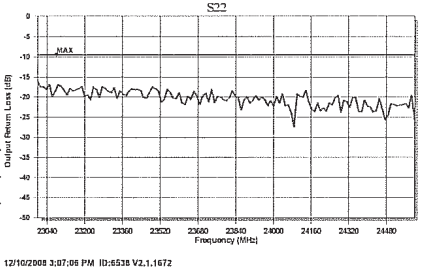

23000	-16.05
23200	-19.78
23400	-17.96
23600	-18.92
23800	-20.99
24000	-22.20
24200	-23.40
24400	-22.21
24600	-25.61
MAX	-16.05
SPEC:	-9.54
ID:6538	PASS

12/10/2008 3:07:06 PM ID:6538 V2.1.1672

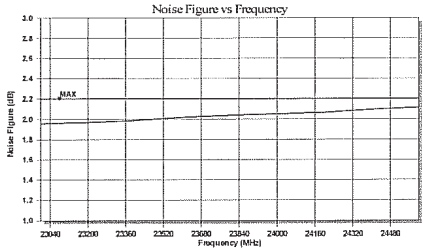

23000	1.96
23200	1.97
23400	1.99
23600	2.02
23800	2.04
24000	2.05
24200	2.06
24400	2.09
24600	2.11
MAX	2.11
SPEC:	2.20
ID:6554	PASS

12/10/2008 4:01:03 PM ID:6554 V2.1.1672

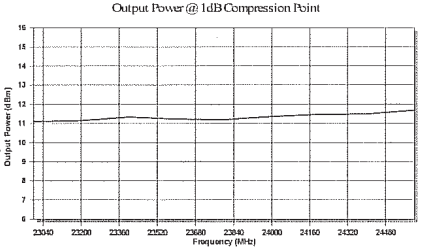

23000	11.10
23200	11.15
23400	11.33
23600	11.23
23800	11.20
24000	11.36
24200	11.46
24400	11.48
24600	11.67
MIN	11.10
SPEC:	0.00
ID:6539	PASS

12/10/2008 3:10:12 PM ID:6539 V2.1.1672

Printed On: 12/10/2008 4:40:33 PM

PASS

Rework Final Test

WEEE

100 Davids Drive
Hauppauge, NY 11788
Tel: (631) 436-7400

Serial #
1108762

Model #
JDM2-23002450-22-OPSH-FM

Project #
MQ0162287

Customer
CONAE / COMISION NACIONAL

Customer PO
1408

Stock #
1611

Voltage (V)
+12V

Current (mA)
157 Pass <= 200

Temp (°C)
-30

Tested By
Richard Schwinn

Comments

Printed On: 8/28/2008 4:42:49 PM

PASS

Final Test

WEEE

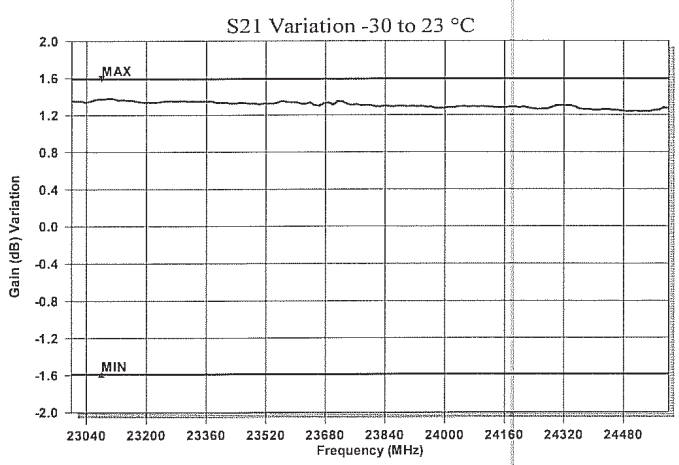

8/28/2008 11:50:12 AM ID:2352 V2.1.1651

23000	1.35
23200	1.33
23400	1.33
23600	1.34
23800	1.30
24000	1.28
24200	1.28
24400	1.25
24600	1.27
MIN	1.24
SPEC:	-1.59
MAX	1.38
SPEC:	1.59
ID:2352	PASS

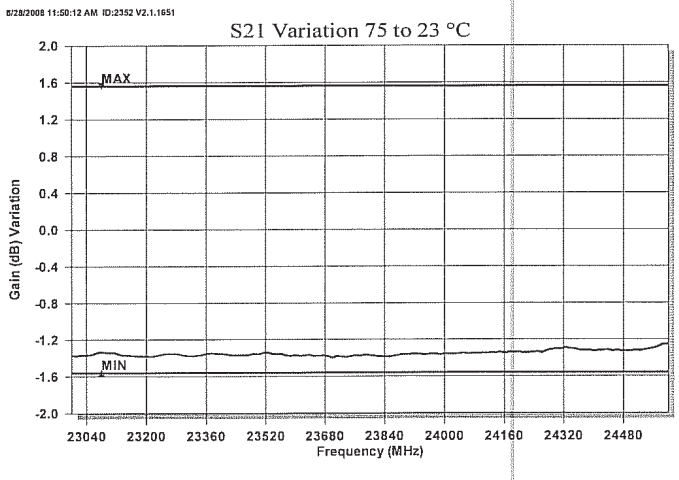

8/28/2008 12:00:24 PM ID:2360 V2.1.1651

23000	-1.38
23200	-1.38
23400	-1.36
23600	-1.37
23800	-1.37
24000	-1.36
24200	-1.34
24400	-1.33
24600	-1.26
MIN	-1.40
SPEC:	-1.56
MAX	-1.26
SPEC:	1.56
ID:2360	PASS

A.1.6 Noise Diode

NOISE COM, INC.
25 EASTMANS ROAD
PARSIPPANY, NJ 07054
(973) 386-9696

CALIBRATION LABORATORY
NOISE SOURCE CALIBRATION REPORT

MODEL NO: NC5342 **CUSTOMER:** RADAR SYSTEMS TECHNOLOGY, INC. **SER NO.:** W395

P.O. # : **SPECIFICATION:** OPT. 2 & 4 **REV:** -

BIAS CONDITIONS: 28 VDC 5.7mA **DATE:** 8/22/08

FREQ GHz	ENR dB	FREQ GHz	ENR dB
22.80	25.04		
23.80	25.48		
24.80	25.09		
LIMITS:	25 Min.	LIMITS:	25 Min.

FLATNESS: 0.44 **HUMIDITY:** <70% **TEMP:** 70 - 80 Deg. (F) / 21 - 27 Deg. (C)

FLATNESS SPEC: +/- .5 **Max**

TESTED BY: _____

INSPECTED BY: _____ **DATE:** AUG 25 2008

STANDARD USED: 346B **SERIAL NUMBER:** 3328A03551 **TRACE NUMBER:** SP3276

RSS UNCERTAINTY: +/- .18 dB

TEST STATION 2

Page 1 of 1

A.1.7 Wave Guide Termination (Match Load)

millitech®

Test Data Sheet*

Customer:	Mollendo Equipment Co. , Inc.	**P.O. No:**	466/Con
Model No:	WTR-42-S0000	**Serial No:**	103
Description:	Termination,wr-42	**Date:**	5/12/05
Sales Order:	A12933.009	**Ref No:**	

Operating / Test Conditions

Test Frequency: 18.0 – 26.5 GHz

Test Data

Test Parameter	Specification	Measurement	
VSWR (max):	1.03:1	1.03:1	

*****CAUTIONS*****

****Waveguide flange #4-40 torque 5~6 in-lb****
*****DO NOT exceed 30 dBm input power*****

Comments:

Signatures

Technician: Helena Drowski **Quality Assurance:**
Print Name: Helena Drowski **Print Name:**

*Covers Series WTR, WAC, TLD, TSC

Millitech, Inc. • 29 Industrial Dr. East • Northampton, MA 01060
Ph. (413) 582-9620 • Fax (413) 582-9622
Email: info@millitech.com • Web Site: www.millitech.com

A.2 Ka Band Receiver

A.2.1 Ortho-Mode Transducer (OMT)

millitech®

Orthomode Transducer Test Data Sheet*

Customer:	Mollendo Equipment Co., Inc	**P.O. No:**	598/CON
Model No:	OMT-28-SS250	**Serial No:**	66
Description:	Transducer, Orthomode ,WR-28	**Date:**	3/7/06
Sales Order:	A13178.014	**Ref No:**	24232

Operating / Test Conditions

Test Frequency: 35.587- -37.412 GHz **Center Frequency:** 36.5 GHz

Test Data

Test Parameter	Specification	Measurement			
Insertion Loss (max):	Not specified dB	0.18dB	side	0.50dB	thru
Isolation (min):	25.0 dB	37.95dB	side	28.55dB	thru
VSWR (typ):	1.4:1	1.32:1	side	1.15:1	thru

*****CAUTIONS*****

****Waveguide flange #4-40 torque 5~6 in-lb****
*****DO NOT exceed 100 W input power*****

Comments:

Signatures

Technician: Bonnie Poku **Quality Assurance:**
Print Name: Bonnie Poku **Print Name:**

*Covers Series OMT

Millitech, Inc. • 29 Industrial Dr. East • Northampton, MA 01060
Ph. (413) 582-9620 • Fax (413) 582-9622
Email: info@millitech.com • Web Site: www.millitech.com

FRM000246 REV01 ECO# 0408-24-03

A.2.2 Circulator Switch

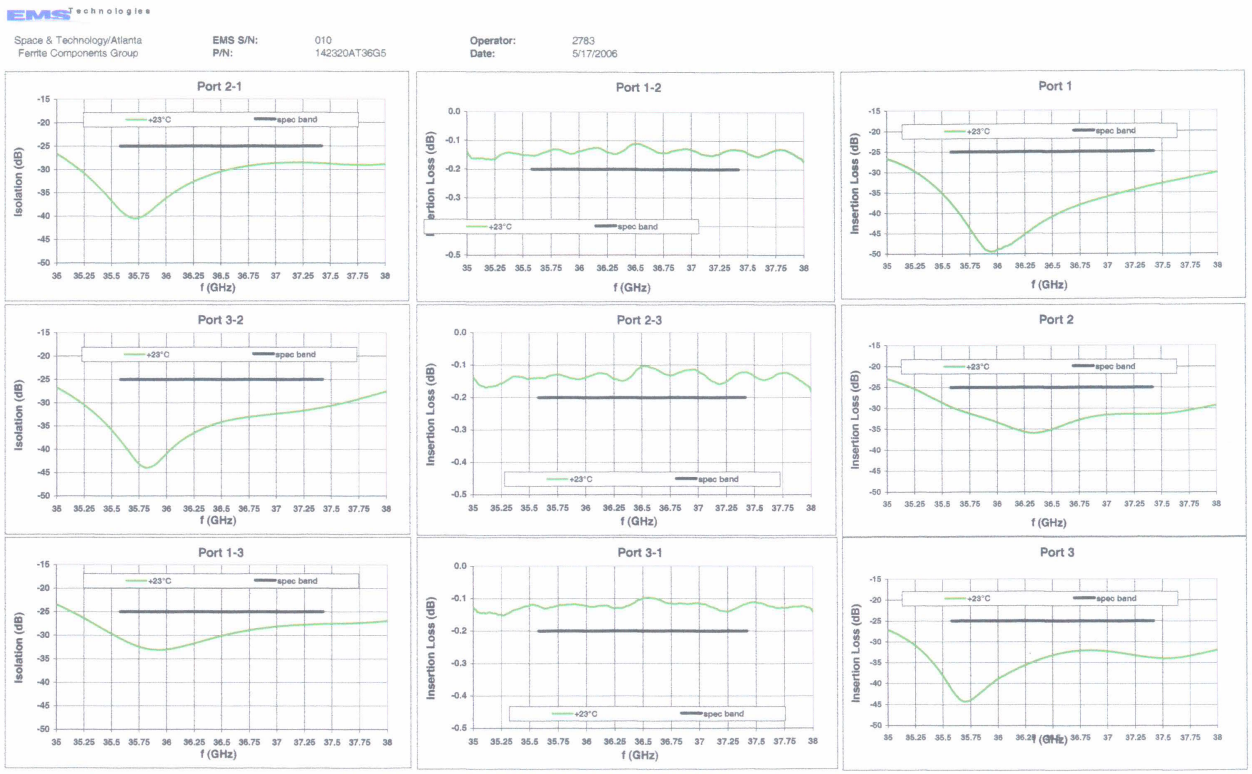

A.2.3 Isolator

EMS Technologies

Space & Technology/Atlanta
Ferrite Components Group

EMS S/N: 005
P/N: 142319AT36G5

Operator: 2783
Date: 5/19/2006

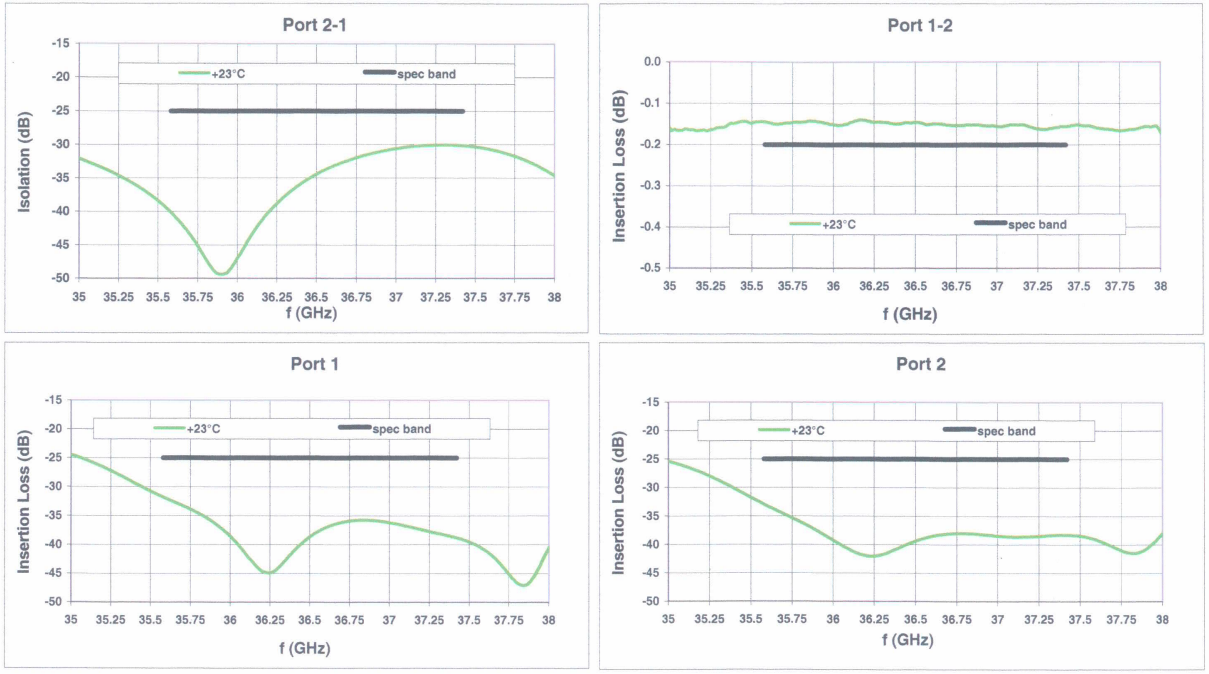

A.2.4 Coupler

millitech®

Coupler Test Data Sheet*

Customer:	Mollendo Equipment Co.Inc.	**P.O. No:**	466/CON
Model No:	CL3-28-S2000	**Serial No:**	329
Description:	Coupler,3-Port High Directivity	**Date:**	5/5/05
Sales Order:	A12933.002	**Ref No:**	

Specifications and Requirements

Frequency:	26.5-40.0	GHz	**VSWR Main Port:**	1.05:1	
Insertion Loss:	0.8	dB (max)	**VSWR Secondary Port:**	1.10:1	
Coupling:	20	dB	**Directivity:**	33.00	dB (min)
Flatness:	+/-0.7	dB (max)			

Operating / Test Conditions

Test Frequency: 26.5-40.0 GHz

Test Data

Frequency (GHz)	Coupling (dB)	Insertion Loss (dB)	Flatness (dB)	Directivity (dB)	VSWR Main	VSWR Secondary
26.50 33.25 40.00	19.75 20.53 19.90	0.48	+/-0.48	35.00 39.0(Typical)	1.05:1	1.04:1

*****CAUTIONS*****

****Waveguide flange #4-40 torque 5~6 in-lb****

Comments:

Signatures

Technician: Helena Drowski **Quality Assurance:**

Print Name: Helena Drowski **Print Name:**

*Covers Series CL3, CGC

Millitech, Inc. • 29 Industrial Dr. East • Northampton, MA 01060
Ph. (413) 582-9620 • Fax (413) 582-9622
Email: info@millitech.com • Web Site: www.millitech.com

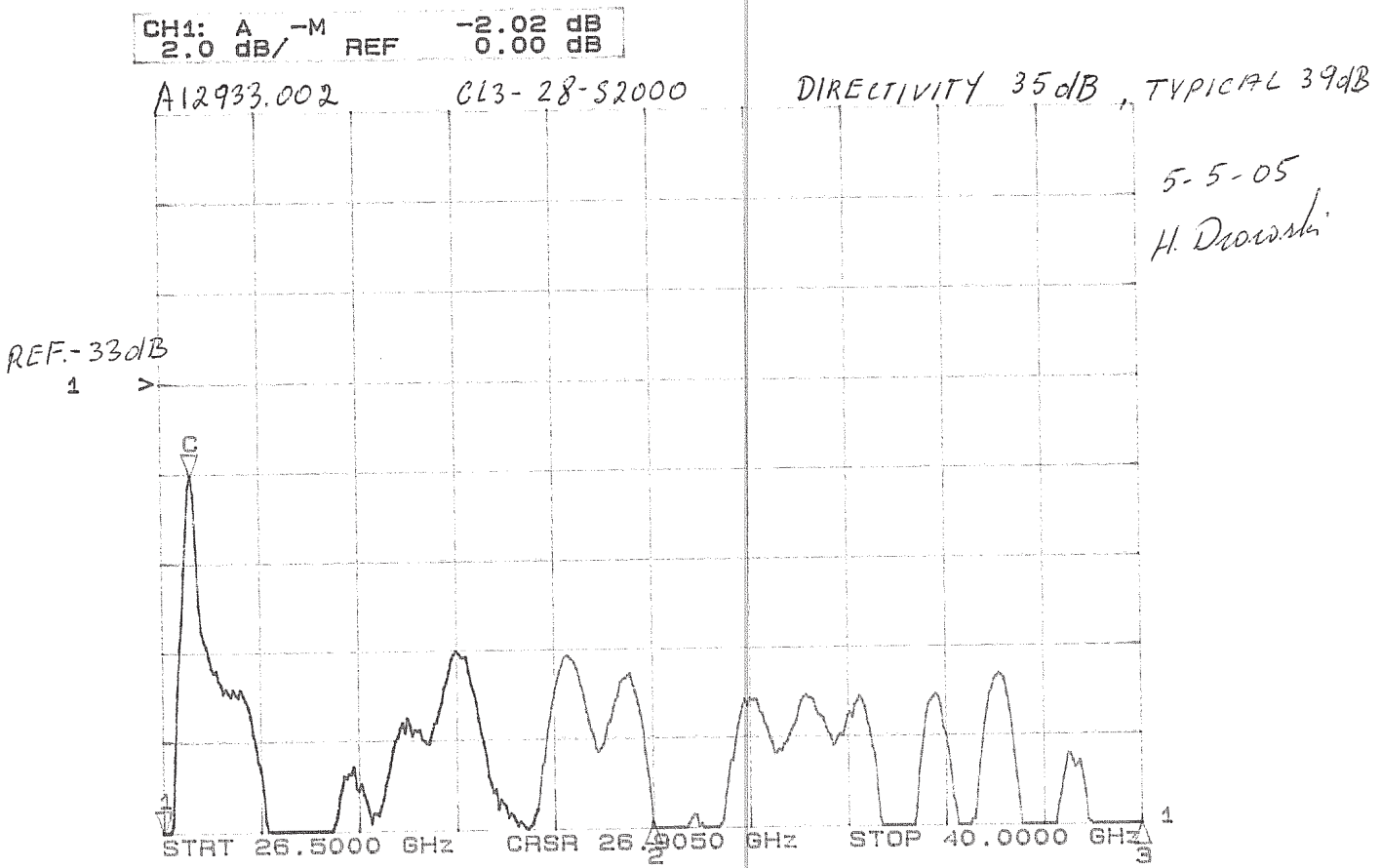
CH1: A -M
2.0 dB/ REF
-2.02 dB
0.00 dB
A12933.002
CL3-28-S2000
DIRECTIVITY 35dB, TYPICAL 39dB
5-5-05
H. Drowski
REF.-33dB
1 >
C
STRT 26.5000 GHz
CRSR 26.9050 GHz
STOP 40.0000 GHz

A.2.5 Filter

millitech®

Filter Test Data Sheet*

Customer:	Mollendo Equipment Co., Inc.	**P.O. No:**	466/CON
Model No:	FNP-28-03000	**Serial No:**	27
Description:	Filter, Bandpass, Narrow	**Date:**	06/14/05
Sales Order:	A12933.008	**Ref No:**	

Operating / Test Conditions

Frequency Passband: 36.0 – 37.0 GHz **Center Frequency:** 36.5 GHz

Test Data

Test Parameter	Specification	Measurement
Insertion Loss (max):	1.60 dB	0.51 dB
VSWR (max):	1.50:1	1.29:1
Rejection Low:	40.0 dB (min) @ 34.9 GHz	45.56 dB (min) @ 34.9 GHz
Rejection High:	30.0 dB (min) @ 38.2 GHz	39.72 dB (min) @ 38.2 GHz

*****CAUTIONS*****

****Waveguide flange #4-40 torque 5~6 in-lb****

Comments:

Signatures

Technician: Bonnie Poku **Quality Assurance:**
Print Name: Bonnie Poku **Print Name:**

*Covers Series FHP, FLP, FNP

Millitech, Inc. • 29 Industrial Dr. East • Northampton, MA 01060
Ph. (413) 582-9620 • Fax (413) 582-9622
Email: info@millitech.com • Web Site: www.millitech.com

FRM000235 REV01 ECO# 0408-24-03

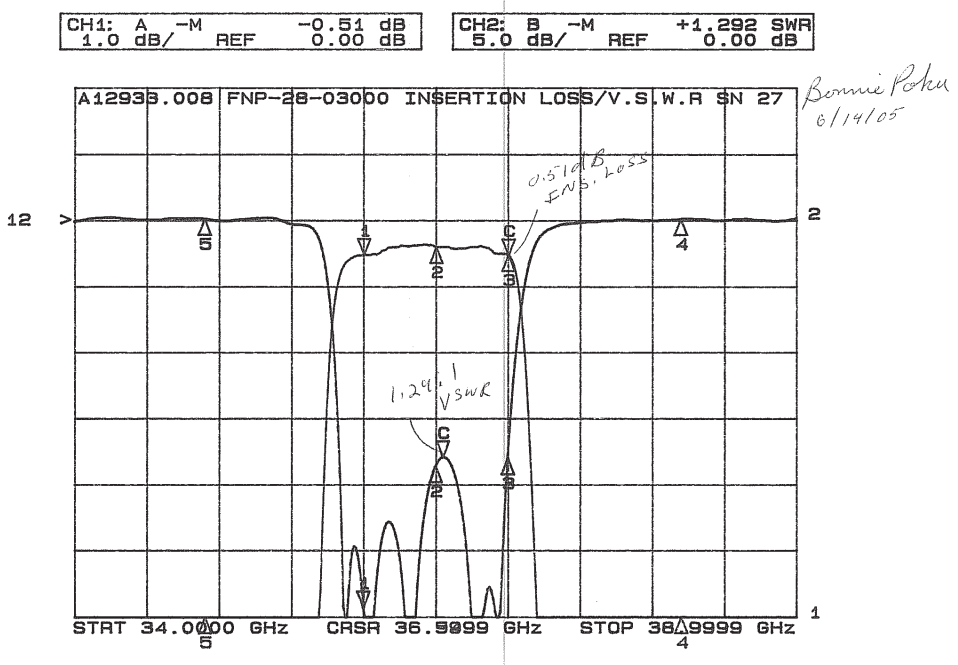
CH1: A -M -0.51 dB
1.0 dB/ REF 0.00 dB
CH2: B -M +1.292 SWR
5.0 dB/ REF 0.00 dB
A12933.008 FNP-28-03000 INSERTION LOSS/V.S.W.R SN 27
Bonnie Pokin 6/14/05
0.51dB INS. LOSS
1.29:1 VSWR
12
2
1
STRT 34.0000 GHz
CRSR 36.5099 GHz
STOP 38.9999 GHz

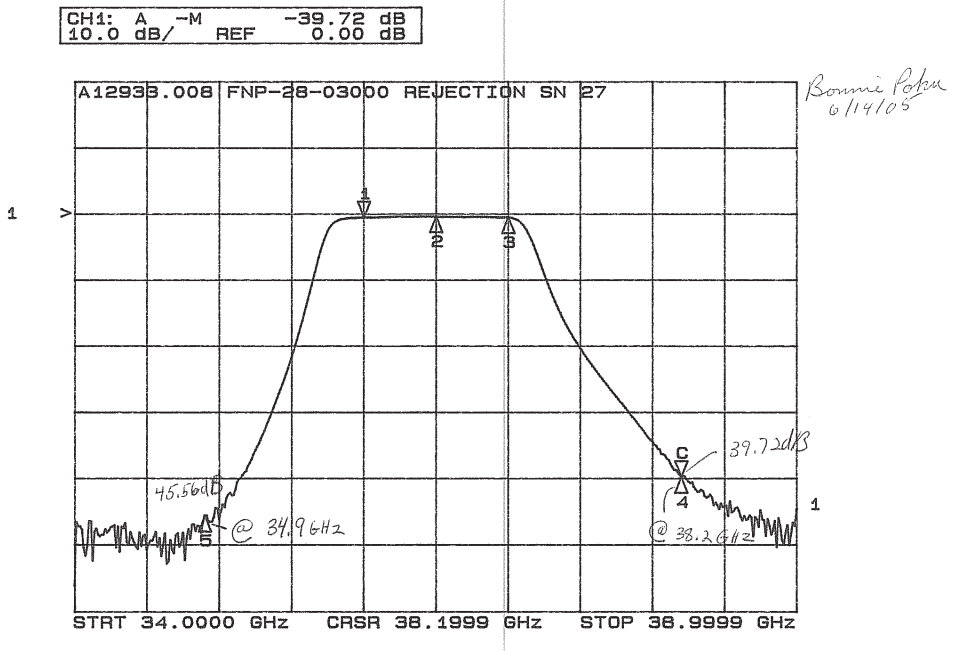
CH1: A -M -39.72 dB
10.0 dB/ REF 0.00 dB
A12933.008 FNP-28-03000 REJECTION SN 27
Bonnie Pokin 6/14/05
45.56dB @ 34.96Hz
39.72dB @ 38.2GHz
1
STRT 34.0000 GHz
CRSR 38.1999 GHz
STOP 38.9999 GHz

A.2.6 Low Noise Amplifier (LNA)

MITEQ

100 Davids Drive

Hauppauge, NY 11788

Tel: (631) 436-7400

Serial #
1108775

Model #
JDM2-35503750-27-OPSH-FM

Project #
MQ0162287

Customer
CONAE / COMISION NACIONAL

Customer PO
1408

Stock #
1612

Voltage (V)
+12V

Current (mA)
156 Pass <= 200

Temp (°C)
23

Tested By
Richard Schwinn

Comments

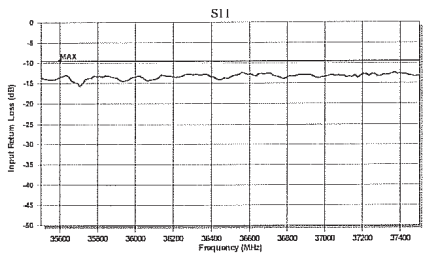

35500	-13.54
35750	-13.79
36000	-13.42
36250	-13.17
36500	-13.45
36750	-13.37
37000	-13.38
37250	-12.67
37500	-13.22
MAX	-12.32
SPEC:	-9.54
ID:6459	PASS

12/9/2008 4:04:23 PM ID:6459 V2.1.1672

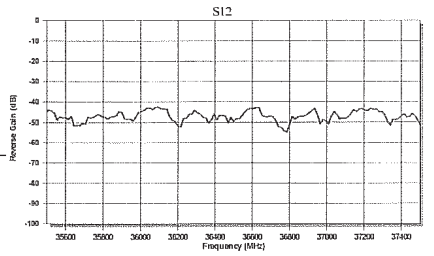

35500	-44.72
35750	-47.54
36000	-44.88
36250	-47.42
36500	-49.67
36750	-52.17
37000	-49.75
37250	-43.80
37500	-51.03
ID:6461	PASS

12/9/2008 4:04:37 PM ID:6461 V2.1.1672

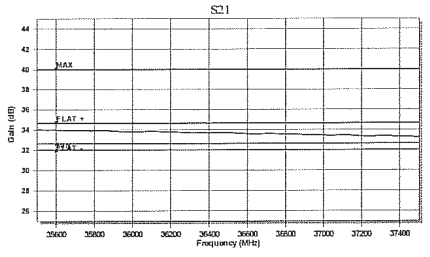

35500	34.03
35750	33.91
36000	33.80
36250	33.75
36500	33.70
36750	33.59
37000	33.44
37250	33.32
37500	33.24
MIN	33.24
SPEC:	32.00
MAX	34.03
SPEC:	40.00
FLAT+/-	0.40
SPEC+/-	1.00
ID:6460	PASS

12/9/2008 4:04:30 PM ID:6460 V2.1.1672

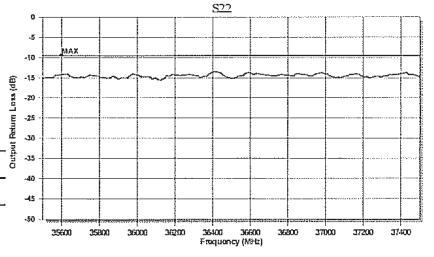

35500	-15.09
35750	-14.28
36000	-14.24
36250	-14.24
36500	-15.05
36750	-14.29
37000	-13.98
37250	-14.88
37500	-14.75
MAX	-13.39
SPEC:	-9.54
ID:6462	PASS

12/9/2008 4:04:43 PM ID:6462 V2.1.1672

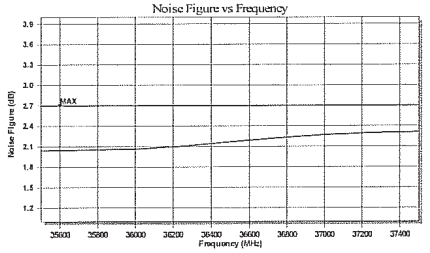

35500	2.04
35750	2.05
36000	2.06
36250	2.10
36500	2.17
36750	2.23
37000	2.27
37250	2.30
37500	2.31
MAX	2.31
SPEC:	2.70
ID:6463	PASS

12/9/2008 4:05:20 PM ID:6463 V2.1.1672

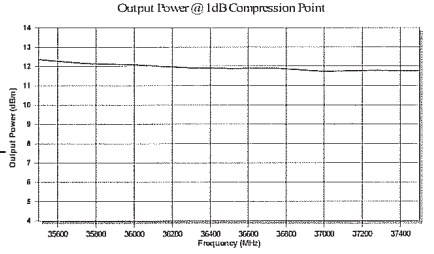

35500	12.35
35750	12.14
36000	12.08
36250	11.92
36500	11.88
36750	11.89
37000	11.73
37250	11.78
37500	11.76
MIN	11.73
SPEC:	0.00
ID:6504	PASS

12/9/2008 5:02:18 PM ID:6504 V2.1.1672

Printed On: 12/10/2008 2:04:39 PM

PASS

Rework Final Test

WEEE

100 Davids Drive
Hauppauge, NY 11788
Tel: (631) 436-7400

Serial #
1108775

Model #
JDM2-35503750-27-OPSH-FM

Project #
MQ0162287

Customer
CONAE / COMISION NACIONAL

Customer PO
1408

Stock #
1612

Voltage (V)
+12V

Current (mA)
155 Pass <= 200

Temp (°C)
-30

Tested By
Richard Schwinn

Comments

Printed On: 9/4/2008 12:00:48 PM

PASS

Final Test

WEEE

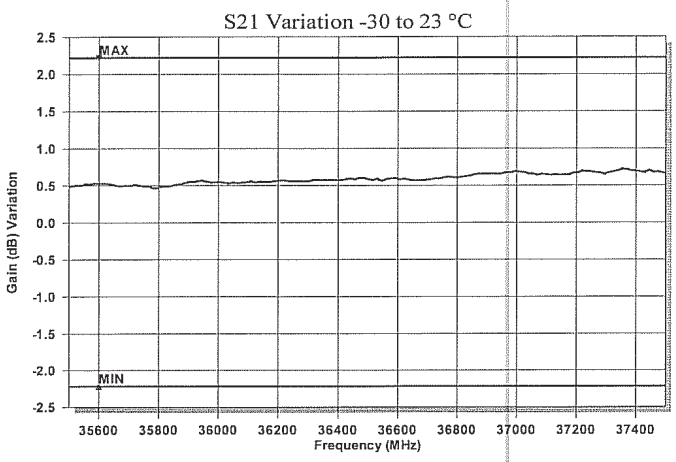

9/2/2008 11:29:31 AM ID:2470 V2.1.1651

35500	0.48
35750	0.49
36000	0.54
36250	0.56
36500	0.58
36750	0.60
37000	0.69
37250	0.68
37500	0.67
MIN	0.47
SPEC:	-2.22
MAX	0.72
SPEC:	2.22
ID:2470	PASS

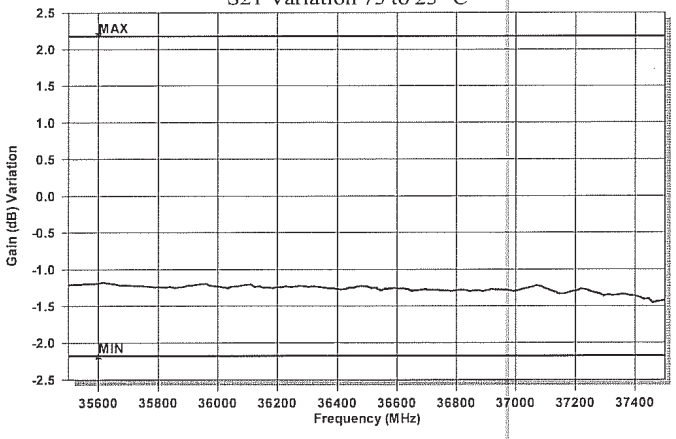

9/2/2008 11:39:10 AM ID:2478 V2.1.1651

35500	-1.22
35750	-1.23
36000	-1.23
36250	-1.24
36500	-1.23
36750	-1.29
37000	-1.29
37250	-1.30
37500	-1.42
MIN	-1.46
SPEC:	-2.18
MAX	-1.18
SPEC:	2.18
ID:2478	PASS

A.2.7 Noise Diode

NOISE COM, INC.
25 EASTMANS ROAD
PARSIPPANY, NJ 07054
(973) 386-9696

CALIBRATION LABORATORY
NOISE SOURCE CALIBRATION REPORT

MODEL NO: NC5328 **CUSTOMER:** RADAR SYSTEMS TECHNOLOGY,INC. **SER NO.:** W397

P.O. # : **SPECIFICATION:** OPT. 2 & 4 **REV:** -

BIAS CONDITIONS: 28 VDC 7.1mA **DATE:** 8/22/08

FREQ GHz	ENR dB	FREQ GHz	ENR dB
35.50	23.51		
36.50	23.95		
37.50	23.37		

LIMITS:	23 Min.	LIMITS:	23 Min.

FLATNESS: 0.58 **HUMIDITY:** <70% **TEMP:** 70 - 80 Deg. (F) / 21 - 27 Deg. (C)

FLATNESS SPEC: +/- .5 **Max**

TESTED BY: _____

INSPECTED BY: _____ **DATE:** AUG 25 2008

STANDARD USED: TN162 **SERIAL NUMBER:** 3328A03551 **TRACE NUMBER:** SP4603

RSS UNCERTAINTY: +/- .18 dB

TEST STATION 2

Page 1 of 1

A.2.8 Wave Guide Termination (Match Load)

millitech®

Test Data Sheet*

Customer:	Mollendo Equipment Co., Inc.	**P.O. No:**	466/CON
Model No:	WTR-28-S0000	**Serial No:**	283
Description:	Termination ,WR-28	**Date:**	05/02/05
Sales Order:	A12933.010	**Ref No:**	

Operating / Test Conditions

Test Frequency: 26.5-40.0 GHz

Test Data

Test Parameter	Specification	Measurement	
VSWR (max):	1.03:1	1.03:1	

*****CAUTIONS*****

****Waveguide flange #4-40 torque 5~6 in-lb****
*****DO NOT exceed28 dBm input power*****

Comments:

Signatures

Technician: Helena Drowski
Print Name: Helena Drowski
Quality Assurance:
Print Name:

*Covers Series WTR, WAC, TLD, TSC

Millitech, Inc. • 29 Industrial Dr. East • Northampton, MA 01060
Ph. (413) 582-9620 • Fax (413) 582-9622
Email: info@millitech.com • Web Site: www.millitech.com

APPENDIX B
MWR RECEIVER SCHEMATICS

B.1 K Band Receiver Schematics

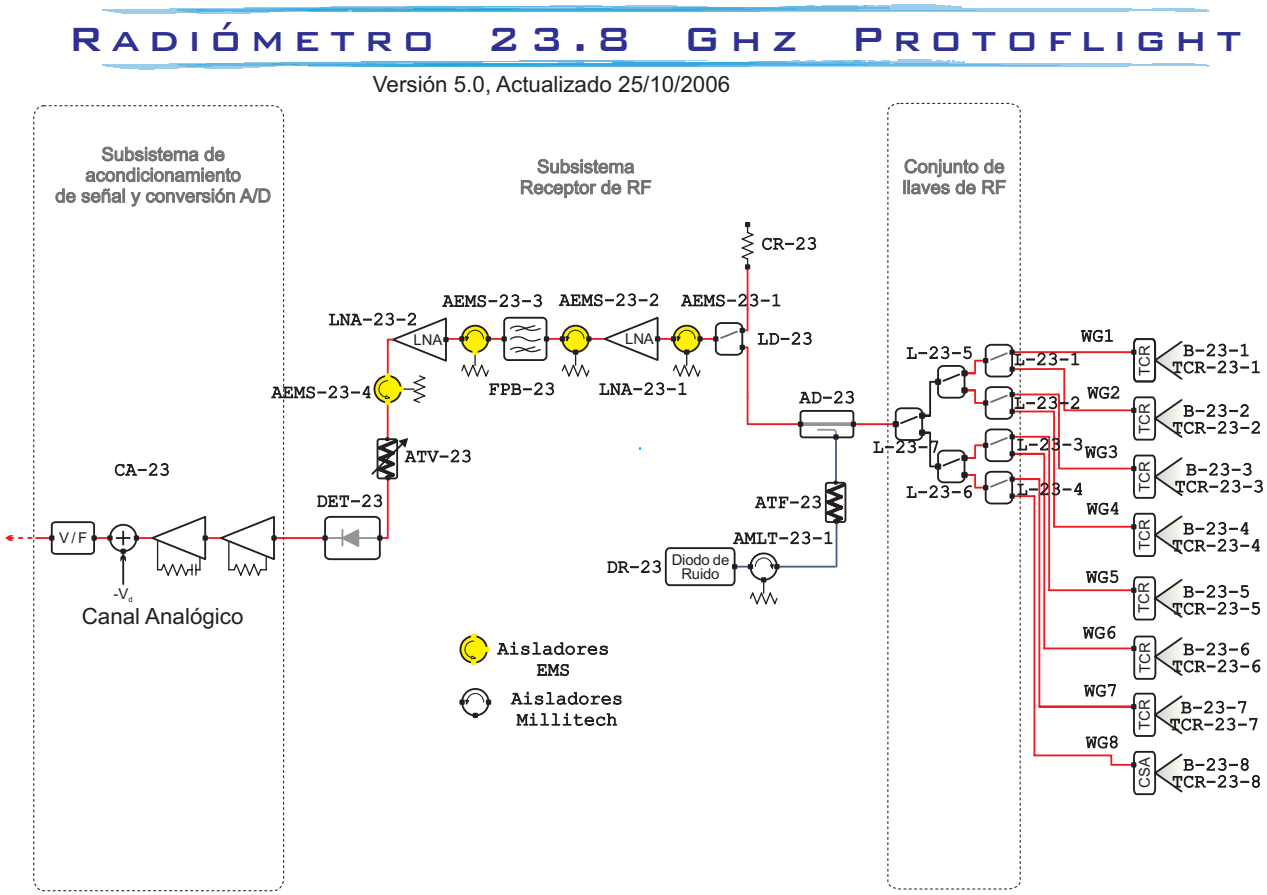

B.2 Ka Band Receiver Schematics

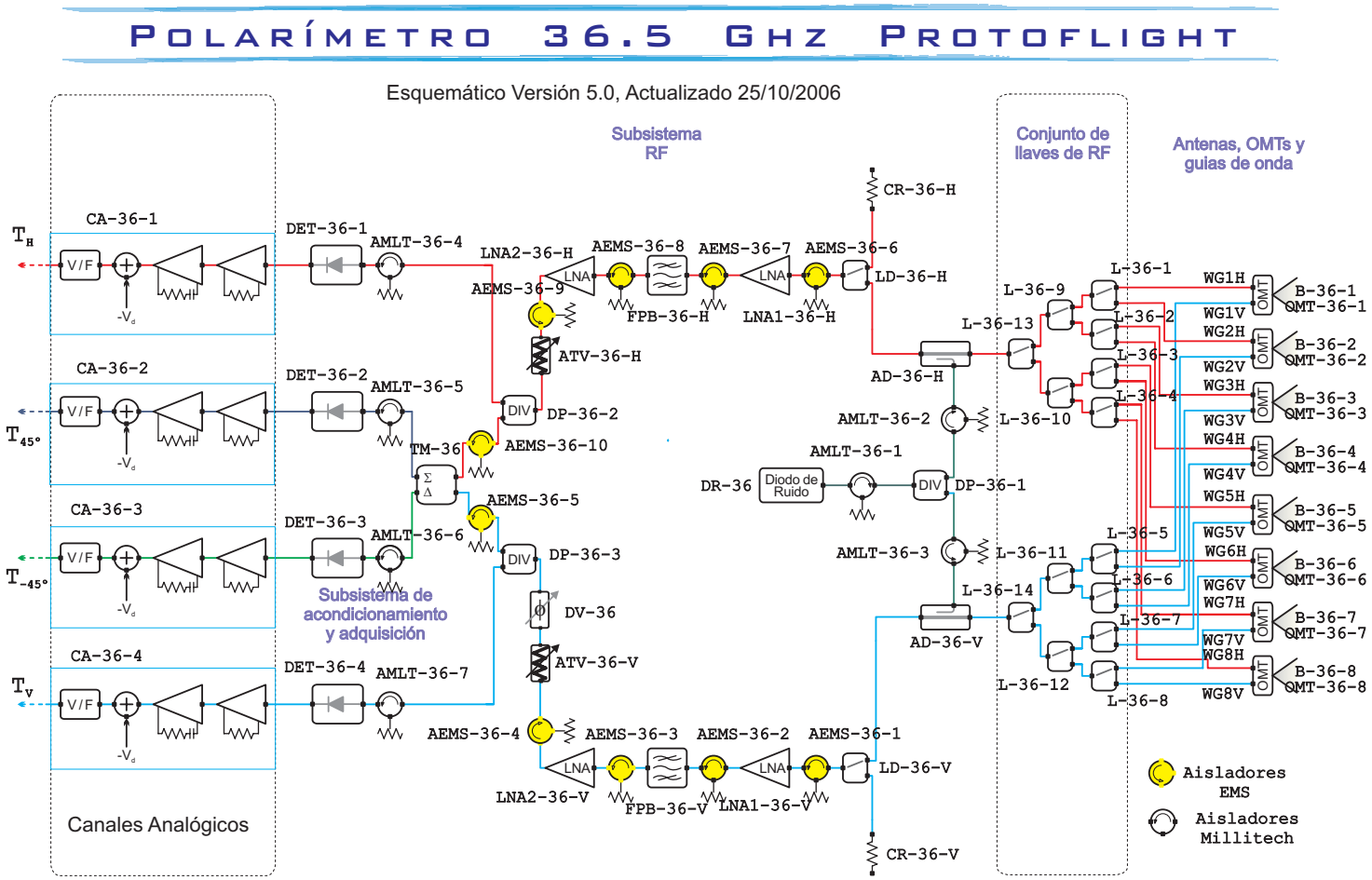

APPENDIX C
MWR WAVEGUIDE LENGTHS

C.1 Waveguide Length Computation Example

Feed Horn 8 – OMT Horizontal path (green)

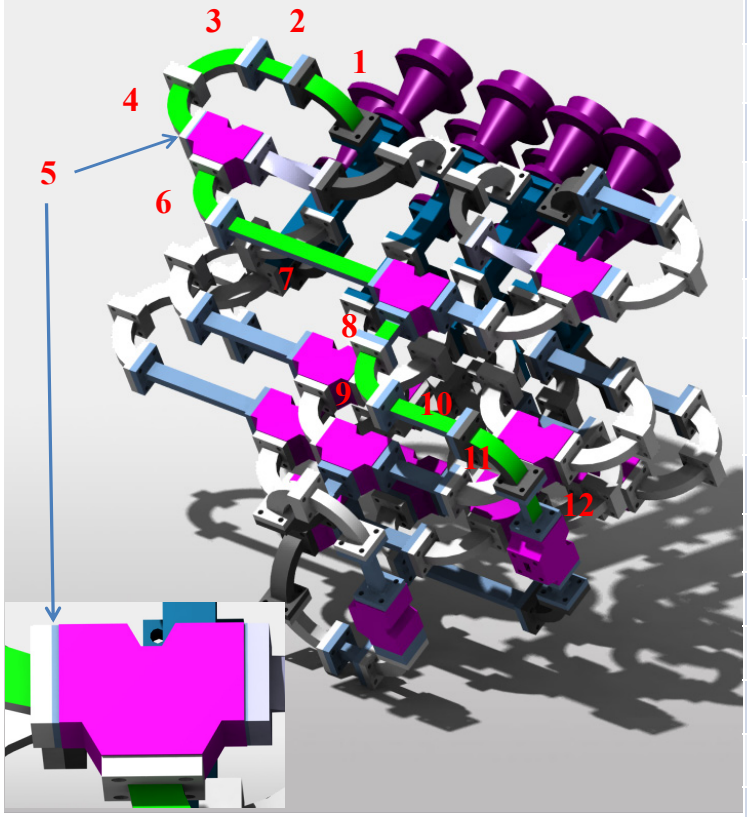

WG	L (mm)	Code
1	39.898	CE90
2	30.308	TGAM30.31-36
3	39.898	CH90
4	39.898	CH90
5	1.366	TGAM1.37-36
SW1		Dickie Switch
6	39.898	CH90
7	102.540	TGAM102.54-36
SW2		Dickie Switch
8	23.272	TGAM23.27-36
9	39.898	CH90
10	50.652	TGAM50.65-36
11	39.898	CE90
12	33.345	TGAM33.34-36
SW3		Dickie Switch

241.483mm + 4*CH90+2*CE90

C.2 K Band Waveguide Lengths

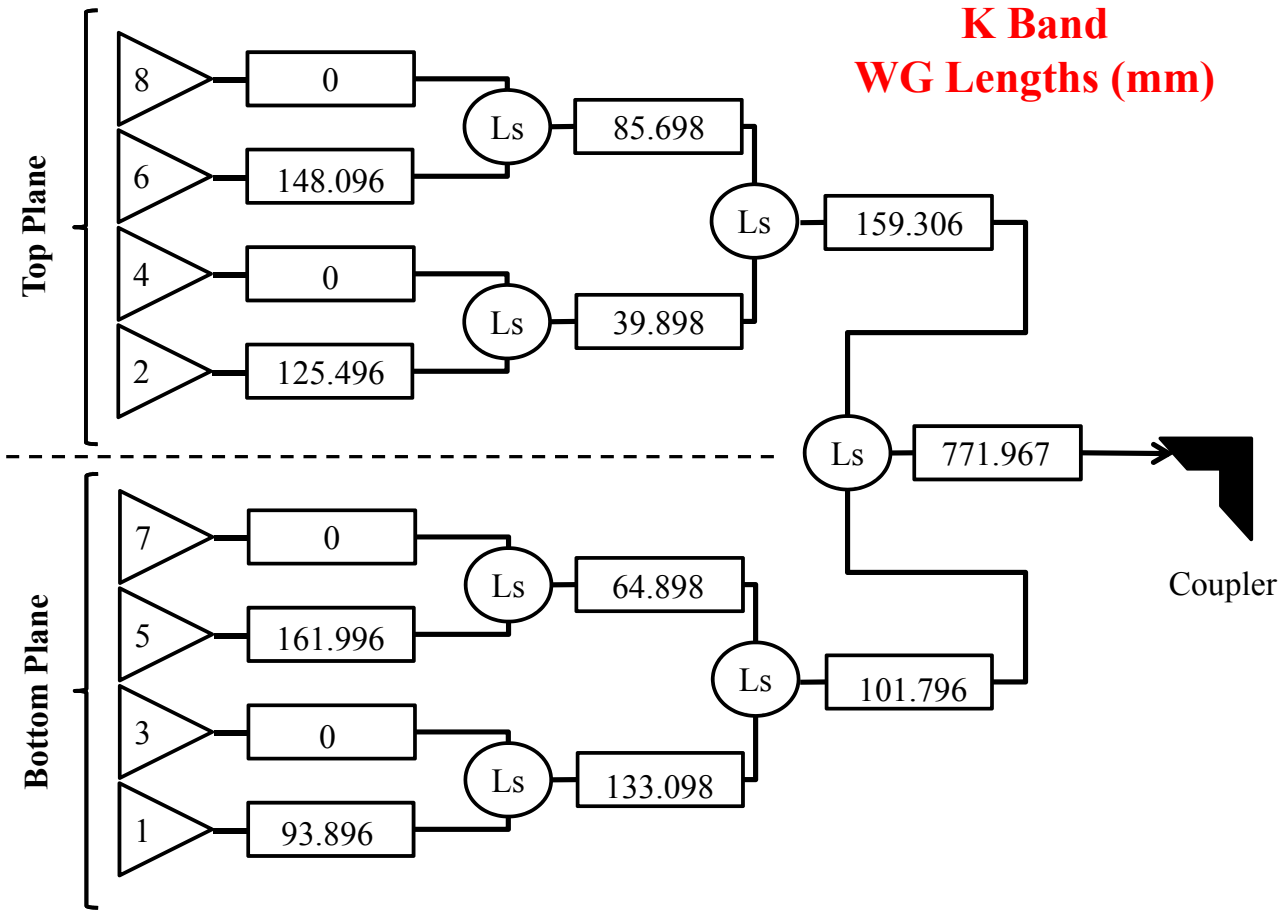

C.3 Ka Band V-pol Waveguide Lengths

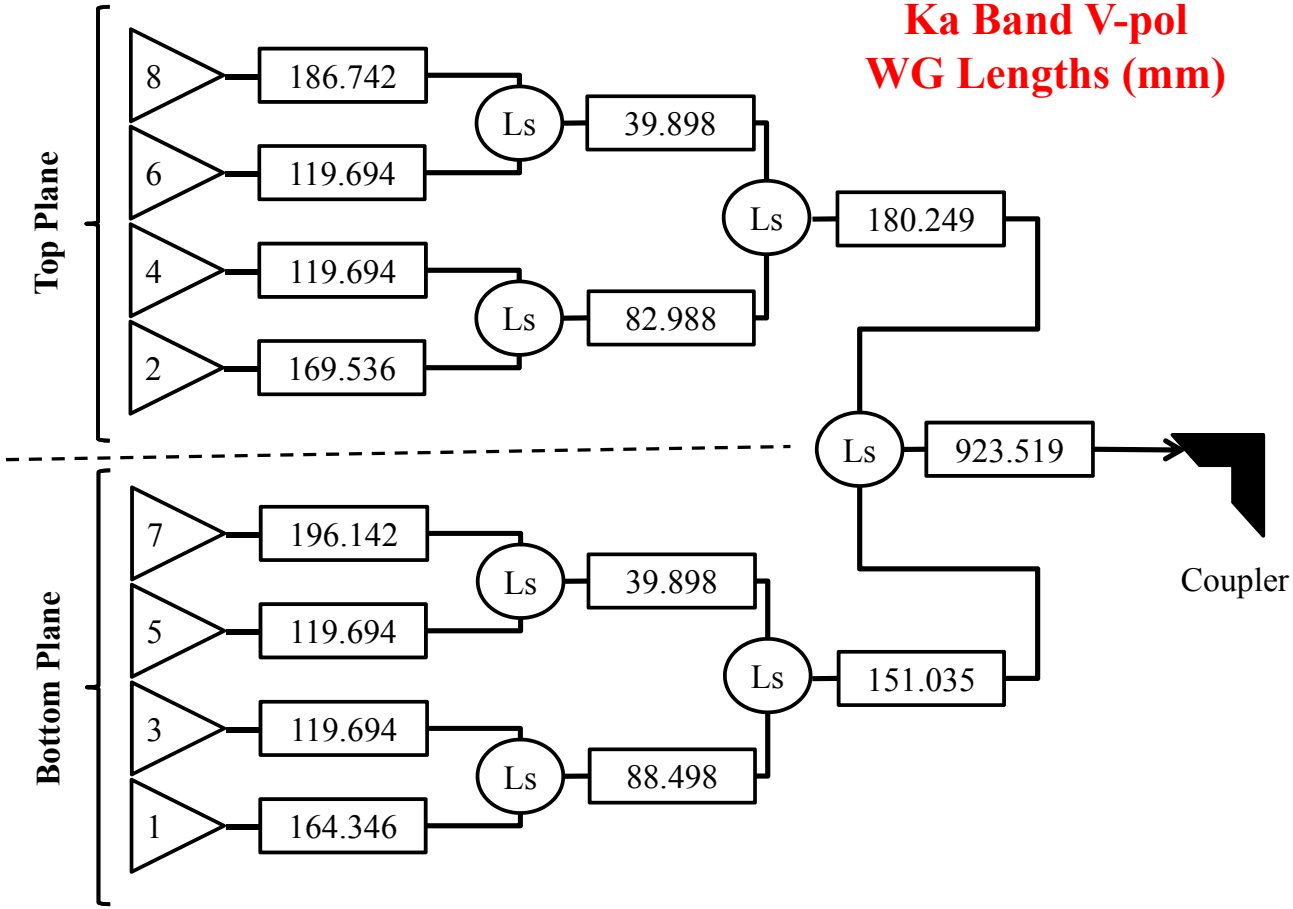

C.4 Ka Band H-pol Waveguide Lengths

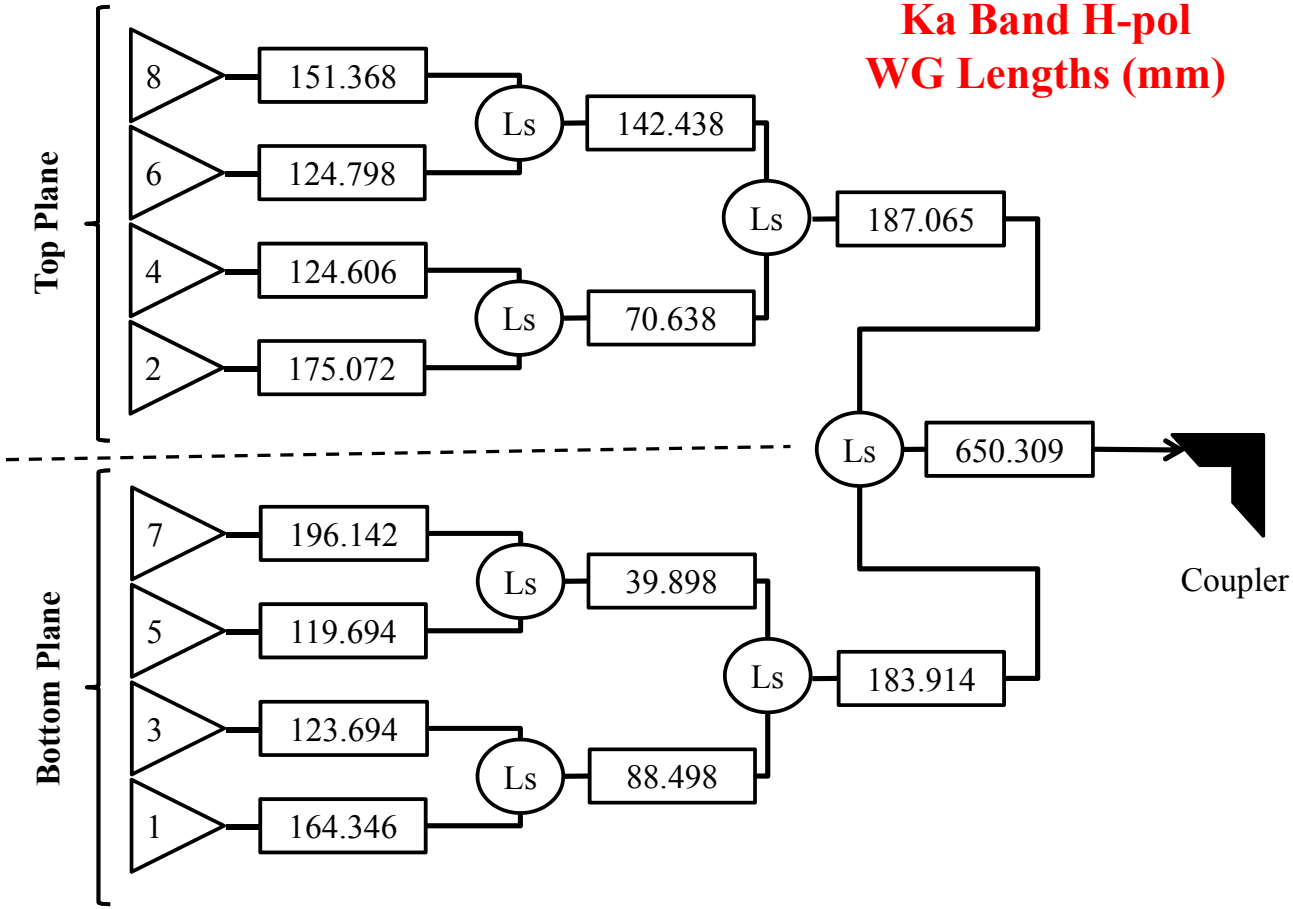

APPENDIX D
MWR SWITCH MATRICES

D.1 K Band Switch Matrix

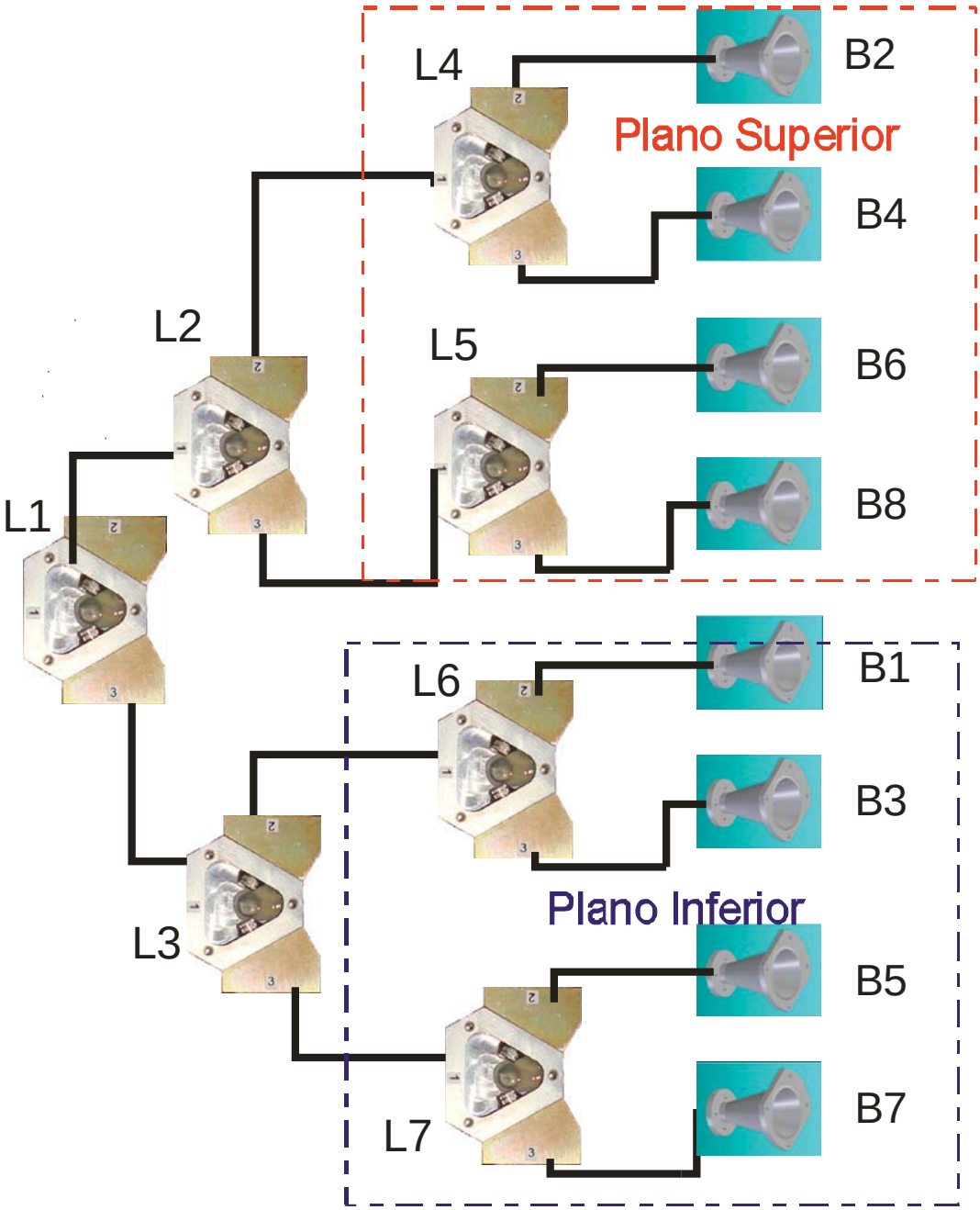

D.2 Ka Band Switch Matrix (H-pol)

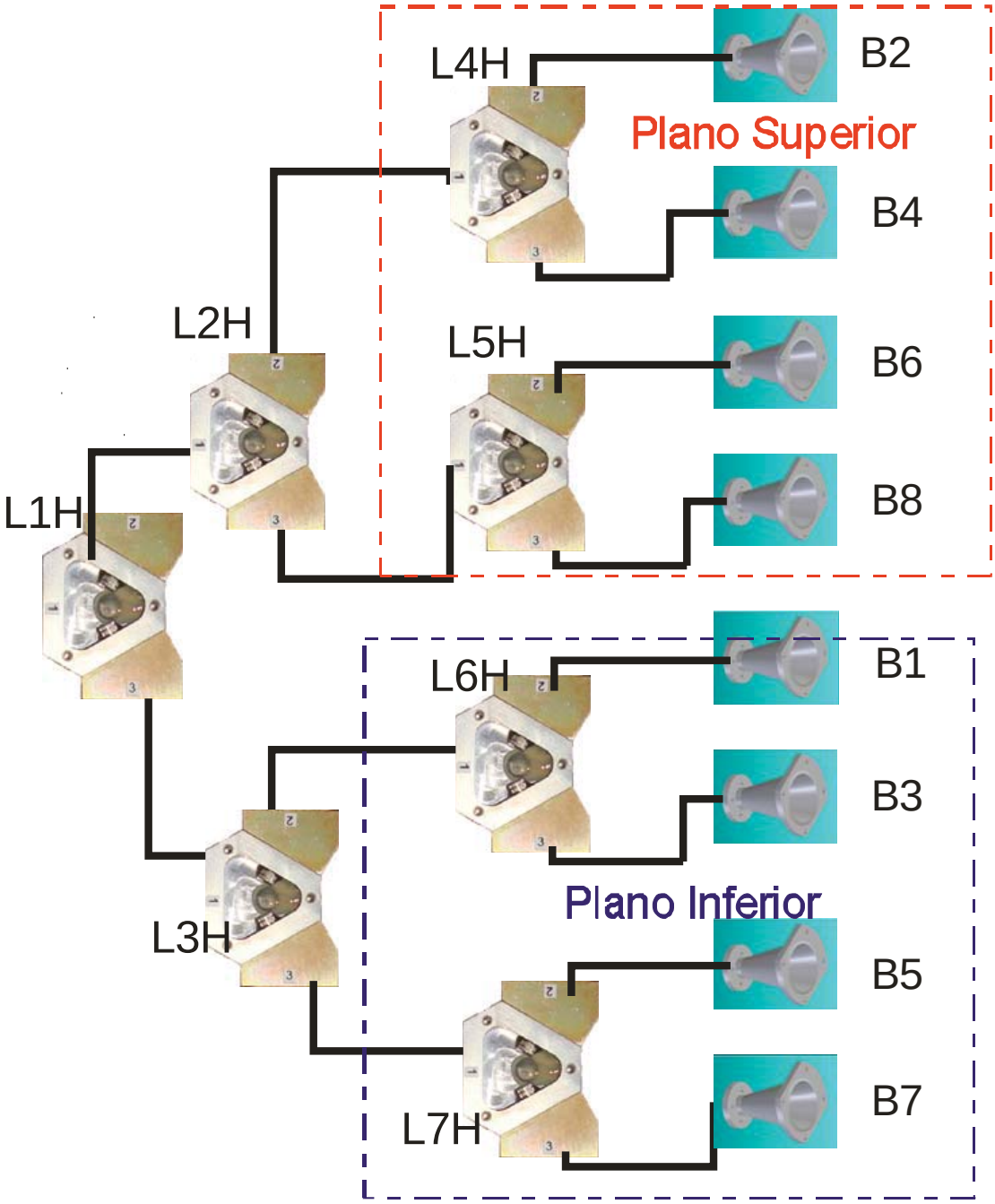

D.3 Ka Band Switch Matrix (V-pol)

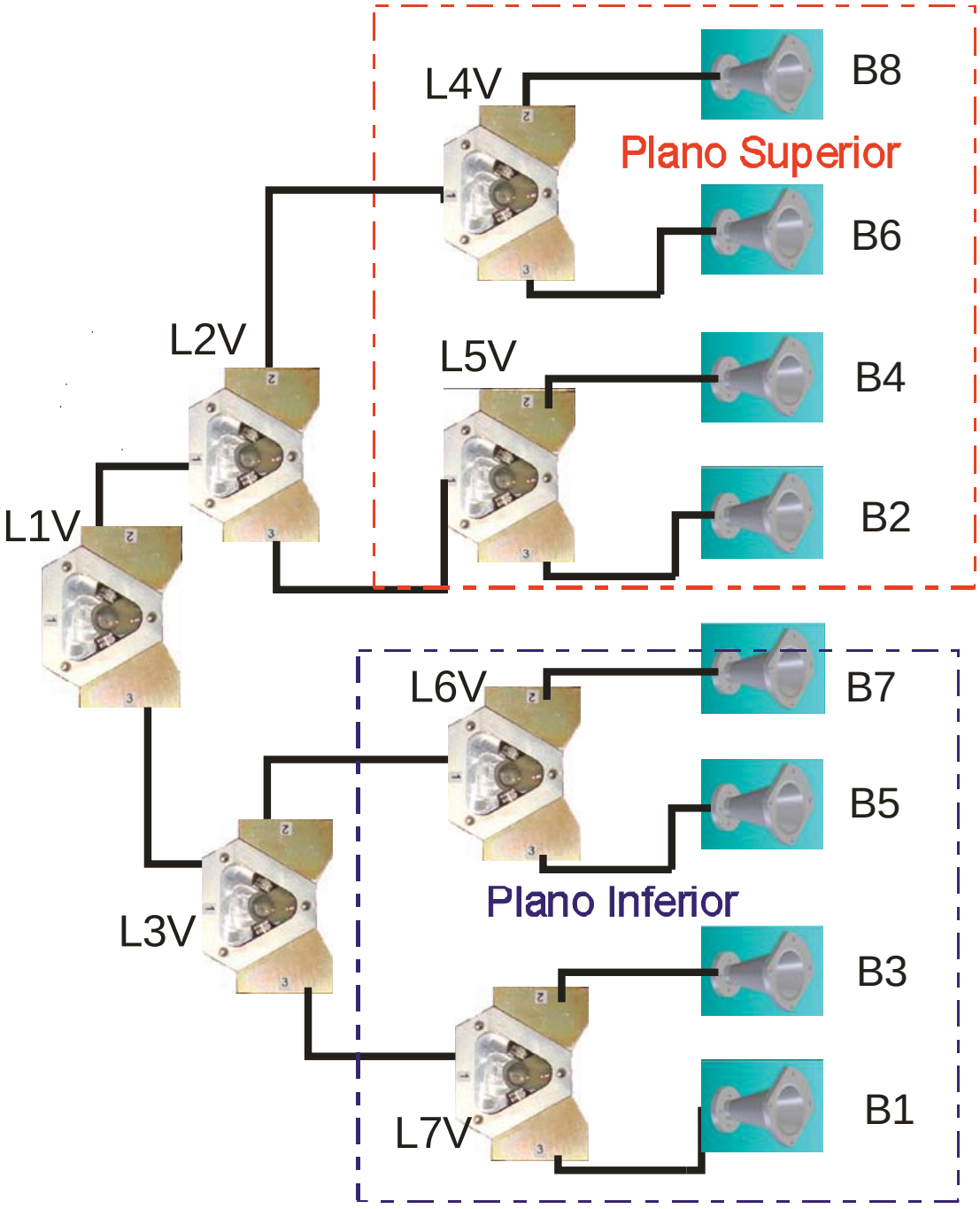

APPENDIX E
MWR THERMAL VACUUM TEST

E.1 K Band Absorber Temperature sensors

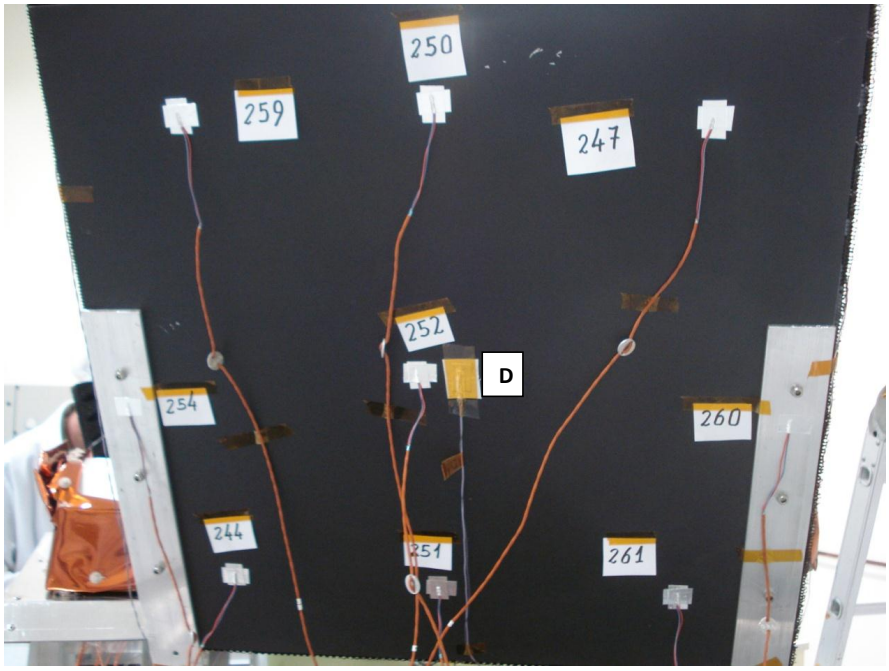

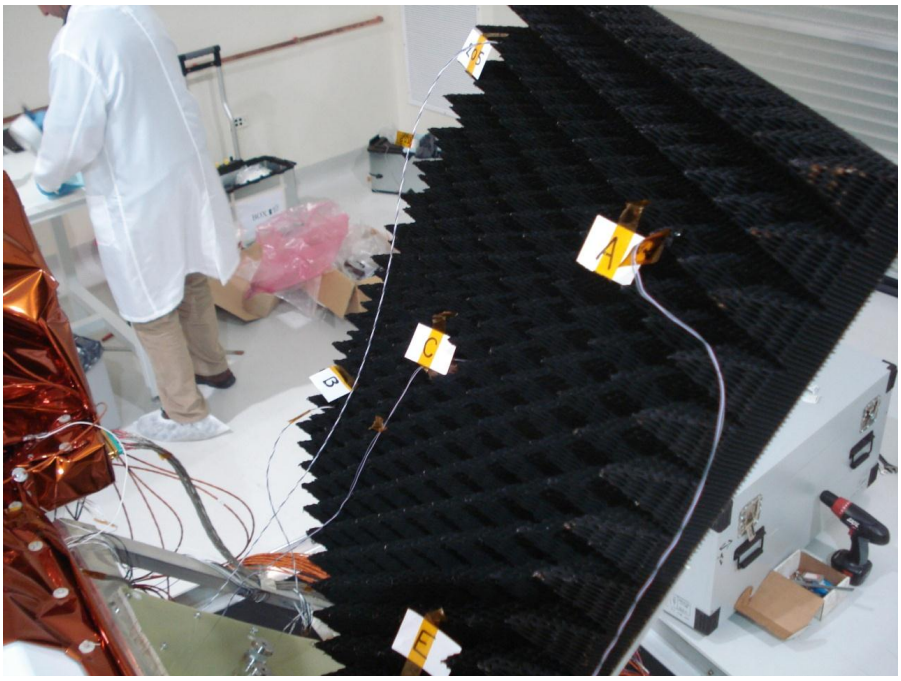

23.8 GHz Absorber

E.2 Ka Band Absorber Temperature sensors

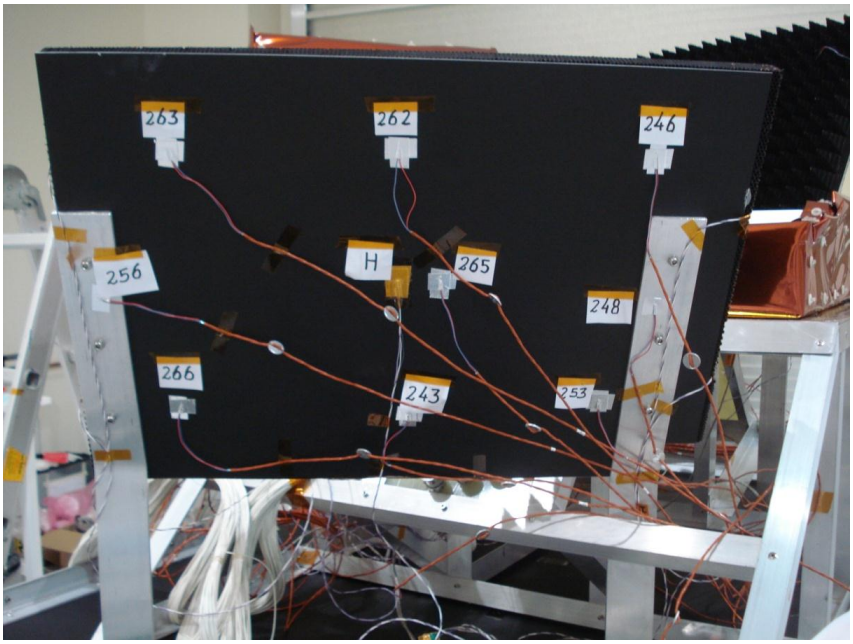

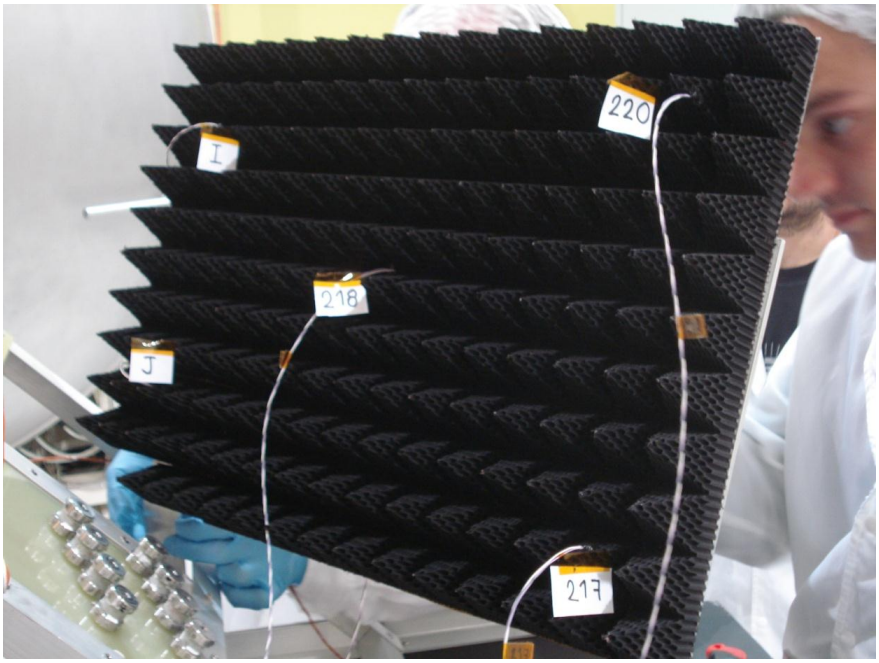

36.5 GHz Absorber

E.3 Thermal Vacuum Test Data Readme

TIME AND DATE (001-006)

COL	DESCRIPTION
1	Day of Month
2	Month Number
3	Year
4	Hour
5	Minute
6	Seconds

MWR Modes & Sampling Sequence (007-008)

COL	DESCRIPTION
7	Mode of Operation
8	Horn ID of the horn being sampled

MODE

Modo de Funcionamiento	MSB del Identificador
Mission	0x05
Stand Alone	0x06
StandBy	0x07
Calibration	0x08
SACalibration	0x0C
Diagnostic	0x09

Tabla 3. Codificación del MSB del (ID)

HORN ID

ANTENA DE 23.8 GHZ	
Bocina de Observación	LSB del Identificador
Bocina 2	0x01
Bocina 4	0x02
Bocina 6	0x03
Bocina 8	0x04
Bocina 1	0x05
Bocina 3	0x06
Bocina 5	0x07
Bocina 7	0x08

ANTENA DE 36.5 GHZ	
Bocina de Observación	LSB del Identificador
Bocina 1	0x01
Bocina 3	0x02
Bocina 5	0x03
Bocina 7	0x04
Bocina 2	0x05
Bocina 4	0x06
Bocina 6	0x07
Bocina 8	0x08

MWR Measurement Counts (009-023)

OFFSET_1 = 8

Column No = OFFSET_1 + SD no

Datos de Ciencia	Subsistema	Source	Data
SD-1	MWR – 36.5 GHz	Horizontal Polarization	**Signal**
SD-2	MWR – 36.5 GHz	Horizontal Polarization	**Signal+Noise**
SD-3	MWR – 36.5 GHz	Horizontal Polarization	**Load**
SD-4	MWR – 36.5 GHz	+45º Phase	**Signal**
SD-5	MWR – 36.5 GHz	+45º Phase	**Signal+Noise**
SD-6	MWR – 36.5 GHz	+45º Phase	**Load**
SD-7	MWR – 36.5 GHz	-45º Phase	**Signal**
SD-8	MWR – 36.5 GHz	-45º Phase	**Signal+Noise**
SD-9	MWR – 36.5 GHz	-45º Phase	**Load**
SD-10	MWR – 36.5 GHz	Vertical Polarization	**Signal**
SD-11	MWR – 36.5 GHz	Vertical Polarization	**Signal+Noise**
SD-12	MWR – 36.5 GHz	Vertical Polarization	**Load**
SD-13	MWR – 23.8 GHz	Horizontal Polarization	**Signal**
SD-14	MWR – 23.8 GHz	Horizontal Polarization	**Signal+Noise**
SD-15	MWR – 23.8 GHz	Horizontal Polarization	**Load**

MWR Telemetry (024-087)

OFFSET_2 = 23

Column No = OFFSET_2 + Parameter no

Parámetro N °	Nombre de la señal	Nombre Sensor	Medición de TEMPERATURA	Subsistema
1	T1	MT_1	Detector 2 (+45)Rx 36GHz	Rx-Front-end
2	T2	MT_2	Detector 3 (-45) Rx 36GHz	Rx-Front-end
3	T3	MT_3	Detector 4 (V) Rx 36GHz	Rx-Front-end
4	T4	MT_4	L23-1	Swich Matrix 23Ghz
5	T5	MT_5	L23-2	Swich Matrix 23Ghz
6	T6	MT_6	L23-3	Swich Matrix 23Ghz
7	T7	MT_7	L23-4	Swich Matrix 23Ghz
8	T8	MT_8	L23-5	Swich Matrix 23Ghz
9	T9	MT_9	Dicke LOAD 36GHz_V/ CALIBRACION	Rx-Front-end
10	T10	MT_10	RED Dicke LOAD 36GHz_V/ CALIBRACION	Rx-Front-end
11	T11	MT_11	Dicke LOAD 23GHz CALIBRACION	Rx-Front-end
12	T12	MT_12	RED Dicke LOAD 23GHz CALIBRACION	Rx-Front-end
13	T13	MT_13	Diodo de Ruido Rx 23GHz	Rx-Front-end
14	T14	MT_14	Diodo de Ruido Rx 36GHz	Rx-Front-end
15	T15	MT_15	Detector Rx 23GHz	Rx-Front-end
16	T16	MT_16	Detector 1 (H) Rx 36GHz	Rx-Front-end
17	T17	MT_17	CTA-7	MRBOX
18	T18	MT_18	CTA-8	Rx-Front-end
19	T19	MT_19	CTA-9	Rx-Front-end
20	T20	MT_20	CTA-10	Rx-Front-end
21	T21	MT_21	BOCINA 6 RX 23GHz	Plano de Bocinas 23 GHZ
22	T22	MT_22	BOCINA 6 RX 36GHz	Plano de Bocinas 36 GHZ
23	T23	MT_23	Dicke LOAD 36GHz_H/ CALIBRACION	Rx-Front-end
24	T24	MT_24	RED Dicke LOAD 36GHz_H/ CALIBRACION	Rx-Front-end
25	T25	MT_25	Bocina 8	RF Switches
26	T26	MT_26	LUP BOX	MRBOX
27	T27	MT_27	CTA-1	Rx-Front-end
28	T28	MT_28	CTA-2	Rx-Front-end
29	T29	MT_29	CTA-3	Rx-Front-end
30	T30	MT_30	CTA-4	Rx-Front-end
31	T31	MT_31	CTA-5	Rx-Front-end
32	T32	MT_32	CTA-6	Rx-Front-end
33	T33	MT_33	L23-6	Swich Matrix 23Ghz
34	T34	MT_34	L23-7	Swich Matrix 23Ghz
35	T35	MT_35	L36V-1	Swich Matrix 36Ghz
36	T36	MT_36	L36V-2	Swich Matrix 36Ghz
37	T37	MT_37	L36V-3	Swich Matrix 36Ghz
38	T38	MT_38	L36V-4	Swich Matrix 36Ghz
39	T39	MT_39	L36V-5	Swich Matrix 36Ghz
40	T40	MT_40	L36V-6	Swich Matrix 36Ghz
41	T41	MT_41	L36V-7	Swich Matrix 36Ghz
42	T42	MT_42	L36H-1	Swich Matrix 36Ghz
43	T43	MT_43	L36H-2	Swich Matrix 36Ghz
44	T44	MT_44	L36H-3	Swich Matrix 36Ghz
45	T45	MT_45	L36H-4	Swich Matrix 36Ghz
46	T46	MT_46	L36H-5	Swich Matrix 36Ghz
47	T47	MT_47	L36H-6	Swich Matrix 36Ghz
48	T48	MT_48	L36H-7	Swich Matrix 36Ghz

Tabla 7. Detalle de los datos de Telemetría de Temperatura

Parámetro N °	Nombre de la señal	Nombre Sensor	Descripción	Subsistema
49	N/A	MV_1	N/A	N/A
50	N/A	MV_2	N/A	N/A
51	V+12_CA	MV_3	Tensión +12V Canales analógicos	Latchup Board
52	V-12_CA	MV_4	Tensión -12V Canales analógicos	Latchup Board
53	RF-LNA-23-1-P12	MV_5	Tensión de alimentación del primer LNA del RX 23GHz	Latchup Board
54	V+5_CA	MV_6	Tensión 5V Canales analógicos	Latchup Board
55	N/A	MV_7	N/A	N/A
56	N/A	MV_8	N/A	N/A

Tabla 8. Detalle de los datos de Telemetría de Tensiones

Parámetro N °	Nombre de la señal	Nombre Sensor	Descripción	Subsistema
57	RF-LNA-23-1-P12	MI_1	Monitor de corriente del primer LNA del RX 23GHz	Latchup Board
58	RF-LNA2-36-V-P12	MI_2	Monitor de corriente del 2do LNA V del RX 36GHz	Latchup Board
59	N/A	MI_3	N/A	N/A
60	RF-LNA2-36-H-P12	MI_4	Monitor de corriente del 2do LNA H del RX 36GHz	Latchup Board
61	RF-LNA1-36-H-P12	MI_5	Monitor de corriente del 1er LNA H del RX 36GHz	Latchup Board
62	RF-LNA-23-2-P12	MI_6	Monitor de corriente del 2do LNA del RX 23GHz	Latchup Board
63	N/A	MI_7	N/A	N/A
64	RF-LNA1-36-V-P12	MI_8	Monitor de corriente del 1er LNA V del RX 36GHz	Latchup Board

Tabla 9. Detalle de los datos de Telemetría de Corrientes

Thermal Control Parameters (088-089)

COL	DESCRIPTION
88	Thermal Control
89	Thermal Control

Cyclic Redundancy Check - CRC (090-091)

COL	DESCRIPTION
90	First 8 bit (0-255)
91	Last 8 bit (0-255)

External Temperature Sensors (092-132)

	23 GHz
	36 GHz

COL	DESCRIPTION
92	101
93	102
94	103
95	104
96	105
97	106
98	107
99	108
100	109
101	110
102	111
103	112
104	113 - ABS 23 A
105	114
106	115
107	116
108	117
109	118 - ABS 23 B
110	119 - Sensor Inside 23 GHz HORN
111	120 - Sensor Inside 36 GHz HORN
112	201
113	202 - ABS 23 E
114	203 - ABS 23 D
115	204 - ABS 23 C
116	205 - ABS 23
117	206
118	207
119	208
120	209
121	210
122	211
123	212
124	213 - ABS 36 H
125	214 - ABS 36 I
126	215 - ABS 36 J
127	216
128	217- ABS 36
129	218 - ABS 36
130	219
131	220 - ABS 36

CHAMBER Temperature Sensors (132-155)

COL	DESCRIPTION
132	TC#243- ABS 36
133	TC#245
134	TC#246- ABS 36
135	TC#247- ABS 23
136	TC#248- ABS 36
137	TC#249
138	TC#250- ABS 23
139	TC#251- ABS 23
140	TC#252- ABS 23
141	TC#253- ABS 36
142	TC#254- ABS 23
143	TC#255
144	TC#256- ABS 36
145	TC#257
146	TC#258
147	TC#259- ABS 23
148	TC#260- ABS 23
149	TC#261- ABS 23
150	TC#262- ABS 36
151	TC#263- ABS 36
152	TC#264
153	TC#265- ABS 36
154	TC#266- ABS 36

APPENDIX F
MWR LEVEL 1 DATA PRODUCTS

F.1 CONAE L1A Data (HDF5)

MWR L1A Product HDF5 Data Format Reference

Authors: Felipe Madero

Date: Feb 29, 2012

COMISION NACIONAL DE ACTIVIDADES ESPACIALES
ARGENTINA

Table of Contents

1 Description of Hdf5 Global Metadata Attributes 3
1.1 Group '/' . . . 3
1.2 Group 'Global Metadata/Acquisition' . . . 3
1.3 Group 'Global Metadata/Downloading/Pass Id %s' . . . 4
1.4 Group 'Global Metadata/Mission' . . . 5
1.5 Group 'Global Metadata/Platform' . . . 5
1.6 Group 'Global Metadata/Platform/Orbit' . . . 5
1.7 Group 'Global Metadata/Product' . . . 7
1.8 Group 'Global Metadata/Product/Stats' . . . 8
1.9 Group 'Global Metadata/Production' . . . 9
1.10 Group 'Global Metadata/Sensor' . . . 10
1.11 Group 'Global Metadata/Software' . . . 12

2 Description of Hdf5 Datasets 13
2.1 Group 'Block Attributes' . . . 13
2.2 Group 'Calibration/Geometric Data' . . . 14
2.3 Group 'Calibration/Radiometric Data' . . . 16
2.4 Group 'Converted Telemetry' . . . 19
2.5 Group 'Navigation' . . . 31
2.6 Group 'Raw MWR Data' . . . 33
2.7 Group 'SAC-D Telemetry' . . . 37

1 Description of Hdf5 Global Metadata Attributes

1.1 Group '/'

Root group for the product.

- **hdf5_especification_filename**

  description: Filename of the .xml hdf5 estructure especification file from which this product was created.
  default value: mwr_l0a_l1a_hdf5_esp.3_0.xml
  datatype: string

1.2 Group 'Global Metadata/Acquisition'

Information related to the acquisition of data by the sensor.

- **Cycle Number**

  description: Counter of weekly cycles (103 orbits) since Aquarius's Commisioning end.
  datatype: 4 bytes signed integer

- **End Time GPS**

  description: GPS time tag for the last MWR data included in the product (seconds since 1980/01/06 00:00:00 UTC)
  datatype: 4 bytes unsigned integer

- **End Time UTC**

  description: UTC time time tag for the last MWR data included in the product
  datatype: string

- **Length Seconds**

  description: Elapsed time period between the first and last MWR data included in the product
  datatype: 4 bytes unsigned integer

- **MWR Reference System Pass Number**

  description: Id of revolution inside the weekly cycle. Consecutive numbers 1 to 103 represent geographically adjacent revolutions. Refer to 'MWR Reference System Pass Number to In Cycle Pass Number Map' to map between these two ids.
  datatype: 1 byte unsigned integer

- **Orbit End Time UTC**

  description: UTC time time tag for the end of the MWR orbit (descending crossing of the south pole)
  datatype: string

- **Orbit Node Longitude**

  description: Longitude of orbit ascending node (equatorial crossing at PM node)
  datatype: 4 bytes IEEE floating point

- **Orbit Node Time UTC**

  description: UTC time time tag for orbit ascending node (equatorial crossing at PM node)
  datatype: string

- **Orbit Number**

  description: Counter of revolutions since launch.
  datatype: 4 bytes signed integer

- **Orbit Start Time UTC**

  description: UTC time time tag for the start of the MWR orbit (ascending crossing of the south pole)
  datatype: string

- **Overlapped Orbit End Time UTC**

  description: UTC time time tag for end of the Overlapped MWR orbit (end of the MWR orbit plus 10 minutes)
  datatype: string

- **Overlapped Orbit Start Time UTC**

  description: UTC time time tag for start of the Overlapped MWR orbit (start of the MWR orbit minus 10 minutes)
  datatype: string

- **Pass Number in Cycle**

  description: Id of revolution inside the weekly cycle. Consecutive numbers 1 to 103 represent revolutions adjacent in time. Refer to 'MWR Reference System Pass Number to In Cycle Pass Number Map' to map between these two ids.
  datatype: 1 byte unsigned integer

- **Start Time GPS**

  description: GPS time tag for the first MWR data included in the product (seconds since 1980/01/06 00:00:00 UTC)
  datatype: 4 bytes unsigned integer

- **Start Time UTC**

  description: UTC time time tag for the first MWR data included in the product
  datatype: string

1.3 Group 'Global Metadata/Downloading/Pass Id %s'

Information related to the download Pass Id %s

More than one instance of this group, and its subgroups, may be present in the product. Each instance will be identificated with an Id replacing the %s character sequences.

- **Agency Id**

  description: Identification of space agency that downloaded this data.
  datatype: string

- **Country Id**

  description: Identification of the country the space agency that downloaded this data belongs to.
  datatype: string

- **Facility Id**

  description: Identification of the facility inside the space agency that downloaded this data.
  datatype: string

- **Service Id**

  description: Identification of the service inside the space agency that downloaded this data.
  datatype: string

- **Start Time UTC**

  description: UTC time tag for the start of the downloading of this data.
  datatype: string

1.4 Group 'Global Metadata/Mission'

Information related to the mission.

- **Name**

  description: Full name for the mission associated to this product.
  default value: SAC-D Aquarius
  datatype: string

1.5 Group 'Global Metadata/Platform'

Information related to the platform.

- **Name**

  description: Full name of the spacecraft platform associated to this product.
  default value: SAC-D
  datatype: string

- **Reference Time**

  description: Main reference time system used in relation with platform information.
  default value: GPS
  datatype: string

1.6 Group 'Global Metadata/Platform/Orbit'

Information related to the orbit of the platform.

- **Mean Argument Perigee Degrees**

  description: Mean Argument of Perigee for the orbit of the platform associated to the product
  default value: 90.0
  datatype: 4 bytes IEEE floating point

- **Mean Eccentricity**

  description: Mean Eccentricity for the orbit of the platform associated to the product
  default value: 0.0012
  datatype: 4 bytes IEEE floating point

- **Mean Equatorial Altitude Km**

  description: Mean Altitude, when crossing above the equator, for the orbit of the platform associated to the product
  default value: 657.0
  datatype: 4 bytes IEEE floating point

- **Mean Inclination Degrees**

  description: Mean Inclination for the orbit of the platform associated to the product
  default value: 98.01
  datatype: 4 bytes IEEE floating point

- **Mean Local Time of ascending Node**

  description: Mean Local Time of Ascending Node for the orbit of the platform associated to the product
  default value: 06:00 PM
  datatype: string

- **Mean Period Min**

  description: Mean minutes required by the platform in order to complete a revolution.
  default value: 98.0
  datatype: 4 bytes IEEE floating point

- **Mean SemiMajor Axis Km**

  description: Mean Semimajor Axis for the orbit of the platform associated to the product
  default value: 7028.87
  datatype: 4 bytes IEEE floating point

- **Revisit Cycle Days**

  description: Number of days needed by the platform in order to pass above the same point in earth.
  default value: 7
  datatype: 1 byte signed integer

- **Revisit Cycle Revolutions**

  description: Number of revolutions needed by the platform in order to pass above the same point in earth.
  default value: 103
  datatype: 1 byte unsigned integer

- **Type**

  description: Description of the main characteristics of the orbit of the platform associated to the product
  default value: Frozen, Almost circular, Dawn-Dusk, Sun Synchronous
  datatype: string

1.7 Group 'Global Metadata/Product'

Information related to the product contents.

- **CODS Attitude Vector Algorithm Version**

  description: Version of Algorithm used to generate included CODS attitude vectors (if applicable)
  datatype: string

- **CODS State Vector Algorithm Version**

  description: Version of Algorithm used to generate included CODS state vectors (if applicable)
  datatype: string

- **Data Format**

  description: Base product data format.
  default value: NCSA-HDF5
  datatype: string

- **Data Format Version**

  description: Base product data format version.
  datatype: string

- **Data Type**

  description: Identifies the kind of data present in the product. One of SCI (Science data), CAL (Calibration data), ENG (Engineering data).
  datatype: string

- **Geometric Tables Update Id**

  description: Update Id of Geometric Calibration Tables included in the product.
  datatype: string

- **Level**

  description: Indication of the production level. One of L0A, L1A, L1B.
  default value: L1A
  datatype: string

- **Level Version**

  description: Version number for the level of this product.
  default value: 3.0
  datatype: string

- **Name**

  description: Full name of the product, used also in file names. Format: EO_YYYMMDD _HHMMSS_SERVICE_SPACECRAFT_SENSOR_LEVEL_DATA. Where time info refers to UTC time tag associated to the start of the overlapped orbit, SERVICE is Production Service Id, SPACECRAFT is Platform Name, SENSOR is Sensor Name, LEVEL is Product Level, DATA is Product Data Type.
  datatype: string

- **Radiometric Tables Update Id**

  description: Update Id of Radiometric Calibration Tables included in the product.
  datatype: string

- **Reference Coordinate System**

  description: Reference coordinate system used to generate geographical information for this product.
  default value: J2000
  datatype: string

- **Reference Datum**

  description: Reference datum used to generate geographical information for this product.
  default value: WGS84
  datatype: string

- **Title**

  description: Identifies Sensor Name, and Product Level.
  default value: MWR Level-1A Data
  datatype: string

1.8 Group 'Global Metadata/Product/Stats'

Statistics for the product contents.

- **Number of CSDP frames**

  description: Number of Conae Science Data Packages whose data is included in the product
  datatype: 4 bytes unsigned integer

- **Number of CSDP frames with CRC error**

  description: Number of Conae Science Data Packages whose data is included in the product that contains CRC errors
  datatype: 4 bytes unsigned integer

- **Number of MWR Data frames**

  description: Number of MWR data/housekeeping frames whose data is included in the product
  datatype: 4 bytes unsigned integer

- **Number of Quaternion Vectors**

  description: Number of quaternion vectors included in the product
  datatype: 4 bytes unsigned integer

- **Number of SAC-D Telemetry frames**

  description: Number of SAC-D telemetry frames included in the product
  datatype: 4 bytes unsigned integer

- **Number of SAC-D Telemetry frames with CRC error**

  description: Number of SAC-D telemetry frames included in the product that contains CRC errors
  datatype: 4 bytes unsigned integer

- **Number of State Vectors**

  description: Number of state vectors included in the product
  datatype: 4 bytes unsigned integer

- **Number of missing CSDP frames**

  description: Number of Conae Science Data Packages missing in the package sequence included in the product
  datatype: 4 bytes unsigned integer

- **Number of missing MWR Data frames**

  description: Number of MWR data/housekeeping frames missing in the frame sequence included in the product
  datatype: 4 bytes unsigned integer

1.9 Group 'Global Metadata/Production'

Information related to the production activity.

- **Agency Id**

  description: Identification of space agency that generated this product
  datatype: string

- **Center**

  description: Identification of the facility and agency that generated this product.
  datatype: string

- **Center Reference Time**

  description: Main reference time system used in the results of the production.
  default value: UTC
  datatype: string

- **Contact Organization Name**

  description: Address of the Production Center
  datatype: string

- **Control Parameters**

  description: Command line arguments of the program used to generate this product.
  datatype: string

- **Country Id**

  description: Identification of the country the space agency that generated this product belongs to.
  datatype: string

- **Facility Id**

  description: Identification of the facility inside the space agency that generated this product.
  datatype: string

- **Input Files**

  description: List of input files used to generate this product.
  datatype: string

- **Service Id**

  description: Identification of the service inside the space agency that generated this product.
  datatype: string

- **Start Time UTC**

  description: UTC time tag for the start of the generation of this product.
  datatype: string

1.10 Group 'Global Metadata/Sensor'

Information related to the sensor.

- **BeamWidth Degrees**

  description: Length in degrees of the beam received by a horn.
  default value: 1.7
  datatype: 4 bytes IEEE floating point

- **Frequency Bands**

  description: List of frequency bands of the sensor.
  default value: 23.8 GHz (K) - 36.5 GHz (Ka)
  datatype: string

- **K Band BandWidth MHz**

  description: Measured bandwidth around the central frequency for the K band H polarization
  default value: 400.0
  datatype: 4 bytes IEEE floating point

- **Ka Band BandWidth MHz**

  description: Measured bandwidth around the central frequency for the Ka band at all polarizations
  default value: 1000.0
  datatype: 4 bytes IEEE floating point

- **MWR Reference System Pass Number to In Cycle Pass Number Map**

  description: Map between the two systems used to identify a particular revolution inside the weekly cycle: MWR Reference System Pass Number and Cycle Pass Number
  default value: 001: 100 , 002: 041 , 003: 085 , 004: 026 , 005: 070 , 006: 011 , 007: 055 , 008: 099 , 009: 040 , 010: 084 , 011: 025 , 012: 069 , 013: 010 , 014: 054 , 015: 098 , 016: 039 , 017: 083 , 018: 024 , 019: 068 , 020: 009 , 021: 053 , 022: 097 , 023: 038 , 024: 082 , 025: 023 , 026: 067 , 027: 008 , 028: 052 , 029: 096 , 030: 037 , 031: 081 , 032: 022 , 033: 066 , 034: 007 , 035: 051 , 036: 095 , 037: 036 , 038: 080 , 039: 021 , 040: 065 , 041: 006 , 042: 050 , 043: 094 , 044: 035 , 045: 079 , 046: 020 , 047: 064 , 048: 005 , 049: 049 , 050: 093 , 051: 034 , 052: 078 , 053: 019 , 054: 063 , 055: 004 , 056: 048 , 057: 092 , 058: 033 , 059: 077 , 060: 018 , 061: 062 , 062: 003 , 063: 047 , 064: 091 , 065: 032 , 066: 076 , 067: 017 , 068: 061 , 069: 002 , 070: 046 , 071: 090 , 072: 031 , 073: 075 , 074: 016 , 075: 060 , 076: 001 , 077: 045 , 078: 089 , 079: 030 , 080: 074 , 081: 015 , 082: 059 , 083: 103 , 084: 044 , 085: 088 , 086: 029 , 087: 073 , 088: 014 , 089: 058 , 090: 102 , 091: 043 , 092: 087 , 093: 028 , 094: 072 , 095: 013 , 096: 057 , 097: 101 , 098: 042 , 099: 086 , 100: 027 , 101: 071 , 102: 012 , 103: 056
  datatype: string

- **Name**

  description: Name of the sensor.
  default value: MWR
  datatype: string

- **Number of beams per channel**

  description: Number of beams/horns per channel
  default value: 8
  datatype: 1 byte unsigned integer

- **Number of channels**

  description: Number of channels measured by the sensr
  default value: 5
  datatype: 1 byte unsigned integer

- **Off Nadir Pointing Degrees**

  description: Off nadir central pointing for each band.
  default value: 23.8 GHz 47.95El/143.73Az - 36.5 GHz 47.95El/36.27Az
  datatype: string

- **Polarizations**

  description: List of all central frequencies and associated polarizations.
  default value: 23.8 GHz H - 36.5 GHz H - 36.5 GHz V - 36.5 GHz +45 - 36.5 GHz -45
  datatype: string

- **Spatial Resolution Km**

  description: Length of the footprint of a horn at the earth surface.
  default value: 54.23
  datatype: 4 bytes IEEE floating point

- **Swath Width Km**

  description: Total distance covered at the earth surface by the 8 horns of a band and polarization pair.
  default value: 367.89
  datatype: 4 bytes IEEE floating point

1.11 Group 'Global Metadata/Software'

Information related to the software used to generate the product.

- **Name**

  description: Name of the software that generated this product
  datatype: string

- **Release**

  description: Configuration control release name of the software that generated this product
  datatype: string

- **Version**

  description: Version of the software that generated this product
  datatype: string

2 Description of Hdf5 Datasets

2.1 Group 'Block Attributes'

Raw values of variables obtained from CSDP headers and trailers, associated to MWR data frames.

Datasets

- **csdp_packet_sequence_count**

  description: CSDP primary header packet sequence count. Increments for each CSDP frame with PAD data.
  datatype: 2 bytes unsigned integer
  size: Number of MWR Data frames

- **csdp_source_sequence_count**

  description: CSDP secondary header source sequence count. Increments for each CSDP frame with PAD data associated to MWR data
  datatype: 2 bytes unsigned integer
  size: Number of MWR Data frames

- **missing_mwr_frames**

  description: Indicates the number of missing MWR data frames before the current one
  datatype: 2 bytes unsigned integer
  size: Number of MWR Data frames

- **pad_csdp_crc**

  description: CRC of the CSDP frame as calculated by PAD
  datatype: 2 bytes unsigned integer
  size: Number of MWR Data frames

- **pad_csdp_crc_is_valid**

  description: Equal to 1 if CSDP CRC was validated
  valid values: [0,1]
  datatype: 1 byte unsigned integer
  size: Number of MWR Data frames

- **pad_csdp_fill**

  description: Fill bytes at the end of CSDP MWR frames
  datatype: 1 byte unsigned integer
  size: Number of MWR Data frames x 182

- **tlm_qual**

  description: Telemetry quality: indicates the degree of quality of the MWR data frame contents
  valid values: [5=good quality, 4, 3, 2, 1=poor quality]
  datatype: 1 byte unsigned integer
  size: Number of MWR Data frames

- **tlm_qual_flags**

  description: Telemetry quality flags: bitmask indicating invalid data in MWR data frames
  units: bitmask
  valid values: byte0: bit7 (msb) = tm_t01, ..., bit0 = tm_t08; byte1: bit7 = tm_t09, ..., bit0 = tm_t16;

byte2: bit7 = tm_t17, ..., bit0 = tm_t24; byte3: bit7 = tm_t25, ..., bit0 = tm_t32; byte4: bit7 = tm_t33, ..., bit0 = tm_t40; byte5: bit7 = tm_t41, ..., bit0 = tm_t48; byte6: bit7 = vm_v01, ..., bit0 = vm_v08; byte7: bit7 = im_i01, ..., bit0 = im_i08; byte8: bit7 = sacd_vbusa_rtu1, bit6 = sacd_vbusb_rtu1, bit5 = K H antenna, bit4 = K H antenna plus noise, bit3 = K H load, bit2 = Ka H antenna, bit1 = Ka H antenna plus noise, bit0 = Ka H load; byte9: bit7 = Ka V antenna, bit6 = Ka V antenna plus noise, bit5 = Ka V load, bit4 = Ka +45 antenna, bit3 = Ka +45 antenna plus noise, bit2 = Ka +45 load, bit1 = Ka -45 antenna, bit0 = Ka -45 antenna plus noise; byte10: bit7 = Ka -45 load
datatype: 1 byte unsigned integer
size: Number of MWR Data frames x 11

2.2 Group 'Calibration/Geometric Data'

Calibration data needed to perform geometric processing.

Datasets

- **k_h_line_of_sight**

  description: Line of sight of each horn of K band H polarization, expressed in the platform fixed coordinate system.
  datatype: 4 bytes IEEE floating point
  size: Number of beams per channel x 3

- **k_h_n3db_approximating_ellipse**

  This dataset is optional, it may be present on the product only due to specific user request.

  description: Lines of sight of the center, first semimajor axis, first semiminor axis, second semimajor axis, second semiminor axis, of the ellipse that approximates the -3dB contour for all horns of K band H polarization, expressed in the platform fixed coordinate system.
  datatype: 4 bytes IEEE floating point
  size: Number of beams per channel x 5 x 3

- **k_h_n3db_contour**

  This dataset is optional, it may be present on the product only due to specific user request.

  description: Lines of sight of selected points from the -3dB contour for all horns K band H polarization, expressed in the platform fixed coordinate system.
  datatype: 4 bytes IEEE floating point
  size: Number of beams per channel x 20 x 3

- **ka_h_line_of_sight**

  description: Line of sight of each horn of Ka band H polarization, expressed in the platform fixed coordinate system.
  datatype: 4 bytes IEEE floating point
  size: Number of beams per channel x 3

- **ka_h_n3db_approximating_ellipse**

  This dataset is optional, it may be present on the product only due to specific user request.

  description: Lines of sight of the center, first semimajor axis, first semiminor axis, second semimajor axis, second semiminor axis, of the ellipse that approximates the -3dB contour for all horns of Ka band H polarization, expressed in the platform fixed coordinate system.

datatype: 4 bytes IEEE floating point
size: Number of beams per channel x 5 x 3

- **ka_h_n3db_contour**

  This dataset is optional, it may be present on the product only due to specific user request.

  description: Lines of sight of selected points from the -3dB contour for all horns Ka band H polarization, expressed in the platform fixed coordinate system.
  datatype: 4 bytes IEEE floating point
  size: Number of beams per channel x 20 x 3

- **ka_n45_line_of_sight**

  description: Line of sight of each horn of Ka band -45 polarization, expressed in the platform fixed coordinate system.
  datatype: 4 bytes IEEE floating point
  size: Number of beams per channel x 3

- **ka_n45_n3db_approximating_ellipse**

  This dataset is optional, it may be present on the product only due to specific user request.

  description: Lines of sight of the center, first semimajor axis, first semiminor axis, second semimajor axis, second semiminor axis, of the ellipse that approximates the -3dB contour for all horns of Ka band -45 polarization, expressed in the platform fixed coordinate system.
  datatype: 4 bytes IEEE floating point
  size: Number of beams per channel x 5 x 3

- **ka_n45_n3db_contour**

  This dataset is optional, it may be present on the product only due to specific user request.

  description: Lines of sight of selected points from the -3dB contour for all horns Ka band -45 polarization, expressed in the platform fixed coordinate system.
  datatype: 4 bytes IEEE floating point
  size: Number of beams per channel x 20 x 3

- **ka_p45_line_of_sight**

  description: Line of sight of each horn of Ka band +45 polarization, expressed in the platform fixed coordinate system.
  datatype: 4 bytes IEEE floating point
  size: Number of beams per channel x 3

- **ka_p45_n3db_approximating_ellipse**

  This dataset is optional, it may be present on the product only due to specific user request.

  description: Lines of sight of the center, first semimajor axis, first semiminor axis, second semimajor axis, second semiminor axis, of the ellipse that approximates the -3dB contour for all horns of Ka band +45 polarization, expressed in the platform fixed coordinate system.
  datatype: 4 bytes IEEE floating point
  size: Number of beams per channel x 5 x 3

- **ka_p45_n3db_contour**

  This dataset is optional, it may be present on the product only due to specific user request.

description: Lines of sight of selected points from the -3dB contour for all horns Ka band +45 polarization, expressed in the platform fixed coordinate system.
datatype: 4 bytes IEEE floating point
size: Number of beams per channel x 20 x 3

- **ka_v_line_of_sight**

  description: Line of sight of each horn of Ka band V polarization, expressed in the platform fixed coordinate system.
  datatype: 4 bytes IEEE floating point
  size: Number of beams per channel x 3

- **ka_v_n3db_approximating_ellipse**

  This dataset is optional, it may be present on the product only due to specific user request.

  description: Lines of sight of the center, first semimajor axis, first semiminor axis, second semimajor axis, second semiminor axis, of the ellipse that approximates the -3dB contour for all horns of Ka band V polarization, expressed in the platform fixed coordinate system.
  datatype: 4 bytes IEEE floating point
  size: Number of beams per channel x 5 x 3

- **ka_v_n3db_contour**

  This dataset is optional, it may be present on the product only due to specific user request.

  description: Lines of sight of selected points from the -3dB contour for all horns Ka band V polarization, expressed in the platform fixed coordinate system.
  datatype: 4 bytes IEEE floating point
  size: Number of beams per channel x 20 x 3

- **line_of_sight_horn_id**

  description: Horn id associated to line of sight datasets.
  valid values: [1,...,8]
  datatype: 1 byte unsigned integer
  size: Number of beams per channel

- **platform_to_attitude_alignment_matrix**

  description: Platform fixed to Attitude fixed alignment matrix. Transformation from a vector expressed in the Platform fixed reference system to a vector expressed in the Attitude control subsystem fixed reference system.
  datatype: 4 bytes IEEE floating point
  size: 3 x 3

2.3 Group 'Calibration/Radiometric Data'

Calibration data needed to perform radiometric processing.

Datasets

- **beta_params_horn_id**

  description: Horn id associated to beta params datasets.
  valid values: [1,...,8]
  datatype: 1 byte unsigned integer
  size: Number of beams per channel

- **k_h_beta_params**

  description: Beta params for K band H polarization: B1 (coupler input temperature offset), B2 (coupler input temperature weight), B3 (squared coupler input temperature weight), B4 (reference load temperature weight), B5 (average front end temperature weight).
  datatype: 4 bytes IEEE floating point
  size: Number of beams per channel x 5

- **k_h_noise_diode_temperature**

  description: Noise diode temperature for K band H polarization.
  units: kelvins
  datatype: 4 bytes IEEE floating point
  size: 1

- **k_h_temperature_sensors**

  description: Selected temperature sensors for radiometric correction formulae of K band H polarization: T0A (reference load temperature A), T0B (reference load temperature B), T1 (switch 1 temperature), T2 (switch 2 temperature), T3 (switch 3 temperature), T4 (horn temperature)
  datatype: 1 byte unsigned integer
  size: Number of beams per channel x 6

- **ka_h_beta_params**

  description: Beta params for Ka band H polarization: B1 (coupler input temperature offset), B2 (coupler input temperature weight), B3 (squared coupler input temperature weight), B4 (reference load temperature weight), B5 (average front end temperature weight).
  datatype: 4 bytes IEEE floating point
  size: Number of beams per channel x 5

- **ka_h_noise_diode_temperature**

  description: Noise diode temperature for Ka band H polarization.
  units: kelvins
  datatype: 4 bytes IEEE floating point
  size: 1

- **ka_h_temperature_sensors**

  description: Selected temperature sensors for radiometric correction formulae of Ka band H polarization: T0A (reference load temperature A), T0B (reference load temperature B), T1 (switch 1 temperature), T2 (switch 2 temperature), T3 (switch 3 temperature), T4 (horn temperature)
  datatype: 1 byte unsigned integer
  size: Number of beams per channel x 6

- **ka_n45_beta_params**

  description: Beta params for Ka band -45 polarization: B1 (coupler input temperature offset), B2 (coupler input temperature weight), B3 (squared coupler input temperature weight), B4 (reference load temperature weight), B5 (average front end temperature weight).
  datatype: 4 bytes IEEE floating point
  size: Number of beams per channel x 5

- **ka_n45_noise_diode_temperature**

  description: Noise diode temperature for Ka band -45 polarization.
  units: kelvins
  datatype: 4 bytes IEEE floating point
  size: 1

- **ka_n45_temperature_sensors**

  description: Selected temperature sensors for radiometric correction formulae of Ka band -45 polarization: T0A (reference load temperature A), T0B (reference load temperature B), T1 (switch 1 temperature), T2 (switch 2 temperature), T3 (switch 3 temperature), T4 (horn temperature)
  datatype: 1 byte unsigned integer
  size: Number of beams per channel x 6

- **ka_p45_beta_params**

  description: Beta params for Ka band +45 polarization: B1 (coupler input temperature offset), B2 (coupler input temperature weight), B3 (squared coupler input temperature weight), B4 (reference load temperature weight), B5 (average front end temperature weight).
  datatype: 4 bytes IEEE floating point
  size: Number of beams per channel x 5

- **ka_p45_noise_diode_temperature**

  description: Noise diode temperature for Ka band +45 polarization.
  units: kelvins
  datatype: 4 bytes IEEE floating point
  size: 1

- **ka_p45_temperature_sensors**

  description: Selected temperature sensors for radiometric correction formulae of Ka band +45 polarization: T0A (reference load temperature A), T0B (reference load temperature B), T1 (switch 1 temperature), T2 (switch 2 temperature), T3 (switch 3 temperature), T4 (horn temperature)
  datatype: 1 byte unsigned integer
  size: Number of beams per channel x 6

- **ka_v_beta_params**

  description: Beta params for Ka band V polarization: B1 (coupler input temperature offset), B2 (coupler input temperature weight), B3 (squared coupler input temperature weight), B4 (reference load temperature weight), B5 (average front end temperature weight).
  datatype: 4 bytes IEEE floating point
  size: Number of beams per channel x 5

- **ka_v_noise_diode_temperature**

  description: Noise diode temperature for Ka band V polarization.
  units: kelvins
  datatype: 4 bytes IEEE floating point
  size: 1

- **ka_v_temperature_sensors**

  description: Selected temperature sensors for radiometric correction formulae of Ka band V polarization: T0A (reference load temperature A), T0B (reference load temperature B), T1 (switch 1 temperature), T2 (switch 2 temperature), T3 (switch 3 temperature), T4 (horn temperature)
  datatype: 1 byte unsigned integer
  size: Number of beams per channel x 6

2.4 Group 'Converted Telemetry'

Engineering values of selected variables from sensor and spacecraft hkp telemetry, useful for processing. Mainly voltages, currents, and temperature measurements.

Datasets

- **mwr_hkp_im_i01**

  description: Current Monitor of the first LNA of RX 23GHz. Subsystem: LatchUp Board
  units: milliamperes
  datatype: 4 bytes IEEE floating point
  size: Number of MWR Data frames

- **mwr_hkp_im_i02**

  description: Current Monitor of the second LNA V of RX 36GHz. Subsystem: LatchUp Board
  units: milliamperes
  datatype: 4 bytes IEEE floating point
  size: Number of MWR Data frames

- **mwr_hkp_im_i03**

  description: Disabled Sensor
  units: milliamperes
  datatype: 4 bytes IEEE floating point
  size: Number of MWR Data frames

- **mwr_hkp_im_i04**

  description: Current Monitor of the second LNA H of RX 36GHz. Subsystem: LatchUp Board
  units: milliamperes
  datatype: 4 bytes IEEE floating point
  size: Number of MWR Data frames

- **mwr_hkp_im_i05**

  description: Current Monitor of the first LNA H of RX 36GHz. Subsystem: LatchUp Board
  units: milliamperes
  datatype: 4 bytes IEEE floating point
  size: Number of MWR Data frames

- **mwr_hkp_im_i06**

  description: Current Monitor of the second LNA of RX 23GHz. Subsystem: LatchUp Board
  units: milliamperes
  datatype: 4 bytes IEEE floating point
  size: Number of MWR Data frames

- **mwr_hkp_im_i07**

  description: Disabled Sensor
  units: milliamperes
  datatype: 4 bytes IEEE floating point
  size: Number of MWR Data frames

- **mwr_hkp_im_i08**

  description: Current Monitor of the first LNA V of RX 36GHz. Subsystem: LatchUp Board
  units: milliamperes

datatype: 4 bytes IEEE floating point
size: Number of MWR Data frames

- **mwr_hkp_tm_t01**

  description: Sensor at Detector 2 (+45)Rx 36GHz. Subsystem: Rx-Front-end
  units: celsius degrees
  valid values: [0,50]
  datatype: 4 bytes IEEE floating point
  size: Number of MWR Data frames

- **mwr_hkp_tm_t02**

  description: Sensor at Detector 3 (-45)Rx 36GHz. Subsystem: Rx-Front-end
  units: celsius degrees
  valid values: [0,50]
  datatype: 4 bytes IEEE floating point
  size: Number of MWR Data frames

- **mwr_hkp_tm_t03**

  description: Sensor at Detector 4 (V)Rx 36GHz. Subsystem: Rx-Front-end
  units: celsius degrees
  valid values: [0,50]
  datatype: 4 bytes IEEE floating point
  size: Number of MWR Data frames

- **mwr_hkp_tm_t04**

  description: Sensor at L23-1. Subsystem: Switch Matrix 23 GHz
  units: celsius degrees
  valid values: [0,50]
  datatype: 4 bytes IEEE floating point
  size: Number of MWR Data frames

- **mwr_hkp_tm_t05**

  description: Sensor at L23-2. Subsystem: Switch Matrix 23 GHz
  units: celsius degrees
  valid values: [0,50]
  datatype: 4 bytes IEEE floating point
  size: Number of MWR Data frames

- **mwr_hkp_tm_t06**

  description: Sensor at L23-3. Subsystem: Switch Matrix 23 GHz
  units: celsius degrees
  valid values: [0,50]
  datatype: 4 bytes IEEE floating point
  size: Number of MWR Data frames

- **mwr_hkp_tm_t07**

  description: Sensor at L23-4. Subsystem: Switch Matrix 23 GHz
  units: celsius degrees
  valid values: [0,50]
  datatype: 4 bytes IEEE floating point
  size: Number of MWR Data frames

- **mwr_hkp_tm_t08**

  description: Sensor at L23-5. Subsystem: Switch Matrix 23 GHz
  units: celsius degrees
  valid values: [0,50]
  datatype: 4 bytes IEEE floating point
  size: Number of MWR Data frames

- **mwr_hkp_tm_t09**

  description: Sensor at Dicke LOAD 36GHz_V / CALIBRATION. Subsystem: Rx-Front-end
  units: celsius degrees
  valid values: [0,50]
  datatype: 4 bytes IEEE floating point
  size: Number of MWR Data frames

- **mwr_hkp_tm_t10**

  description: Sensor at RED Dicke LOAD 36GHz_V / CALIBRATION. Subsystem: Rx-Front-end
  units: celsius degrees
  valid values: [0,50]
  datatype: 4 bytes IEEE floating point
  size: Number of MWR Data frames

- **mwr_hkp_tm_t11**

  description: Sensor at Dicke LOAD 23GHz / CALIBRATION. Subsystem: Rx-Front-end
  units: celsius degrees
  valid values: [0,50]
  datatype: 4 bytes IEEE floating point
  size: Number of MWR Data frames

- **mwr_hkp_tm_t12**

  description: Sensor at RED Dicke LOAD 23GHz / CALIBRATION. Subsystem: Rx-Front-end
  units: celsius degrees
  valid values: [0,50]
  datatype: 4 bytes IEEE floating point
  size: Number of MWR Data frames

- **mwr_hkp_tm_t13**

  description: Sensor at Noise Diode Rx 23GHz. Subsystem: Rx-Front-end
  units: celsius degrees
  valid values: [0,50]
  datatype: 4 bytes IEEE floating point
  size: Number of MWR Data frames

- **mwr_hkp_tm_t14**

  description: Sensor at Noise Diode Rx 36GHz. Subsystem: Rx-Front-end
  units: celsius degrees
  valid values: [0,50]
  datatype: 4 bytes IEEE floating point
  size: Number of MWR Data frames

- **mwr_hkp_tm_t15**

  description: Sensor at DETECTOR Rx 23GHz. Subsystem: Rx-Front-end
  units: celsius degrees

valid values: [0,50]
datatype: 4 bytes IEEE floating point
size: Number of MWR Data frames

- **mwr_hkp_tm_t16**

  description: Sensor at Detector 1(H)Rx 36GHz. Subsystem: Rx-Front-end
  units: celsius degrees
  valid values: [0,50]
  datatype: 4 bytes IEEE floating point
  size: Number of MWR Data frames

- **mwr_hkp_tm_t17**

  description: Sensor at CTA-7. Subsystem: MRBOX
  units: celsius degrees
  valid values: [0,50]
  datatype: 4 bytes IEEE floating point
  size: Number of MWR Data frames

- **mwr_hkp_tm_t18**

  description: Sensor at CTA-8. Subsystem: Rx-Front-end
  units: celsius degrees
  valid values: [0,50]
  datatype: 4 bytes IEEE floating point
  size: Number of MWR Data frames

- **mwr_hkp_tm_t19**

  description: Sensor at CTA-9. Subsystem: Rx-Front-end
  units: celsius degrees
  valid values: [0,50]
  datatype: 4 bytes IEEE floating point
  size: Number of MWR Data frames

- **mwr_hkp_tm_t20**

  description: Sensor at CTA-10. Subsystem: Rx-Front-end
  units: celsius degrees
  valid values: [0,50]
  datatype: 4 bytes IEEE floating point
  size: Number of MWR Data frames

- **mwr_hkp_tm_t21**

  description: Sensor at Horn 6 RX 23GHz. Subsystem: Horns Plane 23 GHz
  units: celsius degrees
  valid values: [0,50]
  datatype: 4 bytes IEEE floating point
  size: Number of MWR Data frames

- **mwr_hkp_tm_t22**

  description: Sensor at Horn 6 RX 36GHz. Subsystem: Horns Plane 36 GHz
  units: celsius degrees
  valid values: [0,50]
  datatype: 4 bytes IEEE floating point
  size: Number of MWR Data frames

- **mwr_hkp_tm_t23**

  description: Sensor at Dicke LOAD 36GHz_H / CALIBRACION. Subsystem: Rx-Front-end
  units: celsius degrees
  valid values: [0,50]
  datatype: 4 bytes IEEE floating point
  size: Number of MWR Data frames

- **mwr_hkp_tm_t24**

  description: Sensor at RED Dicke LOAD 36GHz_H / CALIBRACION. Subsystem: Rx-Front-end
  units: celsius degrees
  valid values: [0,50]
  datatype: 4 bytes IEEE floating point
  size: Number of MWR Data frames

- **mwr_hkp_tm_t25**

  description: Sensor at Horn 8. Subsystem: Rx-Switches
  units: celsius degrees
  valid values: [0,50]
  datatype: 4 bytes IEEE floating point
  size: Number of MWR Data frames

- **mwr_hkp_tm_t26**

  description: Sensor at LUP BOX. Subsystem: MRBOX
  units: celsius degrees
  valid values: [0,50]
  datatype: 4 bytes IEEE floating point
  size: Number of MWR Data frames

- **mwr_hkp_tm_t27**

  description: Sensor at CTA-1. Subsystem: Rx-Front-end
  units: celsius degrees
  valid values: [0,50]
  datatype: 4 bytes IEEE floating point
  size: Number of MWR Data frames

- **mwr_hkp_tm_t28**

  description: Sensor at CTA-2. Subsystem: Rx-Front-end
  units: celsius degrees
  valid values: [0,50]
  datatype: 4 bytes IEEE floating point
  size: Number of MWR Data frames

- **mwr_hkp_tm_t29**

  description: Sensor at CTA-3. Subsystem: Rx-Front-end
  units: celsius degrees
  valid values: [0,50]
  datatype: 4 bytes IEEE floating point
  size: Number of MWR Data frames

- **mwr_hkp_tm_t30**

  description: Sensor at CTA-4. Subsystem: Rx-Front-end
  units: celsius degrees

valid values: [0,50]
datatype: 4 bytes IEEE floating point
size: Number of MWR Data frames

- **mwr_hkp_tm_t31**

  description: Sensor at CTA-5. Subsystem: Rx-Front-end
  units: celsius degrees
  valid values: [0,50]
  datatype: 4 bytes IEEE floating point
  size: Number of MWR Data frames

- **mwr_hkp_tm_t32**

  description: Sensor at CTA-6. Subsystem: Rx-Front-end
  units: celsius degrees
  valid values: [0,50]
  datatype: 4 bytes IEEE floating point
  size: Number of MWR Data frames

- **mwr_hkp_tm_t33**

  description: Sensor at L23-6. Subsystem: Switch Matrix 23GHz
  units: celsius degrees
  valid values: [0,50]
  datatype: 4 bytes IEEE floating point
  size: Number of MWR Data frames

- **mwr_hkp_tm_t34**

  description: Sensor at L23-7. Subsystem: Switch Matrix 23GHz
  units: celsius degrees
  valid values: [0,50]
  datatype: 4 bytes IEEE floating point
  size: Number of MWR Data frames

- **mwr_hkp_tm_t35**

  description: Sensor at L36V-1. Subsystem: Switch Matrix 36GHz
  units: celsius degrees
  valid values: [0,50]
  datatype: 4 bytes IEEE floating point
  size: Number of MWR Data frames

- **mwr_hkp_tm_t36**

  description: Sensor at L36V-2. Subsystem: Switch Matrix 36GHz
  units: celsius degrees
  valid values: [0,50]
  datatype: 4 bytes IEEE floating point
  size: Number of MWR Data frames

- **mwr_hkp_tm_t37**

  description: Sensor at L36V-3. Subsystem: Switch Matrix 36GHz
  units: celsius degrees
  valid values: [0,50]
  datatype: 4 bytes IEEE floating point
  size: Number of MWR Data frames

- **mwr_hkp_tm_t38**

  description: Sensor at L36V-4. Subsystem: Switch Matrix 36GHz
  units: celsius degrees
  valid values: [0,50]
  datatype: 4 bytes IEEE floating point
  size: Number of MWR Data frames

- **mwr_hkp_tm_t39**

  description: Sensor at L36V-5. Subsystem: Switch Matrix 36GHz
  units: celsius degrees
  valid values: [0,50]
  datatype: 4 bytes IEEE floating point
  size: Number of MWR Data frames

- **mwr_hkp_tm_t40**

  description: Sensor at L36V-6. Subsystem: Switch Matrix 36GHz
  units: celsius degrees
  valid values: [0,50]
  datatype: 4 bytes IEEE floating point
  size: Number of MWR Data frames

- **mwr_hkp_tm_t41**

  description: Sensor at L36V-7. Subsystem: Switch Matrix 36GHz
  units: celsius degrees
  valid values: [0,50]
  datatype: 4 bytes IEEE floating point
  size: Number of MWR Data frames

- **mwr_hkp_tm_t42**

  description: Sensor at L36H-1. Subsystem: Switch Matrix 36GHz
  units: celsius degrees
  valid values: [0,50]
  datatype: 4 bytes IEEE floating point
  size: Number of MWR Data frames

- **mwr_hkp_tm_t43**

  description: Sensor at L36H-2. Subsystem: Switch Matrix 36GHz
  units: celsius degrees
  valid values: [0,50]
  datatype: 4 bytes IEEE floating point
  size: Number of MWR Data frames

- **mwr_hkp_tm_t44**

  description: Sensor at L36H-3. Subsystem: Switch Matrix 36GHz
  units: celsius degrees
  valid values: [0,50]
  datatype: 4 bytes IEEE floating point
  size: Number of MWR Data frames

- **mwr_hkp_tm_t45**

  description: Sensor at L36H-4. Subsystem: Switch Matrix 36GHz
  units: celsius degrees

valid values: [0,50]
datatype: 4 bytes IEEE floating point
size: Number of MWR Data frames

- **mwr_hkp_tm_t46**

  description: Sensor at L36H-5. Subsystem: Switch Matrix 36GHz
  units: celsius degrees
  valid values: [0,50]
  datatype: 4 bytes IEEE floating point
  size: Number of MWR Data frames

- **mwr_hkp_tm_t47**

  description: Sensor at L36H-6. Subsystem: Switch Matrix 36GHz
  units: celsius degrees
  valid values: [0,50]
  datatype: 4 bytes IEEE floating point
  size: Number of MWR Data frames

- **mwr_hkp_tm_t48**

  description: Sensor at L36H-7. Subsystem: Switch Matrix 36GHz
  units: celsius degrees
  valid values: [0,50]
  datatype: 4 bytes IEEE floating point
  size: Number of MWR Data frames

- **mwr_hkp_vm_v01**

  description: Disabled Sensor
  units: volts
  datatype: 4 bytes IEEE floating point
  size: Number of MWR Data frames

- **mwr_hkp_vm_v02**

  description: Disabled Sensor
  units: volts
  datatype: 4 bytes IEEE floating point
  size: Number of MWR Data frames

- **mwr_hkp_vm_v03**

  description: Voltage +12V Analog Channels. Subsystem: LatchUp Board
  units: volts
  datatype: 4 bytes IEEE floating point
  size: Number of MWR Data frames

- **mwr_hkp_vm_v04**

  description: Voltage -12V Analog Channels. Subsystem: LatchUp Board
  units: volts
  datatype: 4 bytes IEEE floating point
  size: Number of MWR Data frames

- **mwr_hkp_vm_v05**

  description: Supply Voltage of the first LNA of RX 23GHz. Subsystem: LatchUp Board
  units: volts

datatype: 4 bytes IEEE floating point
size: Number of MWR Data frames

- **mwr_hkp_vm_v06**

  description: Voltage 5V Analog Channels. Subsystem: LatchUp Board
  units: volts
  datatype: 4 bytes IEEE floating point
  size: Number of MWR Data frames

- **mwr_hkp_vm_v07**

  description: Disabled Sensor
  units: volts
  datatype: 4 bytes IEEE floating point
  size: Number of MWR Data frames

- **mwr_hkp_vm_v08**

  description: Disabled Sensor
  units: volts
  datatype: 4 bytes IEEE floating point
  size: Number of MWR Data frames

- **pad_atc_data_cell_pwm_setpoint00_current**

  description: Current at active thermal control heater 0
  units: amperes
  datatype: 4 bytes IEEE floating point
  size: Number of MWR Data frames

- **pad_atc_data_cell_pwm_setpoint00_percent**

  description: Duty cycle percent for active thermal control heater 0
  datatype: 4 bytes IEEE floating point
  size: Number of MWR Data frames

- **pad_atc_data_cell_pwm_setpoint00_power**

  description: Power at active thermal control heater 0
  units: watts
  datatype: 4 bytes IEEE floating point
  size: Number of MWR Data frames

- **pad_atc_data_cell_pwm_setpoint01_current**

  description: Current at active thermal control heater 1
  units: amperes
  datatype: 4 bytes IEEE floating point
  size: Number of MWR Data frames

- **pad_atc_data_cell_pwm_setpoint01_percent**

  description: Duty cycle percent for active thermal control heater 1
  datatype: 4 bytes IEEE floating point
  size: Number of MWR Data frames

- **pad_atc_data_cell_pwm_setpoint01_power**

  description: Power at active thermal control heater 1
  units: watts
  datatype: 4 bytes IEEE floating point
  size: Number of MWR Data frames

- **pad_atc_data_cell_pwm_setpoint02_current**

  description: Current at active thermal control heater 2
  units: amperes
  datatype: 4 bytes IEEE floating point
  size: Number of MWR Data frames

- **pad_atc_data_cell_pwm_setpoint02_percent**

  description: Duty cycle percent for active thermal control heater 2
  datatype: 4 bytes IEEE floating point
  size: Number of MWR Data frames

- **pad_atc_data_cell_pwm_setpoint02_power**

  description: Power at active thermal control heater 2
  units: watts
  datatype: 4 bytes IEEE floating point
  size: Number of MWR Data frames

- **pad_atc_data_cell_pwm_setpoint03_current**

  description: Current at active thermal control heater 3
  units: amperes
  datatype: 4 bytes IEEE floating point
  size: Number of MWR Data frames

- **pad_atc_data_cell_pwm_setpoint03_percent**

  description: Duty cycle percent for active thermal control heater 3
  datatype: 4 bytes IEEE floating point
  size: Number of MWR Data frames

- **pad_atc_data_cell_pwm_setpoint03_power**

  description: Power at active thermal control heater 3
  units: watts
  datatype: 4 bytes IEEE floating point
  size: Number of MWR Data frames

- **pad_atc_data_cell_pwm_setpoint04_current**

  description: Current at active thermal control heater 4
  units: amperes
  datatype: 4 bytes IEEE floating point
  size: Number of MWR Data frames

- **pad_atc_data_cell_pwm_setpoint04_percent**

  description: Duty cycle percent for active thermal control heater 4
  datatype: 4 bytes IEEE floating point
  size: Number of MWR Data frames

- **pad_atc_data_cell_pwm_setpoint04_power**

  description: Power at active thermal control heater 4
  units: watts
  datatype: 4 bytes IEEE floating point
  size: Number of MWR Data frames

- **pad_atc_data_cell_pwm_setpoint05_current**

  description: Current at active thermal control heater 5
  units: amperes
  datatype: 4 bytes IEEE floating point
  size: Number of MWR Data frames

- **pad_atc_data_cell_pwm_setpoint05_percent**

  description: Duty cycle percent for active thermal control heater 5
  datatype: 4 bytes IEEE floating point
  size: Number of MWR Data frames

- **pad_atc_data_cell_pwm_setpoint05_power**

  description: Power at active thermal control heater 5
  units: watts
  datatype: 4 bytes IEEE floating point
  size: Number of MWR Data frames

- **pad_atc_data_cell_pwm_setpoint06_current**

  description: Current at active thermal control heater 6
  units: amperes
  datatype: 4 bytes IEEE floating point
  size: Number of MWR Data frames

- **pad_atc_data_cell_pwm_setpoint06_percent**

  description: Duty cycle percent for active thermal control heater 6
  datatype: 4 bytes IEEE floating point
  size: Number of MWR Data frames

- **pad_atc_data_cell_pwm_setpoint06_power**

  description: Power at active thermal control heater 6
  units: watts
  datatype: 4 bytes IEEE floating point
  size: Number of MWR Data frames

- **pad_atc_data_cell_pwm_setpoint07_current**

  description: Current at active thermal control heater 7
  units: amperes
  datatype: 4 bytes IEEE floating point
  size: Number of MWR Data frames

- **pad_atc_data_cell_pwm_setpoint07_percent**

  description: Duty cycle percent for active thermal control heater 7
  datatype: 4 bytes IEEE floating point
  size: Number of MWR Data frames

- **pad_atc_data_cell_pwm_setpoint07_power**

  description: Power at active thermal control heater 7
  units: watts
  datatype: 4 bytes IEEE floating point
  size: Number of MWR Data frames

- **pad_atc_data_cell_pwm_setpoint08_current**

  description: Current at active thermal control heater 8
  units: amperes
  datatype: 4 bytes IEEE floating point
  size: Number of MWR Data frames

- **pad_atc_data_cell_pwm_setpoint08_percent**

  description: Duty cycle percent for active thermal control heater 8
  datatype: 4 bytes IEEE floating point
  size: Number of MWR Data frames

- **pad_atc_data_cell_pwm_setpoint08_power**

  description: Power at active thermal control heater 8
  units: watts
  datatype: 4 bytes IEEE floating point
  size: Number of MWR Data frames

- **pad_atc_data_cell_pwm_setpoint09_current**

  description: Current at active thermal control heater 9
  units: amperes
  datatype: 4 bytes IEEE floating point
  size: Number of MWR Data frames

- **pad_atc_data_cell_pwm_setpoint09_percent**

  description: Duty cycle percent for active thermal control heater 9
  datatype: 4 bytes IEEE floating point
  size: Number of MWR Data frames

- **pad_atc_data_cell_pwm_setpoint09_power**

  description: Power at active thermal control heater 9
  units: watts
  datatype: 4 bytes IEEE floating point
  size: Number of MWR Data frames

- **pad_atc_data_cell_pwm_setpoint10_current**

  description: Current at active thermal control heater 10
  units: amperes
  datatype: 4 bytes IEEE floating point
  size: Number of MWR Data frames

- **pad_atc_data_cell_pwm_setpoint10_percent**

  description: Duty cycle percent for active thermal control heater 10
  datatype: 4 bytes IEEE floating point
  size: Number of MWR Data frames

- **pad_atc_data_cell_pwm_setpoint10_power**

  description: Power at active thermal control heater 10
  units: watts
  datatype: 4 bytes IEEE floating point
  size: Number of MWR Data frames

- **pad_atc_data_cell_pwm_setpoint11_current**

  description: Current at active thermal control heater 11
  units: amperes
  datatype: 4 bytes IEEE floating point
  size: Number of MWR Data frames

- **pad_atc_data_cell_pwm_setpoint11_percent**

  description: Duty cycle percent for active thermal control heater 11
  datatype: 4 bytes IEEE floating point
  size: Number of MWR Data frames

- **pad_atc_data_cell_pwm_setpoint11_power**

  description: Power at active thermal control heater 11
  units: watts
  datatype: 4 bytes IEEE floating point
  size: Number of MWR Data frames

- **sac_vbusa_rtu1**

  description: SAC-D bus A voltage RTU1 measurements interpolated to MWR time tags
  units: volts
  datatype: 4 bytes IEEE floating point
  size: Number of MWR Data frames

- **sac_vbusb_rtu1**

  description: SAC-D bus B voltage RTU1 measurements interpolated to MWR time tags
  units: volts
  datatype: 4 bytes IEEE floating point
  size: Number of MWR Data frames

2.5 Group 'Navigation'

Navigation data for the orbit, consisting of SAC-D orbit and attitude data. Based on the best available source. Orbit data sources in decreasing quality order: Cods Definitive Ephemerides, Cods Post Fact Ephemerides, Raw Spacecraft Telemetry, Cods Predicted Ephemerides. Attitude data sources in decreasing quality order: Cods Interpolated Attitude, Raw Spacecraft Telemetry.

Attributes

- **name:** Attitude Data Source
  description: Source of the attitude vectors include in the product. One of: Cods Interpolated Attitude, Raw Spacecraft Telemetry
  datatype: str

- **name:** Attitude Data Time Between Samples In Seconds
  description: Seconds between quaternion vector samples included in the product
  datatype: f4

- **name:** Orbit Data Source
  description: Source of the state vectors included in the product. One of: Cods Definitive Ephemerides, Cods Post Fact Ephemerides, Raw Spacecraft Telemetry, Cods Predicted Ephemerides
  datatype: str

- **name:** Orbit Data Time Between Samples In Seconds
  description: Seconds between state vector samples included in the product
  datatype: f4

Datasets

- **att_ang**

  description: roll, pitch, yaw associated to transformation from a vector expressed in the Orbital reference system to a vector expressed in the Platform fixed reference
  units: degrees
  valid values: <-180,...,180; -180,...,180; -180,...,180>
  datatype: 4 bytes IEEE floating point
  size: Number of Quaternion Vectors x 3

- **att_flags**

  description: Attitude vectors description and quality flags
  units: bitmask
  valid values: bit5 (msb) = cods vectors; bit4 = vector passed consistency tests; bit3 = science mode attitude; bit2 = yaw steering attitude; bit1 = ongoing propulsion maneuver; bit0 (lsb) = ongoing attitude maneuver
  datatype: 1 byte unsigned integer
  size: Number of Quaternion Vectors

- **att_is_valid**

  description: Equal to 1 if attitude vector is valid for science purposes
  valid values: [0,1]
  datatype: 1 byte unsigned integer
  size: Number of Quaternion Vectors

- **att_quaternion**

  description: J2000 to platform quaternion. Transformation from a vector expressed in the J2000 inertial system to a vector expressed in the Platform fixed reference system
  units: normalized 4-tuple
  valid values: <-1,...,1; -1,...,1; -1,...,1; -1,...,1>
  datatype: 4 bytes IEEE floating point
  size: Number of Quaternion Vectors x 4

- **att_time**

  description: GPS time tag of attitude data (seconds since 1980/01/06 00:00:00 UTC)
  units: seconds
  datatype: 8 bytes IEEE floating point
  size: Number of Quaternion Vectors

- **orb_flags**

  description: Orbit vectors description and quality flags
  units: bitmask
  valid values: bit7 (msb) = cods vectors; bit6 = vector passed consistency tests; bit5 = sps solution vectors; bit4 = nkf solution vectors; bit3 = problems with gps time; bit2 = problems with sps convergence; bit1 = problems with nkf convergence; bit0 (lsb) = ongoing propulsion maneuver
  datatype: 1 byte unsigned integer
  size: Number of State Vectors x 3

- **orb_is_valid**

  description: Equal to 1 if orbit vector is valid for science purposes
  valid values: [0,1]
  datatype: 1 byte unsigned integer
  size: Number of State Vectors x 3

- **orb_lla**

  description: Orbit position vector in latitude, longitude, altitude (WGS84 datum)
  units: degrees,meters
  valid values: <-90,...,90, -180,...,180, 650000,...,660000>
  datatype: 4 bytes IEEE floating point
  size: Number of State Vectors x 3

- **orb_pos**

  description: Orbit position vector in J2000 inertial reference frame (mean vernal equinox, mean equator, at Terrestrial time J2000)
  units: meters
  valid values: <-7100000,...,7100000; -7100000,...,7100000; -7100000,...,7100000>
  datatype: 4 bytes IEEE floating point
  size: Number of State Vectors x 3

- **orb_time**

  description: GPS time tag of orbit vectors (seconds since 1980/01/06 00:00:00 UTC)
  units: seconds
  datatype: 8 bytes IEEE floating point
  size: Number of State Vectors

- **orb_vel**

  description: Orbit velocity vector in J2000 inertial reference frame (mean vernal equinox, mean equator, at Terrestrial time J2000)
  units: meters per second
  valid values: <-7600,...,7600; -7600,...,7600; -7600,...,7600>
  datatype: 4 bytes IEEE floating point
  size: Number of State Vectors x 3

2.6 Group 'Raw MWR Data'

Raw values of variables obtained from MWR data frames.

Datasets

- **mwr_atc_param_1**

  description: Parameter 1 of last active thermal control command received by MWR. Heater id and an indication of the kind of command received (either duty cycle configuration or redundancy selection).
  valid values: [0x20,...,0x37]
  datatype: 1 byte unsigned integer
  size: Number of MWR Data frames

- **mwr_atc_param_2**

description: Parameter 2 of last active thermal control command received by MWR. Either duty cycle configuration value or redundancy selection value for the heater.
valid values: [0x20,...,0x7F]
datatype: 1 byte unsigned integer
size: Number of MWR Data frames

- **mwr_hkp_im**

  description: Raw counts for the 8 MWR current measurements
  datatype: 2 bytes unsigned integer
  size: Number of MWR Data frames x 8

- **mwr_hkp_tm**

  description: Raw counts for the 48 MWR temperature measurements
  datatype: 2 bytes unsigned integer
  size: Number of MWR Data frames x 48

- **mwr_hkp_vm**

  description: Raw counts for the 8 MWR voltage measurements
  datatype: 2 bytes unsigned integer
  size: Number of MWR Data frames x 8

- **mwr_horn_id**

  description: Raw horn id for both K and Ka bands
  valid values: [0x1,...,0x8]
  datatype: 1 byte unsigned integer
  size: Number of MWR Data frames

- **mwr_k_band_horn_id**

  description: Id of measured horn for K band
  valid values: [1,..,8]
  datatype: 1 byte unsigned integer
  size: Number of MWR Data frames

- **mwr_k_h_antenna**

  description: Raw counts for K band H polarization antenna measurement
  datatype: 2 bytes unsigned integer
  size: Number of MWR Data frames

- **mwr_k_h_antenna_plus_noise**

  description: Raw counts for K band H polarization antenna plus noise measurement
  datatype: 2 bytes unsigned integer
  size: Number of MWR Data frames

- **mwr_k_h_load**

  description: Raw counts for K band H polarization reference load measurement
  datatype: 2 bytes unsigned integer
  size: Number of MWR Data frames

- **mwr_ka_band_horn_id**

  description: Id of measured horn for Ka band
  valid values: [1,..,8]
  datatype: 1 byte unsigned integer
  size: Number of MWR Data frames

- **mwr_ka_h_antenna**

  description: Raw counts for Ka band H polarization antenna measurement
  datatype: 2 bytes unsigned integer
  size: Number of MWR Data frames

- **mwr_ka_h_antenna_plus_noise**

  description: Raw counts for Ka band H polarization antenna plus noise measurement
  datatype: 2 bytes unsigned integer
  size: Number of MWR Data frames

- **mwr_ka_h_load**

  description: Raw counts for Ka band H polarization reference load measurement
  datatype: 2 bytes unsigned integer
  size: Number of MWR Data frames

- **mwr_ka_n45_antenna**

  description: Raw counts for Ka band -45 polarization antenna measurement
  datatype: 2 bytes unsigned integer
  size: Number of MWR Data frames

- **mwr_ka_n45_antenna_plus_noise**

  description: Raw counts for Ka band -45 polarization antenna plus noise measurement
  datatype: 2 bytes unsigned integer
  size: Number of MWR Data frames

- **mwr_ka_n45_load**

  description: Raw counts for Ka band -45 polarization reference load measurement
  datatype: 2 bytes unsigned integer
  size: Number of MWR Data frames

- **mwr_ka_p45_antenna**

  description: Raw counts for Ka band +45 polarization antenna measurement
  datatype: 2 bytes unsigned integer
  size: Number of MWR Data frames

- **mwr_ka_p45_antenna_plus_noise**

  description: Raw counts for Ka band +45 polarization antenna plus noise measurement
  datatype: 2 bytes unsigned integer
  size: Number of MWR Data frames

- **mwr_ka_p45_load**

  description: Raw counts for Ka band +45 polarization reference load measurement
  datatype: 2 bytes unsigned integer
  size: Number of MWR Data frames

- **mwr_ka_v_antenna**

  description: Raw counts for Ka band V polarization antenna measurement
  datatype: 2 bytes unsigned integer
  size: Number of MWR Data frames

- **mwr_ka_v_antenna_plus_noise**

  description: Raw counts for Ka band V polarization antenna plus noise measurement
  datatype: 2 bytes unsigned integer
  size: Number of MWR Data frames

- **mwr_ka_v_load**

  description: Raw counts for Ka band V polarization reference load measurement
  datatype: 2 bytes unsigned integer
  size: Number of MWR Data frames

- **mwr_mode**

  description: MWR operation mode
  valid values: 0x05 = mission; 0x06 = stand alone; 0x07 = stand by; 0x08 = calibration; 0x0c = stand alone calibration; 0x09 = diagnostic
  datatype: 1 byte unsigned integer
  size: Number of MWR Data frames

- **mwr_sync_word**

  description: Sync word of the MWR frame
  datatype: 4 bytes unsigned integer
  size: Number of MWR Data frames

- **mwr_time**

  description: GPS time tag for MWR frame including milliseconds (seconds since 1980/01/06 00:00:00 UTC)
  units: seconds
  datatype: 8 bytes IEEE floating point
  size: Number of MWR Data frames

- **mwr_time_ms**

  description: GPS time tag for MWR frame (milliseconds since mwr_time_s)
  units: milliseconds
  datatype: 2 bytes unsigned integer
  size: Number of MWR Data frames

- **mwr_time_s**

  description: GPS time tag for MWR frame (seconds since 1980/01/06 00:00:00 UTC)
  units: seconds
  datatype: 4 bytes unsigned integer
  size: Number of MWR Data frames

- **pad_atc_data_cell_pwm_setpoint**

  description: Active thermal control raw duty cycle configuration value for each of the 12 heaters.
  datatype: 1 byte unsigned integer
  size: Number of MWR Data frames x 12

- **pad_atc_data_configuration_report**

  description: Partitioned dump of active thermal control configuration.
  datatype: 4 bytes unsigned integer
  size: Number of MWR Data frames

- **pad_hkp**

  description: Raw PAD housekeeping associated to the MWR frame.
  datatype: 1 byte unsigned integer
  size: Number of MWR Data frames x 20

2.7 Group 'SAC-D Telemetry'

SAC-D raw telemetry frames associated to the orbit.

Datasets

- **sacd_telemetry**

  description: SAC-D raw telemetry blocks. 4000 bytes every 8 seconds
  datatype: 1 byte unsigned integer
  size: Number of SAC-D Telemetry frames x 4000

- **sacd_telemetry_crc_is_valid**

  description: Equal to 1 if SAC-D raw telemetry CRC was validated.
  valid values: [0,1]
  datatype: 1 byte unsigned integer
  size: Number of SAC-D Telemetry frames

F.2 CONAE L1B Data (HDF5)

MWR L1B Product HDF5 Data Format Reference

Authors: Felipe Madero

Date: Feb 29, 2012

COMISION NACIONAL DE ACTIVIDADES ESPACIALES
ARGENTINA

Table of Contents

1 Description of Hdf5 Global Metadata Attributes 3
1.1 Group '/' . . . 3
1.2 Group 'Global Metadata/Acquisition' . . . 3
1.3 Group 'Global Metadata/Mission' . . . 4
1.4 Group 'Global Metadata/Platform' . . . 5
1.5 Group 'Global Metadata/Platform/Orbit' . . . 5
1.6 Group 'Global Metadata/Product' . . . 6
1.7 Group 'Global Metadata/Product/Stats' . . . 8
1.8 Group 'Global Metadata/Production' . . . 9
1.9 Group 'Global Metadata/Sensor' . . . 10
1.10 Group 'Global Metadata/Software' . . . 11

2 Description of Hdf5 Datasets 12
2.1 Group 'Ancillary Data' . . . 12
2.2 Group 'Geolocation Data' . . . 13
2.3 Group 'MWR Calibrated Radiometric Data' . . . 23
2.4 Group 'Quality indicators' . . . 23

1 Description of Hdf5 Global Metadata Attributes

1.1 Group '/'

Root group for the product.

- **hdf5_especification_filename**

  description: Filename of the .xml hdf5 estructure especification file from which this product was created.
  default value: mwr_l1b_hdf5_esp.2_0.xml
  datatype: string

1.2 Group 'Global Metadata/Acquisition'

Information related to the acquisition of data by the sensor.

- **Cycle Number**

  description: Counter of weekly cycles (103 orbits) since Aquarius's Commisioning end.
  datatype: 4 bytes signed integer

- **End Time GPS**

  description: GPS time tag for the last MWR data included in the product (seconds since 1980/01/06 00:00:00 UTC)
  datatype: 4 bytes unsigned integer

- **End Time UTC**

  description: UTC time time tag for the last MWR data included in the product
  datatype: string

- **Length Seconds**

  description: Elapsed time period between the first and last MWR data included in the product
  datatype: 4 bytes unsigned integer

- **Mwr Reference System Pass Number**

  description: Id of revolution inside the weekly cycle. Consecutive numbers 1 to 103 represent geographically adjacent revolutions. Refer to 'MWR Reference System Pass Number to In Cycle Pass Number Map' to map between these two ids.
  datatype: 1 byte unsigned integer

- **Orbit End Time UTC**

  description: UTC time time tag for the end of the MWR orbit (descending crossing of the south pole)
  datatype: string

- **Orbit Node Longitude**

  description: Longitude of orbit ascending node (equatorial crossing at PM node)
  datatype: 4 bytes IEEE floating point

- **Orbit Node Time UTC**

  description: UTC time time tag for orbit ascending node (equatorial crossing at PM node)
  datatype: string

- **Orbit Number**

  description: Counter of revolutions since launch.
  datatype: 4 bytes signed integer

- **Orbit Start Time UTC**

  description: UTC time time tag for the start of the MWR orbit (ascending crossing of the south pole)
  datatype: string

- **Overlapped Orbit End Time UTC**

  description: UTC time time tag for end of the Overlapped MWR orbit (end of the MWR orbit plus 10 minutes)
  datatype: string

- **Overlapped Orbit Start Time UTC**

  description: UTC time time tag for start of the Overlapped MWR orbit (start of the MWR orbit minus 10 minutes)
  datatype: string

- **Pass Number in Cycle**

  description: Id of revolution inside the weekly cycle. Consecutive numbers 1 to 103 represent revolutions adjacent in time. Refer to 'MWR Reference System Pass Number to In Cycle Pass Number Map' to map between these two ids.
  datatype: 1 byte unsigned integer

- **Start Time GPS**

  description: GPS time tag for the first MWR data included in the product (seconds since 1980/01/06 00:00:00 UTC)
  datatype: 4 bytes unsigned integer

- **Start Time UTC**

  description: UTC time time tag for the first MWR data included in the product
  datatype: string

1.3 Group 'Global Metadata/Mission'

Information related to the mission.

- **Name**

  description: Full name for the mission associated to this product.
  default value: SAC-D Aquarius
  datatype: string

1.4 Group 'Global Metadata/Platform'

Information related to the platform.

- **Name**

  description: Full name of the spacecraft platform associated to this product.
  default value: SAC-D
  datatype: string

- **Reference Time**

  description: Main reference time system used in relation with platform information.
  default value: GPS
  datatype: string

1.5 Group 'Global Metadata/Platform/Orbit'

Information related to the orbit of the platform.

- **Mean Argument Perigee Degrees**

  description: Mean Argument of Perigee for the orbit of the platform associated to the product
  default value: 90.0
  datatype: 4 bytes IEEE floating point

- **Mean Eccentricity**

  description: Mean Eccentricity for the orbit of the platform associated to the product
  default value: 0.0012
  datatype: 4 bytes IEEE floating point

- **Mean Equatorial Altitude Km**

  description: Mean Altitude, when crossing above the equator, for the orbit of the platform associated to the product
  default value: 657.0
  datatype: 4 bytes IEEE floating point

- **Mean Inclination Degrees**

  description: Mean Inclination for the orbit of the platform associated to the product
  default value: 98.01
  datatype: 4 bytes IEEE floating point

- **Mean Local Time of ascending Node**

  description: Mean Local Time of Ascending Node for the orbit of the platform associated to the product
  default value: 06:00 PM
  datatype: string

- **Mean Period Min**

  description: Mean minutes required by the platform in order to complete a revolution.
  default value: 98.0
  datatype: 4 bytes IEEE floating point

- **Mean SemiMajor Axis Km**

  description: Mean Semimajor Axis for the orbit of the platform associated to the product
  default value: 7028.87
  datatype: 4 bytes IEEE floating point

- **Revisit Cycle Days**

  description: Number of days needed by the platform in order to pass above the same point in earth.
  default value: 7
  datatype: 1 byte signed integer

- **Revisit Cycle Revolutions**

  description: Number of revolutions needed by the platform in order to pass above the same point in earth.
  default value: 103
  datatype: 1 byte unsigned integer

- **Type**

  description: Description of the main characteristics of the orbit of the platform associated to the product
  default value: Frozen, Almost circular, Dawn-Dusk, Sun Synchronous
  datatype: string

1.6 Group 'Global Metadata/Product'

Information related to the product contents.

- **CODS Attitude Vector Algorithm Version**

  description: Version of Algorithm used to generate CODS attitude vectors used to generate this product (if applicable)
  datatype: string

- **CODS State Vector Algorithm Version**

  description: Version of Algorithm used to generate CODS state vectors used to generate this product (if applicable)
  datatype: string

- **Data Format**

  description: Base product data format.
  default value: NCSA-HDF5
  datatype: string

- **Data Format Version**

  description: Base product data format version.
  datatype: string

- **Data Type**

  description: Identifies the kind of data present in the product. One of SCI (Science data), CAL (Calibration data), ENG (Engineering data).
  datatype: string

- **Geometric Tables Update Id**

  description: Update Id of Geometric Calibration Tables used to generate this product
  datatype: string

- **Level**

  description: Indication of the production level.
  default value: L1B
  datatype: string

- **Level Version**

  description: Version number for the level of this product.
  default value: 2.0
  datatype: string

- **Name**

  description: Full name of the product, used also in file names. Format: EO_YYYMMDD_ HHMMSS_SERVICE_SPACECRAFT_SENSOR_LEVEL_DATA. Where time info refers to UTC time tag associated to the start of the overlapped orbit, SERVICE is Production Service Id, SPACECRAFT is Platform Name, SENSOR is Sensor Name, LEVEL is Product Level, DATA is Product Data Type.
  datatype: string

- **Radiometric Tables Update Id**

  description: Update Id of Radiometric Calibration Tables used to generate this product
  datatype: string

- **Reference Coordinate System**

  description: Reference coordinate system used to generate geographical information for this product.
  default value: J2000
  datatype: string

- **Reference Datum**

  description: Reference datum used to generate geographical information for this product.
  default value: WGS84
  datatype: string

- **Title**

  description: Identifies Sensor Name, and Product Level.
  default value: MWR Level-1B Data
  datatype: string

1.7 Group 'Global Metadata/Product/Stats'

Statistics for the product contents.

- **Number of MWR lines**

  description: Number of MWR lines included in this product.
  datatype: 4 bytes unsigned integer

- **Number of MWR lines where the geolocation algorithm failed**

  description: Number of MWR lines included in this product that contains geolocation errors. One counter for each band: K H, Ka H, Ka V, Ka +45, Ka -45.
  datatype: 4 bytes unsigned integer

- **Number of MWR lines whose input data has CRC error**

  description: Number of MWR lines included in this product that contains CRC errors. One counter for each band: K H, Ka H, Ka V, Ka +45, Ka -45.
  datatype: 4 bytes unsigned integer

- **Number of MWR lines whose input data was flagged as invalid**

  description: Number of MWR lines whose input data was flagged as invalid. One counter for each band: K H, Ka H, Ka V, Ka +45, Ka -45.
  datatype: 4 bytes unsigned integer

- **Number of MWR samples where the geolocation algorithm failed**

  description: Number of MWR samples included in this product that contains geolocation errors. One counter for each band: K H, Ka H, Ka V, Ka +45, Ka -45.
  datatype: 4 bytes unsigned integer

- **Number of MWR samples whose input data has CRC error**

  description: Number of MWR samples included in this product that contains CRC errors. One counter for each band: K H, Ka H, Ka V, Ka +45, Ka -45.
  datatype: 4 bytes unsigned integer

- **Number of MWR samples whose input data was flagged as invalid**

  description: Number of MWR samples whose input data was flagged as invalid. One counter for each band: K H, Ka H, Ka V, Ka +45, Ka -45.
  datatype: 4 bytes unsigned integer

- **Number of filled MWR samples**

  description: Number of MWR samples that were filled in this product, due to missing frames. One counter for each band: K H, Ka H, Ka V, Ka +45, Ka -45.
  datatype: 4 bytes unsigned integer

- **Number of missing MWR lines**

  description: Number of missing MWR lines for the line sequence included in this product.
  datatype: 4 bytes unsigned integer

1.8 Group 'Global Metadata/Production'

Information related to the production activity.

- **Agency Id**
  description: Identification of space agency that generated this product
  datatype: string

- **Center**
  description: Identification of the facility and agency that generated this product.
  datatype: string

- **Center Reference Time**
  description: Main reference time system used in the results of the production.
  default value: UTC
  datatype: string

- **Contact Organization Name**
  description: Address of the Production Center
  datatype: string

- **Control Parameters**
  description: Command line arguments of the program used to generate this product.
  datatype: string

- **Country Id**
  description: Identification of the country the space agency that generated this product belongs to.
  datatype: string

- **Facility Id**
  description: Identification of the facility inside the space agency that generated this product.
  datatype: string

- **Input Files**
  description: List of input files used to generate this product.
  datatype: string

- **Service Id**
  description: Identification of the service inside the space agency that generated this product.
  datatype: string

- **Start Time UTC**
  description: UTC time tag for the start of the generation of this product.
  datatype: string

1.9 Group 'Global Metadata/Sensor'

Information related to the sensor.

- **BeamWidth Degrees**

  description: Length in degrees of the beam received by a horn.
  default value: 1.7
  datatype: 4 bytes IEEE floating point

- **Frequency Bands**

  description: List of frequency bands of the sensor.
  default value: 23.8 GHz (K) - 36.5 GHz (Ka)
  datatype: string

- **K Band BandWidth MHz**

  description: Measured bandwidth around the central frequency for the K band H polarization
  default value: 400.0
  datatype: 4 bytes IEEE floating point

- **Ka Band BandWidth MHz**

  description: Measured bandwidth around the central frequency for the Ka band at all polarizations
  default value: 1000.0
  datatype: 4 bytes IEEE floating point

- **MWR Reference System Pass Number to In Cycle Pass Number Map**

  description: Map between the two systems used to identify a particular revolution inside the weekly cycle: MWR Reference System Pass Number and Cycle Pass Number
  default value: 001: 100 , 002: 041 , 003: 085 , 004: 026 , 005: 070 , 006: 011 , 007: 055 , 008: 099 , 009: 040 , 010: 084 , 011: 025 , 012: 069 , 013: 010 , 014: 054 , 015: 098 , 016: 039 , 017: 083 , 018: 024 , 019: 068 , 020: 009 , 021: 053 , 022: 097 , 023: 038 , 024: 082 , 025: 023 , 026: 067 , 027: 008 , 028: 052 , 029: 096 , 030: 037 , 031: 081 , 032: 022 , 033: 066 , 034: 007 , 035: 051 , 036: 095 , 037: 036 , 038: 080 , 039: 021 , 040: 065 , 041: 006 , 042: 050 , 043: 094 , 044: 035 , 045: 079 , 046: 020 , 047: 064 , 048: 005 , 049: 049 , 050: 093 , 051: 034 , 052: 078 , 053: 019 , 054: 063 , 055: 004 , 056: 048 , 057: 092 , 058: 033 , 059: 077 , 060: 018 , 061: 062 , 062: 003 , 063: 047 , 064: 091 , 065: 032 , 066: 076 , 067: 017 , 068: 061 , 069: 002 , 070: 046 , 071: 090 , 072: 031 , 073: 075 , 074: 016 , 075: 060 , 076: 001 , 077: 045 , 078: 089 , 079: 030 , 080: 074 , 081: 015 , 082: 059 , 083: 103 , 084: 044 , 085: 088 , 086: 029 , 087: 073 , 088: 014 , 089: 058 , 090: 102 , 091: 043 , 092: 087 , 093: 028 , 094: 072 , 095: 013 , 096: 057 , 097: 101 , 098: 042 , 099: 086 , 100: 027 , 101: 071 , 102: 012 , 103: 056
  datatype: string

- **Name**

  description: Name of the sensor.
  default value: MWR
  datatype: string

- **Number of beams per channel**

description: Number of beams/horns per channel
default value: 8
datatype: 1 byte unsigned integer

- **Number of channels**

  description: Number of channels measured by the sensr
  default value: 5
  datatype: 1 byte unsigned integer

- **Off Nadir Pointing Degrees**

  description: Off nadir central pointing for each band.
  default value: 23.8 GHz 47.95El/143.73Az - 36.5 GHz 47.95El/36.27Az
  datatype: string

- **Polarizations**

  description: List of all central frequencies and associated polarizations.
  default value: 23.8 GHz H - 36.5 GHz H - 36.5 GHz V - 36.5 GHz +45 - 36.5 GHz -45
  datatype: string

- **Spatial Resolution Km**

  description: Length of the footprint of a horn at the earth surface.
  default value: 54.23
  datatype: 4 bytes IEEE floating point

- **Swath Width Km**

  description: Total distance covered at the earth surface by the 8 horns of a band and polarization pair.
  default value: 367.89
  datatype: 4 bytes IEEE floating point

1.10 Group 'Global Metadata/Software'

Information related to the software used to generate the product.

- **Name**

  description: Name of the software that generated this product
  datatype: string

- **Release**

  description: Configuration control release name of the software that generated this product
  datatype: string

- **Version**

  description: Version of the software that generated this product
  datatype: string

2 Description of Hdf5 Datasets

2.1 Group 'Ancillary Data'

Ancillary data useful for higher level processing

Datasets

- **ascending_flag**

  description: Indicator of whether the spacecraft is ascending or descending.
  valid values: 0 = descending; 1 = ascending
  datatype: 1 byte unsigned integer
  size: Number of MWR lines

- **k_h_surface_type**

  description: Surface type associated to K band H polarization measurement.
  valid values: -1 = unknown; 0 = land; 1 = ocean; 2 = coast; 3 = near coast; 4 = ice; 5 = possible ice
  datatype: 1 byte signed integer
  size: Number of MWR lines x Number of beams per channel

- **ka_h_surface_type**

  description: Surface type associated to Ka band H polarization measurement.
  valid values: -1 = unknown; 0 = land; 1 = ocean; 2 = coast; 3 = near coast; 4 = ice; 5 = possible ice
  datatype: 1 byte signed integer
  size: Number of MWR lines x Number of beams per channel

- **ka_n45_surface_type**

  description: Surface type associated to Ka band -45 polarization measurement.
  valid values: -1 = unknown; 0 = land; 1 = ocean; 2 = coast; 3 = near coast; 4 = ice; 5 = possible ice
  datatype: 1 byte signed integer
  size: Number of MWR lines x Number of beams per channel

- **ka_p45_surface_type**

  description: Surface type associated to Ka band +45 polarization measurement.
  valid values: -1 = unknown; 0 = land; 1 = ocean; 2 = coast; 3 = near coast; 4 = ice; 5 = possible ice
  datatype: 1 byte signed integer
  size: Number of MWR lines x Number of beams per channel

- **ka_v_surface_type**

  description: Surface type associated to Ka band V polarization measurement.
  valid values: -1 = unknown; 0 = land; 1 = ocean; 2 = coast; 3 = near coast; 4 = ice; 5 = possible ice
  datatype: 1 byte signed integer
  size: Number of MWR lines x Number of beams per channel

2.2 Group 'Geolocation Data'

Geolocation Data associated to MWR measurements

Attributes

- **name:** Cell Length x
  description: Grid cell length over x axis of the geolocation grid.
  datatype: u2
- **name:** Cell Length y
  description: Grid cell length over y axis of the geolocation grid.
  datatype: u2

Datasets

- **k_h_azimuth_angle_to_moon**

  description: Azimuth angle to moon for K band H polarization measurement.
  units: degrees
  valid values: [-180,...,180]
  datatype: 4 bytes IEEE floating point
  size: Number of MWR lines x Number of beams per channel
- **k_h_azimuth_angle_to_spacecraft**

  description: Azimuth angle to spacecraft for K band H polarization measurement.
  units: degrees
  valid values: [-180,...,180]
  datatype: 4 bytes IEEE floating point
  size: Number of MWR lines x Number of beams per channel
- **k_h_azimuth_angle_to_sun**

  description: Azimuth angle to sun for K band H polarization measurement.
  units: degrees
  valid values: [-180,...,180]
  datatype: 4 bytes IEEE floating point
  size: Number of MWR lines x Number of beams per channel
- **k_h_latitude**

  description: Latitude for K band H polarization measurement.
  units: degrees
  valid values: [-90,...,90]
  datatype: 4 bytes IEEE floating point
  size: Number of MWR lines x Number of beams per channel
- **k_h_longitude**

  description: Longitude for K band H polarization measurement.
  units: degrees
  valid values: [-180,...,180]
  datatype: 4 bytes IEEE floating point
  size: Number of MWR lines x Number of beams per channel

- **k_h_n3db_approximating_ellipse_lat**

  This dataset is optional, it may be present on the product only due to specific user request.

  description: Latitude of the center, first semimajor axis, first semiminor axis, second semimajor axis, second semiminor axis, of the ellipse that approximates the -3dB contour, for K band H polarization
  units: degrees
  valid values: [-90,...,90]
  datatype: 4 bytes IEEE floating point
  size: Number of MWR lines x Number of beams per channel x 5

- **k_h_n3db_approximating_ellipse_lon**

  This dataset is optional, it may be present on the product only due to specific user request.

  description: Longitude of the center, first semimajor axis, first semiminor axis, second semimajor axis, second semiminor axis, of the ellipse that approximates the -3dB contour, for K band H polarization
  units: degrees
  valid values: [-180,...,180]
  datatype: 4 bytes IEEE floating point
  size: Number of MWR lines x Number of beams per channel x 5

- **k_h_n3db_contour_lat**

  This dataset is optional, it may be present on the product only due to specific user request.

  description: Latitude of selected points from the -3dB contour, for K band H polarization.
  units: degrees
  valid values: [-90,...,90]
  datatype: 4 bytes IEEE floating point
  size: Number of MWR lines x Number of beams per channel x 20

- **k_h_n3db_contour_lon**

  This dataset is optional, it may be present on the product only due to specific user request.

  description: Longitude of selected points from the -3dB contour, for K band H polarization.
  units: degrees
  valid values: [-180,...,180]
  datatype: 4 bytes IEEE floating point
  size: Number of MWR lines x Number of beams per channel x 20

- **k_h_range_to_spacecraft**

  description: Distance between spacecraft and position of K band H polarization measurement.
  units: meters
  datatype: 4 bytes IEEE floating point
  size: Number of MWR lines x Number of beams per channel

- **k_h_zenith_angle_to_moon**

  description: Zenith (incidence) angle to moon for K band H polarization measurement.
  units: degrees
  valid values: [0,...,90]
  datatype: 4 bytes IEEE floating point
  size: Number of MWR lines x Number of beams per channel

- **k_h_zenith_angle_to_spacecraft**

  description: Zenith (incidence) angle to spacecraft for K band H polarization measurement.
  units: degrees
  valid values: [0,...,90]
  datatype: 4 bytes IEEE floating point
  size: Number of MWR lines x Number of beams per channel

- **k_h_zenith_angle_to_sun**

  description: Zenith (incidence) angle to sun for K band H polarization measurement.
  units: degrees
  valid values: [0,...,90]
  datatype: 4 bytes IEEE floating point
  size: Number of MWR lines x Number of beams per channel

- **ka_h_azimuth_angle_to_moon**

  description: Azimuth angle to moon for Ka band H polarization measurement.
  units: degrees
  valid values: [-180,...,180]
  datatype: 4 bytes IEEE floating point
  size: Number of MWR lines x Number of beams per channel

- **ka_h_azimuth_angle_to_spacecraft**

  description: Azimuth angle to spacecraft for Ka band H polarization measurement.
  units: degrees
  valid values: [-180,...,180]
  datatype: 4 bytes IEEE floating point
  size: Number of MWR lines x Number of beams per channel

- **ka_h_azimuth_angle_to_sun**

  description: Azimuth angle to sun for Ka band H polarization measurement.
  units: degrees
  valid values: [-180,...,180]
  datatype: 4 bytes IEEE floating point
  size: Number of MWR lines x Number of beams per channel

- **ka_h_latitude**

  description: Latitude for Ka band H polarization measurement.
  units: degrees
  valid values: [-90,...,90]
  datatype: 4 bytes IEEE floating point
  size: Number of MWR lines x Number of beams per channel

- **ka_h_longitude**

  description: Longitude for Ka band H polarization measurement.
  units: degrees
  valid values: [-180,...,180]
  datatype: 4 bytes IEEE floating point
  size: Number of MWR lines x Number of beams per channel

- **ka_h_n3db_approximating_ellipse_lat**

  This dataset is optional, it may be present on the product only due to specific user request.

description: Latitude of the center, first semimajor axis, first semiminor axis, second semimajor axis, second semiminor axis, of the ellipse that approximates the -3dB contour, for Ka band H polarization
units: degrees
valid values: [-90,...,90]
datatype: 4 bytes IEEE floating point
size: Number of MWR lines x Number of beams per channel x 5

- **ka_h_n3db_approximating_ellipse_lon**

  This dataset is optional, it may be present on the product only due to specific user request.

  description: Longitude of the center, first semimajor axis, first semiminor axis, second semimajor axis, second semiminor axis, of the ellipse that approximates the -3dB contour, for Ka band H polarization
  units: degrees
  valid values: [-180,...,180]
  datatype: 4 bytes IEEE floating point
  size: Number of MWR lines x Number of beams per channel x 5

- **ka_h_n3db_contour_lat**

  This dataset is optional, it may be present on the product only due to specific user request.

  description: Latitude of selected points from the -3dB contour, for Ka band H polarization.
  units: degrees
  valid values: [-90,...,90]
  datatype: 4 bytes IEEE floating point
  size: Number of MWR lines x Number of beams per channel x 20

- **ka_h_n3db_contour_lon**

  This dataset is optional, it may be present on the product only due to specific user request.

  description: Longitude of selected points from the -3dB contour, for Ka band H polarization.
  units: degrees
  valid values: [-180,...,180]
  datatype: 4 bytes IEEE floating point
  size: Number of MWR lines x Number of beams per channel x 20

- **ka_h_range_to_spacecraft**

  description: Distance between spacecraft and position of Ka band H polarization measurement.
  units: meters
  datatype: 4 bytes IEEE floating point
  size: Number of MWR lines x Number of beams per channel

- **ka_h_zenith_angle_to_moon**

  description: Zenith (incidence) angle to moon for Ka band H polarization measurement.
  units: degrees
  valid values: [0,...,90]
  datatype: 4 bytes IEEE floating point
  size: Number of MWR lines x Number of beams per channel

- **ka_h_zenith_angle_to_spacecraft**

  description: Zenith (incidence) angle to spacecraft for Ka band H polarization measurement.
  units: degrees

valid values: [0,...,90]
datatype: 4 bytes IEEE floating point
size: Number of MWR lines x Number of beams per channel

- **ka_h_zenith_angle_to_sun**

  description: Zenith (incidence) angle to sun for Ka band H polarization measurement.
  units: degrees
  valid values: [0,...,90]
  datatype: 4 bytes IEEE floating point
  size: Number of MWR lines x Number of beams per channel

- **ka_n45_azimuth_angle_to_moon**

  description: Azimuth angle to moon for Ka band -45 polarization measurement.
  units: degrees
  valid values: [-180,...,180]
  datatype: 4 bytes IEEE floating point
  size: Number of MWR lines x Number of beams per channel

- **ka_n45_azimuth_angle_to_spacecraft**

  description: Azimuth angle to spacecraft for Ka band -45 polarization measurement.
  units: degrees
  valid values: [-180,...,180]
  datatype: 4 bytes IEEE floating point
  size: Number of MWR lines x Number of beams per channel

- **ka_n45_azimuth_angle_to_sun**

  description: Azimuth angle to sun for Ka band -45 polarization measurement.
  units: degrees
  valid values: [-180,...,180]
  datatype: 4 bytes IEEE floating point
  size: Number of MWR lines x Number of beams per channel

- **ka_n45_latitude**

  description: Latitude for Ka band -45 polarization measurement.
  units: degrees
  valid values: [-90,...,90]
  datatype: 4 bytes IEEE floating point
  size: Number of MWR lines x Number of beams per channel

- **ka_n45_longitude**

  description: Longitude for Ka band -45 polarization measurement.
  units: degrees
  valid values: [-180,...,180]
  datatype: 4 bytes IEEE floating point
  size: Number of MWR lines x Number of beams per channel

- **ka_n45_n3db_approximating_ellipse_lat**

  This dataset is optional, it may be present on the product only due to specific user request.

  description: Latitude of the center, first semimajor axis, first semiminor axis, second semimajor axis, second semiminor axis, of the ellipse that approximates the -3dB contour, for Ka band -45 polarization

units: degrees
valid values: [-90,...,90]
datatype: 4 bytes IEEE floating point
size: Number of MWR lines x Number of beams per channel x 5

- **ka_n45_n3db_approximating_ellipse_lon**

  This dataset is optional, it may be present on the product only due to specific user request.

  description: Longitude of the center, first semimajor axis, first semiminor axis, second semimajor axis, second semiminor axis, of the ellipse that approximates the -3dB contour, for Ka band -45 polarization
  units: degrees
  valid values: [-180,...,180]
  datatype: 4 bytes IEEE floating point
  size: Number of MWR lines x Number of beams per channel x 5

- **ka_n45_n3db_contour_lat**

  This dataset is optional, it may be present on the product only due to specific user request.

  description: Latitude of selected points from the -3dB contour, for Ka band -45 polarization.
  units: degrees
  valid values: [-90,...,90]
  datatype: 4 bytes IEEE floating point
  size: Number of MWR lines x Number of beams per channel x 20

- **ka_n45_n3db_contour_lon**

  This dataset is optional, it may be present on the product only due to specific user request.

  description: Longitude of selected points from the -3dB contour, for Ka band -45 polarization.
  units: degrees
  valid values: [-180,...,180]
  datatype: 4 bytes IEEE floating point
  size: Number of MWR lines x Number of beams per channel x 20

- **ka_n45_range_to_spacecraft**

  description: Distance between spacecraft and position of Ka band -45 polarization measurement.
  units: meters
  datatype: 4 bytes IEEE floating point
  size: Number of MWR lines x Number of beams per channel

- **ka_n45_zenith_angle_to_moon**

  description: Zenith (incidence) angle to moon for Ka band -45 polarization measurement.
  units: degrees
  valid values: [0,...,90]
  datatype: 4 bytes IEEE floating point
  size: Number of MWR lines x Number of beams per channel

- **ka_n45_zenith_angle_to_spacecraft**

  description: Zenith (incidence) angle to spacecraft for Ka band -45 polarization measurement.
  units: degrees

valid values: [0,...,90]
datatype: 4 bytes IEEE floating point
size: Number of MWR lines x Number of beams per channel

- **ka_n45_zenith_angle_to_sun**

  description: Zenith (incidence) angle to sun for Ka band -45 polarization measurement.
  units: degrees
  valid values: [0,...,90]
  datatype: 4 bytes IEEE floating point
  size: Number of MWR lines x Number of beams per channel

- **ka_p45_azimuth_angle_to_moon**

  description: Azimuth angle to moon for Ka band +45 polarization measurement.
  units: degrees
  valid values: [-180,...,180]
  datatype: 4 bytes IEEE floating point
  size: Number of MWR lines x Number of beams per channel

- **ka_p45_azimuth_angle_to_spacecraft**

  description: Azimuth angle to spacecraft for Ka band +45 polarization measurement.
  units: degrees
  valid values: [-180,...,180]
  datatype: 4 bytes IEEE floating point
  size: Number of MWR lines x Number of beams per channel

- **ka_p45_azimuth_angle_to_sun**

  description: Azimuth angle to sun for Ka band +45 polarization measurement.
  units: degrees
  valid values: [-180,...,180]
  datatype: 4 bytes IEEE floating point
  size: Number of MWR lines x Number of beams per channel

- **ka_p45_latitude**

  description: Latitude for Ka band +45 polarization measurement.
  units: degrees
  valid values: [-90,...,90]
  datatype: 4 bytes IEEE floating point
  size: Number of MWR lines x Number of beams per channel

- **ka_p45_longitude**

  description: Longitude for Ka band +45 polarization measurement.
  units: degrees
  valid values: [-180,...,180]
  datatype: 4 bytes IEEE floating point
  size: Number of MWR lines x Number of beams per channel

- **ka_p45_n3db_approximating_ellipse_lat**

  This dataset is optional, it may be present on the product only due to specific user request.

  description: Latitude of the center, first semimajor axis, first semiminor axis, second semi-major axis, second semiminor axis, of the ellipse that approximates the -3dB contour, for Ka band +45 polarization

units: degrees
valid values: [-90,...,90]
datatype: 4 bytes IEEE floating point
size: Number of MWR lines x Number of beams per channel x 5

- **ka_p45_n3db_approximating_ellipse_lon**

  This dataset is optional, it may be present on the product only due to specific user request.

  description: Longitude of the center, first semimajor axis, first semiminor axis, second semimajor axis, second semiminor axis, of the ellipse that approximates the -3dB contour, for Ka band +45 polarization
  units: degrees
  valid values: [-180,...,180]
  datatype: 4 bytes IEEE floating point
  size: Number of MWR lines x Number of beams per channel x 5

- **ka_p45_n3db_contour_lat**

  This dataset is optional, it may be present on the product only due to specific user request.

  description: Latitude of selected points from the -3dB contour, for Ka band +45 polarization.
  units: degrees
  valid values: [-90,...,90]
  datatype: 4 bytes IEEE floating point
  size: Number of MWR lines x Number of beams per channel x 20

- **ka_p45_n3db_contour_lon**

  This dataset is optional, it may be present on the product only due to specific user request.

  description: Longitude of selected points from the -3dB contour, for Ka band +45 polarization.
  units: degrees
  valid values: [-180,...,180]
  datatype: 4 bytes IEEE floating point
  size: Number of MWR lines x Number of beams per channel x 20

- **ka_p45_range_to_spacecraft**

  description: Distance between spacecraft and position of Ka band +45 polarization measurement.
  units: meters
  datatype: 4 bytes IEEE floating point
  size: Number of MWR lines x Number of beams per channel

- **ka_p45_zenith_angle_to_moon**

  description: Zenith (incidence) angle to moon for Ka band +45 polarization measurement.
  units: degrees
  valid values: [0,...,90]
  datatype: 4 bytes IEEE floating point
  size: Number of MWR lines x Number of beams per channel

- **ka_p45_zenith_angle_to_spacecraft**

  description: Zenith (incidence) angle to spacecraft for Ka band +45 polarization measurement.
  units: degrees

valid values: [0,...,90]
datatype: 4 bytes IEEE floating point
size: Number of MWR lines x Number of beams per channel

- **ka_p45_zenith_angle_to_sun**

  description: Zenith (incidence) angle to sun for Ka band +45 polarization measurement.
  units: degrees
  valid values: [0,...,90]
  datatype: 4 bytes IEEE floating point
  size: Number of MWR lines x Number of beams per channel

- **ka_v_azimuth_angle_to_moon**

  description: Azimuth angle to moon for Ka band V polarization measurement.
  units: degrees
  valid values: [-180,...,180]
  datatype: 4 bytes IEEE floating point
  size: Number of MWR lines x Number of beams per channel

- **ka_v_azimuth_angle_to_spacecraft**

  description: Azimuth angle to spacecraft for Ka band V polarization measurement.
  units: degrees
  valid values: [-180,...,180]
  datatype: 4 bytes IEEE floating point
  size: Number of MWR lines x Number of beams per channel

- **ka_v_azimuth_angle_to_sun**

  description: Azimuth angle to sun for Ka band V polarization measurement.
  units: degrees
  valid values: [-180,...,180]
  datatype: 4 bytes IEEE floating point
  size: Number of MWR lines x Number of beams per channel

- **ka_v_latitude**

  description: Latitude for Ka band V polarization measurement.
  units: degrees
  valid values: [-90,...,90]
  datatype: 4 bytes IEEE floating point
  size: Number of MWR lines x Number of beams per channel

- **ka_v_longitude**

  description: Longitude for Ka band V polarization measurement.
  units: degrees
  valid values: [-180,...,180]
  datatype: 4 bytes IEEE floating point
  size: Number of MWR lines x Number of beams per channel

- **ka_v_n3db_approximating_ellipse_lat**

  This dataset is optional, it may be present on the product only due to specific user request.

  description: Latitude of the center, first semimajor axis, first semiminor axis, second semi-major axis, second semiminor axis, of the ellipse that approximates the -3dB contour, for Ka band V polarization

units: degrees
valid values: [-90,...,90]
datatype: 4 bytes IEEE floating point
size: Number of MWR lines x Number of beams per channel x 5

- **ka_v_n3db_approximating_ellipse_lon**

  This dataset is optional, it may be present on the product only due to specific user request.

  description: Longitude of the center, first semimajor axis, first semiminor axis, second semimajor axis, second semiminor axis, of the ellipse that approximates the -3dB contour, for Ka band V polarization
  units: degrees
  valid values: [-180,...,180]
  datatype: 4 bytes IEEE floating point
  size: Number of MWR lines x Number of beams per channel x 5

- **ka_v_n3db_contour_lat**

  This dataset is optional, it may be present on the product only due to specific user request.

  description: Latitude of selected points from the -3dB contour, for Ka band V polarization.
  units: degrees
  valid values: [-90,...,90]
  datatype: 4 bytes IEEE floating point
  size: Number of MWR lines x Number of beams per channel x 20

- **ka_v_n3db_contour_lon**

  This dataset is optional, it may be present on the product only due to specific user request.

  description: Longitude of selected points from the -3dB contour, for Ka band V polarization.
  units: degrees
  valid values: [-180,...,180]
  datatype: 4 bytes IEEE floating point
  size: Number of MWR lines x Number of beams per channel x 20

- **ka_v_range_to_spacecraft**

  description: Distance between spacecraft and position of Ka band V polarization measurement.
  units: meters
  datatype: 4 bytes IEEE floating point
  size: Number of MWR lines x Number of beams per channel

- **ka_v_zenith_angle_to_moon**

  description: Zenith (incidence) angle to moon for Ka band V polarization measurement.
  units: degrees
  valid values: [0,...,90]
  datatype: 4 bytes IEEE floating point
  size: Number of MWR lines x Number of beams per channel

- **ka_v_zenith_angle_to_spacecraft**

  description: Zenith (incidence) angle to spacecraft for Ka band V polarization measurement.
  units: degrees
  valid values: [0,...,90]
  datatype: 4 bytes IEEE floating point
  size: Number of MWR lines x Number of beams per channel

- **ka_v_zenith_angle_to_sun**

  description: Zenith (incidence) angle to sun for Ka band V polarization measurement.
  units: degrees
  valid values: [0,...,90]
  datatype: 4 bytes IEEE floating point
  size: Number of MWR lines x Number of beams per channel

2.3 Group 'MWR Calibrated Radiometric Data'

MWR calibrated radiometric measurements

Datasets

- **k_h_antenna_temperature**

  description: K band H polarization antenna temperature measurement
  units: celsius degrees
  datatype: 4 bytes IEEE floating point
  size: Number of MWR lines x Number of beams per channel

- **ka_h_antenna_temperature**

  description: Ka band H polarization antenna temperature measurement
  units: celsius degrees
  datatype: 4 bytes IEEE floating point
  size: Number of MWR lines x Number of beams per channel

- **ka_n45_antenna_temperature**

  description: Ka band -45 polarization antenna temperature measurement
  units: celsius degrees
  datatype: 4 bytes IEEE floating point
  size: Number of MWR lines x Number of beams per channel

- **ka_p45_antenna_temperature**

  description: Ka band +45 polarization antenna temperature measurement
  units: celsius degrees
  datatype: 4 bytes IEEE floating point
  size: Number of MWR lines x Number of beams per channel

- **ka_v_antenna_temperature**

  description: Ka band V polarization antenna temperature measurement
  units: celsius degrees
  datatype: 4 bytes IEEE floating point
  size: Number of MWR lines x Number of beams per channel

2.4 Group 'Quality indicators'

Datasets indicating quality of measurements and measurements positions

Datasets

- **filled_mwr_samples**

  description: Bitmask indicating the filling MWR samples included in the product.
  units: bitmask
  valid values: byte0: bit7 (msb) = Horn 1 of K band H polarization, ..., bit0 = Horn 8 of K band H polarization; byte1: bit7 (msb) = Horn 1 of Ka band H polarization, ..., bit0 = Horn 8 of Ka band H polarization; byte2: bit7 (msb) = Horn 1 of Ka band V polarization, ..., bit0 = Horn 8 of Ka band V polarization; byte3: bit7 (msb) = Horn 1 of Ka band +45 polarization, ..., bit0 = Horn 8 of Ka band +45 polarization; byte4: bit7 (msb) = Horn 1 of Ka band -45 polarization, ..., bit0 = Horn 8 of Ka band -45 polarization;
  datatype: 1 byte unsigned integer
  size: Number of MWR lines x Number of channels

- **k_h_quality**

  description: Quality of each MWR sample of K band H polarization. Indicates the degree of quality of the data. [5=good quality, 4, 3, 2, 1=poor quality]
  valid values: [5=good quality, 4, 3, 2, 1=poor quality]
  datatype: 1 byte unsigned integer
  size: Number of MWR lines x Number of beams per channel

- **ka_h_quality**

  description: Quality of each MWR sample of Ka band H polarization. Indicates the degree of quality of the data. [5=good quality, 4, 3, 2, 1=poor quality]
  valid values: [5=good quality, 4, 3, 2, 1=poor quality]
  datatype: 1 byte unsigned integer
  size: Number of MWR lines x Number of beams per channel

- **ka_n45_quality**

  description: Quality of each MWR sample of Ka band -45 polarization. Indicates the degree of quality of the data. [5=good quality, 4, 3, 2, 1=poor quality]
  valid values: [5=good quality, 4, 3, 2, 1=poor quality]
  datatype: 1 byte unsigned integer
  size: Number of MWR lines x Number of beams per channel

- **ka_p45_quality**

  description: Quality of each MWR sample of Ka band +45 polarization. Indicates the degree of quality of the data. [5=good quality, 4, 3, 2, 1=poor quality]
  valid values: [5=good quality, 4, 3, 2, 1=poor quality]
  datatype: 1 byte unsigned integer
  size: Number of MWR lines x Number of beams per channel

- **ka_v_quality**

  description: Quality of each MWR sample of Ka band V polarization. Indicates the degree of quality of the data. [5=good quality, 4, 3, 2, 1=poor quality]
  valid values: [5=good quality, 4, 3, 2, 1=poor quality]
  datatype: 1 byte unsigned integer
  size: Number of MWR lines x Number of beams per channel

- **missing_mwr_lines**

  description: Indicates the number of missing MWR lines before the current one
  datatype: 2 bytes unsigned integer
  size: Number of MWR lines

- **mwr_samples_with_crc_errors**

  description: Bitmask indicating the MWR samples whose input data contains CRC errors.
  units: bitmask
  valid values: byte0: bit7 (msb) = Horn 1 of K band H polarization, ..., bit0 = Horn 8 of K band H polarization; byte1: bit7 (msb) = Horn 1 of Ka band H polarization, ..., bit0 = Horn 8 of Ka band H polarization; byte2: bit7 (msb) = Horn 1 of Ka band V polarization, ..., bit0 = Horn 8 of Ka band V polarization; byte3: bit7 (msb) = Horn 1 of Ka band +45 polarization, ..., bit0 = Horn 8 of Ka band +45 polarization; byte4: bit7 (msb) = Horn 1 of Ka band -45 polarization, ..., bit0 = Horn 8 of Ka band -45 polarization;
  datatype: 1 byte unsigned integer
  size: Number of MWR lines x Number of channels

- **mwr_samples_with_geolocation_errors**

  description: Bitmask indicating the MWR samples where the geolocation algorithm failed.
  units: bitmask
  valid values: byte0: bit7 (msb) = Horn 1 of K band H polarization, ..., bit0 = Horn 8 of K band H polarization; byte1: bit7 (msb) = Horn 1 of Ka band H polarization, ..., bit0 = Horn 8 of Ka band H polarization; byte2: bit7 (msb) = Horn 1 of Ka band V polarization, ..., bit0 = Horn 8 of Ka band V polarization; byte3: bit7 (msb) = Horn 1 of Ka band +45 polarization, ..., bit0 = Horn 8 of Ka band +45 polarization; byte4: bit7 (msb) = Horn 1 of Ka band -45 polarization, ..., bit0 = Horn 8 of Ka band -45 polarization;
  datatype: 1 byte unsigned integer
  size: Number of MWR lines x Number of channels

- **mwr_samples_with_invalid_data**

  description: Bitmask indicating the MWR samples whose input data was tagged as invalid.
  units: bitmask
  valid values: byte0: bit7 (msb) = Horn 1 of K band H polarization, ..., bit0 = Horn 8 of K band H polarization; byte1: bit7 (msb) = Horn 1 of Ka band H polarization, ..., bit0 = Horn 8 of Ka band H polarization; byte2: bit7 (msb) = Horn 1 of Ka band V polarization, ..., bit0 = Horn 8 of Ka band V polarization; byte3: bit7 (msb) = Horn 1 of Ka band +45 polarization, ..., bit0 = Horn 8 of Ka band +45 polarization; byte4: bit7 (msb) = Horn 1 of Ka band -45 polarization, ..., bit0 = Horn 8 of Ka band -45 polarization;
  datatype: 1 byte unsigned integer
  size: Number of MWR lines x Number of channels

F.3 CFRSL L1 Data (.mat)

The File Name:

Qyyyydddhhmmss_MWR_L1_Vn.0

%%%

yyyy : year

ddd : Julian Day (day of the year)

hh,mm,ss : hours, minutes, seconds (start of the file)

L1 : Level of the data product

Vn.0: version of the calibration

The file Structure:

%%%

it is a Matlab structure (.mat) that consists of three main structure (three radiometers):

1) RX23H

2) RX37H

3) RX37V

Each of these main structures is divided to eight sub-structures representing the eight horns for that specific radiometer:

B1

B2

B3

B4

B5

B6

B7

B8

Inside of each of these horns there are three variables and three sub-structures

Variables:

1)Lat ➔ Latitude in deg

2)Lon ➔ Longitude in deg

3) EIA ➔ earth incidence angle (deg)

4) Tin ➔ Brightness temperature at the input of the coupler

5) Tb ➔ Calibrated main-beam antenna brightness temperature

6) time ➔ time in matlab serial date format

7)Ca ➔ Antenna Counts

8)Cn ➔ Antenna + Noise Counts

9)Co ➔ Reference Load Counts

You can use matlab command datestr(time) to see sampling time and date for each sample.

Sub-Structures:

1) calib_coeff : This structure contains the following calibration coefficients

slope, offset, b

2) Telem_Temp :This structure contains 5 temperature sensor measurements in K=> To T1 T2 T3 T4

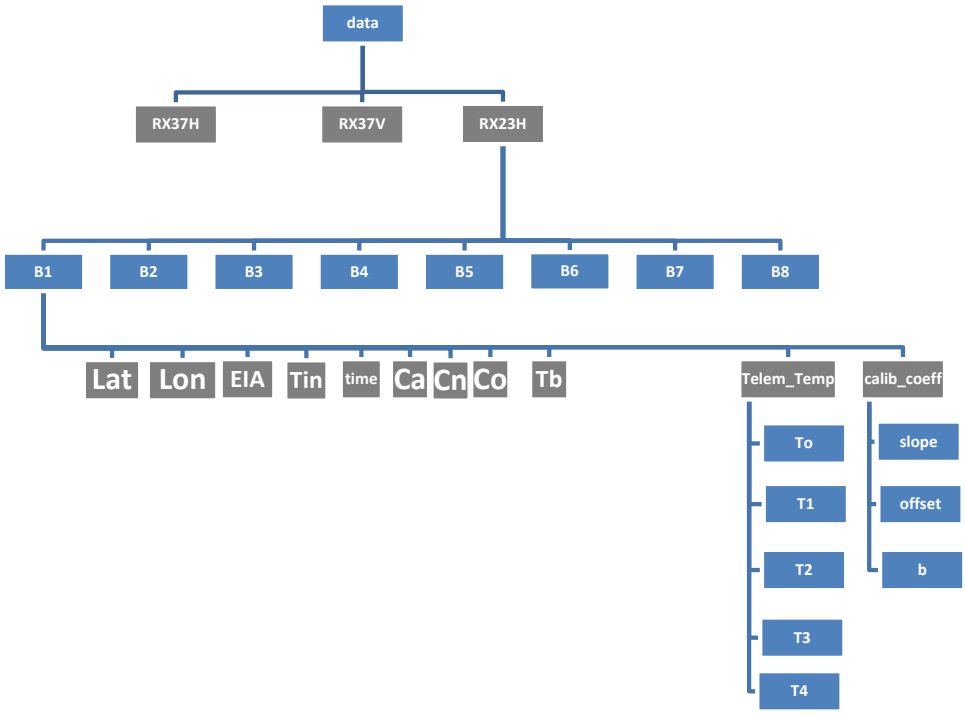
data
RX37H
RX37V
RX23H
B1
B2
B3
B4
B5
B6
B7
B8
Lat
Lon
EIA
Tin
time
Ca
Cn
Co
Tb
Telem_Temp
calib_coeff
To
T1
T2
T3
T4
slope
offset
b

LIST OF REFERENCES

[1] J. C. Gallo, "Aquarius/SAC-D Microwave Radiometer Critical Design Review," (Buenos Aires, Argentina), August 22-24, 2007.

[2] S. S. Khan, "Simulation of Brightness Temperatures for The Microwave Radiometer on The Aquarius/SAC-D Mission," Master's thesis, School of Electrical Engineering & Computer Science, University of Central Florida, 2009.

[3] "NASA Aquarius Mission Overview."
weblink - http://aquarius.nasa.gov/overview.html/.

[4] "NASA Aquarius Mission Science:Discovery & Exploration."
weblink - http://aquarius.nasa.gov/science-discovery.html.

[5] "NASA Aquarius Mission Basics & Exploration."
weblink - http://aquarius.nasa.gov/overview-mission.html.

[6] G. Lagerloef, F. Colomb, D. L. Vine, F. Wentz, S. Yueh, C. Ruf, J. Lilly, J. Gunn, Y. Chao, A. deCharon, G. Feldman, and C. Swift, "The aquarius/sac-d mission: Designed to meet the salinity remote-sensing challenge," *Oceanography:Special Issue on Salinity*, vol. 21, pp. 68–81, mar 2008.

[7] Y. K., A. Sen, D. Caruso, G. Lagerloef, R. Colomb, D. L. Vine, and S.Yueh, "Aquarius/SAC-D Mission Overview," in *Proc. SPIE Conf. Sens. Syst. and Next-Generation Satellites X*, (Stockholm, Sweden), p. 63610I, 2006.

[8] G. Evans and C. W. McLeish, *RF Radiometer Handbook*. Dedham, MA: Artech House, 1977.

[9] R. K. M. F. T. Ulaby and A. K. Fung, *Microwave remote sensing: active and passive. Volumn I, Microwave Remote Sensing Fundamentals and Radiometry*. Norwood, MA: Artech House, 1981.

[10] F. Wentz, P. Ashcroft, and C. Gentemann, "Post-launch calibration of the trmm microwave imager," *Geoscience and Remote Sensing, IEEE Transactions on*, vol. 39, pp. 415 –422, feb 2001.

[11] K. Gopalan, L. Jones, S. Biswas, S. Bilanow, T. Wilheit, and T. Kasparis, "A Time-Varying Radiometric Bias Correction for The TRMM Microwave Imager," *IEEE Trans. Geosci. Rem. Sens.*, vol. 47, Oct. 2009.

[12] P. Gaiser, K. St Germain, E. Twarog, G. Poe, W. Purdy, D. Richardson, W. Grossman, W. Jones, D. Spencer, G. Golba, J. Cleveland, L. Choy, R. Bevilacqua, and

P. Chang, "The windsat spaceborne polarimetric microwave radiometer: sensor description and early orbit performance," *Geoscience and Remote Sensing, IEEE Transactions on*, vol. 42, pp. 2347 – 2361, nov. 2004.

[13] "Satellite Toolkit." weblink - http://www.stk.com/.

[14] S. Biswas, L. Jones, S. Khan, J.-C. Gallo, and D. Roca, "Mwr and windsat intersatellite radiometric calibration plan," in *Microwave Radiometry and Remote Sensing of the Environment (MicroRad), 2010 11th Specialist Meeting on*, pp. 266 –271, march 2010.

[15] T. Meissner and F. Wentz, "The complex dielectric constant of pure and sea water from microwave satellite observations," *Geoscience and Remote Sensing, IEEE Transactions on*, vol. 42, pp. 1836 – 1849, sept. 2004.

[16] G. Elsaesser, "A parametric optimal estimation retrieval of the nonprecipitating parameters over the global oceans," Master's thesis, Colorado State University, Fort Collins, CO, 2006.

[17] T. Wilheit, "A model for the microwave emissivity of the ocean's surface as a function of wind speed," *Geoscience Electronics, IEEE Transactions on*, vol. 17, pp. 244 –249, oct. 1979.

[18] J. Hollinger, "Passive microwave measurements of sea surface roughness," *Geoscience Electronics, IEEE Transactions on*, vol. 9, pp. 165 –169, july 1971.

[19] A. Stogryn, "The emissivity of sea foam at microwave frequencies," in *Antennas and Propagation Society International Symposium, 1971*, vol. 9, pp. 169 – 171, sep 1971.

[20] C. Elachi and J. Zyl, *Introduction to the physics and techniques of remote sensing*. Wiley series in remote sensing, Wiley-Interscience, 2006.

[21] F. Wentz, "Measurement of oceanic wind vector using satellite microwave radiometers," *Geoscience and Remote Sensing, IEEE Transactions on*, vol. 30, pp. 960 –972, sep 1992.

[22] P. W. rosenkranz, "Water vapor microwave continuum absorption: A comparison of measurements and models," *Radio Science*, vol. 33, pp. 919–928, 1998.

[23] H. J. Liebe, G. A. Hufford, and T. Manabe, "A model for the complex permittivity of water at frequencies below 1 THz," *International Journal of Infrared and Millimeter Waves*, vol. 12, pp. 659–675, July 1991.

[24] H. Liebe, P. Rosenkranz, and G. Hufford, "Atmospheric 60-ghz oxygen spectrum: New laboratory measurements and line parameters," *Journal of Quantitative Spectroscopy and Radiative Transfer*, vol. 48, no. 56, pp. 629 – 643, 1992. Special Issue Conference on Molecular Spectroscopic Databases.

[25] P. W. Rosenkranz, "Absorption of Microwaves by Atmospheric Gases," in *Atmospheric Remote Sensing By Microwave Radiometry* (M. A. Janssen, ed.), p. 37, 1993.

[26] B. Geerts and E. Linacre, "The height of the tropopause." `http://www-das.uwyo.edu/~geerts/cwx/notes/chap01/tropo.html`, 1997. [Online; accessed 19-March-2012].

[27] M. Wisler and J. Hollinger, *Estimation of Marine Environmental Parameters Using Microwave Radiometric Remote Sensing Systems.* NAVAL RESEARCH LAB WASHINGTON D C., NRL memorandum report no. 3661, Defense Technical Information Center, 1977.

[28] "Sensor Data Record Files (SDR)," in *WindSat Data Products Users' Manual: Sensor and Environmental Data Records* (Ted. Lungu, ed.), Version 3.0, D-29825, January, 2006.

[29] S. Biswas, K. Gopalan, L. Jones, and S. Bilanow, "Correction of Time-Varying Radiometric Errors in TRMM Microwave Imager Calibrated Brightness Temperature Products," *IEEE Geosci, Rem. Sens. Letters.*, 2010. accepted for publication.

[30] C. S. May, "Engineering evaluation of multi-beam satellite antenna boresight pointing using land/water crossings," Master's thesis, School of Electrical Engineering & Computer Science, University of Central Florida, 2012.

[31] M. M. Jacob and M. Labanda, "Mwr calibration anomaly report - preliminary version," *Technical Memo, CONAE Ground Segment and Application*, March, 2012.

[32] C. Ruf, S. Keihm, and M. Janssen, "Topex/poseidon microwave radiometer (tmr). i. instrument description and antenna temperature calibration," *Geoscience and Remote Sensing, IEEE Transactions on*, vol. 33, pp. 125 –137, jan 1995.

[33] F. J. Wentz, "The effect of clouds and rain on the aquarius salinity retrieval," *Remote Sensing Systems Technical Memorandum 3031805*, Mar 18 2005.